The Impact of Ligand Design on the Coordination Chemistry and Reactivity of Metal Pincer Complexes

Sarath Wanniarachchi
Marquette University

THE IMPACT OF LIGAND DESIGN ON THE COORDINATION CHEMISTRY AND REACTIVITY OF METAL PINCER COMPLEXES

by

Sarath Wanniarachchi, B.Sc. (Hons)

A Dissertation submitted to the Faculty of the Graduate School,
Marquette University,
in Partial Fulfillment of the Requirements for
the Degree of Doctor of Philosophy

Milwaukee, Wisconsin

May 2012

ABSTRACT

THE IMPACT OF LIGAND DESIGN ON THE COORDINATION CHEMISTRY AND REACTIVITY OF METAL PINCER COMPLEXES

Sarath Wanniarachchi, B.Sc. (Hons)

Marquette University, 2012

Pincer ligands are uninegative tridentate metal-coordinating agents of the form $[XZY]^-$ where Z is the central, anchoring Lewis donor while X and Y are flanking Lewis donors. Ever since initial reports of transition metal pincer complexes were published in the late 1970's, there has been burgeoning interest in such complexes because of their desirable robust nature, generally simple syntheses, and the spectacular chemical transformations that they can mediate. In this research project, two new sets of pincer ligands with a diarylamido anchor and either two pyrazolyl nitrogenous flanking donors (NNN pincer) or one pyrazolyl and one diphenylphosphine donor (NNP pincer) have been prepared and their late transition metal complexes have been studied.

First, for tricarbonylrhenium(I) complexes it was demonstrated that the NNN pincers bind in bidentate or *fac*- tridentate modes. By increasing steric bulk at the 3-pyrazolyl position near the metal, the *fac*-$Re(CO)_3$ moiety distorts the ligand to enhance ligand-centered reactivity.

Second, for carbonylrhodium(I) complexes, (NNN)Rh(CO), substitution at the *para*-aryl positions predictably modulates the electronic properties and chemical reactivity. Oxidative addition reactions of the (NNN)Rh(CO) with iodoalkanes proceed about three orders of magnitude faster than those reported for the Monsanto catalyst, $[Rh(CO)_2I_2]^-$.

Third, there is also interest in metal complexes of redox-active ligands because it is hoped that one could use the ligand as an electron reservoir to help arbitrate difficult multi-electron processes. For $(NNN)Rh^{III}XYZ$, varying non-pincer ligands(X, Y, and Z) changes the $(NNN)/(NNN)^+$ oxidation potential by 700 mV. An empirical ligand

additivity model was discovered that predicts the half wave potential of the ligand-based redox couple. Such a model is envisioned to be important for future considerations when designing complexes for exothermic electron transfer reactions.

Finally, a comparison of related (NNN)Rh(CO), (NNP)Rh(CO) and (PNP)Rh(CO) complexes revealed that substitutions of pyrazolyl for diphenylphosphine primarily impacts sterics (not electronics), thereby affecting kinetics of reactions. The PPh_2 moiety permits the isolation of a coordinatively-unsaturated 16-electron rhodium(III) complex that showed metal ligand cooperativity in its reactions with HI. The hemilability of the (NNP)Rh fragment was also demonstrated by reactions with t-BuNC.

ACKNOWLEDGMENTS

Sarath Wanniarachchi, B. Sc (Hons)

I especially want to thank my advisor, Prof.James R. Gardinier for his guidance during my research and study at Marquette University. His perpetual energy and enthusiasm in research had motivated all his advisees, including me. Besides my advisor, I would like to thank the rest of my dissertation committee Prof.Rajendra Rathore and Prof. Yi Chae S, for their encouragement, insightful comments, and the support. I would like to thanks my group members Dr.Brendan Liddle, Dr. Chengeto Gwengo, Dr. Tyler J. Morin, Heidi Tatlock, Brandon Kizer and Jeewantha Sampath for their support and valuable conversations. I thank my teachers and colleagues at the Ruhuna University.

My deepest gratitude goes to my parents and elder brother for their unflagging love and support throughout my life; this dissertation is simply impossible without them. They provided the best possible environment for me to grow up and attend school. Although they are no longer with us, they are forever remembered. I am sure they share our joy and happiness in the Nirvana. I thank my family siblings for their support and encouragement. I most want to thank my wife Shriya for her love, sacrifice, and kind indulgence. I also credit my son Nirad for inspiring and amazing me every day. Also I thank Shriya's mom for providing us unending encouragement and support.

I would like to acknowledge Marquette University, Ruhuna University and National Science Foundation for financial support. The generous support from Arthur J. Schmitt Foundation is greatly appreciated.

TABLE OF CONTENTS

LIST OF TABLES

LIST OF FIGURES

LIST OF SCHEMES

CHAPTER 1

INTRODUCTION

1.1. General introduction of pincer ligands and their metal complexes. Pincer ligands are loosely characterized as being uninegative, tridentate, meridionally- metal-coordinating agents. Derivatives with different overall charge or that are sometimes facially-coordinating are also given the moniker of pincer. These ligands are categorized by the nature of donor atoms along the ligand scaffold and are given general abbreviations of the type DXD that correspond to the central anchoring donor, X, and flanking donors, D (**Figure 1.1**). The flexibility of the DXD pincer platform provides

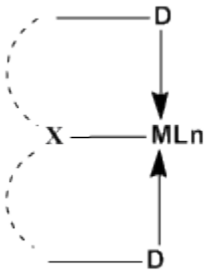

Figure 1.1. General representation of a pincer ligand
MLn=Metal complex, **X**,**D**=DonoratomO, S,N, P, C

ample opportunity to design the ligand architecture by changing the anchoring or flanking donors or the linkers connecting the various donor atoms. **Chart 1.1** displays a small sample of various charge-neutral and anionic pincer frameworks.[1]

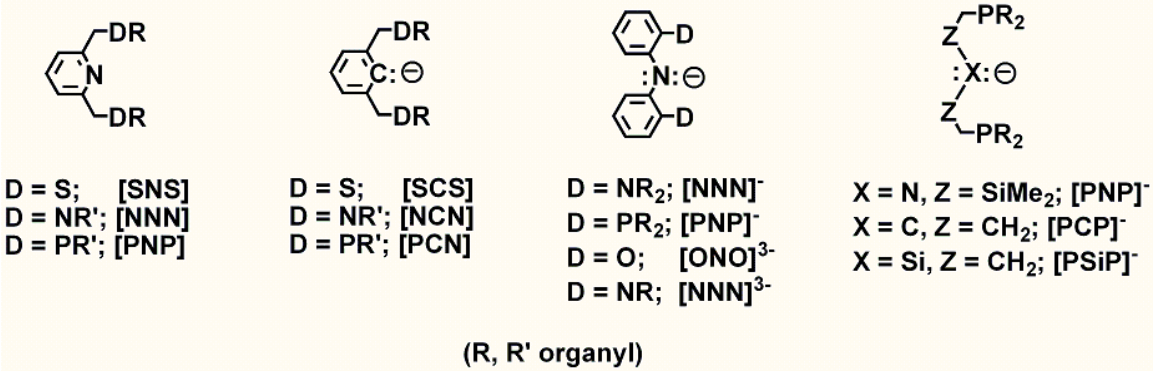

Chart 1.1.Selected examples of pincer ligands in literature.

Metal pincer complexes are typically robust structures with high thermal stability and many researchers are currently investigating pincer complexes for various applications ranging from homogeneous catalysis to the development of chemical sensors and switches.[2]The persistent high level of interest in such complexes is due to, in part, to the ability of fine tune the steric and electronic properties of the pincer ligand in a systematic manner. Such modifications can alter the physical and electronic properties, and, hence, the reactivity of the complexes. As will be seen, very different reactivities can be displayed by pincers with similar (-NR_2vs -NH_2 flankers) or the same donor sets. In other words, not all NNN- pincer complexes (for instance) behave the same! Part of the work of this thesis is aimed at uncovering the origin of such phenomena.

1.2. Overview of "classical" stoichiometric bond activation and catalytic activity.

Pincer complexes have been employed in various stoichiometric bond activation reactions and catalytic processes that continue to promote intrigue into their possible uses. For instance, pincer complexes have been used to probe the limits of C-X oxidative addition reactions,[3] and catalytic processes such as the Heck reaction,[4] Suzuki-

Miyauracoupling,[5]olefin polymerization,[6]decarbonylation of ketones,[7]asymmetric allylicalkylation,[8]and hydrogen transfer reactions.[9]Only C-X oxidative addition and transfer hydrogenation reactions are discussed in the following sections since these will be used as benchmarks to test reactivity of newly developed pincers later in the thesis.

Oxidative addition and reductive elimination reactions (**Scheme 1.1**) are very important and widely studied class of reactions initiated by transition metal complexes since they are often the rate limiting steps of catalytic cycles. The rate-limiting oxidative addition reaction of iodomethane to square planar Rh(I) complexes in the Monsanto industrial process for the production of acetic acid from methanol is a prime example. Oxidative addition of C-X bond (X = Cl, Br, I) to Rh(I) complexes has been steadily rising over the past few years as these can be envisioned as starting points to the formation of new carbon–carbon, carbon–nitrogen, and carbon–oxygen bonds.[10]

Scheme 1.1. Oxidative addition of X-Y bond to a metal complex

For example, terdentate NNN- pincer ligand systems can act as electron rich donors to enhance the nucleophilicity of low-valent late transition metal centers. This enhanced nucleophilicity might be exploited to control the catalytic processes at the metal center.[11]Studies on Rh(I) complexes clearly indicate that electron rich Rh(I) complexes undergo faster oxidative addition than electron poor counterparts. This observation is exemplified by the work of Doris Kunz and coworkers[12] who reported a highly nucleophilicrhodium(I) carbonyl complex **1** that contains two N-heterocyclic carbene

moieties. This complex is unique in that it has the highest yet reported rate for the oxidative addition of CH_3I. Complex **1** also reacts at room temperature with benzyl bromide **(Figure 1-2)** to give the benzylrhodium(III) complex **2.** Typicallyrhodium(I) complexes only react with benzyl bromide at high temperature, if at all. Even more remarkable is the report from the Ozerov group that describes an oxidative addition

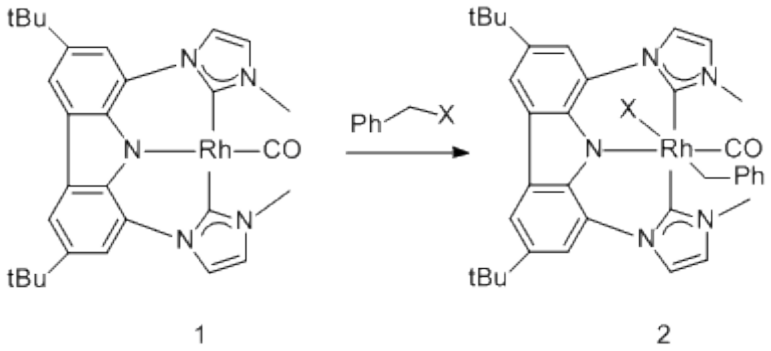

Figure 1.2. Oxidative addition of benzyl bromide by (CNC) Rh pincer complex

reaction between the (PNP)Rh(I) complex **3** and haloarenes, Ar-X (X = Cl, Br) **(Figure 1.3)**. The strong aryl halide bonds (BDE Ph-Br = 353 kJ/mol, BDE Ph-Cl = 408

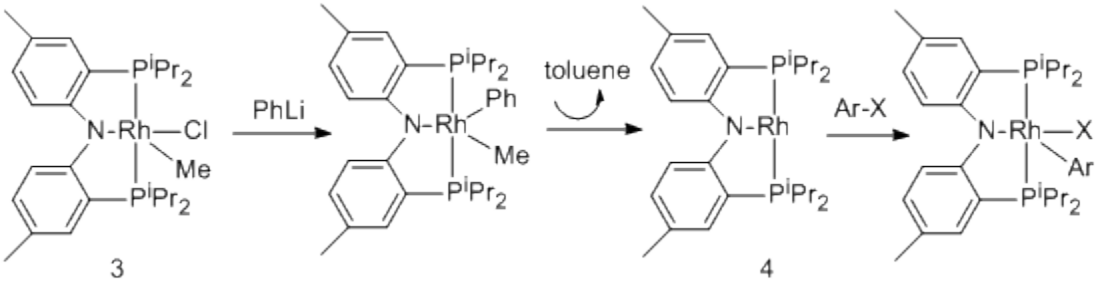

Figure 1.3. Oxidative addition of Ar-X to (PNP)Rh complex

kJ/mol) combined with the bulky nature of the organic and the typically modest nucleophilicity of rhodium(I) usually prevents such OA reactions with other

rhodium(I)complexes. The three-coordinate Rh(I) intermediate **4** was proposed as the reactive species in these reactions; the fluorobenzene adduct of **4** can be isolated.[3]

Hydrogenation of ketones (**Scheme1.2**) catalyzed by transition metal complexes is a fundamental process for the production of wide range of alcohols and amines using mild conditions.[13] Transfer hydrogenation has economic and environmental advantages as it avoids the use of more diffusing and inflammable dihydrogen gas and hazardous reducing agents.[14]Ruthanium, rhodium and iridium metal complexes are the most active and selective transfer hydrogenation catalysis.

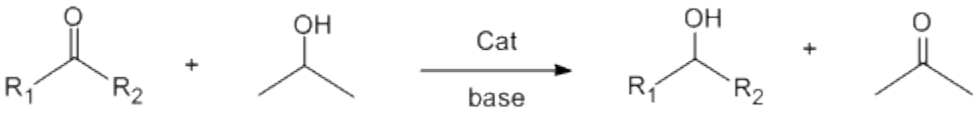

Scheme 1.2. Hydrogenation of ketons

A large number of metal complexes have been found to be highly efficient catalysts for transfer hydrogenation of ketones and a majority of these are ruthenium-centered catalysts.[15]Of the various pincer complexes studied (**Figure 1.4**), Van Koten showed [16] that NCN and PCP pincer complexes **5** and **6** efficiently convert cyclohexanone to cyclohexanol using KOH/isopropanol system with TOF 1100 and 10000 h^{-1} respectively. Grutzmacher's NCC pincer complex **7** converts cyclohexanone to cyclohexanol[17] with a turnover frequency (TOF) of 7.5 x 10^5 h^{-1}. Baratta's CNN pincer complex **8** showed [18] remarkable conversion with a TOF of 1.5 x 10^6 h^{-1}. Transfer hydrogenation can occur by a variety of different mechanisms.[14]Many (all) invoke a metal-hydride intermediate. Such a hydride intermediate was thought to be the catalytic active species in the transfer hydrogenation process of **8**.[19]The hydridoruthenium

complex **9** (**Figure 1.5**) was isolated from the reaction between **8** and sodium isopropoxide. Then, complex **9** was found to react with acetophenone in 2-propanol in the absence of base to give 1-phenylethanol and acetone with a TOF of 4.8 x 10^{4} h^{-1}. Clearly, variation in pincer ligand design and of the metal environment have important influences on the transfer hydrogenation reactions – new designs may lead to even more improved performance in catalytic reactions.

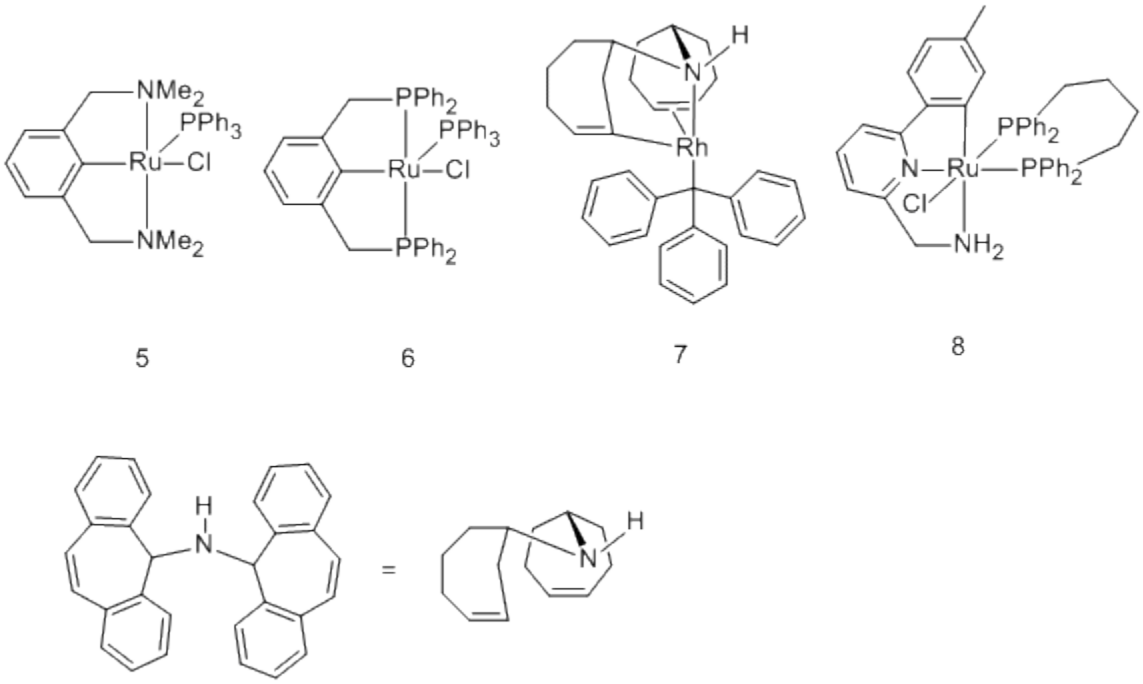

Figure 1.4. NCN, PCP and CNC, CNN pincer complexes used in transfer .hydrogenation

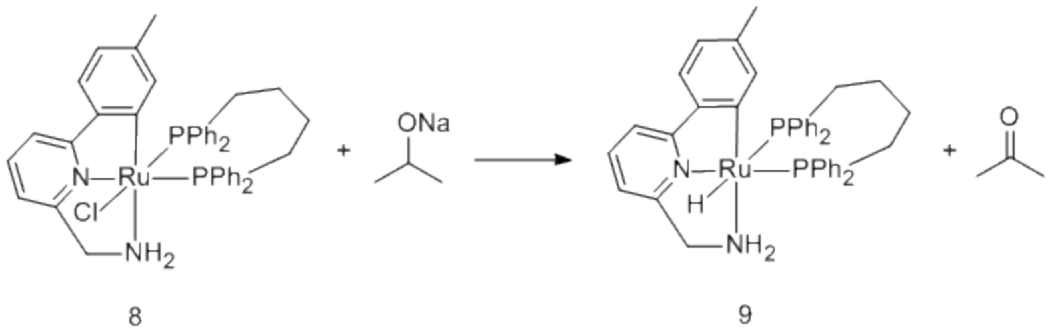

8 9

Figure 1.5. Isolation of hydridoruthenium intermediate of the CNN pincer complex

1.3. More recent developments: "non-classical" reactivity of pincer complexes.

Very recently new modes of reactivity of metal pincer complexes have been identified where the ligand plays an active role in chemical reactions. These can be divided into three main categories: (i) hemilability; (ii) metal-ligand cooperativity; and (iii) redox non-innocence. A brief (non-comprehensive) overview of each these categories follows.

1.3.1 Hemilability. There has long been interest in different kinds of 'hemilabile' multidentate ligands where one or more donor atoms are firmly bound to a metal center while another donor 'arm' can be readily displaced as in **Scheme-1.3**

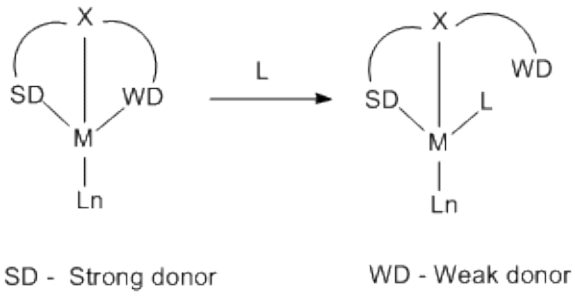

Scheme 1.3. Depiction of a hemilable tridentate ligand.

Metal complexes with various hemilabile ligands have been found to be active catalysis for range of chemical transformations including hydrogenation, carbonylation, olefin dimerization and small molecular activation.[20,21]A majority of hemilabile ligands are bidentate[22] with both 'hard' and 'soft' flanking donors to give disparity in their interactions with a metal center but other hemilabile ligands with higher denticities and homogeneous donor sets are also known. [23] Recently, there has been a growing interest in complexes of hemilabile terdentate, anionic 'pincer' ligands [24] owing to the remarkable chemical transformations that can be mediated by such species.[25,] In this vein, a very recent manuscript by the van der Vlugt group describes a study of three hemilabile PNN complexes of rhodium(I) (**Figure 1.6**).[26] The authors provided compelling

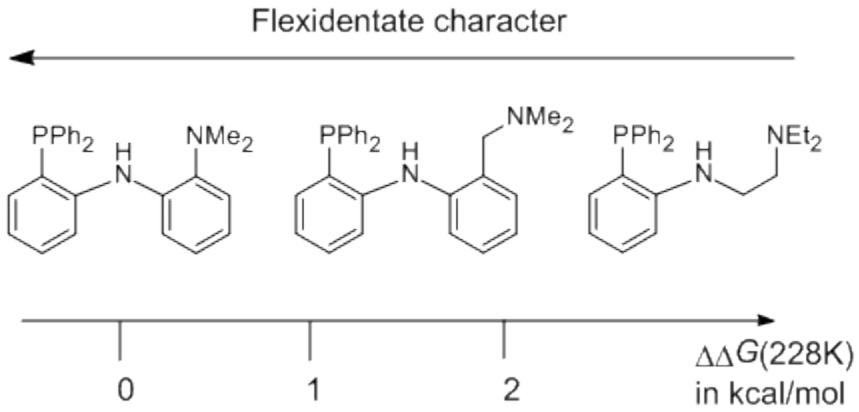

Figure 1.6. Three pincer ligands in increasing order of hemi-lability from ref 26.

Spectroscopic evidence that various (PNN)Rh(CNR)$_2$ complexes were hemilabile and contained four-coordinate rhodium with κ^2*PN*-pincer ligands but in no case was a complex structurally-authenticated. Instead, theoretical calculations were used to support the assertion of hemilability. Part of the goals of this thesis work will be set toward exploiting the crystallinity of pyrazolyl-containing pincer systems to structurally verify

the elusive $\kappa^2 PN$ -coordination mode of the (PNN)Rh$(CNR)_2$ systems, by first learning how to prepare such ligands. The presence of a hemilabile ligand in a metal complex may significantly influence the reactivity and promote new transformations.

1.3.2 Metal ligand cooperativity .In most of transition metal catalysis, the catalytic activity is based on the metal center. That is, throughout a catalytic cycle, the metal oxidation state and coordination number changes and the metal's supporting ligands are not involved in bond-making or -breaking. When the metal and its supporting ligand both participate in the catalytic activation of a substrate by undergoing reversible structural changes then metal-ligand cooperation is said to exist. Two of the main strategies for promoting metal-ligand cooperativity include placing a ligand-centered lone pair adjacent to a vacant metal coordination site or to incorporate aromatic rings adjacent to both a methylene and a metal so as to encourage aromatization/dearomatization processes.

The imido group acts as a cooperative ligand in early transition metal complexes. Even unactivated C-H bonds can be reversibly added across M=N bond.[27] (Figure 1.7). Amido ligand acts as cooperating ligands in catalyzed hydrogenation of unsaturated ketones.

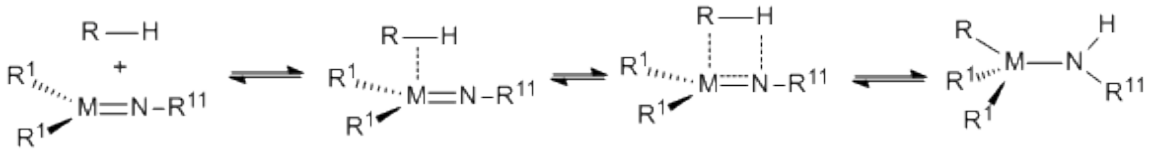

Figure 1.7. C-H activation promoted byimido complexes (M=Ti, Zr; R'=siloxy or Cp, Cp*)

Noyori's Ru(II) amido complex operates[28] metal ligand by functional mechanism and cleaves dihydrogen to give Ru amino dihydride complex which converts ketones in to alchols**.(Figure 1.8).**

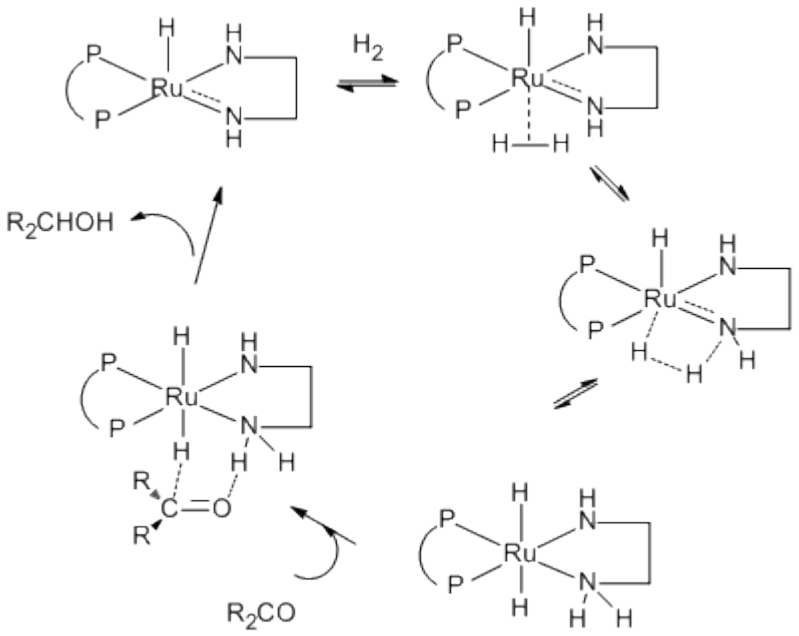

Figure 1.8. Selected steps in the catalytic cycle of the Noyori–Morrismechanism, highlighting the role of the cooperating amido ligand inthe heterolytic cleavage of the H_2 molecule

Recently Milstein[29] has discovered new modes of metal ligand cooperation involving aromatization- dearomatization processes of PNP and PNN pyridine based pincer complexes. These metal complexes undergo deprotonation at the pyridinylmethylenic carbon resulting in dearomatization of the pyridine ring **(Figure.1.9)**. This dearomatized pyridine complex activates strong bonds like C-H, N-H,

H-H etc. by cooperation between the metal and ligand (which regains the aromatization). There is no change in the formal oxidation state of the metal center in this process.

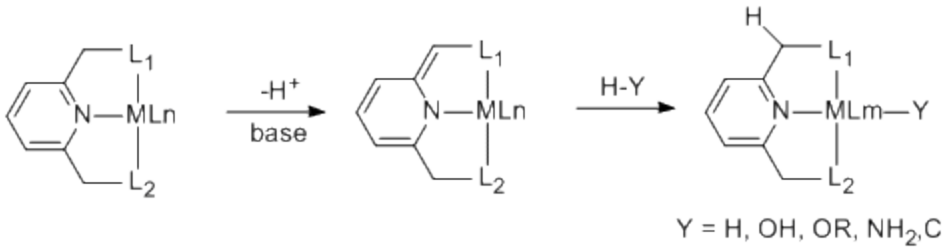

Figure 1.9. Activation of strong bond by metal ligand cooperation

The reaction of complex **10** with a base results dearomatized **11**, which activates C-D bond in C_6D_6 **(Figure 1.10)** and concomitantly forms re-aromatized lutidine-anchored pincer **12**.

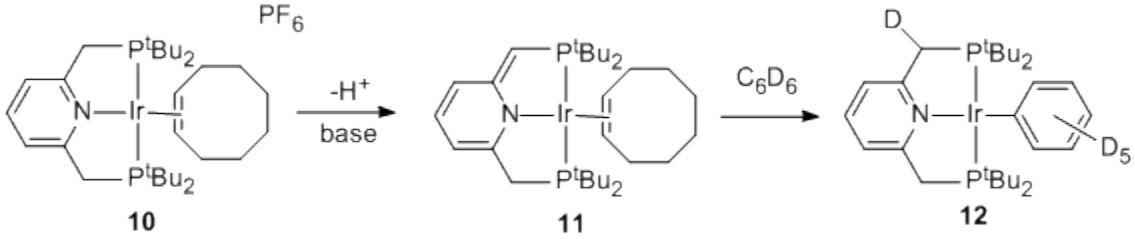

Figure 1.10. C-H activation by metal ligand cooperation

Similarly, dearomatized ruthenium complex **14** reacts with dihydrogen **(Figure 1.11)** to give *trans* dihydride complex, **15**, with a re-aromatized pyridine ligand. The stability of the complex **15** can be controlled by selective substitution of L_1 and L_2 with different

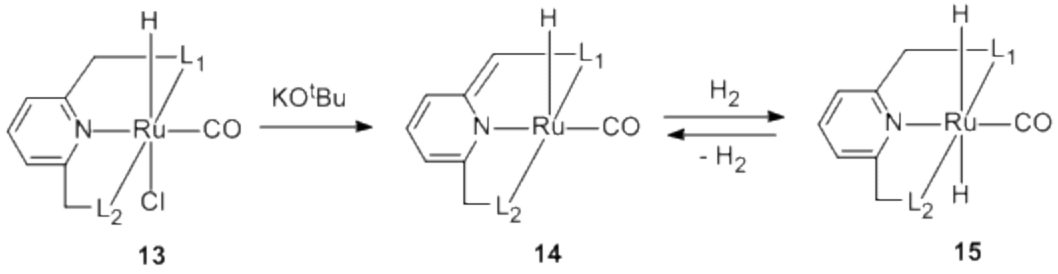

Figure 1.11. Activation of dihydrogen by dearomatized Ru intermediate

phosphines. Ir complex **16** reacts with H_2 to provide Ir(III) *trans*-dihydride complex **18** When the complex **16** reacts with D_2,formation of the D-Ir-H**(Figure 1-12)** has been

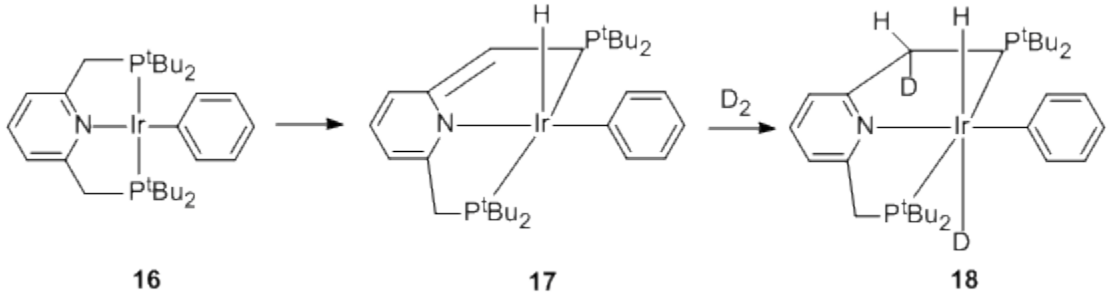

Figure 1.12. Activation of H_2 by Ir(III) intermediate.

observed, with one D atom attached to the pyridinylmethylenic carbon suggesting that dihydrogen is actually activated by dearomatizedIr(III) complex **17**.

The design of efficient catalytic system for splitting water to H_2 and O_2 is among the most desired tasks today. Well-defined metal complexes that catalyze water oxidation require a sacrificial strong oxidant. The dearomatized (PNN)Ru complex **19** reacts with water **(Figure1.13)** to form *trans*-Hydrido–hydroxo complex **20** with the aromatized pyridine ligand.[30]It has been proposed that this compound is probably formed by a mechanism involving coordination of water at the vacant coordination site *trans* to the

hydride ligand, followed by proton migration to the side arm. Heating complex **20** in water for 3 days resulted in evolution of H_2 with formation of **21.** In this process metal oxidation state is unchanged and the cooperation between the metal and the ligand fragment results the water activation. Irradiation of **21** in THF resulted O_2 evolution with concomitant formation of **20**. Photolysis of **21** may form $H_2O_2$and Ru(0) intermediate. This intermediate converts to complex **19** by proton migration from the side arm to the Ru center. It was proposed that H_2O_2 catalytically decomposed in to O_2 and H_2O possibly by complex **19.**

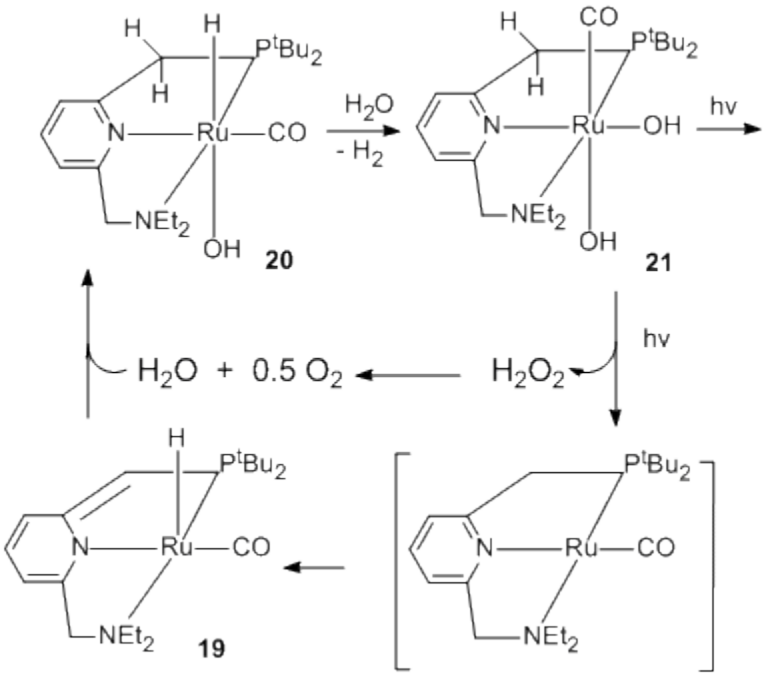

Figure 1.13. Water splitting by dearomatized Ru complex

Oxidative addition of the N-H bond in ammonia to various metal complexes is a highly desirable reaction this can be envisioned as a key step in the formation of complex

nitrogen-containing molecules from a commodity chemical. The OA reaction of ammonia with most transition metal complexes is notoriously difficult because the reaction usually generates simple Werner type Lewis acid base complexes instead of the desired hydrido-amido complex (**Scheme 1.4**). In order to accomplish OA with

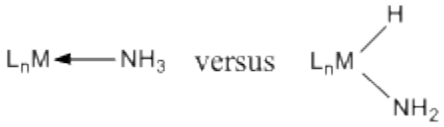

Scheme 1.4. Werner type complex vs hydrido amido complex

ammonia the classical Werner type coordination has to be altered. The imido-hydride complex formed by N-H cleavage should be favored over the traditional Werner complex. One such way to increase the preference for the imido complex is increase the electron density at the metal center. As the coordination of ammonia would transfer substantial electron density towards the already electron rich metal center, such a process is thermodynamically not favored. Hartwig and coworkers[31] developed a new Ir(I) PCP pincer complex **22** (**Figure 1.14**) that has an electron-rich methylidene anchor.

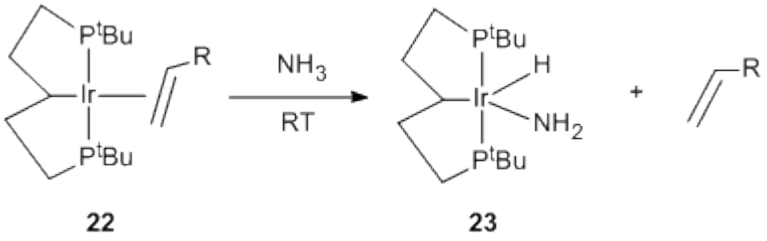

Figure 1.14. Oxidative addition of ammonia at room temperature by (PCP)Ir pincer complex with an electron donation ligand.

Complex **22** is sufficiently nucleophilic to readily react with ammonia at room temperature to form the oxidative addition product **23**.

The (PNP)Ru pincer complex **14** also initiates an N-H activation process but this reaction occurs via a dearomatized ligand intermediate. When the complex **14** ($L_1 = L_2 = P^tBu_2$) is reacted with aniline one hydrogen transfers to the pyridinylmethylenic carbon to give complex **24** and the re-aromatized pyridine ring (**Figure 1.15**).

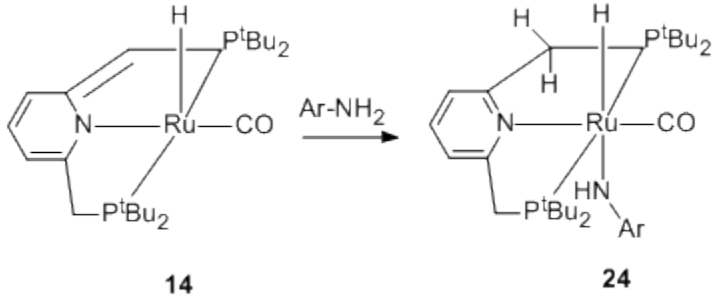

14 **24**

Figure 1.15. Oxidative addition of ammonia at room temperature by (PNP)Ru pincer complex with aniline.

While the above examples of metal – ligand cooperation are based on aromatization-dearomatization of lutidine-anchored PNN and PNP ligands pincers such strategies are also found for other aromatics (acridine)[29b]

1.3.3. Redox-active 'Non-Innocent' Pincer ligands. Recently, there has been great interest in metal complexes of redox-active ligands for fundamental academic studies and for potential use as sensors, catalysts, and other materials.[32]As Jorgensen pointed out in 1966[33] a ligand can be regarded as 'non-innocent' if it does not allow the oxidation state of a metal in a complex to be defined. Often the metal ion in the general form of $[M^{II}L^{0}]$

X_2 type complexes has been assigned an oxidation state of 2^+ assuming L is an "innocent" ligand despite the fact that it may very well have rich redox chemistry. Non – innocent behavior depends on both the ligand and metal. The ligand itself could not be considered as innocent or non-innocent. For example when the metal centered and ligand centered frontier orbitals are at very different energies such that their redox potentials are widely separated then these redox processes can be assigned as metal or ligand-centered without any ambiguity. But when the ligands are redox-active and there is strong mixing between ligand and metal frontier orbitals, assignment of oxidation states to individual metal and ligand fragment is difficult if not impossible. In some cases ligand- and metal-centered orbitals can be so close in energy (within *k*T) such that the complexes display "redox isomerism' or valence tautomerism. For example, the cobalt –dioxolene complex (**Figure 1.16,** bottom) switches between a high spin (S = 5/2) bis-semiquinonatecobalt(II) at high temperatures and a low spin catecholate/semiquinonatecobalt(III) (S = 1/2) at low temperature.[34,35]Therefore the term 'non-innocent' is more appropriately applied to combinations of metal and ligand rather than to redox active ligands alone. In many metal complexes with redox active ligands the ambiguity in assignment of oxidation states to metal and ligand and the confusion concerning the interpretation of the electronic and spectroscopic properties has lasted for many years. Redox active catecholate based complexes and their analogs are extensively studied by Pierpont[36] and Lever.[37,38]

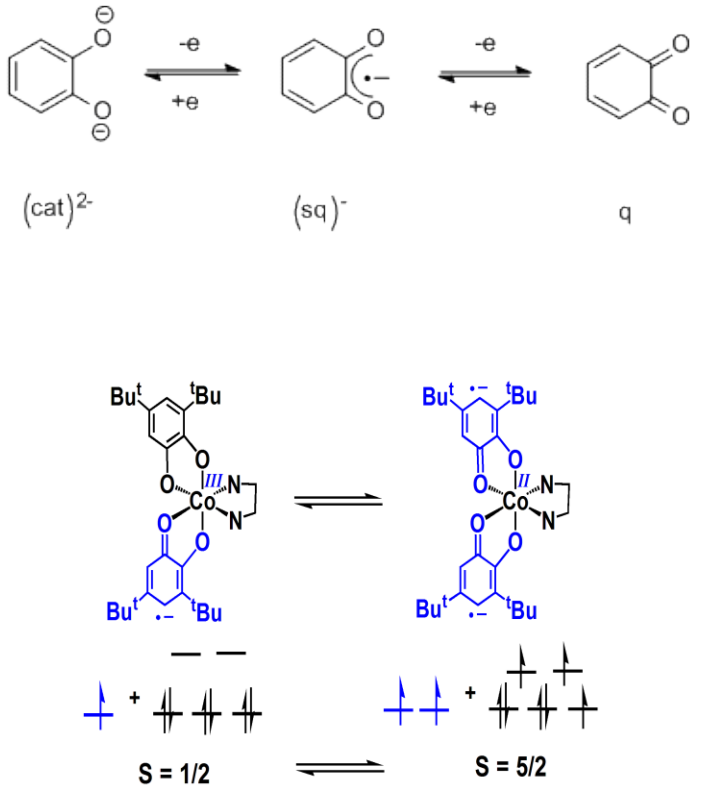

Figure 1.16. The dioxolene redox series (top) and valence tautomeric cobalt complexes (bottom).

Transition metal complexes with redox active ligands are known to exist in the active sites of metalloproteins.[39]The best understood and well known example is galactose oxidase which contains a single Cu(II) ion coordinate to modified tyrosine radical.[40] This site is thought to promote the two-electron oxidation from alcohol to aldehyde in this enzyme. The prospect of utilizing the redox-active ligands to mediate otherwise challenging multi-electron reactions has encouraged further study into the reactivity of synthetic complexes. A sampling of such chemistry is described next.

Heyduk[41]has used amidophenolate ligands to enable oxidative addition and reductive elimination reactions to d^0 zirconium(IV) and tantalum(V) metal complexes.

This ONO and NNN type redox active ligands (**Figure 1.17)** have been used to enable multielectron reactivity, nitrene group transfer at the electron poor tantalum and

Figure 1.17. Redox-active ONO and NNN pincer ligands

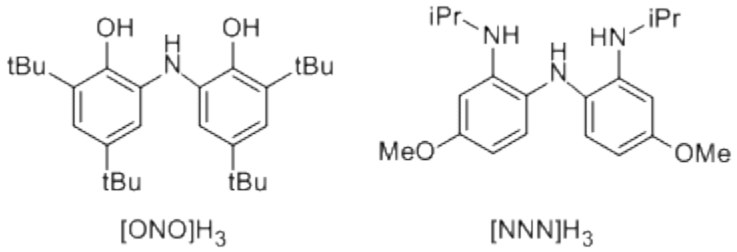

zirconium. While the both NNN and ONO ligands provide appropriate redox reservoir, these two ligands are sterically different. Ligand sterics also play an important role in controlling the coordination geometry and the reactivity at the metal center. The NNN ligand reacts with $TaCl_2Me_3$ to afford five coordinate $[NNN^{cat}]TaCl_2$ while the ONO ligand forms six coordinate $[ONO^{cat}]TaCl_2L$ with a coordinating solvent ligand L. $[ONO^{cat}]TaCl_2L$ undergoes one electron and two electron oxidation with $PhICl_2$to give $[ONO^{sq}]TaCl_3$ and $[ONO^{q}]TaCl_4$ respectively. In contrast, $[NNN^{cat}]TaCl_2$ affords the one-electron oxidized product $[NNN^{sq}]TaCl_3$exclusively.This difference in reactivity was attributed to variable steric constraints imposed by [ONO] and [NNN] ligands. The redox non-innocent nature of these metal complexes has been used to initiate nitrene group transfer reactions. $[NNN^{cat}]TaCl_2$ reacts with aryl azides to give tantalum imide complex $[NNN^{q}]TaCl_2$(=NAr) and N_2 gas, as shown in the middle of **Figure 1.18.** The Lewis-base adduct $[NNN^{cat}]TaCl_2$(py) did not react with aryl azides, due to the lack of an empty

coordination site at the tantalum center. The tantalum imide then reacts with diphenylhydrazine to give diazobenzene, and aniline to regenerate [NNN^{cat}]TaCl$_2$.

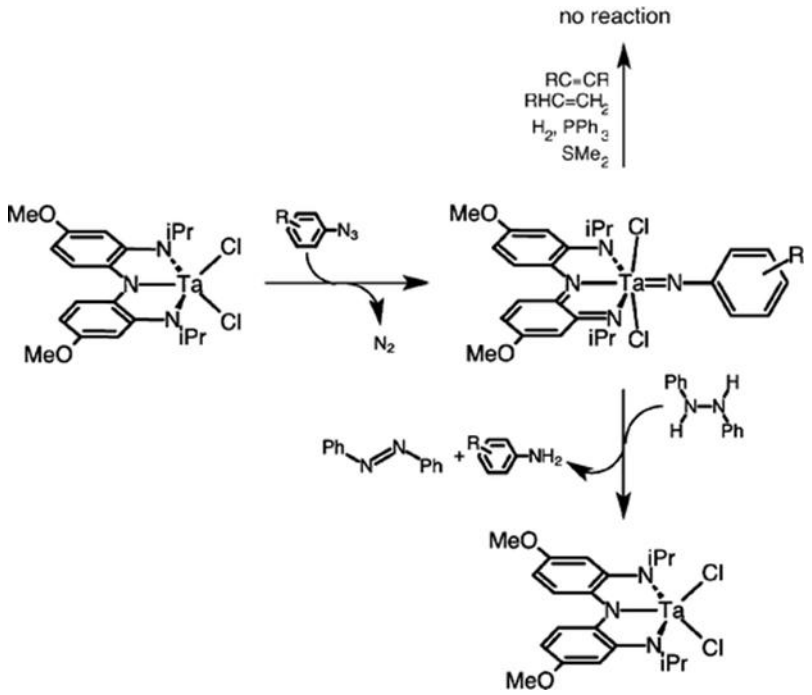

Figure 1.18. Nitrene group transfer reactions described by the Heyduk group.

Other examples of non-innocent ligands acting as electron reservoirs can be seen in electron deficient metal ions that are stabilized by introducing electron rich multidentate ligands such as bulky PNP pincer ligands, as well as electron rich metal centers that are stabilized by introducing reducible ligands such as 2,6-bis[1-(phenylimino)ethyl]pyride. If additional electrons can be temporarily stored or released by a redox active ligand then multielectron chemical transformation can be performed.[42]Iron complexes of bis(imino)pyridine ligands have been shown to be an effective catalysts for the intramolecular [2π-2π] cyclization of dienes and the redox activity of the chelate appears to play an important role in the catalytic activity. Complex

25 reacts with a diene to form the π complex **26**. Both **25** and **26** contain dianionic 2e reduced formed of the 2,6-diiminepyridine ligand. This complex **26** is in equilibrium with complex **27. (Figure 1.19)**

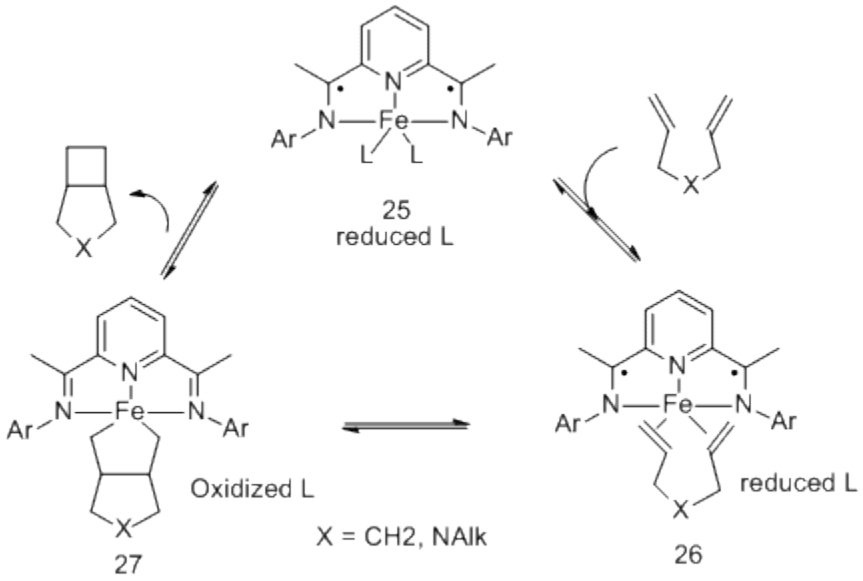

Figure 1.19. Redox non innocent 2,6- diiminepyridine ligand action as an electron reservoir.

This transformation is two electron oxidative addition process and the electrons required for reaction is supplied by the two electron reduced ligand. Throughout this transformation the electron storage capacity of the ligand allows the iron to maintain its Fe^{II} oxidation state.[43]Mindiola group recently reported square planer Ni(II) radical cation complex with PNP pincer ligand.[44] Electron hole mostly resides at the nitrogen and aryl carbon atoms in the ligand without altering Ni oxidation state. It is proposed that this kind of metal ligand cooperativity may find applications in certain type of bond activation processes.

1.4. Purpose of the Thesis research.

Clearly there is a lot of exciting chemistry that can be uncovered from investigations of metal complexes of pincer ligands. What is lacking in the literature, however, are comprehensive, systematic studies that detail the effects of variations in ligand architecture on the physical, electronic properties and on reaction chemistry of the resultant metal complexes. For this work, the generic forms of pincer ligands(and nomenclature used later on) in **Chart 1.2** are the targets of such investigations.

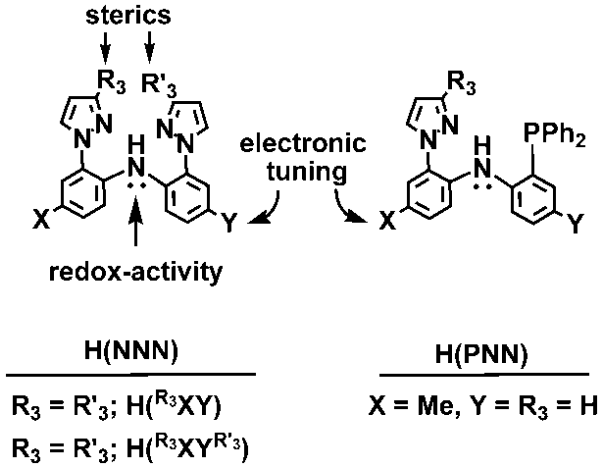

Chart 1.2. Pyrazolyl-containing NNN- and PNN- pincer ligands studied herein

The diarylamido moiety was chosen as an anchor because this species is a well-known electron donor whose redox potential can be predictably tuned by varying the *para*- aryl substituents. Such substitution will permit the evaluation of the effects of redox potential on the reactivity of metal complexes. For instance, it may be possible to address whether (and by how much) replacing hydrogen with methoxy groups will impact rates of oxidative addition or the strength of bond that can be oxidatively-added to a metal center.

Also, it may be possible to determine what substitution patterns would favor a ligand-centered electron transfer to a metal-bound substrate. The pyrazolyl flanking donor is chosen for several reasons. First, given the ubiquitous nature of scorpionate ligands,[2] synthetic methodology to an enormous number of pyrazolyl variants are well-established. The steric profiles of a given pincer ligand can be easily altered by changing the 3-pyrazolyl substituent, R_3, proximal to the metal center. Pyrazolyl-containing ligands are usually easily crystallizable as a result of the multitude of non-covalent interactions that the pyrazolyl groups can participate.[45] Thirdly, the expected six-membered chelate ring formed on metal complexation should give the possibility for structural flexibility where both *mer*- and *fac*- coordination modes should be possible. Finally, if the PNN derivative can be prepared, then the dichotomy in donor strength toward a metal may give rise to hemilabile behavior.

Thus, this thesis first describes the efforts toward preparing both symmetric and asymmetric NNN- pincer ligands and some of their late transition metal complexes. During the preparations if the pincers, it occurred to us that the synthetic intermediates to asymmetric pincers, namely, 2-pyrazolyl-*p*-X-anilines may be interesting bidentate ligands in their own regard. Thus, initial findings regarding their chemistry with group 7 tricarbonyls is described first. Next, the findings of studies examining the influence of sterics on the electronic properties and ligand-centered reactivity of tricarbonylrhenium(I) complexes are reported. In these studies, the ligand centered oxidation behavior is established and it is shown that steric interactions can couse ligand folding. The folded pincers are more reactive than non-folded pincers. In Chapter 5 an in-depth analysis of how varying non-pincer ligands can influence the electrochemical properties of various

rhodium(III) complexes is reported. Then, attention is turned to quantifying how ligand electronics impact reactivity by examining oxidative addition reactions between alkyl halides and carbonylrhodium(I) species as models. Finally attention is turned to the preparation of the PNN ligand and the associated chemistry of rhodium(I) carbonylrhodium(I) derivatives. Here, a comparison between related NNN, PNN, and known PNP complexes reveals that the main influence that flanking donors have on the rhodium chemistry is steric in nature rather than electronic. The results described in this section form the basis for further studies in the Gardinier lab that demonstrate both the structurally adaptive (preferences for *fac*- and *mer*- conformations can be induced) and the hemilabile nature of the PNN ligand in rhodium(I) chemsitry.

CHAPTER 2

TRICARBONYLRHENIUM(I) AND MANGANESE(I) COMPLEXES OF 2-(PYRAZOLYL)-4-TOLUIDINE

2.1. Introduction:

There has been continued interest in $Re^{I}(CO)_3$ chelate complexes owing to their potential biomedical applications[1] as well as to the promising photophysical behavior derived from MLCT transitions[2] that can be exploited in energy and electron transfer studies, [3] in display technology, [4] and even in solar energy conversion and photocatalysis.[5] We have been exploring the reactivity and properties of luminescent complexes of electroactive N,N-chelating ligands based on 2-(pyrazolyl)-*p*-toluidine, $H(pzAn^{Me})$, and other allied derivatives for the latter purposes.[6-8] For instance, our early studies indicated that the simple Lewis adduct of $H(pzAn^{Me})$ and BPh_3 is a thermally unstable species with distinct cyan emission that gives way to the intensely green-blue fluorescent $Ph_2B(pzAn^{Me})$ via elimination of benzene.[6] In this latter case, DFT calculations and experimental observations indicated that emission was a result of a π-π^* transition involving the chelated $(pzAn^{Me})^-$ portion of the complex. Unfortunately, this complex is readily susceptible to solvolysis by alcohols or other protic media. Changing the electronic properties of the ligands by substitution at the 2- or 4- position of the aniline moiety permits a good control over tuning the emission properties (ranging from blue to yellow-green) and can greatly improve stability of the resulting dyes toward

solvolysis. [6,7] We became interested exploring the transition metal chemistry of this ligand scaffold [8] with the hope of discovering complexes that are more robust or kinetically inert and that might possess more unusual electronic properties or even more desirable chemical reactivities than the diphenylboron derivatives. An added incentive to this area of study is that the electronic properties of the transition metal complexes might be chemically switchable by addition of Brønsted acids or bases as in Scheme 1. That is, the capacity for the metal-coordinated aniline ligand to become involved in ligand-

Scheme 2.1. Chemical switching behavior

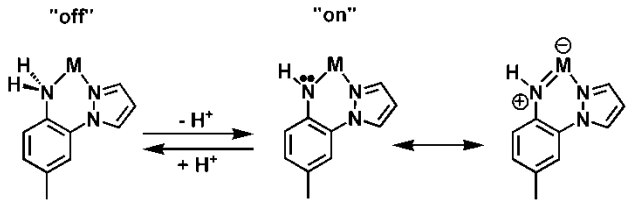

centered one-electron oxidation or possibly even metal-nitrogen multiple bonding should be greatly impaired when the aniline nitrogen is coordinatively saturated, as in the left of Scheme 1. Also, the extent to which the ligand pi-system is conjugated becomes attenuated upon quartenization of nitrogen such that significant changes in the optoelectronic properties of the resultant complexes would be anticipated. We were aware of recent sporadic reports concerning various nickel and palladium complexes of H(pz*An) (pz* = 3,5-dimethylpyrazolyl; An = aniline) and related derivatives [9,10] but surprisingly few details concerning the electronic properties of these transition metal complexes were disseminated. Given the enticing photophysical prospects of tricarbonylrhenium(I) N,N-chelates we detail our initial findings concerning the

preparation, reactivity, and electronic properties of the H($pzAn^{Me}$) complexes of this moiety. We also document our findings concerning the manganese(I) congeners with the intent of providing insight into changes in electronic properties and reactivity as a function of the periodicity of the group 7 metals.

2.2. Experimental

2.2.1. Materials: The compounds $Mn(CO)_5Br$, $TlPF_6$, NEt_4OH were purchased from commercial sources and were used without further purification while $Re(CO)_5Br$ [11] and H($pzAn^{Me}$) [6] were prepared by literature methods. The solvents used in the preparations were dried by conventional methods and distilled under nitrogen prior to use. All reactions were performed under an atmosphere of nitrogen using Schlenk techniques.

2.2.2. Physical measurements: . Midwest MicroLab, LLC, Indianapolis, Indiana 45250, performed all elemental analyses. ^{1}H, ^{13}C, ^{19}F and ^{31}P NMR spectra were recorded on a Varian 400 MHz spectrometer. Chemical shifts were referenced to solvent resonances at δ_H 7.27, δ_C 77.23 for $CDCl_3$; δ_H 5.33 for CD_2Cl_2; δ_H 1.94, δ_C 118.9 for CD_3CN and δ_H 2.05, δ_C 29.92 for acetone-d_6 while those for ^{19}F and ^{31}P NMR spectra were referenced against external standards of $CFCl_3$ (δ_F 0.00 ppm) and 85% $H_3PO_{4(aq)}$ (δ_P 0.00 ppm), respectively. Melting point determinations were made on samples contained in glass capillaries using an Electrothermal 9100 apparatus and are uncorrected. Absorption measurements were recorded on an Agilent 8453 spectrometer. Electrochemical measurements were collected under nitrogen atmosphere at a scan rate of 50 mV/s for samples as 0.1 mM CH_3CN solutions with 0.1 M NBu_4PF_6 as the

supporting electrolyte. A three-electrode cell comprised of an Ag/AgCl electrode (separated from the reaction medium with a semipermeable polymer membrane filter), a platinum working electrode, and a glassy carbon counter electrode was used for the voltammetric measurements. With this set up, the ferrocene/ferrocenium couple had an $E_{1/2}$ value of +0.53 V consistent with the literature value in this solvent.[12]

2.2.3. Synthesis of complexes.

2.2.3.1. *fac*-$MnBr(CO)_3[H(pzAn^{Me})]$, **1a**.

A mixture of 0.495 g (1.80 mmol) $Mn(CO)_5Br$ and 0.312 g (1.80 mmol) $H(pzAn^{Me})$ in 25 ml of toluene was heated at reflux 4 h initially giving an orange solution, then a yellow precipitate. After cooling, the yellow precipitate was isolated by filtration, washed with three 10 ml portions Et_2O, and then dried under vacuum to give 0.579 g (82%) of pure **1a** as a yellow powder. M.p.: 215-223° C, dec. Anal. Calc. for $C_{13}H_{11}BrMnN_3O_3$: C, 39.82; H, 2.83; N, 10.72. Found: C, 39.56; H, 3.07; N, 10.44%. IR (KBr, cm^{-1}) υ_{co} 2029, 1923, 1902; (CH_2Cl_2, cm^{-1}) υ_{co} 2033, 1940, 1919; (CH_3CN, cm^{-1}) υ_{co} major: 2029, 1936, 1913; minor: 2050, 1954. ^1H NMR (CD_2Cl_2): δ_H 8.31 (s, 1H, H_3-pz), 8.12 (s, 1H, H_5-pz), 7.29 (s, 1H, H_3-An), 7.22 (br s, 2H, $H_{5/6}$-An), 6.72 (s, 1 H, H_4-pz), 4.98 (br s, 1H, NH_a), 4.10 (br s, 1H, NH_b), 2.43 (s, 3H, CH_3). ^1H NMR (CD_3CN): (major resonances only, see Supporting Information) δ 8.23 (br s, 2H, $H_{3\&5}$-pz), 7.40 - 7.20 (br m, 3H, H_3,H_5,H_6-An), 6.71 (s, 1H, H_4-pz), 5.85 (br s., 1H, NH), 4.09 (br s, 1H, NH), 2.38 (s, 3H, CH_3). ^{13}C NMR (CD_3CN): δ_C 140.9, 136.9, 135.2, 133.3, 132.0, 129.6, 123.6, 121.4, 109.8, 20.6. UV-Vis (CH_3CN) λ_{max}, nm (ε, $M^{-1}cm^{-1}$): 213 (43,200), 256 (16,900), 284 (10,100), 371 (1,600). $E^{ox}_{1/2}$ (V versus Ag/AgCl:ΔE (E_a-E_c,

mV): i_c/i_a): 0.98 V: 120 mV: 0.44. Single crystals of **1a** suitable for x-ray diffraction studies were grown by layering a dichloromethane solution with hexanes and allowing solvents to diffuse.

2.2.3.2. *fac*-$ReBr(CO)_3[H(pzAn^{Me})]$, **1b**.

A mixture of 0.526 g (1.30 mmol) $Re(CO)_5Br$ and 0.225 g (1.30 mmol) $H(pzAn^{Me})$ in 20 ml of toluene was heated at reflux 4 h giving a colorless precipitate. After cooling to room temperature, the precipitate was isolated by filtration, washed with two 5 mL portions Et_2O, and then dried under vacuum 12 h to give 0.582 g (86%) of **1b** as a colorless powder. M.p.: 294-306°C, dec. to black solid. Anal. Calc. for $C_{13}H_{11}BrN_3O_3Re$: C, 29.83; H, 2.12; N, 8.03. Found: C, 29.65; H, 2.24; N, 8.37%. IR (KBr, cm^{-1}) υ_{co} 2019, 1903, 1884; (CH_2Cl_2, cm^{-1}) υ_{co} 2029, 1921, 1900; (CH_3CN, cm^{-1}) υ_{co} major: 2025, 1917, 1894; minor: 2040, 1935. ^1H NMR (CD_2Cl_2): δ_H 8.16 (dd, *J* = 2, 1 Hz, 1H, H_3-pz), 8.09 (dd, *J* = 3, 1 Hz, 1H, H_5-pz), 7.31 (s, 1H, H_3-An), 7.28 (part of AB m, 1H, $H_5/_6$-An), 7.19 (part of AB m, 1H, $H_{5/6}$-An), 6.73 (dd, *J* = 3, 2 Hz, 1 H, H_4-pz), 5.29 (br d, *J* = 11 Hz, 1H, NH_a), 4.60 (br d, *J* = 11 Hz, 1H, NH_b), 2.46 (s, 3H, CH_3). ^1H NMR (CD_3CN): δ_H 8.27 (dd, *J* = 3, 1 Hz, 1H, H_5-pz), 8.10 (dd, *J* = 2, 1 Hz, 1H, H_3-pz), 7.42 (s, 1H, H_3-An), 7.25 (AB m, 2H, H_5- and H_6-An), 6.72 (dd, *J* = 3, 2 Hz, 1 H, H_4-pz), 6.29 (br d, *J* = 12 Hz, 1H, NH_a), 4.73 (br d, *J* = 12 Hz, 1H, NH_b), 2.40 (s, 3H, CH_3). ^{13}C NMR (CD_3CN): δ_C 210, 207, 149, 138, 135, 133, 132, 130, 125, 122, 110, 21. UV-Vis (CH_3CN) λ_{max}, nm (ε, $M^{-1}cm^{-1}$): 219 (16,600), 249 (8,100), 286 (2,800), 303 (1,200). $E^{ox}_{1/2}$ ($(E_a+E_c)/2$ V, ΔE (E_a-E_c) mV, i_c/i_a): 1.32 V, 120 mV, 0.55. Single crystals of **1b**

suitable for X-ray diffraction studies were grown by layering a dichloromethane solution with hexanes and allowing solvents to diffuse.

2.2.3.3. {*fac*-Mn(CH_3CN)$(CO)_3$[H($pzAn^{Me}$)]}(PF_6), **2a**.

A mixture of 0.393 g (1.00 mmol) **1a** and 0.350 g (1.00 mmol) $TlPF_6$ in 20 mL dry acetonitrile was heated at reflux for 20 h under nitrogen. After cooling to room temperature, the yellow solution of **2a** and colorless precipitate (TlBr) were separated by cannula filtration. Solvent was removed under vacuum to leave 0.442 g (89%) of **2a** as a yellow powder. M.p.: 192-196°C dec. Anal. Calc. for $C_{15}H_{14}F_6MnN_4O_3P$: C, 36.16 ; H, 2.83; N, 11.25. Found: C, 36.12; H, 2.97; N, 11.43%. IR (KBr, cm^{-1}) υ_{co} 2052, 1956, 1919; (CH_2Cl_2, cm^{-1}) υ_{co} 2052, 1954; (CH_3CN, cm^{-1}) υ_{co} 2050, 1954. ^{1}H NMR (CD_2Cl_2): δ_H 8.20 (s, 1H, H_5-pz), 8.05 (s, 1H, H_3-pz), 7.30 (br part of AB, 1H, Ar), 7.29 (s, 1H, Ar), 7.25 (br part of AB, 1H, Ar), 6.79 (br s, 1H, H_4-pz), 5.01 (br d, J = 11.6 Hz, 1H, NH), 4.17 (br d, J = 11.6 Hz, 1H, NH), 2.44 (s, 3H, $ArCH_3$), 2.32 (s, 3H, CH_3CN). ^{1}H NMR (CD_3CN): δ_H 8.31 (s, 1H, H_5-pz), 8.14 (s, 1H, H_3-pz), 7.39 (s, 1H, Ar), 7.31 (br part of AB, 1H, Ar), 7.21 (br part of AB, 1H, Ar), 6.76 (br s, 1H, H_4-pz), 5.57 (br s, 1H, NH), 4.60 (br s, 1H, NH), 2.35 (br s, 3H, $ArCH_3$), 1.96 (br s, 8H, CH_3CN and residual solvent of CD_3CN). ^{13}C NMR (CD_3CN): resonances not resolved. ^{19}F NMR (CD_3CN): δ_F -72.7 (J_{FP} = 707 Hz). ^{31}P NMR (CD_3CN): δ_P -144.6 (J_{PF} = 707 Hz). UV-Vis (CH_3CN) λ_{max}, nm (ε, $M^{-1}cm^{-1}$): 213 (37,100), 255 (14,800), 281 (9,200), 371 (1,600). $E^{ox}_{1/2}$ ((E_a+E_c)/2 V, ΔE (E_a-E_c) mV, i_c/i_a): 1.42 V, 150 mV, 0.33. Single crystals of **2a** suitable for X-ray diffraction studies were grown by layering a dichloromethane solution with Et_2O and allowing the solvents to slowly diffuse.

2.2.3.4. {*fac*-Re(CH_3CN)$(CO)_3$[H($pzAn^{Me}$)]}(PF_6), **2b**.

A mixture of 0.136 g (0.259 mmol) **1b** and 0.090 g (0.26 mmol) $TlPF_6$ in 20 mL dry acetonitrile was heated at reflux for 20 h under nitrogen. After cooling to room temperature, the colorless solution of **2b** and precipitate (TlBr) were separated by cannula filtration. Solvent was removed under vacuum to leave 0.163 g (78%) of **2b** as a colorless powder. M.p.: 165-186 °C dec. to black solid. Anal. Calc. for $C_{15}H_{14}F_6N_4O_3PRe$: C, 28.62; H, 2.24; N, 8.90. Found: C, 28.55; H, 2.02; N, 8.99%. IR: (KBr, cm^{-1}) υ_{co} 2035, 1925, 1905; (CH_2Cl_2, cm^{-1}) υ_{co} 2044, 1936; (CH_3CN, cm^{-1}) υ_{co} 2040, 1935. ^{1}H NMR (CD_2Cl_2): δ_H 8.19 (dd, J = 2, 1 Hz, 1H, H_5-pz), 8.05 (dd, J = 3, 1 Hz, 1H, H_3-pz), 7.31 (br part of AB, 1H, Ar), 7.30 (s, 1H, Ar), 7.26 (br part of AB, 1H, Ar), 6.80 (dd, J = 3, 2 Hz, 1H, H_4-pz), 5.32 (br d, J = 12 Hz, 1H, NH), 5.14 (br d, J = 12 Hz, 1H, NH), 2.46 (s, 3H, $ArCH_3$), 2.41 (s, 3H, CH_3CN). ^{1}H NMR (CD_3CN): δ_H 8.34 (d, J = 3 Hz, 1H, H_5-pz), 8.14 (d, J = 2 Hz, 1H, H_3-pz), 7.45 (s, 1H, H_3-An), 7.32 (AB m, 2H, H_5- and H_6-An), 6.79 (dd, J = 3, 2 Hz, 1 H, H_4-pz), 6.36 (br d, J = 12 Hz, 1H, NH_a), 5.83 (br d, J = 12 Hz, 1H, NH_b), 2.41 (s, 3H, CH_3-An), 2.22 (s, 3H, CH_3CN-Re). ^{13}C NMR (CD_3CN): δ_C 193.4, 192.2, 148.7, 138.8, 133.9, 132.3, 130.8, 125.4, 123.7, 122.9, 118.5, 110.9, 20.7, 3.99. UV-Vis (CH_3CN) λ_{max}, nm (ε, $M^{-1}cm^{-1}$): 216 (18,000), 251 (7,600), 285 (3,800), 307 (1,200). ^{19}F NMR (CD_3CN): δ_F -72.9 (J_{FP} = 707 Hz). ^{31}P NMR (CD_3CN): δ_P -144.6 (J_{PF} = 707 Hz). $E^{ox}_{1/2}$ ((E_a+E_c)/2 V, ΔE (E_a-E_c) mV, i_c/i_a): 1.76 V, 110 mV, 0.34. Single crystals of **2b** suitable for X-ray diffraction studies were grown by vapor diffusion of Et_2O into a CH_2Cl_2 solution of the complex.

2.2.3.5. [*fac*-Mn$(CO)_3$(μ-$pzAn^{Me}$)]$_2$, **3a**.

A 2.6 mL aliquot of a 0.10 M solution (0.26 mmol) of $(NEt_4)(OH)$ in MeOH was added to a solution of 0.100 g (0.255 mmol) **1a** in 4 mL MeCN which immediately gave a yellow-brown solution. After leaving the solution undisturbed and protected from light for 5 d, the very dark solution was decanted from the yellow crystals and a thin layer of manganese metal (on the walls of the reaction vessel). The crystals were mechanically separated, washed with Et_2O, and dried under vacuum to give 0.016 g (20%) of **3a**. M.p.: 265-282°C. Anal. Calcd for $C_{26}H_{20}Mn_2N_6O_6$: C, 50.18; H, 3.24; N, 13.50. Found: C, 50.12: H, 2.97; N, 13.13%. IR (KBr, cm^{-1}) υ_{co} 2002, 1905, 1884; (CH_3CN, cm^{-1}) υ_{co} 2004, 1906. ^1H NMR (CD_3CN): δ_H 8.62 (d, J = 2 Hz, 1H, H_5-pz), 8.50 (d, J = 1 Hz, 1H, H_3-pz), 7.45 (s, 1H), 7.09 (part of AB, 1H), 7.01 (dd, J = 2,1 Hz, 1H, H_4-pz), 6.97 (part of AB, 1H), 2.35 (s, 3H); NH not observed. ^{13}C NMR (CD_3CN): not sufficiently soluble for reasonable acquisition times. UV-Vis (CH_3CN) λ_{max}, nm (absorbance of Satd. Soln.): 235 (2.101), 286 (0.630), 326 (0.322), 368 (0.174). X-ray quality crystals removed directly from the mother liquor (without washing and drying) were found to contain two acetonitrile molecules of solvation per formula unit, **$3a \cdot 2CH_3CN$.**

2.2.3.6. [*fac*-$Re(CO)_3(\mu\text{-}pzAn^{Me})]_2$, **3b**.

Method A (from **1b**). A 2.3 mL portion of 0.10 M (0.23 mmol) solution of $(NEt_4)(OH)$ in MeOH was added to a solution of 0.120 g (0.229 mmol) **1b** in 20 mL CH_3CN, which immediately gave a yellow solution. The yellow color dissipated within minutes and over several hours colorless blocks began to form. After two days left undisturbed, the crystals were isolated by filtration and drying under vacuum to give 0.052 g (51%) of **3b**. M.p.: 278-290°C dec. to black solid. Anal. Calc. for

$C_{26}H_{20}N_6O_6Re_2$: C, 35.29; H, 2.28; N, 9.50. Found: C, 35.65; H, 2.00; N, 9.17%. IR: (KBr, cm^{-1}) υ_{co} 2006, 1886, 1873; (CH_3CN, cm^{-1}) υ_{co} 2007, 1893. ^1H NMR (CD_3CN): δ_H 8.60 (d, *J* = 2 Hz, 2H, H_5-pz), 8.37 (d, *J* = 1 Hz, 1H, H_3-pz), 7.45 (s, 1H, Ar), 7.06 (part of AB, 1H), 6.97 (dd, J = 2,1 Hz, 1H, H_4-pz), 6.96 (part of AB, 1H), 3.48 (br s, 1H, NH), 2.39 (s, 3H, CH_3). δ_H (acetone-d_6): 8.85 (d, *J* = 2 Hz, 1H, H_5-pz), 8.61 (d, *J* = 1 Hz, 1H, H_3-pz), 7.57 (s, 1H, Ar), 7.15 (part of AB, 1H), 7.06 (dd, J = 2,1 Hz, 1H, H_4-pz), 7.03 (part of AB, 1H), 3.57 (br s, 1H, NH), 2.36 (s, 3H, CH_3). ^{13}C NMR (CD_3CN): not sufficiently soluble to obtain spectra in reasonable acquisition times. UV-Vis (CH_3CN) λ_{max}, nm (absorbance, Satd. Soln.): 232 (0.737), 262 (0.393), 306 (0.119), 334 (0.042). X-ray quality crystals removed directly from the mother liquor (without drying) were found to contain two acetonitrile molecules of solvation per formula unit, **3b·2CH$_3$CN.**

Method B (from **2b**). A 1.62 mL portion of a 0.142 M (0.230 mmol) solution of (NEt_4)(OH) in MeOH was added to a solution of 0.145 g (0.230 mmol) **2b** in 20 mL CH_3CN, which immediately gave a yellow solution. The yellow color dissipated within minutes and over several hours colorless blocks began to form. After two days left undisturbed, the crystals were isolated by filtration and drying under vacuum to give 0.048 g (47% yield) of **3b** whose spectroscopic characterization data were identical to above.

2.3. Single crystal X-ray crystallography

X-ray intensity data from a yellow plate of $MnBr(CO)_3[H(pzAn^{Me})]$ (**1a**), a colorless block of $ReBr(CO)_3[H(pzAn^{Me})]$ (**1b**), a yellow block of $\{Mn(CH_3CN)(CO)_3[H(pzAn^{Me})]\}(PF_6)$ (**2a**), a colorless block of

{Re(CH_3CN)$(CO)_3$[H($pzAn^{Me}$)]}(PF_6) (**2b**), a yellow prism of [$Mn(CO)_3$(μ-$pzAn^{Me}$)]$_2$·2CH_3CN (**3a**·2CH_3CN), and a colorless prism of [$Re(CO)_3$(μ-$pzAn^{Me}$)]$_2$·**2**CH_3CN (**3b**·2CH_3CN) were measured at 100(2) K (except **2b** which was collected at 130(2) K) with a Bruker AXS 3-circle diffractometer equipped with a SMART2 [13] CCD detector using either Cu(Kα) or Mo(Kα) radiation as indicated in Tables 1 and 2. Raw data frame integration and Lp corrections were performed with SAINT+.[14] Final unit cell parameters were determined by least-squares refinement of 5995 reflections from the data set of **1a**, 5750 reflections from the data set of **1b**, of 5222 reflections from that of **2a**, 6385 reflections from that of **2b**, 7062 reflections of **3a**·2CH_3CN, 5148 reflections from that of **3b**·2CH_3CN, 7188 reflections from that of **3**·2CH_3CN, with $I > 2\sigma(I)$ for each. Analysis of the data showed negligible crystal decay during collection in each case. Direct methods structure solutions, difference Fourier calculations and full-matrix least-squares refinements against F^2 were performed with SHELXTL. [15] Numerical absorption corrections based on the real shapes of the crystals were applied to the data of each **1a**, **2a**, and **3b**·2CH_3CN while semi-empirical absorption corrections based on the multiple measurement of equivalent reflections was applied to the data of each **1b**, **2b**, and **3a**·2CH_3CN with SADABS. [14] All non-hydrogen atoms were refined with anisotropic displacement parameters. Hydrogen atoms were placed in geometrically idealized positions and included as riding atoms. The X-ray crystallographic parameters and further details of data collection and structure refinements are presented in Tables 1 and 2.

Table 2.1. Crystallographic Data Collection and Structure Refinement for $MnBr(CO)_3[H(pzAn^{Me})]$ (**1a**), $\{Mn(CH_3CN)(CO)_3[H(pzAn^{Me})]\}(PF_6)$ (**2a**), and $[Mn(CO)_3(\mu\text{-}pzAn^{Me})]_2 \cdot 2CH_3CN$ (**3a**$\cdot 2CH_3CN$).

Compound	**1a**	**2a**	**3a**$\cdot 2CH_3CN$
Formula	$C_{13}H_{11}BrMnN_3O_3$	$C_{15}H_{14}F_6MnN_4O_3P$	$C_{30}H_{26}Mn_2N_8O_6$
Formula weight	392.10	498.21	704.47
Crystal system	Monoclinic	Triclinic	Triclinic
Space Group	$P2_1/n$	P- $\bar{1}$	P- $\bar{1}$
a, Å	10.9987(2)	12.5631(3)	7.8903(9)
b, Å	11.5636(2)	10.9887(2)	8.6499(10)
c, Å	11.5075(2)	21.2710(3)	11.7547(14)
α, deg	90	104.2360(10)	90.476(2)
β, deg	101.4420(10)	95.4760(10)	90.678(2)
γ, deg	90	101.0720(10)	102.619(2)
V, $Å^3$	1434.49(4)	979.65(4)	782.78(16)
Z	4	2	1
T, K	100(2)	100(2)	100(2)
ρ calcd, Mg m^{-3}	1.816	1.689	1.494
λ, Å	1.54178	1.54178	0.71073
μ, mm^{-1}	10.877[a]	7.029[a]	0.863[b]
F(000)	776	500	360
θ Range (^{o})	5.08 to 67.02	3.79 to 61.12	1.73 to 31.89
Reflections Collected	11721	7913	12823
Indep. Reflns [R_{int}]	2478 [0.0238]	2831 [0.0223]	4977 [0.0191]
Data/Restraints/Parameters	2478/0/234	2831/0/328	4977/0/260
Goodness of fit on F^2	1.004	0.989	0.973
R[I>2σ(I)][c](all data)	0.0232 (0.0254)	0.0330 (0.0383)	0.0291 (0.0331)
*w*R[d] (all data)	0.0550 (0.0559)	0.0864 (0.0873)	0.0761 (0.0785)
ρ_{fin} (max/min) ($eÅ^{-3}$)	0.441/-0.261	0.440/-0.336	0.435/-0.196

[a](Cu Kα). [b](Mo Kα). [c]$R = \Sigma||F_o|-||F_c||/\Sigma|F_o|$. [d]$wR = [\Sigma w(|F_o^2|-|F_c^2|)^2/\Sigma w|F_o^2|^2]^{1/2}$

Table 2.2. Crystallographic Data Collection and Structure Refinement for $ReBr(CO)_3[H(pzAn^{Me})]$ (**1b**), $\{Re(CH_3CN)(CO)_3[H(pzAn^{Me})]\}(PF_6)$ (**2b**), and $[Re(CO)_3(\mu\text{-}pzAn^{Me})]_2 \cdot 2CH_3CN$ (**3b**$\cdot 2CH_3CN$).

Compound	**1b**	**2b**	**3b**$\cdot 2CH_3CN$
Formula	$C_{13}H_{11}BrReN_3O_3$	$C_{15}H_{14}F_6ReN_4O_3P$	$C_{30}H_{26}Re_2N_8O_6$
Formula weight	523.36	629.47	966.98
Crystal system	Monoclinic	Orthorhombic	Triclinic
Space Group	$P2_1/n$	Fdd2	P- $\bar{1}$
a, Å	11.0882(10)	17.3199(4)	7.8901(11)
b, Å	11.6050(10)	24.0151(5)	8.7501(12)
c, Å	11.5784(10)	19.0110(4)	11.8549(16)
α, deg	90	90	89.955(2)
β, deg	100.1730(10)	90	89.194(2)
γ, deg	90	90	77.629(2)
V, $Å^3$	1466.5(2)	7907.4(3)	799.37(19)
Z	4	16	1
T, K	100(2)	130(2)	100(2)
ρ calcd, Mg m^{-3}	2.370	2.115	2.009
λ, Å	0.71073	1.54178	0.71073
μ, mm^{-1}	11.023[b]	13.563[a]	7.620[b]
F(000)	976	4800	460
θ Range (°)	2.34 to 31.82	5.94 to 61.41	2.38 to 31.88
Reflections Collected	23627	16358	12928
Indep. Reflns [R_{int}]	4737 [0.0462]	2973 [0.0209]	5068 [0.0242]
Data/Restraints/Parameters	4737/0/234	2973/1/281	5068/0/261
Goodness of fit on F^2	1.010	1.092	1.012
R[$I>2\sigma(I)$][c](all data)	0.0245 (0.0283)	0.0167 (0.0171)	0.0150 (0.0161)
*w*R[d] (all data)	0.0601 (0.0617)	0.0414 (0.0416)	0.0353 (0.0356)
ρ_{fin} (max/min) ($eÅ^{-3}$)	1.802/-1.831	0.418/-0.493	1.053/-1.002

[a](Cu Kα). [b](Mo Kα). [c]$R = \Sigma||F_o|-||F_c||/\Sigma|F_o|$. [d]$wR = [\Sigma w(|F_o^2|-|F_c^2|)^2/\Sigma w|F_o^2|^2]^{1/2}$

2.4. Results and discussion

2.4.1. Syntheses

The ligand H(pzAn^{Me}) was prepared by exploiting modifications of Taillefer's [16] and Buchwald's [17] copper-catalyzed amination reaction between pyrazole and 2-bromo-4-toluidine which gives very good yield of desired product even on a 20 g scale, as described previously by our group.[6] The complexes MBr(CO)$_3$[H(pzAn^{Me})] (M = Mn (**1a**) or Re (**1b**)) were prepared in high yield by straightforward substitution reactions between M(CO)$_5$Br and H(pzAn^{Me}) in toluene (top of Scheme 2). The ionic species

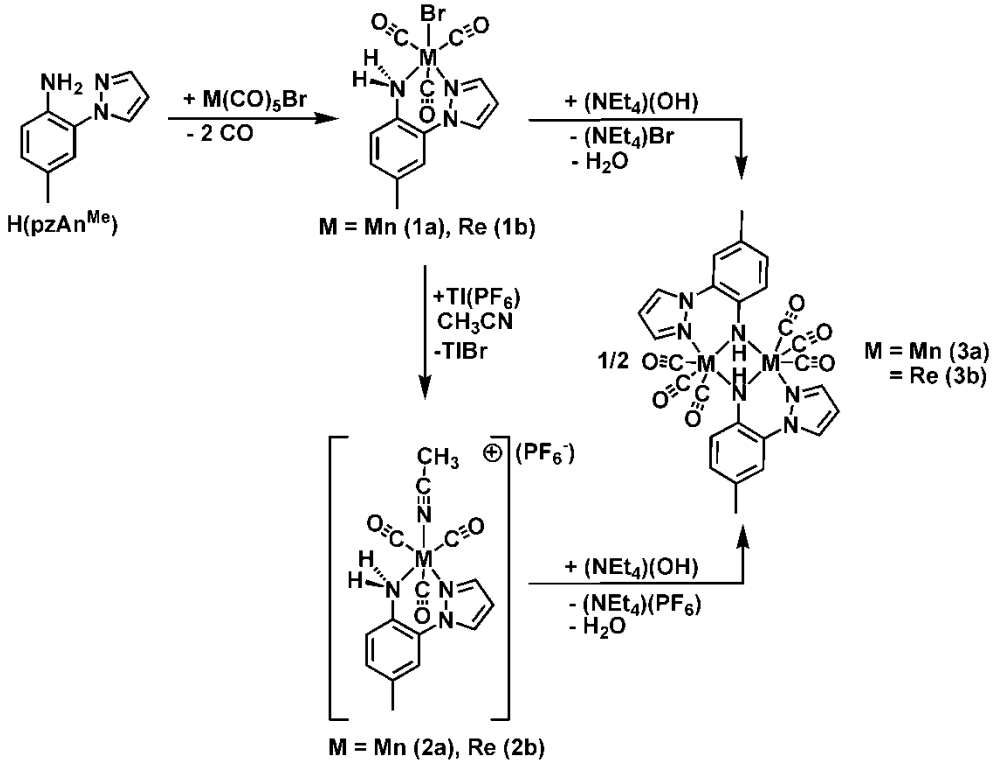

Scheme 2.2. Synthesis of group 7 tricarbonyl complexes of H(pzAn^{Me}). {M(CH$_3$CN)(CO)$_3$[H(pzAn^{Me})]}(PF$_6$) (M = Mn (**2a**) or Re (**2b**)), potentially useful starting materials for further reaction chemistry, are best prepared by metathesis of **1a** or

1b with $TlPF_6$ in acetonitrile (middle of Scheme 2) to give the desired products in good yield.[18] The reactions between either **1a/b** or **2a/b** and one equivalent of $(NEt_4)(OH)$ in CH_3CN (right of Scheme 2) afforded $[M(CO)_3(\mu\text{-}pzAn^{Me})]_2$ (M = Mn (**3a**) or Re (**3b**)), in modest yields (ca. 30% for **3a** versus about 50% for the rhenium derivative **3b**) as poorly soluble crystalline solids after three days at room temperature. Analysis of the mother liquors of the product mixtures by ^1H NMR spectroscopy reveal the presence of free ligand $H(pzAn^{Me})$ and other unidentified products implicating hydrolysis and decomposition of resulting metal complexes as being responsible for the relatively low yields obtained from these reactions. Numerous synthetic routes and conditions (different bases, solvents, reaction temperatures) were explored to **3a/b** but the above preparative routes have most consistently afforded the highest yields of these complexes. The complexes **1a/b** and **2a/b** are slightly soluble in chlorinated solvents or THF, soluble in acetone, soluble with reaction (vide infra) in CH_3CN and more strongly donating solvents (DMF, DMSO, etc.) but are insoluble in hydrocarbons and Et_2O. Complexes **3a** and **3b** exhibit only very slightly solubility in acetone or CH_3CN but are insoluble in most other organic solvents

2.4.2. Description of crystal structures

The solid state structures of all six new compounds **1a**, **1b**, **2a**, **2b**, **3a·2CH$_3$CN**, and **3b·2CH$_3$CN** were obtained from single-crystal X-ray diffraction experiments. The manganese and rhenium compounds are isostructural and the structures of the rhenium derivatives **1b**, **2b**, and **3b·2CH$_3$CN** are given in Fig.2.1 while those of the manganese derivatives **1a**, **2a**, **3a·2CH$_3$CN** can be found in referance 32. Selected bond distances

and angles for all new compounds along are provided in Table 2.3. In all cases, the tricarbonylmetal(I) fragments are arranged in a *facial* manner as found for most other such complexes of N,N-chelating ligands. The compounds **1a/b** and **2a/b** are monomeric while **3a/b** are dimeric as a result of the amido group of the deprotonated aniline moiety bridging metal centers. For the dimeric species **3a** and **3b**, the molecules reside on inversion centers rendering each half of the dimer equivalent by symmetry. As anticipated from the relative sizes of the group 7 metals, the bond distances about the rhenium centers are typically 0.1 Å longer than those for the manganese complexes. The metal-nitrogen bonds involving the pyrazolyl portion of the ligand are detectably shorter than those involving the toluidinyl NH group (Table 2.3) and, for the manganese series (where all structural data were acquired at the same temperature, 100 K), the former bonds are longest for the starting bromide **1a** (Mn-N12 = 2.054(2) Å), followed by the dimeric **3a** (Mn-N12 = 2.048(1) Å), and are shortest for the cation in **2a** (Mn-N12 = 2.045(2) Å). These bond distances are comparable to those observed in related $M(CO)_3$ complexes of pyrazolyl-containing ligands such as $\{Mn(OH_2)(CO)_3[HN{=}C(CH_3)pz^*]\}(BF_4)$ (2.048(4) Å) [19] or $Re(Br)(CO)_3(CH_2pz_2)$ (avg. 2.172(3) Å) [20]. Interestingly, the metal nitrogen bonds of the aniline NH_2 group are longer in the cations of **2a/b** (Mn-N1 = 2.105(2) Å, Re-N1 = 2.226(5) Å) compared to those in the charge neutral compounds **1a/b** (Mn-N1 = 2.091(2) Å, Re-N1 = 2.219(3) Å) but are comparable to other tricarbonyl group 7 metal-aniline complexes such as those distances in $[Mn(CO)_3(\mu\text{-}o\text{-}SC_6H_4NH_2)]_2$ (Mn-NH_2 avg. 2.094(5) Å) [21] and $[Re(CO)_3(H_2N\text{-}p\text{-}tolyl)(bipy)](OSO_2CF_3)$ (Re-NH_2 2.250(3) Å) [22]. In both **3a** and **3b**, the central planar M_2N_2 metallacycle exhibits disparate M-N

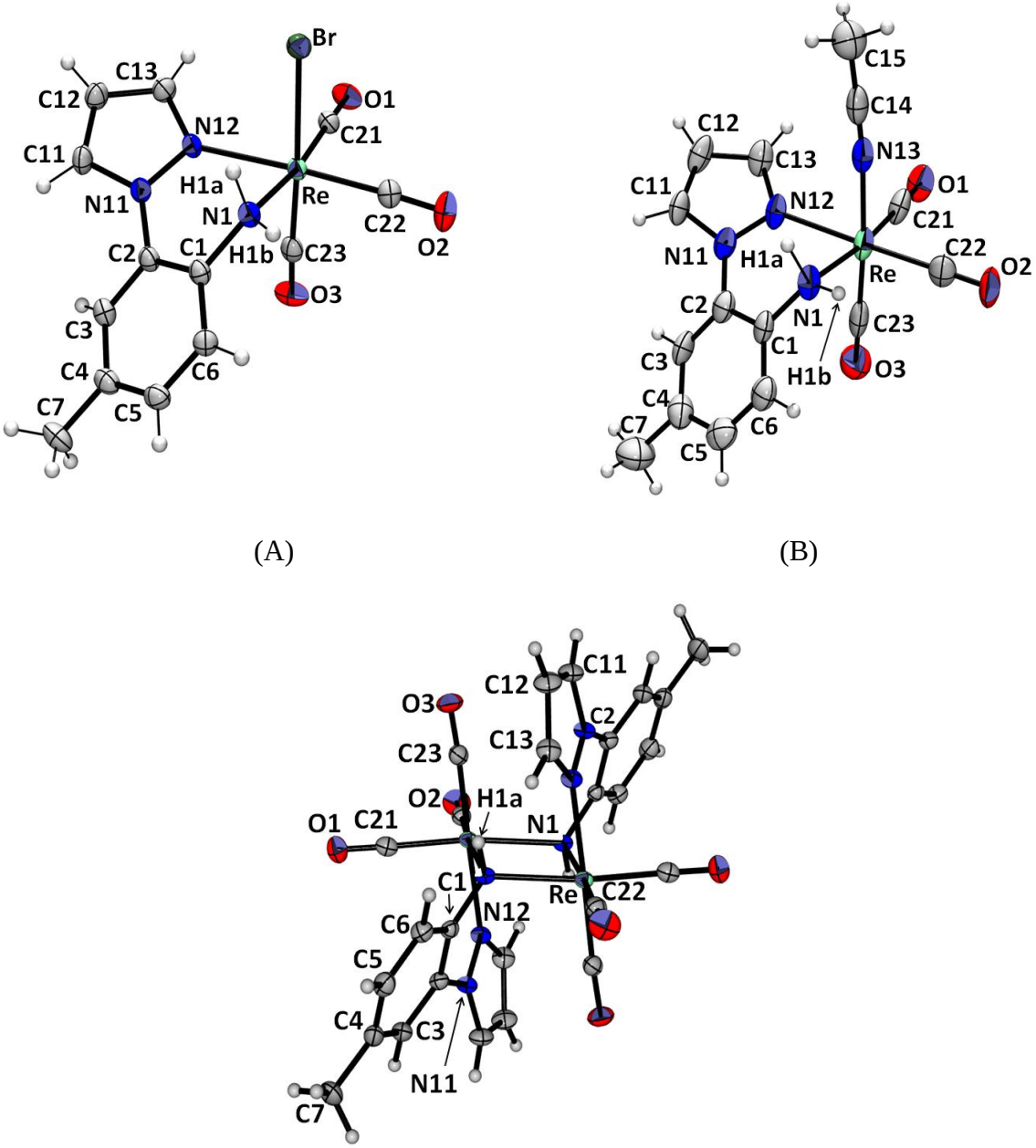

Figure. 2.1. ORTEP drawings (thermal ellipsoids drawn at 50% probability level) with atom labeling of structures of (A) $ReBr(CO)_3[H(pzAn^{Me})]$ (**1b**), (B) $\{Re(CH_3CN)(CO)_3[H(pzAn^{Me})]\}(PF_6)$ (**2b**) and (C) $[Re(CO)_3(\mu\text{-}pzAn^{Me})]_2 \cdot 2CH_3CN$ (**3b**$\cdot$**2**CH_3CN) and with anion in **2b** and solvent in **3b**$\cdot 2CH_3CN$ removed for clarity.

Table 2.3. Selected bond distances and angles for $MnBr(CO)_3[H(pzAn^{Me})]$ (**1a**), $ReBr(CO)_3[H(pzAn^{Me})]$ (**1b**), $\{Mn(CH_3CN)(CO)_3[H(pzAn^{Me})]\}(PF_6)$ (**2a**), $\{Re(CH_3CN)(CO)_3[H(pzAn^{Me})]\}(PF_6)$ (**2b**), $[Mn(CO)_3(\mu\text{-}pzAn^{Me})]_2 \cdot 2CH_3CN$ (**3a**$\cdot 2CH_3CN$), and $[Re(CO)_3(\mu\text{-}pzAn^{Me})]_2 \cdot 2CH_3CN$ (**3b**$\cdot 2CH_3CN$) with labeling as per Fig. 1.

Distances (Å)	**1a**	**1b**	**2a**	**2b**	**3a**	**3b**
M-Br	2.5391(4)	2.6278(4)				
M-N13			2.013(2)	2.151(7)		
M- N12 (pz)	2.054(2)	2.179(3)	2.045(2)	2.180(4)	2.0478(9)	2.1696(16)
M- N1 (NH)	2.091(2)	2.219(3)	2.105(2)	2.226(5)	2.0664(9)	2.1972(15)
M_b- N1 (NH)					2.1035(9)	2.2270(16)
M-C21	1.808(2)	1.909(3)	1.807(3)	1.894(8)	1.8010(12)	1.910(2)
M-C22	1.815(2)	1.922(3)	1.836(3)	1.937(5)	1.8207(12)	1.927(2)
M-C23	1.803(2)	1.896(4)	1.802(3)	1.909(10)	1.8012(12)	1.906(2)
N1⋯N12	2.668	2.731	2.679	2.797	2.741	2.807
M⋯M					3.174	3.435
C21-O1	1.146(3)	1.152(4)	1.141(3)	1.164(9)	1.1439(15)	1.159(2)
C22-O2	1.143(3)	1.147(4)	1.134(3)	1.137(6)	1.1488(15)	1.151(3)
C23-O3	1.145(3)	1.158(4)	1.151(3)	1.160(10)	1.1470(15)	1.155(3)
Angles (°)						
N1-M-N12	80.12(8)	76.77(10)	80.38(9)	78.8(2)	83.55(4)	80.28(6)
N1-M-N1b					80.86(4)	78.13(6)
M-N1-M					99.14(4)	101.87(6)

bond distances (for **3a**: Mn-N1 = 2.0664(9) Å, Mn-N1* = 2.1035(9) Å; for **3b**: Re-N1 = 2.1972(15) Å, Re-N1* = 2.2270(16) Å) that, on average, are shorter than those M-NH_2 bonds for the corresponding complexes **1a** or **1b** (avg. Mn-N 2.085(2) Å; avg. Re-N 2.212(3) Å). The Mn-N bond distances involving the Mn_2N_2 metallacycle in **3b** are slightly shorter but similar to those in $[Mn(CO)_3(\mu\text{-}o\text{-}NHC_6H_4PPh_2)]_2$ (Mn-N1 2.084(3) Å, Mn-N1' 2.084(3) Å, Mn-N avg 2.117(3) Å).[23] For most of the series, the carbonyl bound *trans*- to the pyrazolyl has longer M-C bonds and shorter C-O bonds than the other two carbonyls, the exception being **3a** in which one of the carbonyls in the MnN_2C_2 equatorial plane has longer M-C bonds and shorter C-O bonds than the others. Another point of structural interest is that for **1a/b** and **2a/b** the aniline rings are directed toward the axial carbonyl of the metal rather than the axial bromide or acetonitrile along the N12-N1 hinge axis (Fig. 2.1A or 2.1B gives a good view) rendering the complexes chiral

with low symmetry (C_1). That is, if the complex is viewed from the perspective where two equatorial carbonyls are directed away from the viewer and the third carbonyl is oriented down (placing the ligand in the 'front' of molecule), the pyrazolyl group is oriented either toward the 'left' (such as in the top of Fig. 1) or toward the 'right' side of the molecule, giving two possible enantiomers. For each of these complexes, both enantiomers are found in the solid state associated with one another via weak hydrogen bonding interactions as detailed in the Supporting Information.

2.4.3. IR Spectroscopy

The IR spectra of each complex in the solid state (KBr) consists of one high-energy and two lower energy C-O stretching bands, consistent with a facial tricarbonyl arrangement with local C_{3v} (MC_3N_3) or C_s (MC_3N_2Br) symmetry about the metal, where the lower energy bands are broad and partly resolved in the dimeric cases **3a** and **3b**. The C-O stretching frequencies for solutions of the complexes are, on average, shifted about 9 cm^{-1} higher in energy compared to the solid state spectra and the two lower energy bands are not resolved for the ionic species **2a/b** or the dimeric species **3a/b**. Moreover, the C-O stretching frequencies for the rhenium complexes are lower energy than those for the analogous manganese complexes owing to the more favorable energy match between the carbonyl π^* orbitals and the rhenium 5*d*-orbitals (hence greater back-bonding) versus the manganese 3*d*-orbitals. Within a given series of metal complexes (manganese or rhenium), the carbonyl stretching frequencies follow the usual trend becoming lower in energy with the more electron-rich nature of the complex. Thus, the ν_{C-O} stretches are highest in energy for cationic species (**2a** or **2b**), followed by the charge neutral bromide

complexes (**1a** or **1b**), which are, in turn, higher energy than the dimeric species (**3a** or **3b**). It is noted that the solution IR spectra for the crystalline metal bromide complexes **1a** or **1b** dissolved in CH_3CN had very weak intensity bands (occurring as shoulders to the main bands) for carbonyl stretches with energies comparable to those in **2a** or **2b**. Although the relative intensities of bands were not quantified, these observations are indicative of partial dissociation of **1a/b** in CH_3CN, presumably giving $\{M(CH_3CN)(CO)_3[H(pzan^{Me})]^+\}(Br^-)$, similar to behavior reported for another related system.[24] Such weak intensity bands are absent in the CH_2Cl_2 solution IR spectra.

2.4.4. NMR spectroscopy

The NMR spectra for the complexes confirmed coordination of the ligand and indicated that the geometries observed in the solid state were generally retained in CH_3CN. The spectra of the manganese complexes were less informative than those of the rhenium derivatives owing to the large quadrupole moment of the ^{55}Mn nuclei that gives broad resonances and loss of $^3J_{HH}$ coupling features. Nonetheless, both integration and comparison of chemical shifts of resonances with those of the well-behaved rhenium derivatives allows for indirect interpretation of the manganese spectra. In all of the current coordination complexes, the proton resonances for hydrogens on the pyrazolyl portion of the ligand are shifted downfield while those on the aniline are shifted upfield relative to those of the free ligand in CH_3CN. In both **1b** and **2b**, the hydrogens of the NH_2 group are resolved into a pair of broad doublets (Fig. 2.2) due to germinal coupling ($^2J_{HH}$ = 12 Hz) between 'axial' and 'equatorial' hydrogens of the screw-boat chelate ring conformation found in the solid state; in **1a** and **2a**, the coupling is not always observed

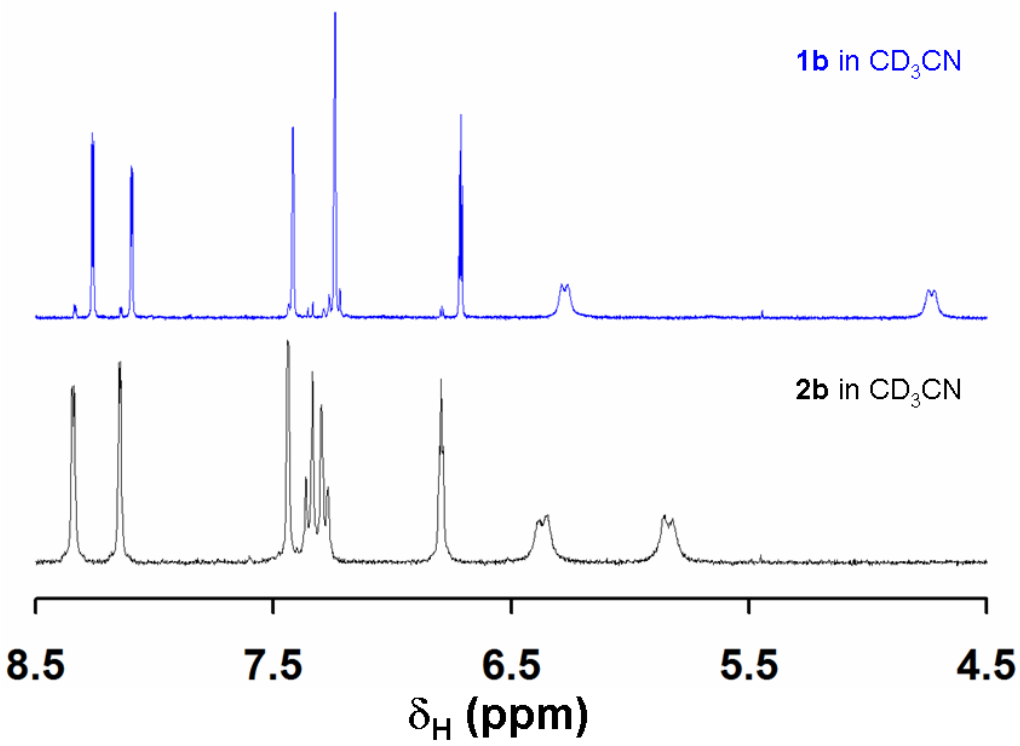

Fig. 2.2. A portion of the ^{1}H NMR spectrum of pure crystalline **1b** (top) and **2b** (bottom) dissolved in CD_3CN.

in each of the two N-H resonances for reasons described above. The chelate ring conformations appear to be energetically locked as two NH resonances are observed even at 70^{o}C in CH_3CN. As also can be seen in the spectra of crystalline **1b** in CD_3CN (Fig. 2.2), the data consists of two sets of overlapping resonances that correspond to those anticipated for **1b** (major component, 98%) and those similar to **2b** (minor component, 2%). That is, the chemical shifts of singlet resonances for pyrazolyl hydrogens, and those for the unique aryl-H and aryl-CH_3 (not shown in Fig. 2.2) are identical in both the spectra of **2b** and the minor component of the spectrum of **1b** but those of the two AB aryl multiplet resonances and the two NH resonances are slightly dissimilar due to differences in counter anions (Br^- versus PF_6^-); Referance 32 further documents the anion dependence of the chemical shifts of these latter resonances. Similar observations are

made for the manganese derivatives. The minor resonances are not present when the same solid samples of **1a** or **1b** are dissolved in either acetone-d_6 or CD_2Cl_2, giving further evidence (in addition to the IR spectral data) that the minor species present in acetonitrile is likely $\{M(CD_3CN)(CO)_3[H(pzAn^{Me})]^+\}(Br^-)$ (M = Mn, Re, as appropriate). Finally, in the spectrum of **3b,** the resonance for the NH occurs at relatively high field (δ_H = 3.48 ppm) likely due to magnetic anisotropy effects experienced by this hydrogen being sandwiched between pi-clouds of both an axial carbonyl and pyrazolyl rings of adjacent metal centers.

2.4.5 Electrochemistry

Since $M^I(CO)_3$ complexes (M = Mn, Re) [25] and the $H(pzAn^{Me})$ ligand [6] are each known electron donors, their electrochemistry was examined by cyclic voltammetry. The cyclic voltammograms for the various compounds obtained in CH_3CN are found in Fig. 2.3. Unfortunately, the poor solubility of the dimeric complexes **3a** and **3b** prohibited reliable electrochemical data from being obtained. The cyclic voltammogram of each metal complex **1a/b** and **2a/b** exhibits an irreversible oxidation (E_{pa} ranging between 1.0 and 1.7 V versus Ag/AgCl, where the cathodic wave is significantly less intense than expected, see ref 32) and an irreversible reduction (E_{pc} ranging between -1.6 and -2.1 V) at potentials more positive than that in the free ligand. The charge neutral derivatives **1a** and **1b** are more easily oxidized by about 0.4 V than the corresponding cationic derivatives **2a** and **2b**, expected from coulombic arguments. Also, the manganese(I) derivatives are more easily oxidized than the corresponding rhenium(I)

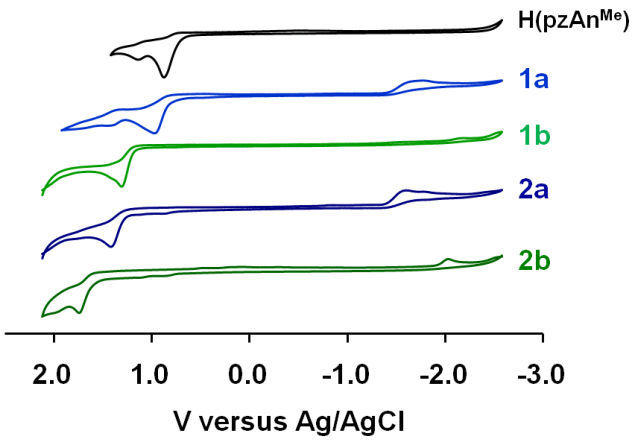

Figure.2. 3. Cyclic voltammograms obtained at scan rates of 50 mV/s for ligand $H(pzAn^{Me})$ (top) and metal complexes in CH_3CN with $(NBu_4)(PF_6)$ as supporting electrolyte.

complexes by about 0.3 V which parallels previous theoretical and experimental results (UV-photoelectron spectroscopy) observed for the $CpM(CO)_3$ [26] and $M(CO)_5Br$ [27] (M = Mn, Re) series of complexes, where it is noted that differences attributed to solvation and structural reorganization of isostructural Mn and Re congeners are negligible such that correlations between experimental gas phase ionization potentials and solution-phase electrochemical experiments are typically maintained [28]. Based upon experimental observations for other $H(pzAn^{Me})$ derivatives [29] as well as the frontier orbitals obtained from single point energy calculations (Supporting Information) which show that the HOMO is centered on the $M(X)(CO)_3$ fragment and the LUMO is essentially a ligand π^* orbital (Fig. 2.4) we very tentatively assign the oxidations in the group 7 metal tricarbonyl complexes as metal-centered and the reductions as ligand-centered in accord with Koopmans theorem.[30]

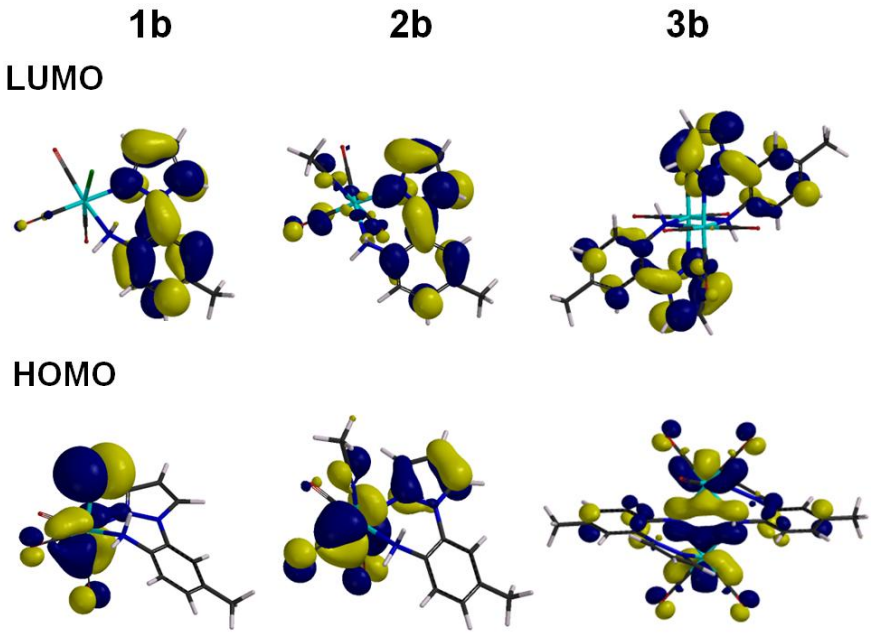

Figure. 2.4. Frontier orbitals [LUMO (top) and HOMO (bottom)] for rhenium complexes **1b** (left), **2b** (center) and **3b** (right) from density functional calculations (BP86/6-31G*//B3LYP/LAVCP*).

2.4.6. Electronic Spectroscopy.

The electronic absorption spectra of all six derivatives were recorded and representative spectra of **1a** and **1b** are given in Fig. 2.5 while complete electronic spectra are found in the ref 32. The poor solubility of **3a** and **3b** has hindered

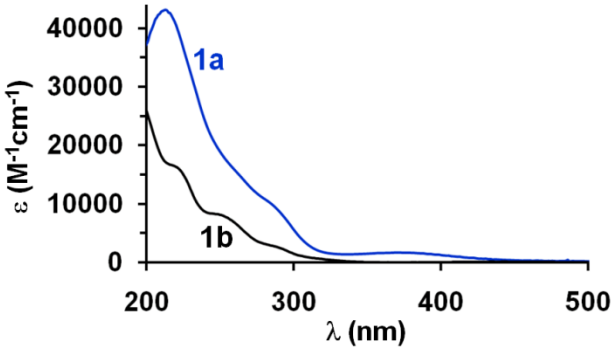

Figure.2.5. Overlay of the electronic absorption spectrum of **1a** (blue line) and **1b** (black line) in CH_3CN.

accurate measurements of their extinction coefficients. Each of the metal complexes has a low-spin d^6 electron configuration as expected from the strong-field carbonyl ligands and as evident from their diamagnetic NMR spectrum. Thus, two *d-d* transitions of low intensity ($\varepsilon < 200\ M^{-1}cm^{-1}$) might be expected for pseudo-octahedral metal centers ($^1A_1 \rightarrow {}^1T_1$ and $^1A_1 \rightarrow {}^1T_2$) as observed in other low-spin d^6 systems.[31] Unfortunately it was not possible to observe these bands as they are likely obscured by the remainder of the absorption bands. Instead, each spectrum consists of a low-energy band $\lambda > 300$ nm of moderately low intensity ($\varepsilon \sim 2{,}000\ M^{-1}cm^{-1}$) that likely corresponds to a metal-to-ligand charge transfer (*MLCT*) or a delocalized metal-ligand-to-ligand charge transfer (*MLLCT*), in analogy to the nicely detailed theoretical and experimental studies on the related $ReCl(CO)_3[HC(3,5\text{-}Me_2pz)_2]$ complex[32]. For the manganese compounds, the lowest energy band tails into the violet region of the visible spectrum giving rise to the yellow color of the compounds while the lowest energy absorption bands for the rhenium complexes are outside the visible range rendering these complexes colorless. The two medium-intensity bands ($\varepsilon \sim 10{,}000\text{-}20{,}000\ M^{-1}cm^{-1}$) and two, intense, high-energy bands (one occurs as a shoulder in the manganese cases) near 200 nm are likely due to π-π^* intraligand transitions based on both energy and intensity considerations. Unfortunately, in contrast to other complexes of $H(pzAn^{Me})$ and its derivatives, none of the current complexes are luminescent in solution or the solid state.

2.5. Concluding remarks

In this study we began a survey of the transition metal coordination chemistry of the electron-rich, N,N-chelating $H(pzAn^{Me})$ ligand by exploring group 7 tricarbonyls. It

was hoped that stable complexes could be obtained and that drastic changes in the electronic properties of the normally non-innocent ligand scaffold would be observed. Moreover, it was also hoped that switching behavior could be observed by cycling reactions of Brønsted acids and bases where the reaction of the complexes with Brønsted bases would restore energetic access to the lone pair on nitrogen responsible for the electron donor properties of aniline derivatives which should be otherwise inhibited when nitrogen is coordinatively-saturated. Thus, four complexes of the type $[M(X)(CO)_3[H(pzAn^{Me})]\}^{n+}$ [X = Br, n = 0, M = Mn (**1a**), M = Re (**1b**); X = CH_3CN, n = 1, M = Mn (**2a**), M = Re (**2b**)] with coordinatively-saturated toluidinyl nitrogens were prepared and characterized both in the solid state and in solution. The relative stabilities of the complexes followed the order **2b** > **2a** > **1b** > **1a** based on chemical reactivities, electrochemical, and spectroscopic properties which also follows the order expected based on both coulombic arguments and periodic trends. The reactions between any of the four complexes and $(NEt_4)(OH)$ as a Brønsted base produced the highly insoluble dimeric $[\textit{fac}\text{-}M(CO)_3(\mu\text{-}pzAn^{Me})]_2$, (M = Mn (**3a**) or M = Re (**3b**)) where the amido nitrogens of the ligands bridge two six coordinate metal centers. Although none of the current complexes exhibited desirable photophysical properties (in stark contrast to chelate complexes with redox-inactive main group Lewis acids which are typically intensely fluorescent) or reversible switching behavior owing to the low solubility of **3a** and **3b**, structurally modified variants of the $H(pzAn^{Me})$ scaffold (using groups that prevent dimerization) can impart such behavior in their tricarbonylrhenium(I) complexes and the successful endeavors by our group in this vein will be disseminated shortly.

CHAPTER 3

CHEMICAL SWITCHING BEHAVIOR OF TRICARBONYLRHENIUM (I) COMPLEXES OF A NEW REDOX ACTIVE 'PINCER' LIGAND.

3.1 Introduction

Simple chemical species that can be dependably switched between multiple, easily-distinguishable (readable), electronic states by external stimuli and that retain their integrity without the need for permanent stimulation are highly desirable for information storage applications in the emerging area of molecular electronics.[1] Numerous organic systems such as diarylethenes, flavylium derivatives, among other more complex examples have been recognized or developed for such purposes.[2] Recently, there has been growing interest in developing similar chemistry for organometallic systems owing to the attractive electronic properties associated with metal centres such as access to multiple oxidation states, different spin states, intense charge transfer absorptions, and large spin-orbit coupling constants that can potentially give rise to interesting photophysical properties.[3]

During the course of our investigations into the coordination chemistry of new pincer ligands[4] (typically meriodonally-coordinating and uninegative species) based on di(2-pyrazolyl-aryl)amine derivatives (left, **Fig.3.1**), it occurred to us that a few of

these complexes might be viable entrants for switching purposes and possibly for information storage applications owing to their interesting optoelectronic properties and chemical reactivity. That is, as diarylamines are well-known electron-donors,[5] pincer ligands based on this scaffold are electrochemically non-innocent;[6] they will

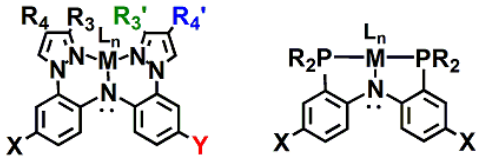

Figure 3.1. Generic depiction of a metal complex of a NNN 'pincer' ligand based on di(2-pyrazolyl-aryl)amine and of a related PNP derivative.

increase the number of available valence states in their transition metal complexes. Moreover, since the electron donor capacity of these ligands relies on nitrogen being coordinatively unsaturated (with a lone pair of electrons), it should be possible to attenuate energetic access to electronic states involving this lone pair (such as any n-π* or dπ-pπ interaction) via quarternization (binding protons or other Lewis acids). Our choice of using pyrazolyl donors is based on the facile syntheses of nearly limitless structural variants that can be exploited to impart control over steric, electronic, and solubility properties (by changing pyrazolyl R groups in **Fig.3.1**). During the course of these studies an important contribution was reported by Ozerov, Nocera, and co-workers[7] regarding a related complex *mer*-(PNP)$Re^{I}(CO)_3$ (**A**) (R = iPr; X = Me, right of **Fig.3.1**). The yellow complex **A** was found to react with triflic acid to produce the colorless {*mer*-[H(PNP)]$Re(CO)_3$}(OTf) (**B**) with a protonated nitrogen. Additionally, oxidation of **A** with AgOTf afforded royal blue {*mer*-[(PNP)]$Re(CO)_3$}(OTf) (**A^+OTf^-**). The IR, EPR spectroscopic data and chemical reactivity of **A^+OTf^-** were indicative of a ligand-centred radical (with relatively weak

coupling to the metal centre). The potential switching behaviour of **A** (or **B**), however, was not addressed despite the interesting colour changes and reversible redox properties. In this chapter we highlight our initial findings concerning the properties and potential switching behaviour of of the $Re(CO)_3$ complexes of di(2-pyrazolyl-*p*-tolyl)amine, **HL**, (R_3=R_3'=R_4=R_4'=H; X=Y=CH_3, **Fig.3 1**). Importantly, this study also allows a comparison of the impact of changing donor groups at the 2,2'-positions on the diarylamine on the electronic properties of resultant $(NNN)Re^{I}(CO)_3$ or $(PNP)Re^{I}(CO)_3$ complexes. Next chapter will more fully detail the chemistry promoted uniquely by complexes of this ligand type (and substituted derivatives) as well as comparisons with the remarkable known chemistry exhibited by related PNP derivatives.[8]

3.2 Experimental

General Considerations.

The compounds pyrazole, CuI, N,N'-dimethylethylenediamine (DMED), anhydrous K_2CO_3 powder, Tl(X = PF_6 or OTf) and (NEt_4)(OH) (1M in MeOH) were purchased from commercial sources and used without further purification while $Re(CO)_5Br$,[9] di(2-bromo-4-tolyl)amine,[10] were prepared by literature methods. The solvents used in the preparations were dried by conventional methods and distilled prior to use. Midwest MicroLab, LLC, Indianapolis, Indiana 45250, performed all elemental analyses. IR spectra were recorded in the 4000-500 cm^{-1} region (as KBr pellets or as CH_2Cl_2 solutions in a cell with KBr windows) on a Nicolet Magna-IR 560 spectrometer. ^{1}H and ^{13}C NMR spectra were recorded on a Varian 400 MHz spectrometer. Chemical shifts were referenced to solvent resonances at δ_H 7.27, δ_C 77.23 for $CDCl_3$; δ_H 5.33, δ_C

54.00 for $CDCl_3$; δ_H 1.94, δ_C 118.9 for CD_3CN and δ_H 2.05, δ_C 29.92 for acetone-d_6. Melting point determinations were made on samples contained in glass capillaries using an Electrothermal 9100 apparatus and are uncorrected. Absorption measurements were recorded on an Agilent 8453 spectrometer. Electrochemical measurements were collected under nitrogen atmosphere at a scan rate of 100 mV/s for samples as 0.1 mM CH_2Cl_2 solutions with 0.1 M NBu_4PF_6 as the supporting electrolyte. A three-electrode cell comprised of an Ag/AgCl electrode (separated from the reaction medium with a semipermeable polymer membrane filter), a platinum working electrode, and a glassy carbon counter electrode was used for the voltammetric measurements. With this set up, the ferrocene/ferrocenium couple had an $E_{1/2}$ value of +0.53 V consistent with the literature value in this solvent.[11] Mass spectrometric measurements recorded in ESI(+) or ESI(-) mode were obtained on a Micromass Q-TOF spectrometer whereas that performed by using direct-probe analyses were made on a VG 70S instrument. For the ESI(+) experiments, formic acid (approximately 0.1 % v/v) was added to the mobile phase (CH_3CN). EPR measurements were obtained using a Bruker ELEXSYS E600 equipped with an ER4116DM cavity resonating at 9.63 GHz, an Oxford Instruments ITC503 temperature controller and ESR-900 helium-flow cryostat. The ESR spectra were recorded with 100kHz field modulation.

Syntheses.

3.2.1. Di(2-(pyrazolyl)-4-tolyl)amine, H(L).

A mixture of 10.82 g (0.030 mol) di(2-bromo-p-tolyl)amine, 7.25 g (0.107mol, 3.5 equiv) pyrazole, 14.72 g (0.107mmol, 3.5 equiv) K_2CO_3, 1.2 mL (0.012 mol, 40 mol %) DMED,

and 10 mL of distilled xylenes was purged with nitrogen 15 min. Then, 0.58 g (3 mmol, 10 mol %) CuI was added as a solid under nitrogen and the mixture was heated at reflux for 36 h under nitrogen. After cooling to room temperature, 200 mL of H_2O was added and the mixture was extracted with three 100 mL portions of CH_2Cl_2. The combined organic layers were dried over $MgSO_4$, filtered, and solvent was removed by rotary evaporation to give an oily residue that was purified by column chromatography on silica gel. Elution using 10:1 hexanes:ethyl acetate (R_f = 0.5) afforded 6.90 g (69 %) of **H(L)** as a white powder, after removing solvent and drying under vacuum. Mp, 89 - 90 ^oC. Anal. Calcd (obs.) for $C_{20}H_{19}N_5$: C, 72.93 (73.05); H, 5.81 (5.97); N, 21.26 (20.88). ^1H NMR: (CD_2Cl_2) 8.48 (s, 1H, NH), 7.72 (dd, *J* = 2, 0.6 Hz, 2H, H_3pz), 7.67 (dd, *J* = 2, 0.6 Hz, 2H, H_5pz), 7.25 (d, *J* = 8 Hz, 2H, Ar), 7.12 (s, 2H, Ar), 7.03 (d, *J* = 8 Hz, 2H, Ar), 6.43(dd, *J* = 2, 0.6 Hz, 2H, H_4pz), 2.30 (s, 6H, $ArCH_3$). ^1H NMR (acetone-d_6) : 8.72 (s, 1H, NH), 7.94 (dd, *J* = 2, 0.6 Hz, 2H, H_3pz), 7.81 (dd, *J* = 2, 0.6 Hz, 2H, H_5pz), 7.36 (d, *J* = 8 Hz, 2H, Ar), 7.29 (d, *J* = 2 Hz, 2H, Ar), 7.19 (dd, *J* = 8, 2 Hz, 2H, Ar), 6.57 (dd, *J* = 2, 0.6 Hz, 2H, H_4pz), 2.41 (s, 6H, $ArCH_3$). ^{13}C NMR: ($CDCl_3$) 140.5, 134.7, 130.7, 130.2, 130.1, 129.0, 125.8, 118.9, 106.7, 20.6. UV-VIS λ_{max}, nm (ε, $M^{-1}cm^{-1}$), CH_2Cl_2: 238 (31,600), 303 (22,700). LRMS (Direct Probe) m/z (Int.) [assign.]: 329 (100) $[HL]^+$, 262 (8) $[HL–Hpz]^+$, 173 (15) $[H_2L–pztolyl]^+$. Single crystals suitable for X-ray diffraction were obtained by slow cooling a hot hexanes solution (supersaturated) to room temperature over the course of a few hours.

3.2.2. *fac*-$ReBr(CO)_3$[H(L)], **1**.

A mixture of 0.510 g (1.27 mmol) $Re(CO)_5Br$ and 0.455g (1.38 mmol) of **H(L)** in 20 mL toluene was heated at reflux 15 h. The resulting precipitate was isolated by filtration, washed with two 5 mL portions Et_2O and dried under vacuum which afforded 0.71 g (83 %) of **1** as a colorless solid. Mp. 272 - 274^oC dec. Anal. Calcd (obs.) for $C_{23}H_{19}BrN_5O_3Re$: C, 40.65 (40.33); H, 2.82 (2.67); N, 10.31 (10.02). IR (KBr) ν_{co} 2020, 1920, 1880 cm^{-1}. IR (CH_2Cl_2) ν_{co} major bands; 2029, 1919, 1896, minor bands; 2038, 1930 cm^{-1}. ^1H NMR: (CD_2Cl_2, 293K): (three species, see text: **I**, 48% of signal integration intensity from well-resolved resonances in the $ArCH_3$, NH, and H_4pz regions of the spectrum; **II**, 42% of signal; **III** 10 % of signal): 11.92 (s, 1H, NH, **II**), 11.40 (s, 1H, NH, **III**), 9.89 (s, 1H, NH, **I**), 8.22 (d, *J* = 3 Hz, 1H, H_5pz, **III**), 8.18 (d, *J* = 3 Hz, 1H, H_5pz, **I**), 8.17 (d, *J* = 2 Hz, 1H, H_3pz, **I**), 8.13 (d, *J* = 2 Hz, 1H, H_3pz, **III**), 8.01 (d, *J* = 3 Hz, 1H, H_5pz, **III**), 7.92 (d, *J* = 2 Hz, 2H, H_3pz, **II**), 7.91(d, *J* = 3 Hz, 3H, H_5pz, **I** and **II**), 7.90 (d, *J* = 2 Hz, 1H, H_3pz, **III**), 7.88 (d, *J* = 3 Hz, 1H, H_5pz, **I**), 7.59-7.54 (m, Ar, 2H, **I**/**II**/**III**), 7.48 (s, 1H, Ar, **III**), 7.36-7.31 (m, Ar, 3H, **I**/**II**/**III** and H_5pz, **I**), 7.30 (s, 1H, Ar, **III**), 7.23-7.08 (m, 2.5H, Ar **I**/**II**/ **III**), 6.86 (d, *J* = 8 Hz, 1H, Ar, **III**), 6.77 (dd, *J* = 3, 2 Hz, 1H, H_4pz, **I**), 6.76 (dd, *J* = 3, 2 Hz, 1H, H_4pz, **III**), 6.61 (dd, *J* = 3, 2 Hz, 1H, H_4pz, **III**), 6.51 (dd, *J* = 3, 2 Hz, 2H, H_4pz, **II**), 6.41 (dd, *J* = 3, 2 Hz, 1H, H_4pz, **I**), 5.94 (d, *J* = 8 Hz, 1H, Ar, **III**), 2.51 (s, 3H, $ArCH_3$, **III**), 2.47 (s, 3H, $ArCH_3$, **I**), 2.44 (s, 3H, $ArCH_3$, **I**), 2.37 (s, 6H, $ArCH_3$, **II**), 2.32 (s, 3H, $ArCH_3$, **III**). ^{13}C NMR: (CD_2Cl_2, 293K) major asymmetric species **I**: 148.00, 141.34, 139.05, 137.68, 135.23, 133.52, 132.09, 128.34, 124.69, 122.81, 119.92, 110.5, 108.37, 21.31, 20.93; symmetric species **II**: 148.85, 139.13, 136.45, 132.97, 130.57, 124.78, 124.24, 110.06, 20.98; minor asymmetric species **III**: 148.89, 142.41, 140.10, 136.93, 136.76, 135.07, 134.99, 131.72, 131.27, 131.06,

130.27, 128.39, 124.74, 124.15, 122.87, 110.53, 108.40, 21.26, 20.91. UV-VIS λ_{max}, nm (ε, $M^{-1}cm^{-1}$), CD_2Cl_2: 230 (49,300), 251 (32,300), 287 (11,100). LRMS ESI(+) m/z (Int.) [assign.]: 743 (4) $[ReBr(CO)_3(HL)+Na(CH_3CN)]^+$, 721 (6) $[ReBr(CO)_3(H_2L)+ CH_3CN]^+$, 718 (7) $[ReBr(CO)_3(HL)+K]^+$, 702 (5) $[ReBr(CO)_3(HL)+Na]^+$, 641 (1) $[Re(CO)_3(H_2L)+CH_3CN]^+$, 600 (100) $[Re(CO)_3(HL)]^+$, 330 (31) $[H_2L]^+$. X-ray quality crystals were grown by layering an acetone solution with hexane and allowing the solvents to slowly diffuse over two days.

3.2.3. {Re(CO)$_3$[H(L)]}(PF$_6$), 2·PF$_6$.

A mixture of 0.208 g (0.306 mmol) of **1** and 0.107 g (0.306 mmol) $TlPF_6$ in 20 mL dry CH_3CN was heated at reflux for 15 h. After cooling to room temperature, TlBr was removed by filtration through Celite, and solvent was removed from the filtrate by rotary evaporation. The residue was washed with two 5 mL portions of Et_2O and was dried under vacuum to give 0.184 g (80 %) of **2·PF$_6$** as a white powder. Mp, 255 – 258 ^oC dec. Anal. Calcd (obs.) for $C_{23}H_{19}F_6N_5O_3PRe$: C, 37.10 (36.99); H, 2.57 (2.32); N, 9.41 (9.16). IR (KBr) ν_{co} 2040, 1950, 1930 cm^{-1}. ^1H NMR: (CD_2Cl_2, 293K) 7.95 (d, J = 2 Hz, 2H, H_3pz), 7.91 (d, J = 3 Hz, 2H, H_5pz), 7.74 (s, 1H, NH), 7.24-7.16 (m, 4H, Ar), 6.58 (dd, J = 3, 2 Hz, 2H, H_4pz), 2.41 (s, 6H, $ArCH_3$). ^{13}C NMR: suitable spectrum of a concentrated solution could not be obtained even after 24 hours acquisition time. UV-VIS λ_{max}, nm (ε, $M^{-1}cm^{-1}$), CD_2Cl_2: 230 (42,500), 245 (34,800), 367 (1,750). LRMS ESI(+) m/z (Int.) [assign.]: 600 (100) $[(HL)Re(CO)_3]^+$. X-ray quality crystals were grown by layering a dichloromethane solution with hexane and allowing the solvents to slowly diffuse over two days.

3.2.4. {Re(CO)$_3$[H(L)]}(OTf), 2·OTf.

A mixture of 0.175 g (0.258 mmol) of **1** and 0.091 g (0.26 mmol) TlOTf in 20 mL dry CH_3CN was heated at reflux for 15 h. After cooling to room temperature, TlBr was removed by filtration through Celite, and solvent was removed from the filtrate by rotary evaporation. The residue was washed with two 5 mL portions of Et_2O and was dried under vacuum to give 0.173 g (90 % based on **1**) of **2·OTf** as a white powder. Mp, 275 - 277^{o}C dec. Anal. Calcd (obs.) for $C_{24}H_{19}F_3N_5O_6ReS$: C, 38.50 (38.78); H, 2.56 (2.72); N, 9.35 (8.99). IR (CH_2Cl_2) ν_{co} 2040, 1938, 1922 cm^{-1}. IR (KBr) ν_{co} 2036, 1947, 1922 cm^{-1}. ^{1}H NMR: (CD_2Cl_2, 293K) 9.79 (s, 1H, NH), 7.93 (d, J = 2 Hz, 2H, H_3pz), 7.89 (d, J = 3 Hz, 2H, H_5pz), 7.25-7.15 (m, 6H, Ar), 6.55 (dd, J = 3, 2 Hz, 2H, H_4pz), 2.39 (s, 6H, $ArCH_3$). ^{13}C NMR: (CD_2Cl_2, 293K) 193.5, 191.3, 148.1, 139.5, 135.9, 133.2, 132.2, 130.7, 125.0, 123.9, 110.1, 21.0. UV-VIS λ_{max}, nm (ε, M^{-1}cm^{-1}), CD_2Cl_2: 230 (43,000), 245 (34,000), 367 (1,700). LRMS ESI(+) m/z (Int.) [assign.]: 600 (100) [(HL)Re(CO)$_3$]$^+$. X-ray quality crystals were grown by layering a dichloromethane solution with hexane and allowing the solvents to slowly diffuse over two days.

3.2.5. Re(CO)$_3$(L), 3.

To a solution of 0.105 g (0.15mmol) **1** in 20 mL of CH_3CN was added 1.50 mL of a 0.103 M (NEt_4)(OH) solution in MeOH (0.155 mmol), immediately giving a yellow solution. The mixture was stirred for 15 min then solvent was removed by rotary evaporation. The residue was washed with two 5 mL portions Et_2O, and the yellow product was extracted with three 10 mL portions of benzene. Benzene was removed by vacuum distillation to afford 0.060 g (67 %) of **3** as a yellow powder. Mp. 295-298^{o}C dec. Anal. Calcd (obs.) for $C_{23}H_{18}N_5O_3Re$: C, 46.15 (45.89); H, 3.03 (3.11); N, 11.70

(11.58). IR (CH_2Cl_2) ν_{co} 2015, 1905, 1885 cm^{-1}. IR (KBr) ν_{co} 2013, 1901, 1876 cm^{-1}. ^1H NMR: (CD_2Cl_2, 293 K) 7.95 (d, *J* = 2 Hz, 2H, H_3pz), 7.92 (d, *J* = 3 Hz, 2H, H_5pz), 7.82 (part of AA'BB', 2H, Ar), 7.12 (part of AA'BB', 2H, Ar), 7.11 (s, 2H, Ar), 6.52 (dd, *J* = 3, 2 Hz, 2H, H_4pz), 2.36 (s, 6H, $ArCH_3$). ^1H NMR: (acetone-d_6) 8.35 (dd, *J* = 2, 1 Hz, 2H, H_3pz), 8.30 (dd, *J* = 2, 1 Hz, 2H, H_5pz), 7.84 (part of AB d, *J* = 8 Hz, 2H), 7.29 (d, *J* = 2, Hz, 2H, Ar), 7.11 (part of AB d, *J* = 9, 2 Hz, 2H, Ar), 6.65 (dd, *J* = 2, 1 Hz, 2H, H_4pz), 2.31 (s, 6H, $ArCH_3$). ^{13}C NMR: (CD_2Cl_2) 196.8, 146.6, 142.9, 130.9, 130.3, 129.0, 128.0, 123.9, 119.4, 108.0, 20.7. HRMS [Direct Probe, m/z] Calc. (Obs) for $C_{23}H_{18}N_5O_3Re$: 599.0968 (599.0973). LRMS (Direct Probe) m/z (Int.) [assign.]: 599 (30) $[LRe(CO)_3]^+$, 515 (58) $[LRe - 3\ CO + H]^+$, 329 (28) $[H_2L]^+$, 173 (100) $[H_2L–pztolyl]^+$, 105 (47) $[H_2Ntolyl]^+$. UV-VIS λ_{max}, nm (ε, $M^{-1}cm^{-1}$), CD_2Cl_2: 229 (40,200), 239 (37,900), 309 (10,600), 353 (8,500), 390 (6,400) . X-ray quality crystals were grown by layering an acetone solution with hexane and allowing the solvents to slowly diffuse over two days.

3.2.6. Acid/base cycling experiments.

UV-Vis spectroscopic experiments. In a typical UV-Vis spectroscopic acid/base cycling experiment, 10 μL aliquots of 1.904 m<u>M</u> acid (HBF_4 or CF_3COOH) in CH_2Cl_2 solution were sequentially added to 3.0 mL of a 0.0635 m<u>M</u> $ReLCO_3$ solution in CH_2Cl_2 where the disappearance of the band at 450 nm was monitored. After one equivalent of acid was added, 10 μL aliquots of 1.904 m<u>M</u> (NEt_4)(OH) solution in dichloromethane were added to the resultant solution. This acid/base cycle was repeated three more times.

Electrochemical experiments. In a representative acid/base cycling experiment monitored by cyclic voltammetry, a solution of 0.0100 g (0.0167 mmol) of $Re(CO)_3$(**L**)

(**3**) and 0.300 g (1.23 mmol) NBu_4PF_6 in 15 mL dry CH_2Cl_2 was treated with 10 μL aliquots of 0.1670 M tetrafluoroboric acid in CH_2Cl_2 where the cyclic voltammogram was recorded between 0.0 to +1.0 V versus Ag/AgCl (the potential values in the main text were calibrated to an external Fc/Fc^+ couple +0.53 V versus Ag/AgCl in CH_2Cl_2) at a scan rate of 100 mV/s after each addition. After the wave centered near +0.53 V versus Ag/AgCl, indicative of **3**, approached a constant near zero baseline current value (after approximately one equivalent of acid added), 10 μL aliquots of 0.1670 M $(NEt_4)(OH)$ in CH_2Cl_2 were added. The voltammograms recorded after each successive base addition, as above. This acid/base cycling process was repeated three more times.

3.2.7. Chemical Oxidation of 3.

Spectrophotometric Titrations. Standard solutions the cation radical 9,10-dimethoxyocta-hydro-1,4:5,8-dimethanoanthracenium hexachloroantimonate, (**CRET**$^+$)(**SbCl$_6^-$**),[12] were prepared by dissolving the cation radical in freshly distilled CH_2Cl_2 and diluting until the absorbance measured at 517 nm was about 1.0, corresponding to a concentration of $1.37x10^{-4}$ M (ε 7,300). For the titrations, 3 mL of this standard solution were used and the spectrum was acquired before and after the addition 10 μL aliquots of 0.00548 M solutions of **3**.

Synthetic Scale. A solution of 0.054g (89 μmol) of (**CRET**$^+$)(**SbCl$_6^-$**) in 15 mL dry, distilled CH_2Cl_2 and the resultant solution was transferred under nitrogen by cannula to a magnetically stirred solution of 0.053 g (89 μmol) **3** in 15 mL CH_2Cl_2. The resultant royal blue solution was stirred 10 min and solvent was removed under vacuum. The blue

solid was washed with two 5 mL portions of pentane and then dried under vacuum to give 0.053 g (64 %) of (**3**$^+$)(**SbCl$_6^-$**) as a blue solid.

Alternatively, a solution of 0.115 g (0.448 mmol) AgOTf in 10 mL CH_2Cl_2 was added to a solution of 0.268 g (0.447 mmol) **3** in 10 mL CH_2Cl_2. After the resulting blue-black mixture had been stirred 1 h, the blue solution was separated from silver metal by filtration. Solvent was removed by vacuum distillation and the blue residue was washed with two 5 mL portions of hexane to leave 0.244 g (73% based on Re) of (**3**$^+$)(**OTf**$^-$) as a blue solid. IR (CH_2Cl_2) ν_{co} 2035, 1932, 1925 cm^{-1}. IR (KBr) ν_{co} 2031, 1941 cm^{-1}. UV-VIS λ_{max}, nm (ε, M^{-1}cm^{-1}), CD_2Cl_2: 488 (1,000), 618 (2,680), 748 (3,600), 892sh (900), 1046sh (460).

3.3. Crystallography.

X-ray intensity data from a colorless block of **H(L)**, a colorless plate of $ReBr(CO)_3$[**H**(**L**)] (**1**), a colorless prism of {$Re(CO)_3$[**H(L)**]}(PF_6), (**2·PF$_6$**), a colorless prism of {$Re(CO)_3$[**H(L)**]}(OTf), (**2·OTf**), and a yellow block of $Re(CO)_3$(**L**), (**3**) were measured **(Fig 3.2 & 3.3)** at 100(2) K with a Bruker AXS 3-circle diffractometer equipped with a SMART2[13] CCD detector using Cu(Kα) radiation. Raw data frame integration and Lp corrections were performed with SAINT+.[14] Final unit cell parameters were determined by least-squares refinement of 7538, 6621, 8198, 9905, and 7176 reflections from the data sets of **H(L), 1**, **2·PF$_6$**, **2·OTf**, and **3**, respectively, with I > 2σ(I) for each. Analysis of the data showed negligible crystal decay during collection in each case. Direct methods structure solutions, difference Fourier calculations and full-

matrix least-squares refinements against F^2 were performed with SHELXTL.[15] Semi-empirical absorption

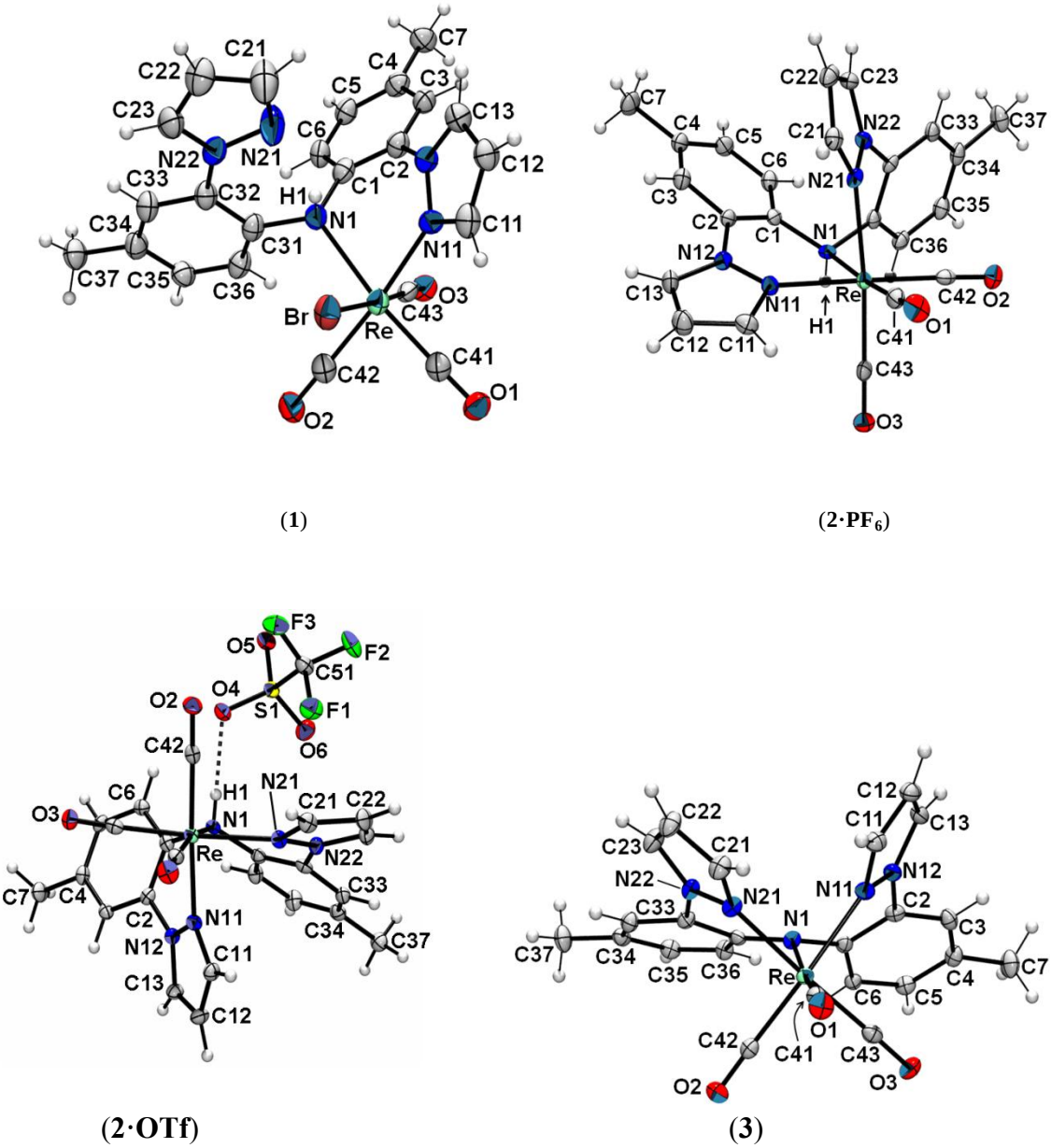

Figure 3.2. Structure Diagrams with Atom Labeling of $ReBr(CO)_3$[**H(L)**] (**1**), {$Re(CO)_3$[**H(L)**]}(PF_6) (**2·PF$_6$**) {$Re(CO)_3$[**H(L)**]}(OTf) (**2·OTf**), and $Re(CO)_3$(**L**), (**3**).

correction based on the multiple measurement of equivalent reflections was applied to the data of **H(L)** with SADABS.[14] An empirical absorption correction of area-detector data for twinned (2:1 component ratio separated by ca 2 degree split) crystals and of **1** was applied with TWINABS.[14] Numerical absorption corrections based on the real shape of the crystals for the remainder of the compounds were applied with SADABS.[14] All non-hydrogen atoms were refined with anisotropic displacement parameters with the following exception. Two alternative positions of PF_6^- anion were found in **2·PF$_6$** from a series of difference Fourier syntheses and were refined with soft geometric restraints (using the SAME instruction in SHELXL). Their relative population was refined to 27/73. The fluorines of the minor disorder component were refined isotropically. The secondary amino nitrogens in **H(L)** and in **2·X** (X = PF_6, OTf) were located and refined whereas the remaining hydrogen atoms in all complexes were placed in geometrically idealized positions and included as riding atoms. The X-ray crystallographic parameters and further details of data collection and structure refinements are presented in **Table 3.1**. Selected bond distances and interatomic angles are found in **Table 3.2** while the remaining distances and angles can be found in the cif files deposited with the CSD.[16]

Compound	**H(L)**	**1**	**2·PF$_6$**	**2·OTf**	**3**
Formula	$C_{20}H_{19}N_5$	$C_{23}H_{19}BrN_5O_3Re$	$C_{23}H_{19}F_6N_5O_3PRe$	$C_{24}H_{19}F_3N_5O_6ReS$	$C_{23}H_{18}N_5O_3Re$
Formula weight	329.40	679.54	744.60	748.70	598.62
Crystal system	Monoclinic	Monoclinic	Monoclinic	Monoclinic	Monoclinic
Space Group	P n	P 2_1/c	P 2_1/c	P 2_1/n	C 2/c
a, Å	7.3364(2)	8.1846(4)	15.6722(7)	8.1784(2)	24.5632(5)
b, Å	16.5933(4)	31.9302(14)	9.6375(4)	18.4766(4)	11.8412(3)
c, Å	14.1016(3)	8.9168(5)	16.8562(7)	17.1772(4)	15.4073(3)
α, deg	90	90	90	90	90
β, deg	98.6740(10)	102.901(3)	103.315(2)	90.9260(10)	110.1570(10)
γ, deg	90	90	90	90	90
V, Å^3	1697.03(7)	2271.5(2)	2477.53(18)	2595.29(10)	4206.86(16)
Z	4	4	4	4	8
T, K	100(2)	100(2)	100(2)	100(2)	100(2)
ρ calcd, Mg m^{-3}	1.289	1.987	1.996	1.916	1.890
λ(Cu Kα), Å	1.54178	1.54178	1.54178	1.54178	1.54178
μ, mm^{-1}	0.631	12.830	10.967	10.561	11.611
Abs. Correction	multi-scan	multi-scan	numerical	numerical	numerical
F(000)	696	1304	1440	1456	2320
θ range [°]	2.66 to 66.41	2.77 to 67.93	2.90 to 67.71	3.51to 67.78	3.83 to 67.85
Reflns collected	13695	35582	20721	21636	17421
Indep. reflns	2889 (R_{int} 0.0242)	4046(R_{int} 0.1068)	4328(R_{int} 0.0372)	4638(R_{int} 0.0197)	3759(R_{int} 0.0199)
T_min/max	0.7865/0.9513	0.2060/0.6279	0.3627/0.6744	0.1306/0.4336	0.1143/0.2748
Data/restraints/ parameters	2889/2/464	4046/0/300	4328/21/392	4638/0/367	3759/0/292
Goodness-of-fit on F^2	0.985	1.042	1.009	1.022	1.002
R[I>2σ(I)][c](all data)	0.0282 (0.0292)	0.0438 (0.0467)	0.0267 (0.0321)	0.0196 (0.0205)	0.0172 (0.0173)
*w*R[d] (all data)	0.0731 (0.0738)	0.1059 (0.1073)	0.0657 (0.0678)	0.0509 (0.0514)	0.0489 (0.0490)

$R = \Sigma||F_o|-||F_c||/\Sigma|F_o|$. [d] $wR = [\Sigma w(|F_o^2|-|F_c^2|)^2/\Sigma w|F_o^2|^2]^{1/2}$

Table 3.1. Crystallographic Data and Refinement Parameters for **H(L)**, $ReBr(CO)_3$[**H**(**L**)] (**1**), {$Re(CO)_3$[**H(L)**]}(X) (X = PF_6 , **2·PF$_6$**; X = OTf, **2·OTf**), and $Re(CO)_3$(**L**), (**3**).

Distance (Å)	**1**	**2·PF$_6$**	**2·OTf**	**3**
Re-Br	2.619	---	---	---
Re-N1	2.265	2.257	2.249	2.163
Re-N11	2.182	2.174	2.169	2.173
Re-N21	---	2.180	2.174	2.148
Re-C41	1.899	1.915	1.910	1.914
Re-C42	1.928	1.944	1.936	1.923
Re-C43	1.946	1.933	1.933	1.948
C41-O1	1.164	1.149	1.150	1.158
C42-O2	1.142	1.129	1.144	1.147
C43-O3	1.091	1.140	1.139	1.138
N1H1•••N21(or O4)	1.913		2.014	
⊥N1•••(C_2Re)[a]	0.383	0.492	0.488	0.191
Angles/torsions (°)				
N1-Re-N11	77.15	77.75	76.61	79.26
N1-Re-N21	---	83.68	83.76	81.57
Fold (N11)[b]	138.81	130.62	123.45	136.17
Fold (N21)[c]	---	159.24	154.62	147.36
ReN11-N12C2	-16.09	14.07	0.61	-14.34
ReN21-N22C32	---	-9.76	-18.36	8.35
pz(N11)-tol(C1)	40.80	43.63	32.29	45.04
pz(N21)-tol(C31)	13.63	27.21	29.82	36.32
tol(C1)- tol(C31)	76.86	74.55	76.03	28.43
Σ∠'s about N1[d]	344.44	334.46	334.85	355.62

pz = mean plane of pyrazolyl ring , tol = mean plane of C_6 ring of tolyl group; [a] Distance of normal vector between N1 and mean plane of atoms Re, C1, and C31; [b] fold angle between Re and the centroids (Ct) of N1 and N11 and Ct of C1 and N12; [c] fold angle between Re and the centroids (Ct) of N1 and N21 and Ct of C31 and N22; [d] involving Re, C1, and C31.

Table 3.2. Summary of Bond Distances and Angles in Rhenium Complexes **1**-**3**.

3.4 Results and Discussion

As detailed in the **section 3.2,** the pincer ligand **HL** is prepared in two steps from commercially-available di(*p*-tolyl)amine by first *ortho*-bromination with elemental bromine to give (2-Br-*p*-tolyl)$_2$NH.[17] Subsequently, a CuI-catalyzed amination reaction of the latter with pyrazole gives the desired ligand in 70% yield.[18] The amination reaction appears to occur stepwise, as small amounts of (2-pz-*p*-tolyl)(2-Br-*p*-tolyl)NH can be isolated from incomplete reactions. As anticipated, **HL** is an electron donor giving an irreversible oxidation (i_{pc}/i_{pa} ~ 0.6; ΔE ~ 490 mV) at about 0.59 V versus Fc/Fc$^+$ in CH_2Cl_2. The colourless toluene-insoluble *fac*-ReBr(CO)$_3$[η^2N-(**HL**)] (**1**) is obtained in high yield by the reaction between the ligand and Re(CO)$_5$Br in toluene. In **1**, the ligand binds rhenium in a *cis*-chelating fashion through two of the three nitrogen donors, one from a pyrazolyl arm and the other from the sp^3-amino nitrogen, giving a pseudo-octahedral ReBrC$_3$N$_2$ kernel. Reaction of **1** with Tl(X = PF_6 or OTf) in CH_3CN affords high yields of very pale yellow {*fac*-Re(CO)$_3$[η^3N-(**HL**)]}(X) (**2·X** or simply **2**) where the ligand is facially-bound to rhenium with all three of its available nitrogen donors. Reaction of either **1** or **2·PF$_6$** with one equivalent of (NE$_4$)(OH) in CH_3CN immediately causes elimination of H_2O and (NEt$_4$)(Br or PF_6) to produce bright yellow *fac*-Re(CO)$_3$[η^3N-(**L**)] (**3**) with a nearly planar central amido nitrogen ($\Sigma\angle$'s about N1 = 356^o).

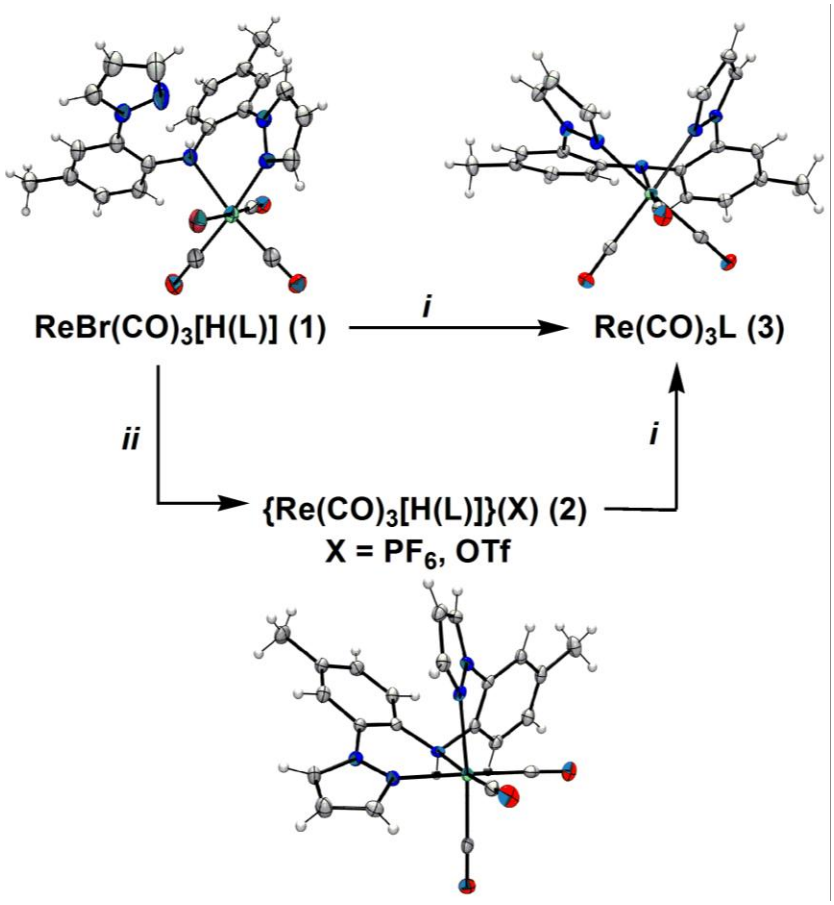

Figure 3.3. Syntheses and structures of *fac*-$Re(CO)_3$ complexes (ORTEP Ellipsoids drawn at 50% probability). Anion removed from **2·PF$_6$** for clarity. Key: *i*. 1 eq. $(NEt_4)(OH)$ in MeOH, CH_3CN, 15 min (69%); *ii*. Tl(PF_6 or OTf), CH_3CN, 12 h (80 %).

It is noted that the low thermal stability of the lithium salt **LiL** (dec. > -15^{o}C) precluded the direct synthesis of **3** from $Re(CO)_5Br$, similar to the preparation of the related PNP complex **A**. It is re-emphasized that in contrast to the PNP derivatives which possess *mer*-$ReCO_3$ cores, the complexes of **HL** have only exhibited *fac*-$ReCO_3$ moieties regardless of synthetic route. As such, the three C-O stretches of each **1**-**3 (Table 3.3)** are consistent with the low symmetry of the complexes and the

average stretching frequencies decrease in the order **2** > **1** > **3** in accord with expectations based on the increasing electron density at metal centres (and greater back- bonding). Interestingly, the IR data (KBr) for **2** and those reported for B are nearly identical despite the very different donor sets and the data for A are more consistent with those of 1 than those of 3. These observations can be reconciled by considering the *trans*-influence of different groups in the *fac*- versus *mer*- complexes.

Compound	$\nu_{C\text{-}O}$ $cm^{-1a,c}$	$E_{1/2}$ (V vs Fc/Fc^{+})[b]
1	2021, 1919, 1882; avg 1941	*irr.* E_{pa} = +1.07, +0.67, +0.23
2	2042, 1952, 1928; avg. 1974	*irr.* E_{pa} =+1.17
3	2013, 1901, 1876; avg. 1930	0.00
A[c]	2026, 1909, 1891; avg. 1942	-0.25
B[c]	2048, 1943, 1928; avg. 1973	*irr.* E_{pa} =+0.93

[a]KBr pellet; [b]CH_2Cl_2 (**1-3**) or CH_3CN(**A**&**B**), 100 mV/s, TBAH [c]Ref. 7.

Table 3.3. IR and electrochemical data for various $Re(CO)_3$ complexes.

Similar to the electrochemistry reported for PNP complexes **A** and **B,** that of **3** is distinct **(Fig. 3.4**) from its protonated derivatives **2·PF$_6$** or **1** (**Table 3.3**). Complex **3** shows a quasi-reversible oxidation[19] in CH_2Cl_2 at 0.00 V versus Fc/Fc^{+} (i_{pc}/i_{pa} = 1, but $\Delta E = E_{pa}\text{-}E_{pc}$ increases as a function of scan rate) whereas the other two complexes have irreversible oxidations ($i_{pc}/i_{pa} << 1$ and $\Delta E >> 59$ mV) at higher potentials.

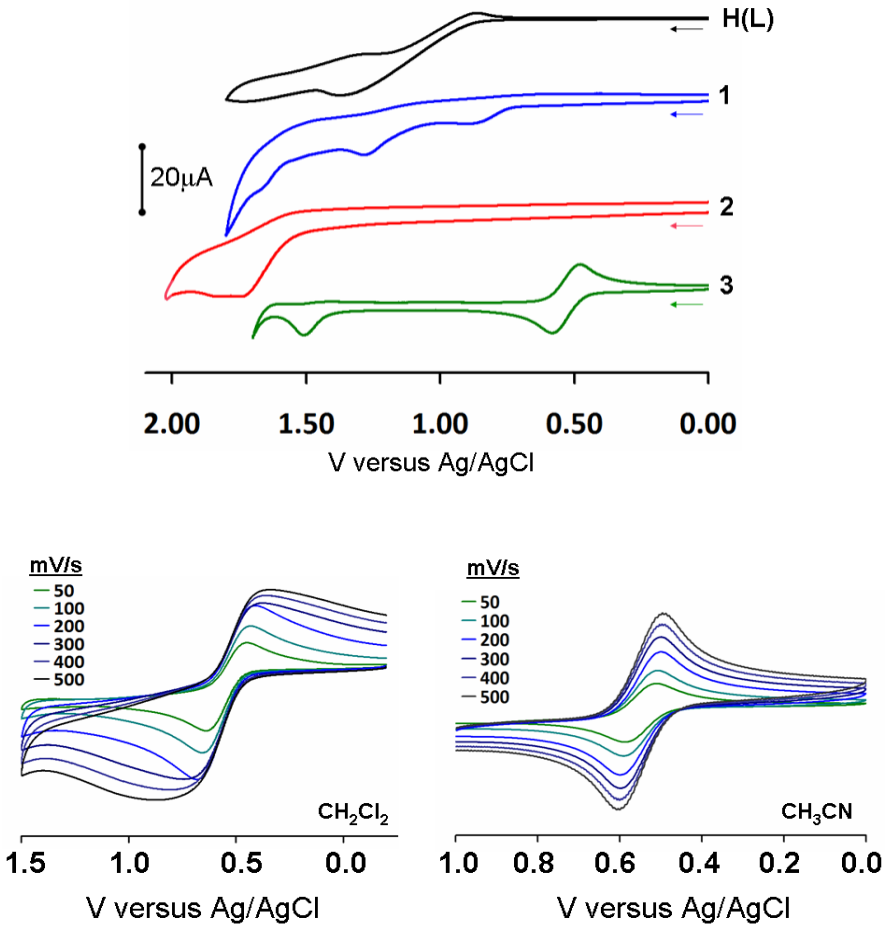

Figure 3.4. Top: Cyclic voltammograms of **3** in CH_2Cl_2 with NBu_4PF_6 as supporting electrolyte recorded at 100 mV/s. Bottom: Scan rate dependence of **3** in CH_2Cl_2 and in CH_3CN

These ligand-based oxidations in **A** or **B** are understandably more favourable than those in **3** and **2** given the relative inductive effects of PR_2 versus pyrazolyl groups on the diarylamine backbone. One-electron oxidation (**Fig. 3.5**) of **3** with AgOTf or organic oxidants forms blue-green ($\mathbf{3}^{+\bullet}$)(**X** = OTf or $SbCl_6$) that appear stable as solids but very slowly decompose ($t_{1/2}$ = 3d) at 295K in CH_2Cl_2 or CH_3CN.

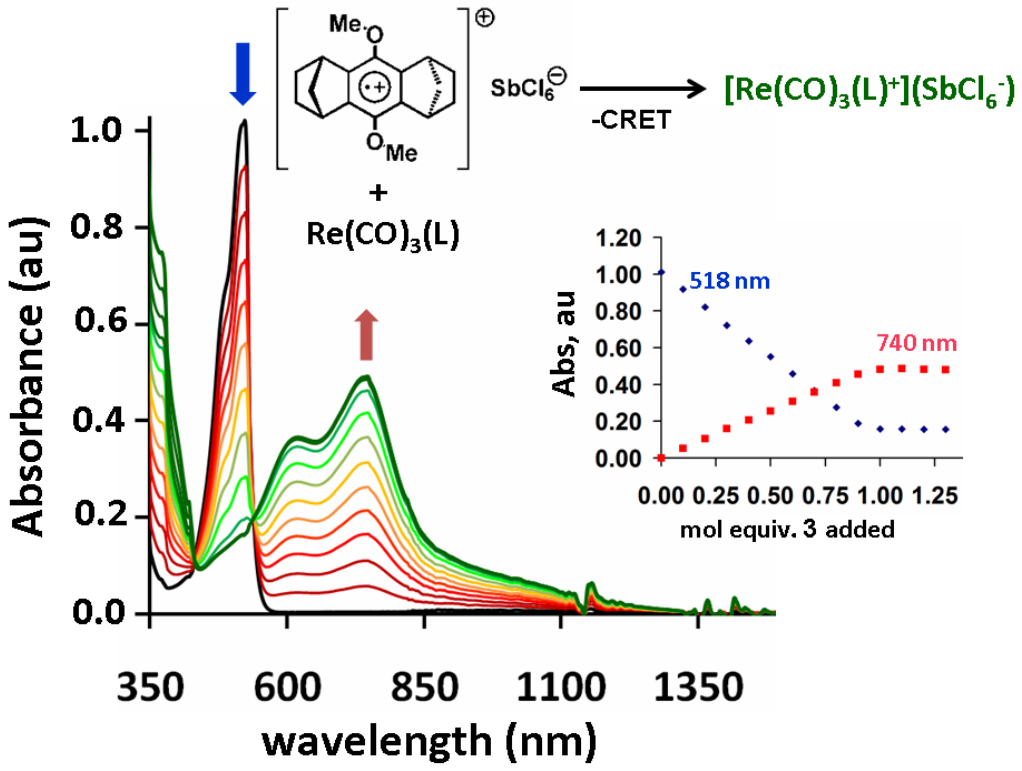

Figure 3.5. Spectrophotometric titration of **3** in CH_2Cl_2 using ($CRET^+$)($SbCl_6^-$) showing uncluttered character of one-electron transfer.

Unfortunately, it has not been possible to obtain X-ray quality crystals of (**3**$^{+\cdot}$)(**X**).

As with **A**$^+$**OTf**$^-$, the IR, and EPR spectroscopic data along with DFT calculations (UB3LYP/LACVP*) of (**3**$^{+\cdot}$) indicate a ligand-centred radical (**Fig. 3.6**). centred at g_{iso} = 2.0177 with a_{iso} = 4.95(7) mT due to the hyperfine interaction between the electronic spin and the $^{185/187}$Re nuclei (I = 5/2). At 10 K the spectrum is pseudo-rhombic and can be adequately simulated with $g_{x,y,z}$ = 2.020, 2.020, 2.005 and $a^{Re}_{x,y,z}$ = 4.0, 5.2, 4.0 mT with inclusion of a small quadrupole interaction P = 0.3 mT, ε = 0.1 mT. The relatively small deviation of g-values from that for the free electron g_e = 2.0023 and small hyperfine coupling are in line with a ligand- rather than a metal-

centred radical.[7,20] These observations are also consistent with theoretical calculations that indicate most of the spin density is located on the ligand.

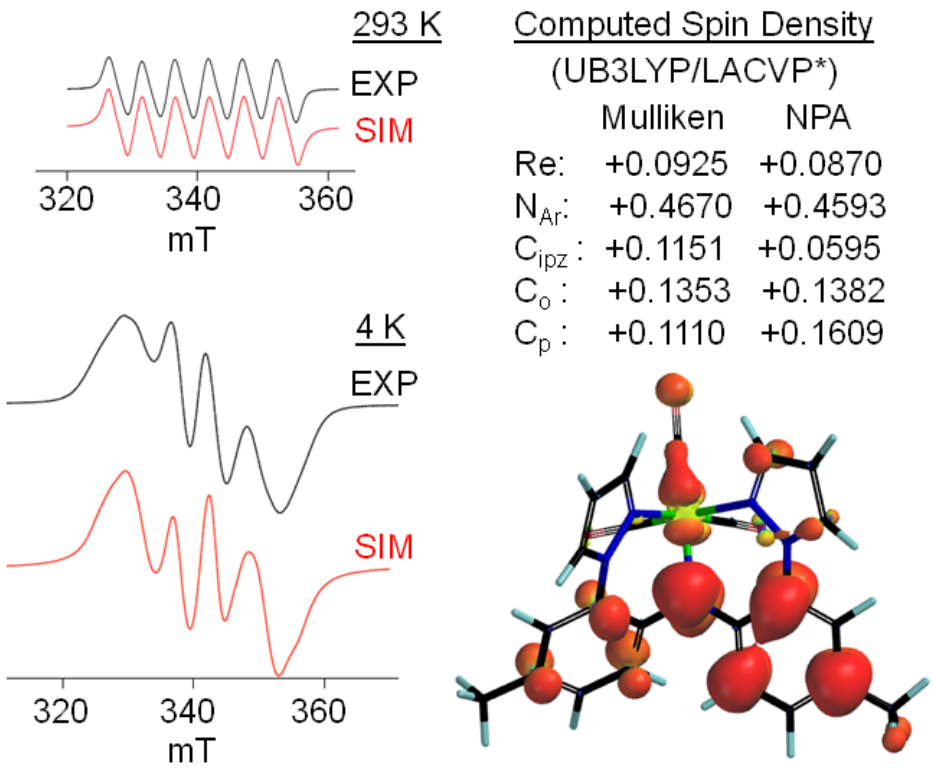

Figure 3.6. Left: X-Band (9.63 GHz) EPR spectra ($\mathbf{3}^{+\cdot}$)($\mathbf{SbCl_6}$) in CH_2Cl_2 at 293 K (top) and 10 K (bottom); Right: Spin density map from DFT calculations (UB3LYP/LACVP*).

The shift in average ν_{co} only increases (**Fig 3.7**) by 41 cm^{-1} on traversing between **3** and $\mathbf{3}^{+\cdot}$ similar to the 38 cm^{-1} increase for the PNP derivatives[7] but less than 50-100 cm^{-1} found for metal-centred oxidations.[21]

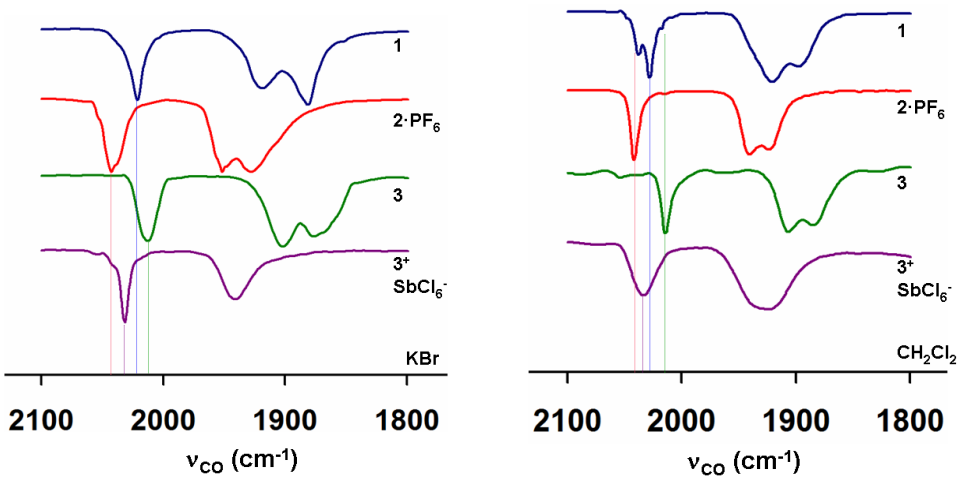

Figure 3.7. Overlay of IR spectroscopic data for carbonyl stretching region of **1** obtained from (a) KBr pellets and (b) from CH_2Cl_2 solutions

The significant differences in the optical spectra of **2·X**, **3**, and $\mathbf{3}^{+\cdot}$ (**Fig 3.8**) and the electrochemical activity of these species prompted further investigation into their potential chemical switching behaviour mediated by Brønsted acids and bases. Thus, the interconversions between **2·X** and **3** using $H(BF_4)$ and $(NEt_4)(OH)$ were monitored by both electronic absorption and voltammetric experiments (**Fig 3.9**). While these initial titration experiments showed the viability of performing AND or even INH logic operations, the reversibility over multiple reaction cycles was variable, being dependent up on the concentration mandated by the analytical technique being employed (10^{-5} M **3** for UV, 10^{-4} M for CV). The more concentrated samples afforded higher reversibility as indicated by the quantity of acid or base required to achieve the maximum signal intensity indicative of **3**.

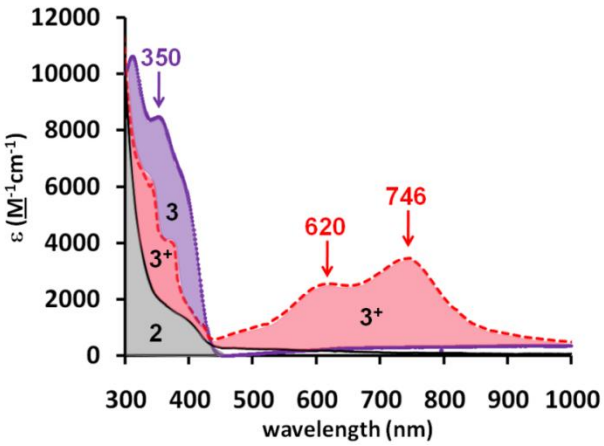

Figure 3.8. Overlay of absorption spectra of **2·PF$_6$** (grey), **3** (violet), and (**3**$^{+\cdot}$)(**SbCl$_6$**) (red) in CH_2Cl_2

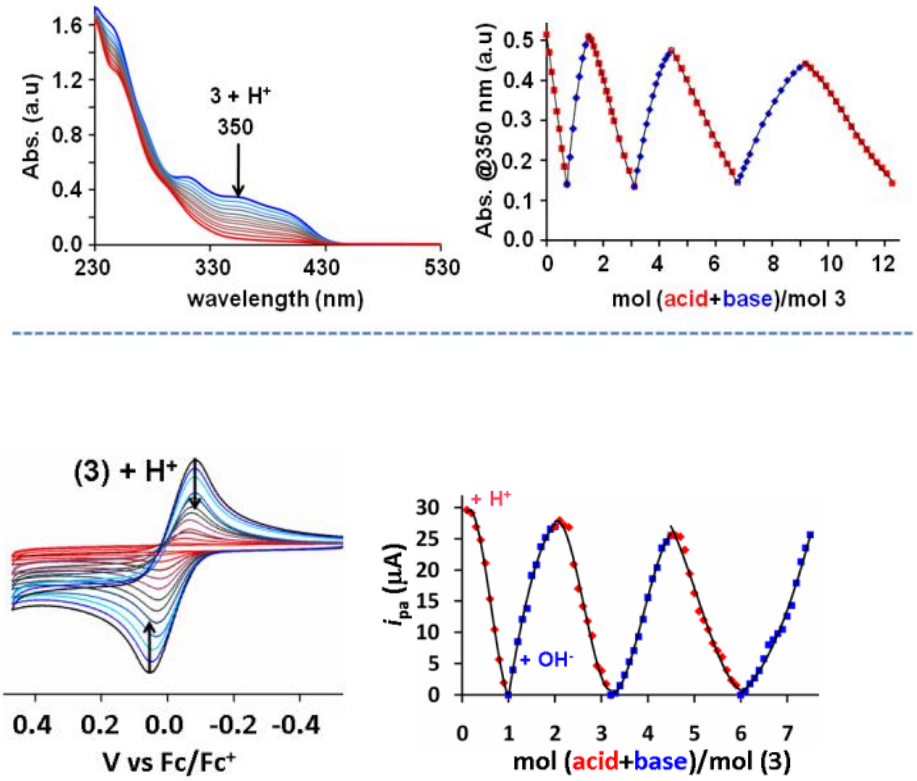

Figure 3.9. UV-Vis spectral (top) and voltammetric (bottom, 100 mV/s) changes attendant upon titration of CH_2Cl_2 solutions of **3** first with a methanolic solution of HBF_4 and then $(NEt_4)(OH)$ in MeOH to in-situ generated **2**. A minimum of three cycles are shown for each

Discussion of NMR spectra and solution structures of 1-3.

The ^{1}H NMR spectrum of pure **1** in various solvents is much more complicated than anticipated from the solid state structure owing to the presence of three species tentatively assigned based on comparison of solution properties [NMR, IR, CV, UV, ESI(+)] of related species and on molecular modeling, as arising from different (interconvertible) geometric and coordination isomers of $ReBr(CO)_3$[**H(L)**], shown in **Scheme 3.1**. That is, if the solid state structure of **1** were retained in solution (similar to the right of Scheme 3.1), the ^{1}H NMR spectrum would be expected to give a single resonance for the N-H group and two sets of signals for each pyrazolyl and tolyl groups arising from the asymmetric nature of ligand bonding (one rhenium-bound and one unbound arm of the ligand). Instead, three species are found in the NMR spectrum of **1** in CH_2Cl_2 (and other chlorinated solvents) that are most easily distinguished by the three resonances above 9 ppm for a nitrogen-bound hydrogen of each (lower left of **Figure 3.10** with assignments in **Table 3.4**). By relative integration, these three species occur in a 48:42:10 ratio at room temperature. Accordingly, there are resonances for three different species in the higher field regions of the NMR spectrum. The second most intense set of resonances corresponds to a symmetric species, presumably [*fac*-$Re(CO)_3[H(L)]^+$}(Br^-) (left of **Scheme 3.1**, vide infra), that shows only a single set of resonances each for pyrazolyl and tolyl group hydrogens. Although the structure on the left of **Scheme 3.1,** appears asymmetric, it is noted that the ^{1}H NMR spectra of **2·X** (X = PF_6, OTf) that have similar solid state structures each show a symmetric ligand environment due to rapid conformational processes that did not reach the slow exchange limit even at -80^{o}C (**Figure 3.11**).

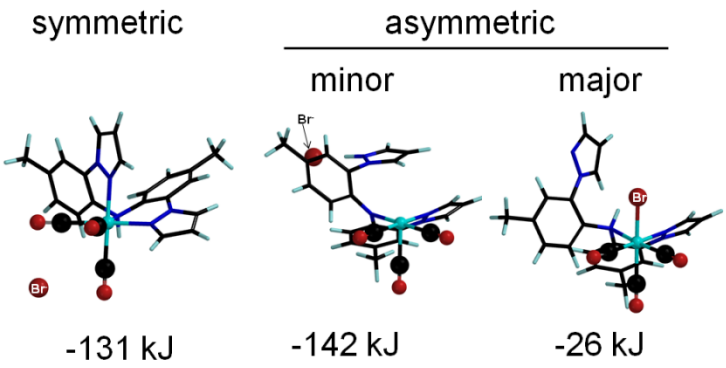

Scheme 3.1. Different low-energy (MMFF) geometric and coordination isomers of $ReBr(CO)_3$[**H(L)**].

Moreover, the chemical shifts of the symmetric bromide species are quite similar to the latter two complexes (**Table 3.4**) where subtle differences are anticipated by the presence of different anions. There are two other species that occur in an approximate 4:1 ratio whose signals are consistent with an asymmetric ligand binding environment (with two sets of pyrazolyl and two sets of tolyl hydrogen resonances for each species). The number or resonances and their chemical shifts are consistent with the expectations described above for **1**, if the solution structures of each species were similar to the solid state. The resonances in the region 6.0 to 6.7 ppm for 4-pyrazolyl hydrogens and in the region 2.2 to 2.5 ppm for tolyl-CH_3 hydrogens are sufficiently resolved **(Figure 3.13)** to allow relative integrations which reproduce the 48 (symmetric): 42 (major asymmetric): 10 (minor asymmetric) ratio observed in the N-H region of the spectrum and also allow assignments to the latter hydrogens. The resonances for the remaining hydrogens of each species could be assigned by examining the cross-peaks in the DQCOSY ^{1}H NMR spectrum (**Figure 3.15**), by their temperature dependence, as well as by comparison of chemical shifts and relative

intensities in different solvents (**Figures 3.17- to 3.19**)

	H(L)	$Re(CO)_3Br[H(L)]$ (**1**)			$[Re(CO)_3[H(L)]^+$ (**2**)		$Re(CO)_3L$ (**3**)
Assign		symm	asym min	asym maj	OTf^-	PF_6^-	
NH	8.48	11.92	11.40	9.89	9.79	7.77	---
H_3pz bnd		7.92	8.13	8.17	7.93	7.95	7.95
H_3pz unb	7.72		7.90	7.31			
H_5pz bnd		7.91	8.22	8.18	7.89	7.92	7.92
H_5pz unb	7.68		8.01	7.88			
H_4pz bnd		6.51	6.76	6.77	6.55	6.58	6.51
H_4pz unb	6.43		6.61	6.41			
Ar_{AB} bnd		7.57	6.86	7.58	7.26	7.22	7.81
Ar_{AB} unb	7.25		7.55	7.21			
$Ar_{AB'}$ bnd		7.32	5.94	7.18	7.19	7.18	7.12
$Ar_{AB'}$ unb	7.03		7.35	7.14			
Ar-H bnd		7.36	7.48	7.35	7.15	7.17	7.10
Ar-H unb	7.12		7.09	7.17			
CH_3 bnd		2.37	2.51	2.47	2.39	2.41	2.36
CH_3 unb	2.30		2.32	2.44			

Table 3.4. Summary of room temperature (293 K) ^{1}H NMR chemical shift data (CD_2Cl_2).

The signals for the major asymmetric species are most likely due to the intact complex **1** (right of Figure) on the basis of IR, cyclic voltammetry and to a lesser extent ESI(+) mass spectrometry for CH_3CN solutions. That is the solid state IR spectrum (**Figure 3.7**, left) for **1** consists of an intense sharp single A_1 (if one assumes C_{3v} local symmetry) C-O stretch at 2020 cm^{-1} which is in between that for **2·X** (2042 cm^{-1}) and **3** (2013 cm^{-1}), as expected. On the other hand, the solution (CH_2Cl_2) spectrum of **1** (**Figure 3.7**, right) consists of three sharp A_1 (if one assumes C_{3v} local symmetry) C-O stretches at 2038, 2029, and 2017 cm^{-1} (minor). The first band is consistent with the energy range for **2·X** and the lowest-energy minor band consistent with the deprotonated amido **3;** the intense band at 2029 is likely due to intact **1**. Moreover, the cyclic voltammogram of **1** recorded in CH_2Cl_2 (**Figure 3.4**) shows an irreversible wave with E_{pa} near +0.86 V (vs Ag/AgCl) due to the Br^-/Br^o couple, a fairly high-current irreversible wave with E_{pa} near +1.26 V consistent with other (NN-L)$Re^{I}Br$/(NN-L)$Re^{II}Br$ couples, and a more intense irreversible wave with E_{pa} near +1.26 V consistent with cationic (NN-L)Re^{I}/(NN-L)Re^{II} couples.[22] The ESI spectrum of **1** (**Figure 3.10-3.12**) also shows that the parent ion (100% relative intensity) at m/z = 600 is due to $\{[H(L)]Re(CO)_3]\}^+$ but even under these conditions peaks for intact **1** and those for intact **1** bound to various cations present (H^+, Na^+, K^+) under the conditions of the experiment (arising from the spectrometer, not impurities in the sample) are still observed. The assignment of the third (minor asymmetric) species as being due to the species in the middle of Scheme 3.1 is the most tentative of the assignments, which is based on the observations from simple molecular mechanics modeling (MMFF) which identified this species as the lowest-energy structure of the

multitude examined. This species can be considered as an intermediate arising from the ionization of **1** to give species such as **2**. An alternative assignment of the minor asymmetric species being due to different conformers of intact **1** where the axial and bromide groups are exchanged such that N-H and Re-CO are in the same direction with HN-ReC torsion near 0^o or a conformer with a *fac*-$Re(CO)_3$ kernel possessing a HN-ReBr torsion of 90^o was disfavored as these conformers were found to be nearly isoergonic, separated only by about 2 kcal in energy (with the latter being lowest energy), but cannot be excluded. Moreover, *trans*-$Re(CO)_3$ isomers seemed also less likely considering that only *fac*- isomers were ever observed throughout the series of coordination complexes of this ligand.

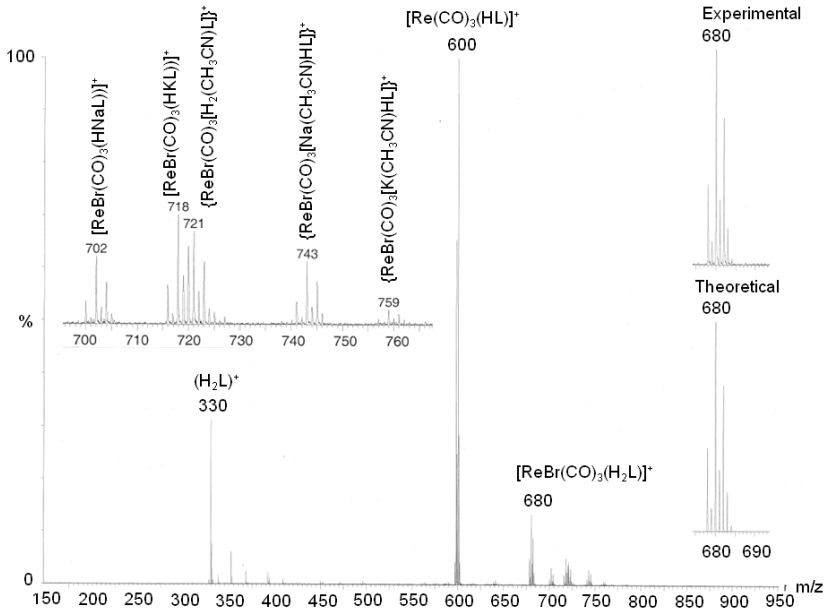

Figure 3.10. ESI(+) mass spectrum of **1** (CH_3CN).

.

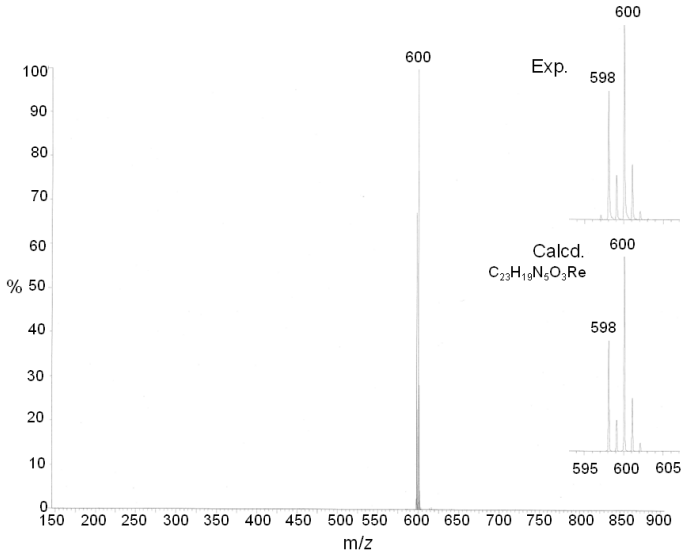

Figure 3.11. ESI(+) mass spectrum of 2·PF_6 (CH_3CN)

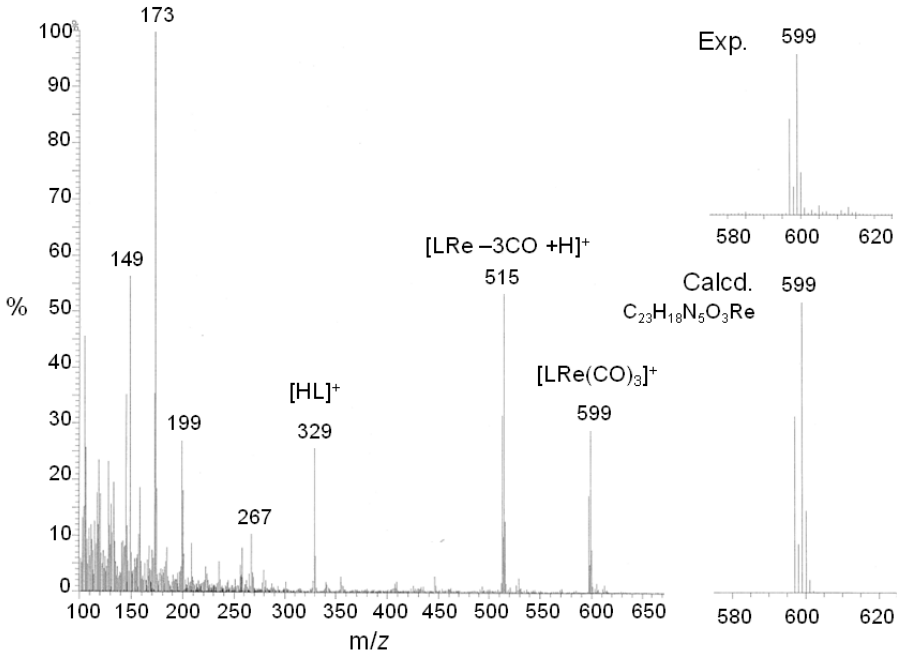

Figure 3.12. Direct Exposure Probe (EI) mass spectrum of 3.

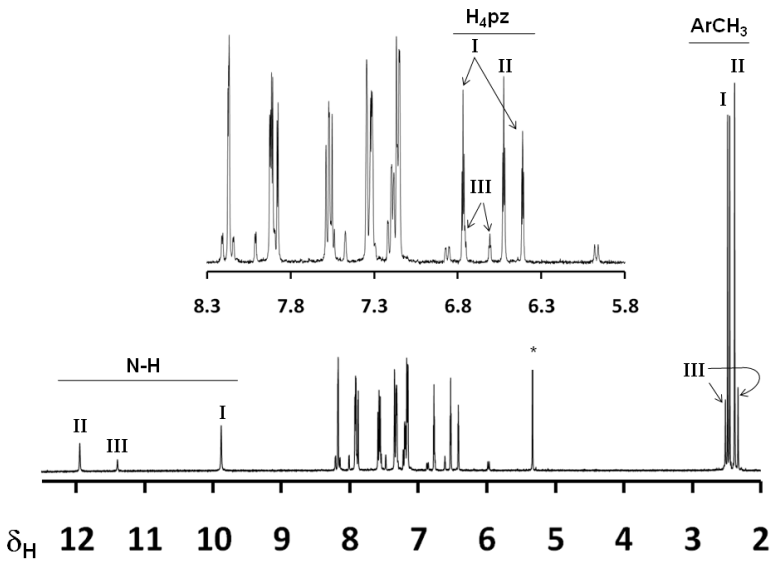

Figure 3.13. The 400 MHz ^{1}H NMR spectrum of **1** in CD_2Cl_2 (*) at 293 K with three main species **I** (major asymmetric), **II** (Symmetric), **III** (minor asymmetric) easily identified in the N-H, H_4pz, and CH_3 regions.

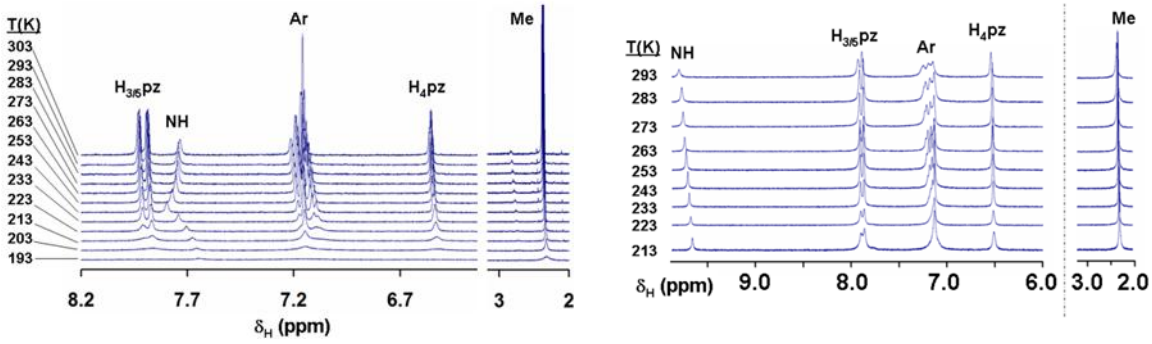

Figure 3.14. Variable temperature ^{1}H NMR spectra of **(a)** $2{\cdot}PF_6$ and **(b)** $2{\cdot}OTf$ in CD_2Cl_2.

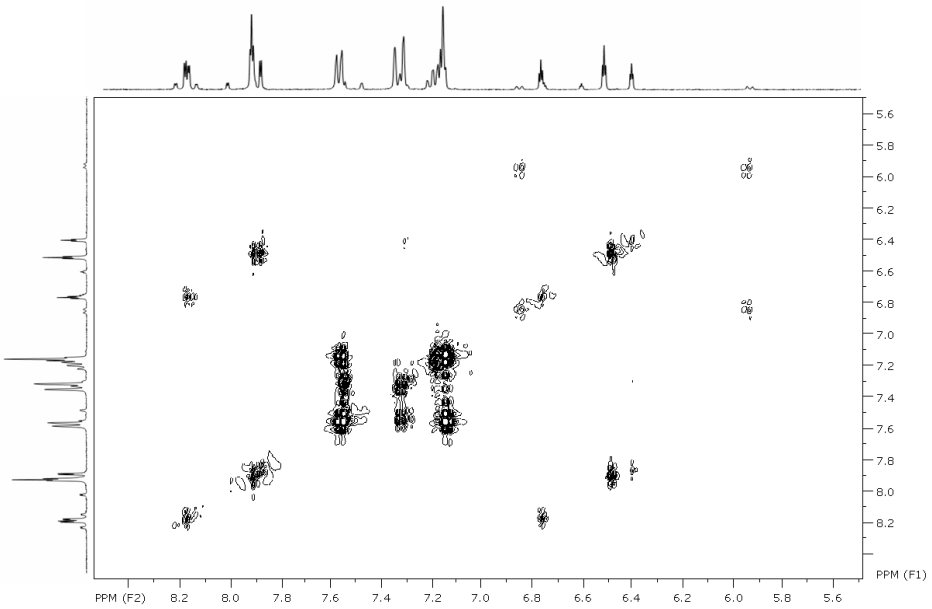

Figure 3.15. The aromatic region of the DQCOSY ^{1}H NMR spectrum (400 MHz) of 1 in CD_2Cl_2 at 293

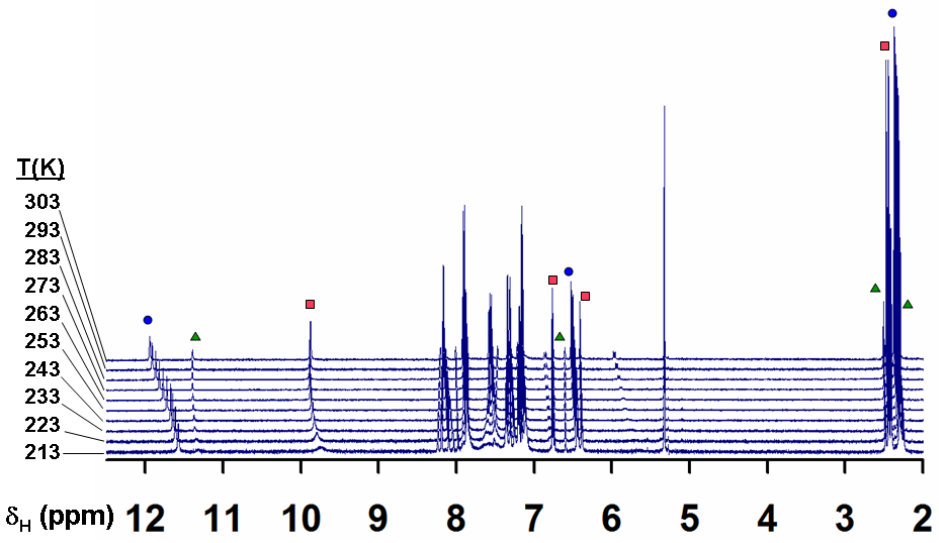

(a)

Figure 3.16.(a) General features of variable temperature ^{1}H NMR spectra of 1 in (a) CD_2Cl_2 (δ_H = 5.33 ppm)

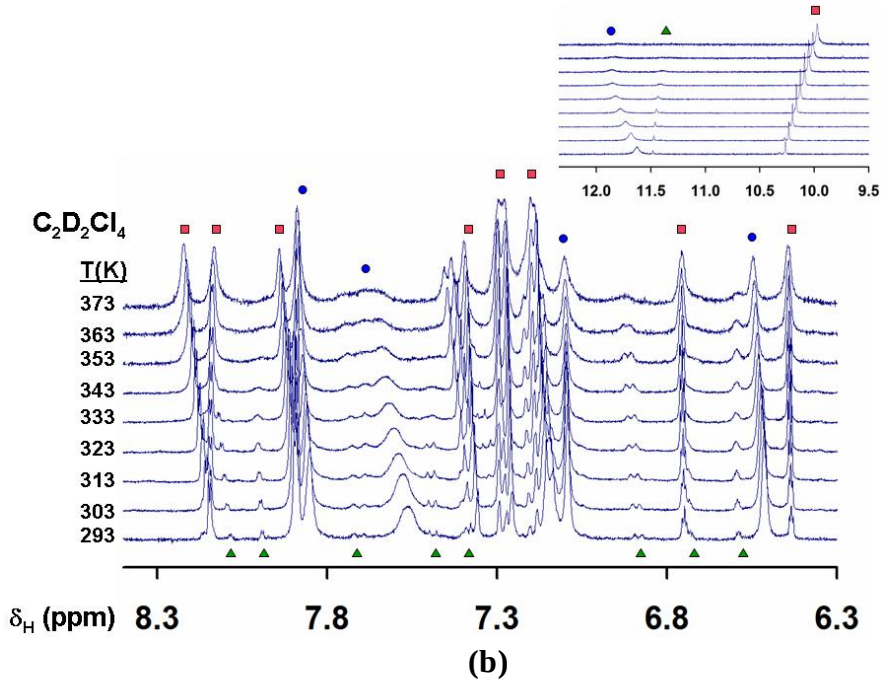

Figure 3.16.(b) General features of variable temperature ^{1}H NMR spectra of 1 in $C_2D_2Cl_4$ (aromatic region emphasized, with NH region inset). Red squares: Major asymmetric species, I; Blue circles: symmetric species, II; green triangles: Minor asymmetric species, III.

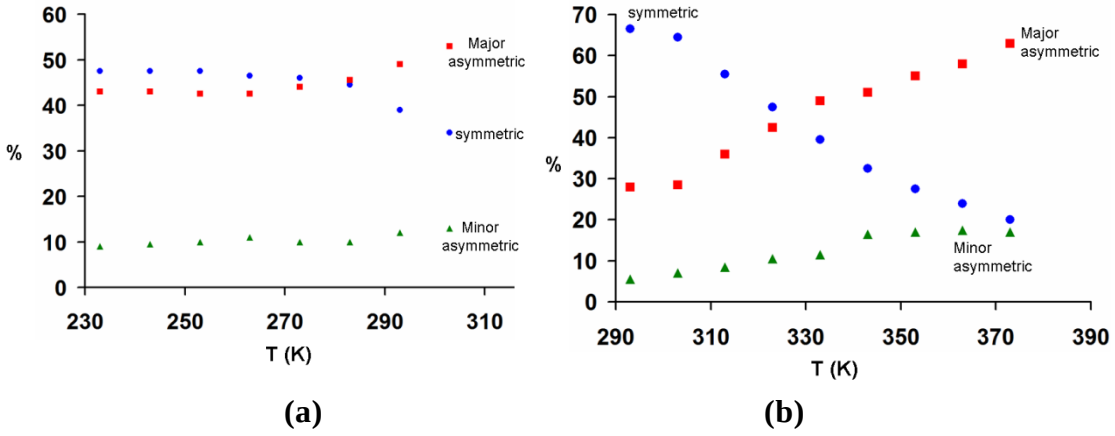

Figure 3.17. Relative composition of three species as a function of temperature, obtained by averaging the relative integrations of N-H, H_4pz, and CH_3- regions of the ^{1}H NMR spectra, of 1 in (a) CD_2Cl_2 and (b) $C_2D_2Cl_4$

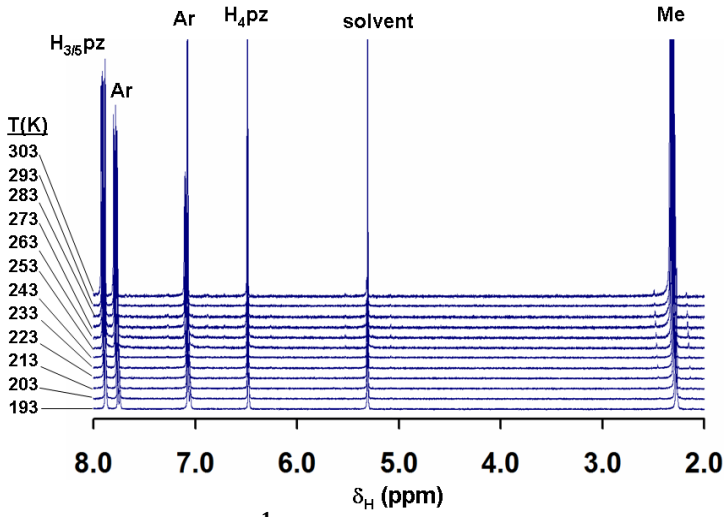

Figure 3.18. Variable temperature ^{1}H NMR spectrum of 3 in CD_2Cl_2.

Computational Details. Calculations utilized the SPARTAN'08 program suite,[23] where gas phase structures of the metal complexes were optimized using the BP86/6-31G* density functional theoretical model owing to the demonstrated success of this model when applied to other complexes.[24] In the current cases, the structures all possess C_1symmetry and the agreement between this model and solid state structures was very good with the computational model (**Figure 3-19)** closely replicating the main features of the solid state structures but with bond distances generally between 0.01 Å to 0.05 Å longer than experimental structures. Single point energy and time-dependent density functional calculations were performed on the energy-minimized structures using the hybrid B3LYP method, which incorporates Becke's three-parameter exchange functional (B3)[25] with the Lee, Yang, and Parr (LYP)[26] correlation functional where the LACVP* effective core potential[27] basis set was employed. The time-dependent density functional calculations were performed on the six lowest-energy singlet and six-lowest energy

triplet excited states of each complex **1**, $\mathbf{2}^{+}$, and **3**, but only the first six excited doublet states of $\mathbf{3}^{+}$ and the results are summarized in ref X

Conclusions

The optical and electrochemical properties of tricarbonylrhenium(I) complexes of a new electroactive NNN-tridentate ligand can be gated by reactions with Brønsted acids or bases which serve to modulate energetic access to the lone pair of electrons

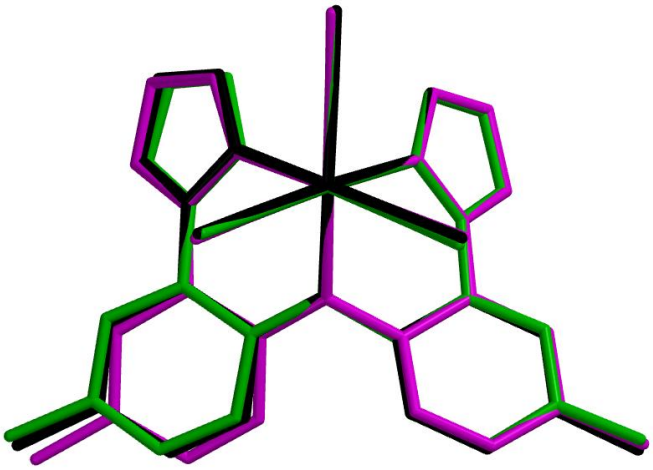

Figure 3.19. Overlay of experimental (green) and calculated structures ((u)BP86/LACVP*) for **3** (black) and $\mathbf{3}^{+}$ (pink) (hydrogens removed for clarity) and selected interatomic distances and angles tabulated.

on the central nitrogen that govern the electrochemical activity and associated electronic (n-π* or dπ- pπ) transitions. It is hoped that appropriate modifications of the ligand on either the pyrazolyls or the diarylamine portion will address the current issues of small signal losses observed during cycling reactions. From this perspective, the PNP ligands or PNN hybrids of Fig. 1 may also offer some advantages for $Re(CO)_3$ –based systems that should be examined.

CHAPTER 4

USING STERICS TO PROMOTE REACTIVITY IN *FAC*-RE(CO)$_3$ COMPLEXES OF SOME 'NON-INNOCENT' NNN-PINCER LIGANDS.

4.1 Introduction: Metal complexes of pincer ligands are receiving increased attention for studies in a wide range of topical areas from catalysis to bioinorganic and materials chemistry.[1] The appeal of these complexes arises from their generally high stability and the unusual reactivity that suitably designed ligands can impart on a metal center. Further interest is educed by emergent reports documenting non-innocent pincer variants that promote unexpected chemistry.[2] We have synthesized a new non-innocent NNN-pincer ligand based on di(2-(pyrazoyl)-*p*-tolyl)amine (Fig.4.1) and its various

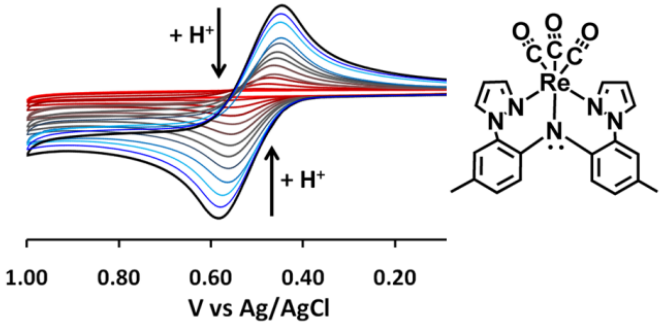

Figure 4.1. The NNN 'pincer' ligands based on di(2-(3-R-pyrazolyl)-*p*-tolyl)amines used in this work.

tricarbonylrhenium(I) complexes.[3] The quasi-reversible electrochemistry associated with the (metal-bound) ligand oxidation could be reproducibly turned 'off' or 'on' by protonation and deprotonation reactions experiments. These results were also suggested by a theoretical (DFT) study that showed that most of the spin density was located on the central amido nitrogen, substantial contributions were found at the *ortho*- and *para*- aryl carbons, and a smaller contribution extended onto a metal d-orbital During the course of that work it occurred to us that if the stability of the ligand cation radical results from hole delocalization over the entire π-conjugated diarylamine framework, it should be possible to alter the stability (i.e. increase the reactivity) of this cation or even its precursors by increasing the aryl-aryl with Brønsted acids or bases, repectively. Moreover, the one-electron oxidized product $[Re(CO)_3(\mathbf{L^H})]^+$ was demonstrated to contain a ligand-centred radical by IR and EPR dihedral angle, effectively disrupting conjugation. Inspection of the structures of $Re(CO)_3(\mathbf{L^H})$ and associated derivatives suggested that this goal could be achieved simply by placing steric bulk at the 3-position of the pyrazolyls. In this chapter we fully document the successful, yet surprising, results of these efforts including the preparation of two new NNN-pincer ligands (R = Me, iPr, Scheme 1) and the properties of their various $Re(CO)_3$ complexes.

4.2. Results and Discussion

Preparation: The syntheses of the ligands and *fac*-$Re(CO)_3$ complexes follows methodology similar to that reported for di(2-(pyrazoyl)-*p*-tolyl)amine, H($\mathbf{L^H}$) and its complexes.[3] The preparative routes to the complexes are summarized in Scheme 4.1. For the ligand syntheses described in the experimental, the CuI-catalyzed amination reactions[4] between HN(2-Br-*p*-tolyl)$_2$[5] and either 3-methyl- or 3-isopropyl-pyrazole[6]

proceeded smoothly to give 60-65% yields of H($\mathbf{L}^{Me}$) or H($\mathbf{L}^{iPr}$) simply by heating neat mixtures for 1 d at 200°C followed by conventional workup. In contrast, low yields of H($\mathbf{L}^{H}$) are obtained when heating neat reaction mixtures because unsubstituted pyrazole distils out of the reaction mixture and condenses as a solid onto cooler parts of the reaction apparatus; here, the addition of minimal xylenes helps to wash pyrazole back to the heterogeneous reaction mixture. The longer reaction time required for the preparation

Scheme 4.1. Summary of preparative routes to the various $Re(CO)_3$ complexes of the NNN-pincer ligands used in this work

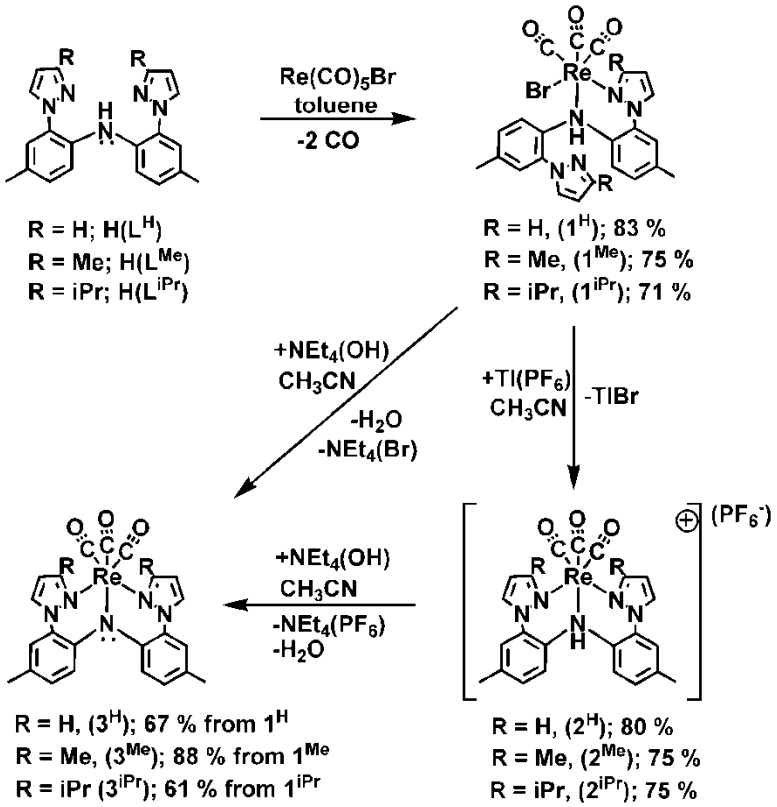

of H($\mathbf{L}^{H}$) (2d, monitored by TLC, 69% isolated yield) is likely limited by the distillation temperature of xylenes (bp = 151 °C). For the 3-organopyrazolyl derivatives, only the desired isomer of H($\mathbf{L}^{Me}$) or H($\mathbf{L}^{iPr}$) as depicted in the top left of Scheme 4.1 was

obtained (from NMR spectral data and crystallographic determinations of the free ligand, H($\mathbf{L^{Me}}$)† and of all metal complexes with these ligands). Hypothetical di(2-(5-R-pyrazolyl)-*p*-tolyl)amine isomers (with both R groups situated proximal rather than distal to the aryls) or mixed 3,5-isomers have not been detected. In the IR spectrum (KBr) of each ligand, the N-H stretching frequency occur as a medium intensity, sharp bands at rather low energy for 2^o arylamines (3261 cm^{-1} for H($\mathbf{L^{H}}$); 3297 cm^{-1} for H($\mathbf{L^{Me}}$); 3296 cm^{-1} for H($\mathbf{L^{iPr}}$)) which typically occur nearer to 3400 cm^{-1}, presumably a result of the intramolecular hydrogen bonding.[7]

The reactions between the free ligands [of general notation H($\mathbf{L^{R}}$)] and $Re(CO)_5Br$ in boiling toluene causes elimination of two equivalents of CO concomitant with the precipitation of the *fac*-$ReBr(CO)_3$[H($\mathbf{L^{R}}$)] complexes ($\mathbf{1^{R}}$) as analytically pure colorless powders. The ensuing reactions of $\mathbf{1^{R}}$ with $TlPF_6$ in CH_3CN provide {*fac*-$Re(CO)_3$[H($\mathbf{L^{R}}$)]}(PF_6) ($\mathbf{2^{R}}$). As found in related diarylamine systems,[8] complexation of the ligands to metal centers causes a progressive red-shift in the N-H stretching frequency with increasing electron density of the metal center. For instance, ν_{NH} = 3243 cm^{-1} for $\mathbf{2^{H}}$ and ν_{NH} = 3147 cm^{-1} for $\mathbf{1^{H}}$. Finally, the reactions of colorless $\mathbf{1^{R}}$ or $\mathbf{2^{R}}$ in CH_3CN with the Brønsted base (NEt_4)(OH) leads immediately to the formation of the corresponding yellow *fac*-$Re(CO)_3$($\mathbf{L^{R}}$) complexes ($\mathbf{3^{R}}$) where the hydrogen on the diarylamine has been eliminated (after reaction with hydroxide to give H_2O). Of the two routes to $\mathbf{3^{R}}$, that starting from $\mathbf{1^{R}}$ is preferred since one less synthetic step is required (and in our hands it was easier to separate $\mathbf{3^{R}}$ from NEt_4Br than from $NEt_4(PF_6)$). In either case, it is noted that the reaction time is best kept short (15 min) as longer reaction times give lower yields due to a slow but competing decomposition reaction that produces increasing

amount of 'free' ligand H($\mathbf{L^R}$); the nature of the rhenium-containing decomposition by-product is unclear. Fortuitously, the separation of $\mathbf{3^R}$ and other products is facilitated by the significantly different solubilities of the desired product and unwanted products in MeOH or in benzene and Et_2O

4.3. Solid state structure

The structures of H(L^{Me}) and the six rhenium complexes 1^R, 2^R, and 3^R (R = Me, iPr) were determined by single crystal X-ray diffraction; those of H(L^H), 1^H, 2^H, and 3^H were reported previously. Structures for the complexes are provided in **Figures 4.2-4.3**

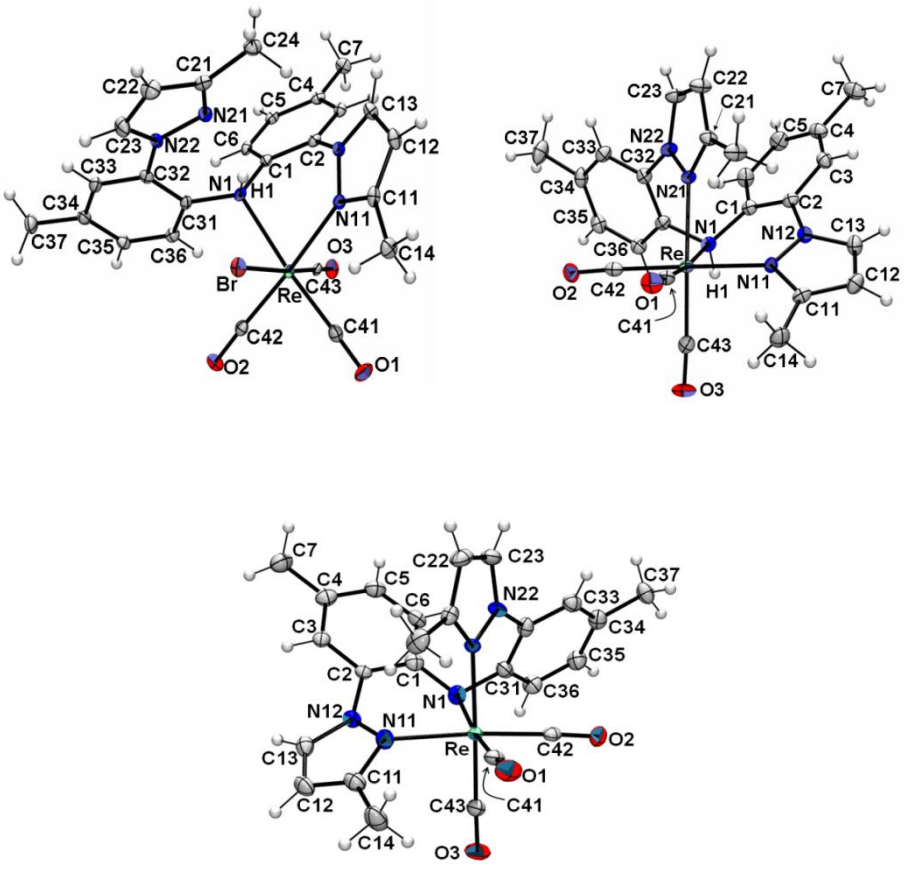

Figure 4.2. (a) Structure of *fac*-ReBr(CO)$_3$[H(L^{Me})], 1^{Me} (b) Structure of the cation in {*fac*-Re(CO)$_3$[H(L^{Me})]}(PF_6), 2^{Me} (c) Structure of *fac*-Re(CO)$_3$(L^{Me}), 3^{Me}.

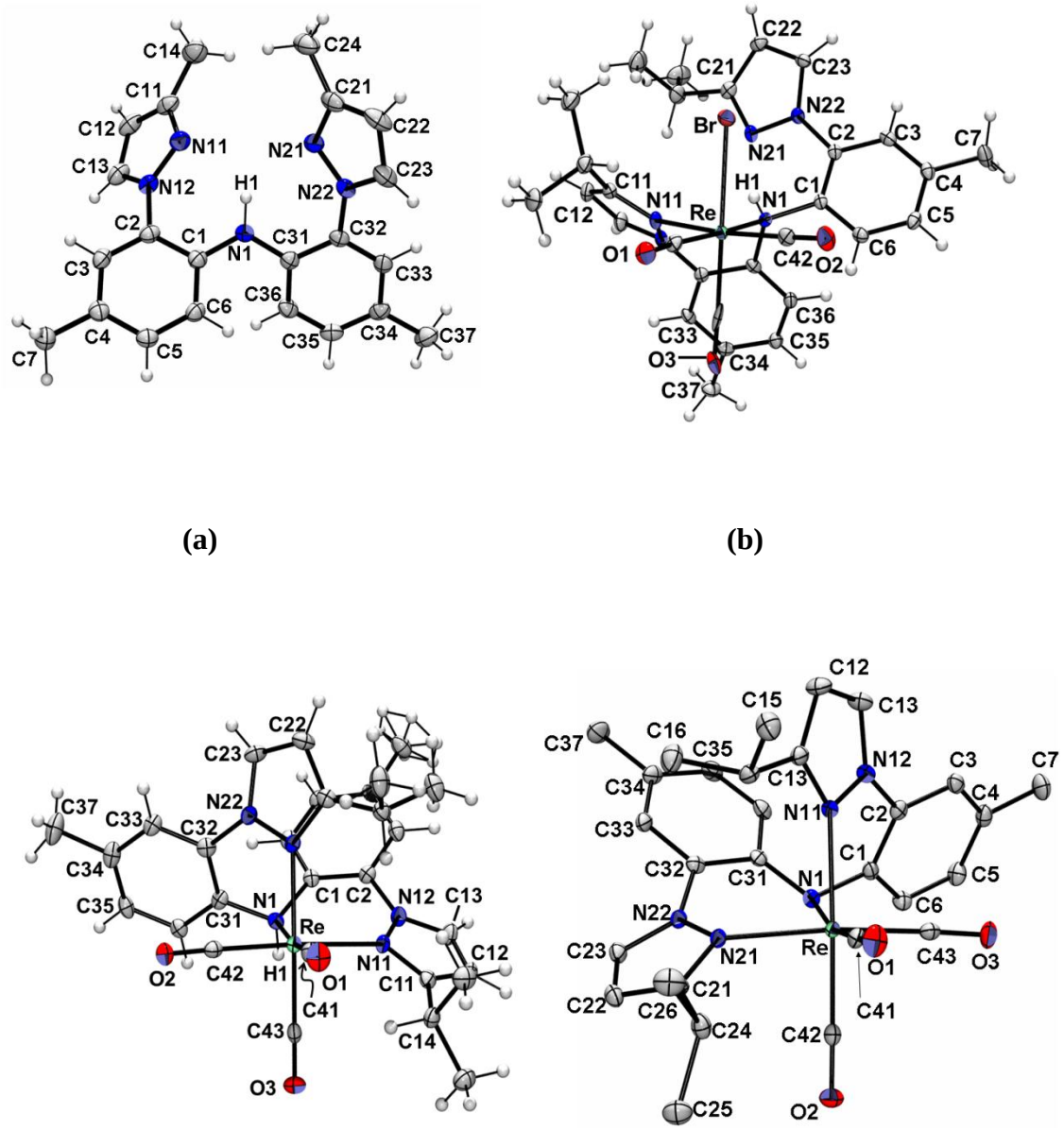

Figure 4.3.(a) Structure of H(LMe) (b) Structure of *fac*-ReBr(CO)$_3$[H(L^{iPr})], 1^{iPr} (c) Structure of cation in {*fac*-Re(CO)3[H(LiPr)]}(PF6), 2^{iPr}. The PF6- anion is removed for clarity.(d) Structure of *fac*-Re(CO)$_3$(L^{iPr}), 3^{iPr}

Selected interatomic distances and angles are listed in **Table 4.1**. All of the rhenium complexes retain the *fac*-$Re(CO)_3$ moiety and all are chiral (with C_1-symmetry) as a result of the various ligand conformations (vide infra).

Distance (Å)	$\mathbf{1}^{H}$	$\mathbf{1}^{Me}$	$\mathbf{1}^{iPr}$	$\mathbf{2}^{H}$	$\mathbf{2}^{Me}$	$\mathbf{2}^{iPr}$	$\mathbf{3}^{H}$	$\mathbf{3}^{Me}$	$\mathbf{3}^{iPr}$	$\mathbf{4}^{iPr}$
Re-Br	2.6193(8)	2.6312(3)	2.6123(3)	---	---	---	---	---	---	---
Re-N1	2.265(6)	2.268(2)	2.263(3)	2.257(4)	2.251(2)	2.265(2)	2.163(2)	2.178(3)	2.183(2)	2.306(1)
Re-N11	2.182(6)	2.198(2)	2.198(2)	2.174(3)	2.175(2)	2.187(2)	2.173(2)	2.191(3)	2.198(2)	2.177(1)
Re-N21	---	---	---	2.180(3)	2.181(2)	2.205(2)	2.148(2)	2.207(3)	2.219(2)	2.185(1)
Re-C41	1.899(8)	1.915(3)	1.932(3)	1.916(5)	1.923(3)	1.921(3)	1.914(3)	1.919(3)	1.923(2)	1.905(2)
Re-C42	1.928(8)	1.922(3)	1.934(3)	1.944(5)	1.927(3)	1.937(3)	1.923(3)	1.921(4)	1.922(2)	1.922(2)
Re-C43	1.946(8)	1.932(3)	1.947(4)	1.933(5)	1.929(3)	1.925(3)	1.948(3)	1.909(3)	1.915((2)	1.925(2)
C41-O1	1.165(9)	1.147(3)	1.132(4)	1.149(5)	1.141(4)	1.144(4)	1.158(3)	1.154(4)	1.150(3)	1.153(2)
C42-O2	1.143(10)	1.147(3)	1.136(4)	1.129(5)	1.148(4)	1.140(4)	1.147(3)	1.155(5)	1.151(3)	1.153(2)
C43-O3	1.091(9)	1.113(3)	1.050(4)	1.140(5)	1.148(4)	1.141(4)	1.138(3)	1.153(4)	1.152(3)	1.146(2)
N1H1•••N21	1.913(9)	2.03(3)	2.13(4)	---	---	---	---	---	---	---
⊥N1•••(C_2Re)[a]	0.383(8)	0.396(2)	0.385(3)	0.492(5)	0.515(3)	0.519(3)	0.191(2)	0.431(3)	0.426(2)	0.576(2)
Angles/torsions (o)										
N1-Re-N11	77.2(2)	77.91(8)	77.61(9)	77.72(13)	77.03(9)	76.30(9)	79.26(8)	76.59(10)	75.27(7)	78.25(5)
N1-Re-N21	---	---	---	83.68(13)	83.45(8)	83.57(8)	81.57(8)	84.27(11)	85.09(7)	83.30(5)
Fold (N11)b	138.8(5)	136.4(2)	135.1(2)	130.6(5)	127.0(4)	125.2(2)	136.2(2)	127.2(3)	125.5(2)	121.0(2)
Fold (N21)c	---	---	---	159.2(4)	152.6(4)	153.2(2)	147.4(2)	164.1(3)	161.9(2)	144.2(2)
ReN11-N12C2	-16.1(9)	-12.8(3)	12.0(4)	14.0(5)	5.1(3)	-1.9(3)	-14.3(3)	-1.3(4)	6.4(3)	-11.6(2)
ReN21-N22C32	---	---	---	-9.8(6)	0.4(4)	15.9(3)	8.3(3)	-36.(4)	-33.0(3)	1.5(2)
pz(N11)-tol(C1)	40.8(6)	39.8(3)	40.7(2)	43.6(5)	38.5(3)	37.3(2)	45.0(2)	38.5(2)	35.7(1)	50.9(1)
pz(N21)-tol(C31)	13.6(6)	23.7(3)	28.6(2)	27.2(5)	29.8(3)	37.2(2)	36.3(2)	37.9(2)	38.6(1)	28.9(1)
tol(C1)- tol(C31)	76.9(6)	66.7(3)	67.5(2)	74.6(4)	71.5(3)	69.7(2)	28.4(2)	78.8(2)	77.9(1)	72.9(1)
Σ∠'s about N1[d]	344.4(7)	343.2(3)	344.2(3)	334.5(4)	332.0(2)	331.7(2)	355.6(2)	338.6(3)	339.2(2)	326.1(2)

pz = mean plane of pyrazolyl ring , tol = mean plane of C6 ring of tolyl group; [a] Distance of normal vector between N1 and mean plane of atoms Re, C1, and C31; [b] fold angle between Re and the centroids (Ct) of N1 and N11 and Ct of C1 and N12; [c] fold angle between Re and the centroids (Ct) of N1 and N21 and Ct of C31 and N22; [d] involving Re, C1, and C31.

Table 4.1. Selected bond distances and interatomic angles for $\mathbf{1}^{R}$, $\mathbf{2}^{R}$, and $\mathbf{3}^{R}$ (R = H, Me, iPr

For the $\mathbf{1}^{R}$ series, the ligand is bound to the metal in a chelating κ^2N- manner via the central amino nitrogen and one pyrazolyl nitrogen. In each of these cases, the amino hydrogen is oriented toward the axial bromide rather than the axial carbonyl. For each, the rhenium-nitrogen bond involving the amino group (Re-N1, or Re-N_{Ar}, ca. 2.27 Å) is longer than that involving the pyrazolyl (Re-N11, or Re-N_{pz}, ca. 2.19 Å). The bond

distances in this series of complexes are typical of other N,N-chelating ligands containing the *fac*-$Re(CO)_3Br$ moiety such as in the closely related $Re(CO)_3Br[H(pzAn^{Me})]$ ($H(pzAn^{Me})$ is 2-pyrazolyl-4-toluidine; Re-Br = 2.628 Å, Re-N_{Ar} = 2.219 Å, and Re-N_{pz} 2.179 Å)[9] or those in the NNN-pincer- relative, $ReBr(CO)_3$[bis(1-methyl-1*H*-benzoimidazol-2-ylmethyl)amine)] (Re-Br, Re-N_{avg} = 2.23-2.28 Å).[10] Within the series $\mathbf{1^R}$, the steric profile of the 3-R-pyrazolyl substituent has the expected but small effect on Re-N_{pz} bond distances with the unsubstituted derivative having a shorter bond (2.18 Å) than the 3-substituted derivatives (ca. 2.20 Å) but there is no significant difference in the Re-N1 (amino nitrogen) bond distances (ca. 2.26 Å). Interestingly, the most striking influence of 3-pyrazolyl substitution occurs with the interatomic distances and angles associated with the 'free' arm of the ligand. For $\mathbf{1^H}$, there is a relatively short hydrogen bonding interaction between the amino hydrogen H1 and the free pyrazolyl nitrogen N21 (N1H1⋯N21: 1.91 Å, 140°) that brings the 'free' pyrazolyl and tolyl groups closer to coplanarity (dihedral between mean planes of 14°) than those rings that are bound to rhenium (dihedral between mean planes of 41°). For $\mathbf{1^{Me}}$ and $\mathbf{1^{iPr}}$, the hydrogen bonding interaction becomes progressively longer (and presumably weaker) and the pz-tolyl dihedral becomes larger with increasing steric bulk (N1H1⋯N21: 2.02 Å, 141° and pz-tolyl dihedral 24° for $\mathbf{1^{Me}}$ and N1H1⋯N21: 2.13 Å, 153° and pz-tolyl dihedral 29° for $\mathbf{1^{iPr}}$). A similar observation is made for the structures of the free ligands [two independent molecules: avg. N1H1⋯N21: 2.04 Å, 132° and pz-tolyl dihedral 30° for H($\mathbf{L^H}$); N1H1⋯N21: 2.20 Å, 129° and pz-tolyl dihedral 43° for H($\mathbf{L^{Me}}$)].

For each ionic derivative $\mathbf{2^R}$, the ligand binds rhenium in a κ^3*N*- manner giving a *fac*-ReN_3C_3 kernel. The average Re-N distances in $\mathbf{2^R}$ are shorter than the corresponding

distances in $\mathbf{1^R}$, as expected from the cationic nature of the former. Within the series of $\mathbf{2^R}$, 3-pyrazolyl substitution results in gradual increase in Re-N_{pz} distances with increasing steric bulk but, as with $\mathbf{1^R}$, substitution has little impact on the Re-N1 distances. In $\mathbf{2^R}$, there are two six-member ReN_3C_2 chelate rings that can be differentiated by small differences in Re-N_{pz} bond lengths, chelate bite and fold angles. As found in Table 4.1, one chelate ring (containing N11) has a shorter Re-N_{pz} bond, a smaller chelate bite (N1ReN11 angle) and a greater chelate ring puckering (more acute fold angle) than the other chelate ring containing N21. The chelate ring with smaller bite and fold angles in $\mathbf{2^R}$ has similar metrical parameters to those found in $\mathbf{1^R}$. A final small but noteworthy effect of changing 3-pyrazolyl substituents is found by examining the local coordination geometry around the amino nitrogen N1. The 3-organopyrazolyl groups in $\mathbf{2^{Me}}$ and $\mathbf{2^{iPr}}$ enforce greater pyramidalization about N1 (relative to the mean plane defined by C1 C31 and Re) compared to the unsubstituted pyrazolyl derivative $\mathbf{2^H}$. That is, the sum of angles about N1 ($\Sigma\angle$'s about N1, not involving N1-H1) and the perpendicular distance between N1 and the mean plane defined by C1 C31 and Re, $\perp$N1$\cdots$(C_2Re), are 332^o and 0.52 Å for $\mathbf{2^{Me}}$ and $\mathbf{2^{iPr}}$ but are 334^o and 0.49 Å for $\mathbf{2^H}$; a planar nitrogen would have ideal values of 360^o and 0 Å. In a manner similar to $\mathbf{2^R}$, the ligands in $\mathbf{3^R}$ bind rhenium in a κ^3*N*- manner giving *fac*-ReN_3C_3 kernels. Deprotonation of the amino hydrogen is accompanied by a significant shortening of the Re-N_{Ar} bond in $\mathbf{3^R}$ (ca. 2.19 Å) relative to the corresponding distances in $\mathbf{1^R}$ (ca. 2.27 Å) or $\mathbf{2^R}$ (ca. 2.26 Å). Within the series $\mathbf{3^R}$, the Re-N_{Ar} bond is longer for derivatives with 3-organo substituents (2.163(2) Å for $\mathbf{3^H}$, 2.178(3) Å for $\mathbf{3^{Me}}$ and 2.183(2) Å for $\mathbf{3^{iPr}}$). As highlighted in Fig 4.4, the structure of $\mathbf{3^H}$ is distinct from those of $\mathbf{3^{Me}}$ and $\mathbf{3^{iPr}}$ in that the

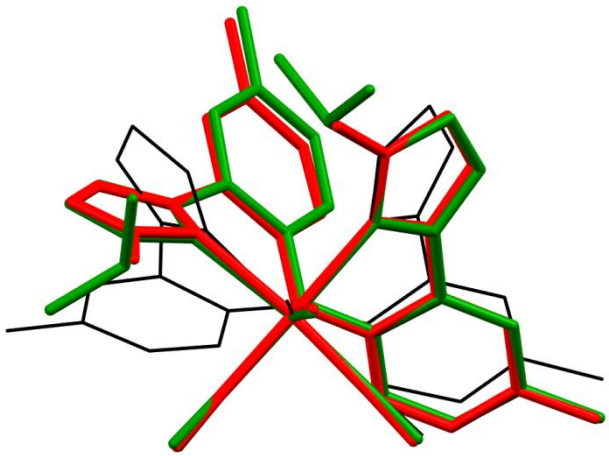

Figure. 4.4. Overlay of structures for $\mathbf{3^R}$ (R = H, black thin wireframe; R = Me, red capped stick; R = iPr, green capped stick) referenced to common $N_{Ar}Re(CO)_3$ cores

former approaches mirror symmetry (disregarding the tolyl-tolyl dihedral and slight differences in chelate ring distortions that give the complex actual C_1 symmetry) with a short average Re-N_{pz} distance (2.16 Å) and a nearly planar amido nitrogen (Σ∠'s about N1 = 356°). In contrast, the latter two complexes more closely resemble their protonated counterparts $\mathbf{2^{Me}}$ and $\mathbf{2^{iPr}}$ each with decidedly C_1 symmetry. Relative to $\mathbf{3^H}$, $\mathbf{3^{Me}}$ and $\mathbf{3^{iPr}}$ have longer Re-N_{pz} bond distances (2.20 Å for $\mathbf{3^{Me}}$ and 2.21 Å for $\mathbf{3^{iPr}}$) and more pyramidal amido nitrogens (Σ∠'s about N1 = 339° for each). Presumably, potential steric interactions involving 3-organopyrazolyl groups enforce the observed C_1 symmetric conformations, and make hypothetical pseudo-C_s symmetric conformations of either $\mathbf{3^{Me}}$ or $\mathbf{3^{iPr}}$ much higher energy.

4.4. Solution Characterization

We previously demonstrated that analytically pure samples of 1^{H}, when dissolved in Lewis donor or chlorocarbon solvents give unexpectedly complex data due to ionization equilibria. That is, both electrochemical measurements (CV) and solution IR spectroscopy showed multiple signals; one main set of signals was thought to be due to intact 1^{H} while another set of lower intensity signals was thought to be for $[Re(CO)_3[H(L^{H})^{+}](Br^{-})$ based on the similarity of the signals with 2^{H}.

For $\mathbf{1^{R}}$ (R = Me, iPr), the collective IR, electrochemical, ESI(+) MS, and NMR data indicate that multiple species also exist in solution with intact $\mathbf{1^{R}}$ being the predominant species at room temperature in either dichloromethane or tetrachloroethane. For $\mathbf{1^{R}}$ (R = Me, iPr), the large disparity in mixture composition renders ^{1}H NMR spectroscopy a more suitable (sensitive) method for illustration of mixture composition than IR or CV data. For instance, a comparison of well-resolved region for the H_4-pyrazolyl resonances in the ^{1}H NMR spectrum is shown in Figure 4.5; full and partial NMR spectra for all species are provided in Figures 4.5-4.10. For $\mathbf{1^{H}}$, resonances for three species (*I*, *II*, and *III*) are easily identified in the bottom of Fig 4.5. Again, based on different experimental lines of evidence, species *I* was previously assigned as the intact $\mathbf{1^{H}}$, species *II* was the six-coordinate ionic species$[Re(CO)_3[k^{3}N\text{-}H(\mathbf{L^{H}})^{+}](Br^{-})$, and species *III* was assigned as the five-coordinate ionic species, $[Re(CO)_3[k^{2}N\text{-}H(\mathbf{L^{H}})^{+}](Br^{-})$. Similarly, for $\mathbf{1^{R}}$ (R = Me, iPr) confident assignments as to the two predominant species that exist in halocarbon solutions can be made from the combination of NMR, IR and cyclic voltammetry. For instance, Figure 4.6 shows the NMR and IR spectra of the various derivatives $\mathbf{1^{Me}}$, $\mathbf{2^{Me}}$,

and $\mathbf{3}^{\mathbf{Me}}$ which demonstrate that when $\mathbf{1}^{\mathbf{Me}}$ is dissolved in CH_2Cl_2, the major species in the resulting mixture is $\mathbf{1}^{\mathbf{Me}}$ while

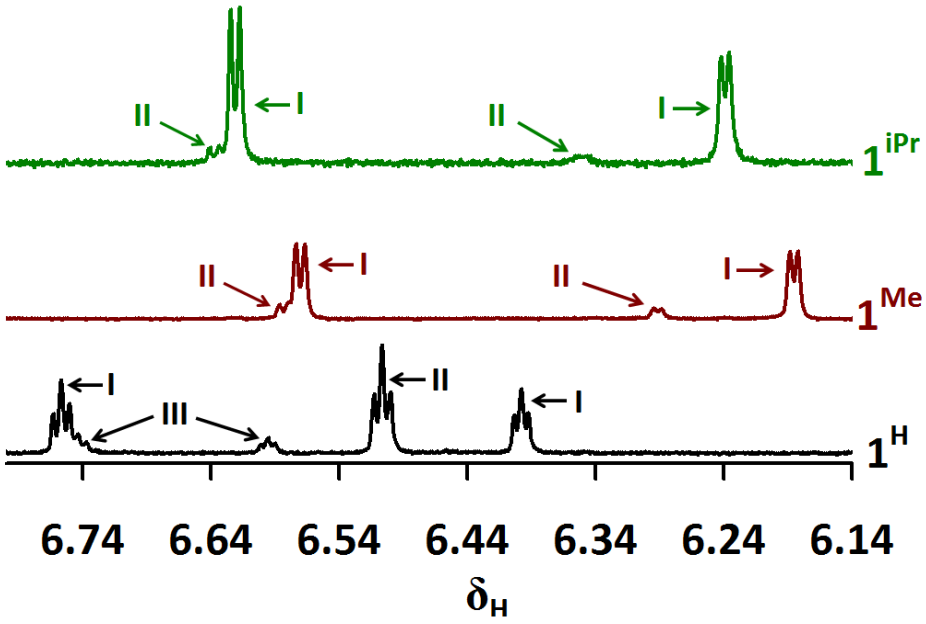

Figure 4.5 Comparison of the H_4-pyrazolyl resonance regions in the 295 K ^{1}H NMR spectra of $\mathbf{1}^{\mathbf{R}}$ (R = H, bottom; Me, middle; iPr, top)

the minor component is likely $[Re(CO)_3[\kappa^2\textit{N}\text{-H}(\mathbf{L}^{\mathbf{Me}})^+](Br^-)$ given the similarity of the ^{1}H NMR resonances and C-O stretching frequencies between $\mathbf{2}^{\mathbf{Me}}$ and the minor component of the mixture obtained from $\mathbf{1}^{\mathbf{Me}}$. The subtle differences in the signals for $\mathbf{2}^{\mathbf{Me}}$ and $[Re(CO)_3[\kappa^2\textit{N}\text{-H}(\mathbf{L}^{\mathbf{Me}})^+](Br^-)$ are likely due to the variable capacity for the different anions to interact (i.e. participate in hydrogen bonding interactions) with acidic protons in the complexes. It is noted from the IR and NMR spectrum of dichloromethane solutions species attributed to ionization isomers of $\mathbf{1}^{\mathbf{Me}}$ are less abundant than those in $\mathbf{1}^{\mathbf{H}}$**)**. In the case of $\mathbf{1}^{\mathbf{iPr}}$, the minor ionization isomers are even less abundant than in $\mathbf{1}^{\mathbf{Me}}$ (Figs. 4.7, 4.11, and 4.12)

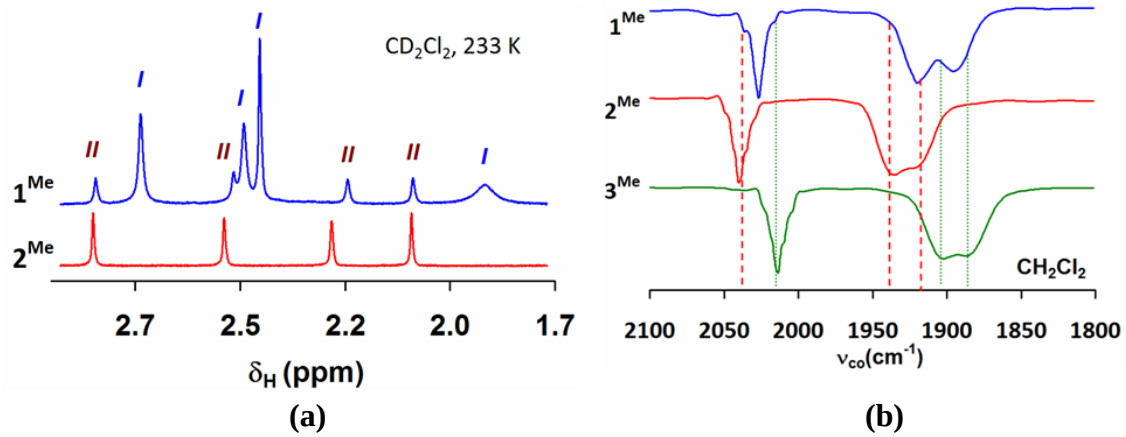

Figure 4.6. Comparison of the up-field (methyl) region of the ^{1}H NMR spectra and the C-O stretching region of the IR spectrum for $\mathbf{1}^{\mathbf{Me}}$, $\mathbf{2}^{\mathbf{Me}}$, and $\mathbf{3}^{\mathbf{Me}}$ in CH_2Cl_2 emphasizing that major component of mixture in CH_2Cl_2 is intact $\mathbf{1}^{\mathbf{Me}}$, while the minor component is likely $[Re(CO)_3[\eta^2$*N*-H($\mathbf{L}^{\mathbf{H}}$)$^+$](Br$^-$

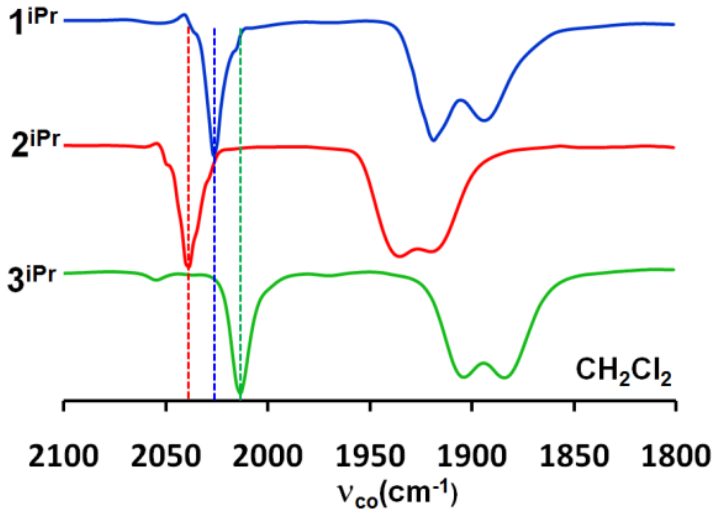

Figure 4.7. Comparison of the C-O stretching region of the IR spectrum of $\mathbf{1}^{\mathbf{iPr}}$, $\mathbf{2}^{\mathbf{iPr}}$, and $\mathbf{3}^{\mathbf{iPr}}$ in CH_2Cl_2

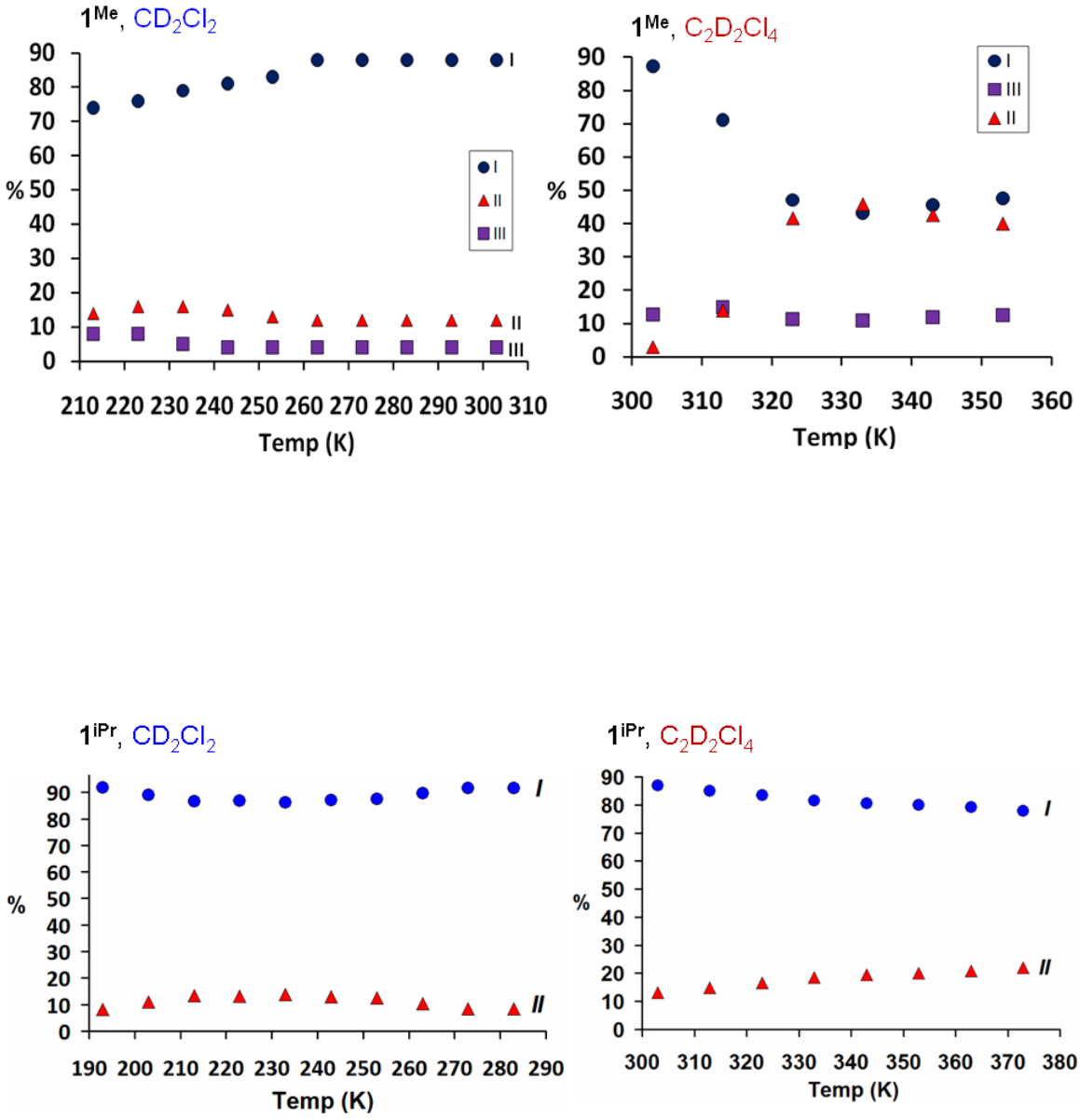

Figure 4.8 Top: Temperature and solvent-dependent composition of mixtures obtained by dissolving pure $\mathbf{1^{Me}}$ in CD_2Cl_2(left) or $C_2D_2Cl_4$ (right) as measured by relative integration ^1H NMR resonances in H_4-pz region of spectra. Bottom: Similar plots for CD_2Cl_2(left) or $C_2D_2Cl_4$ (right) solutions of $\mathbf{1^{iPr}}$ but very minor resonances for thirds species not shown owing to poor signal-to-noise (see ensuing figures) that hinders reliable integrations

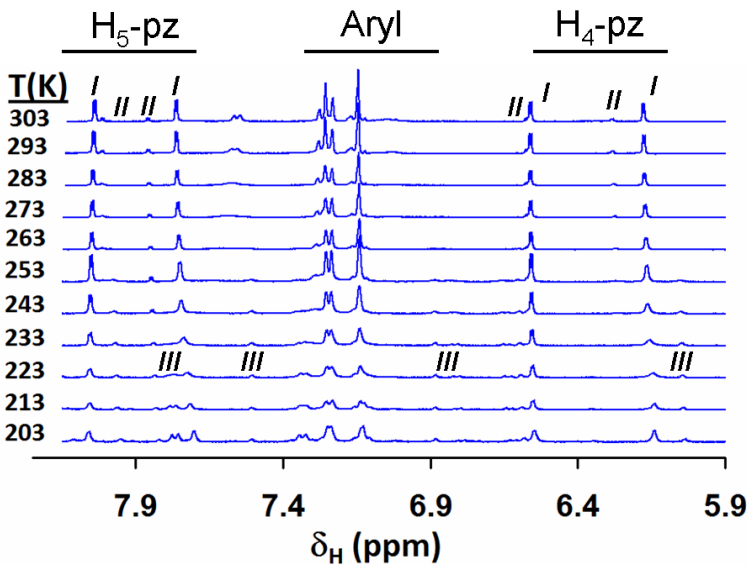

(a)

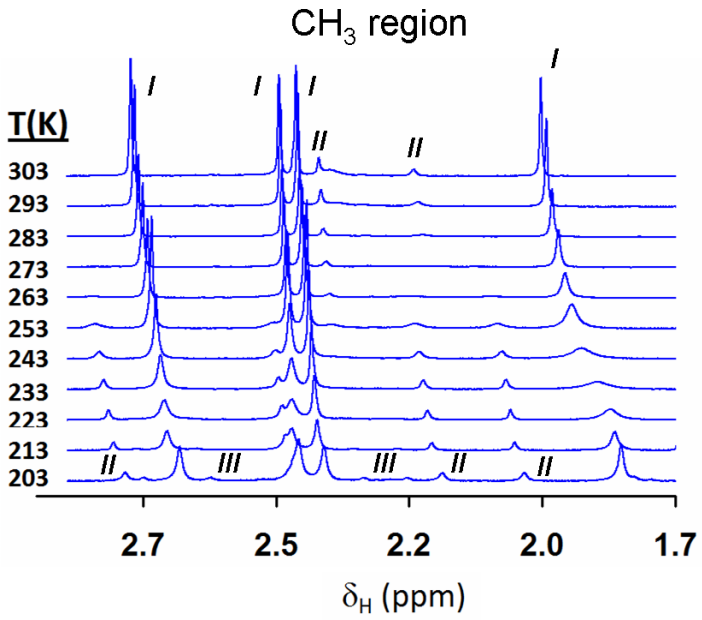

(b)

Figure 4.9. Variable (Low) temperature ^{1}H NMR spectra of **1**^{Me} in CD_2Cl_2 between 193 K and 303 K. (a) aromatic region, (b) methyl region

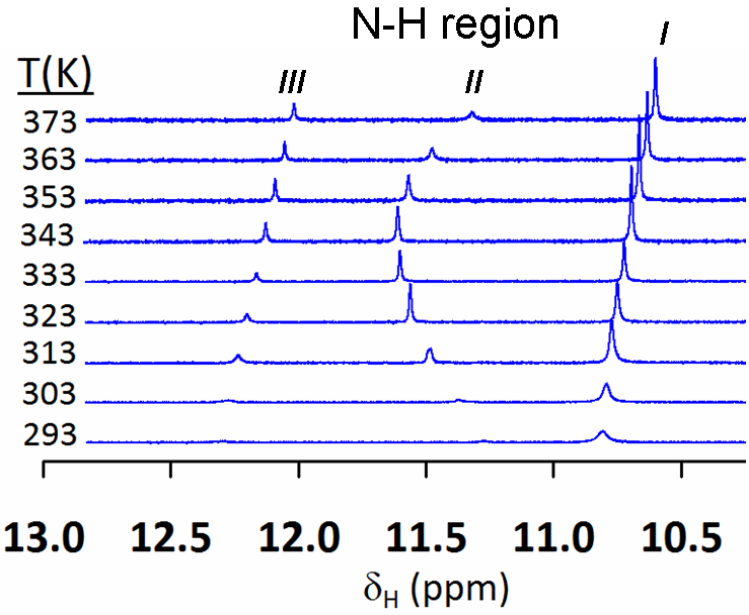

(a)

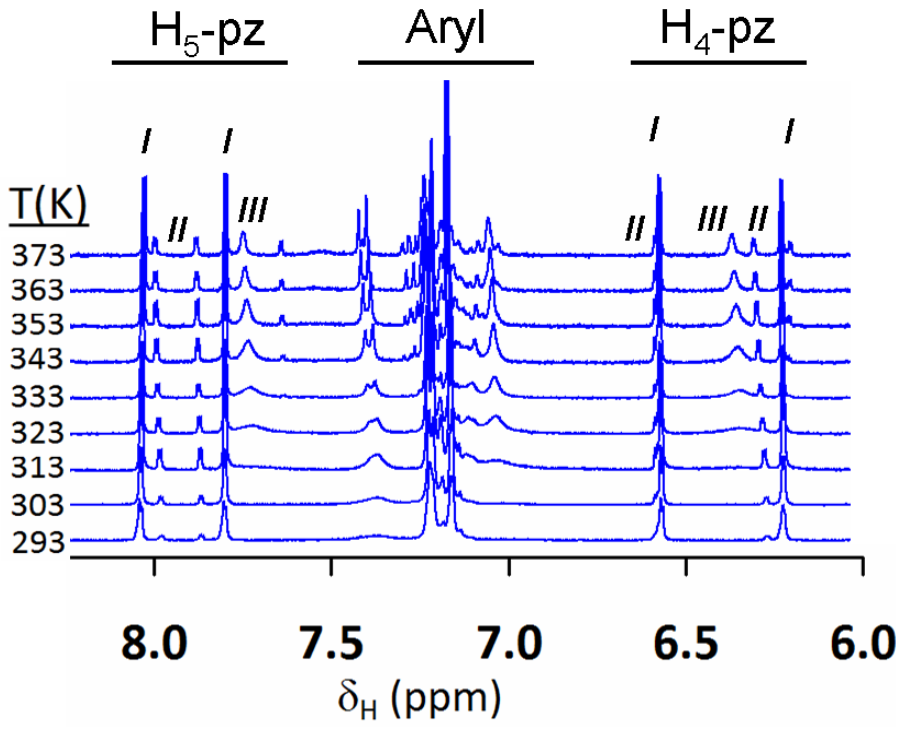

(b)

Figure 4.10. Variable (High) temperature ^{1}H NMR spectra of **1^{Me}** in $C_2D_2Cl_4$ between 293 K and 393 K. (a) N-H region, (b) aromatic region

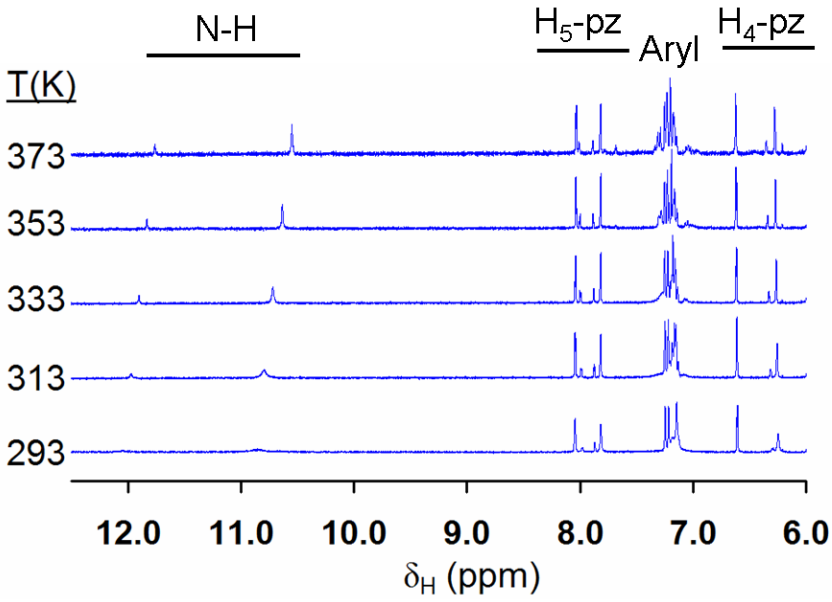

(a)

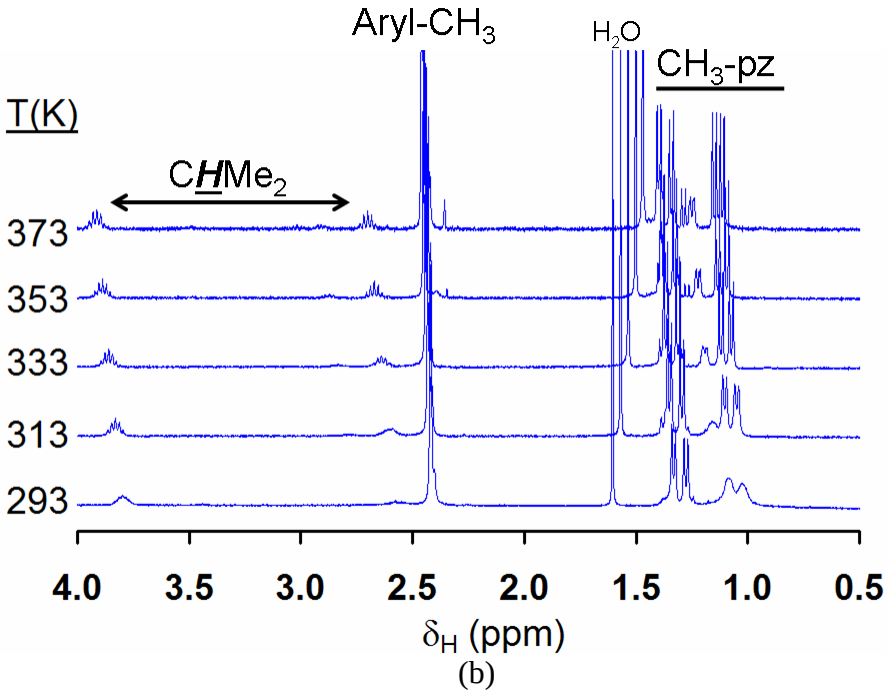

(b)

Figure 4.11. Variable (High) temperature ^{1}H NMR spectra of **1^{iPr}** in $C_2D_2Cl_4$ between 293 K and 373 K. (a) Downfield N-H and aromatic regions; (b) upfield region (where H_2O is an impurity in the solvent).

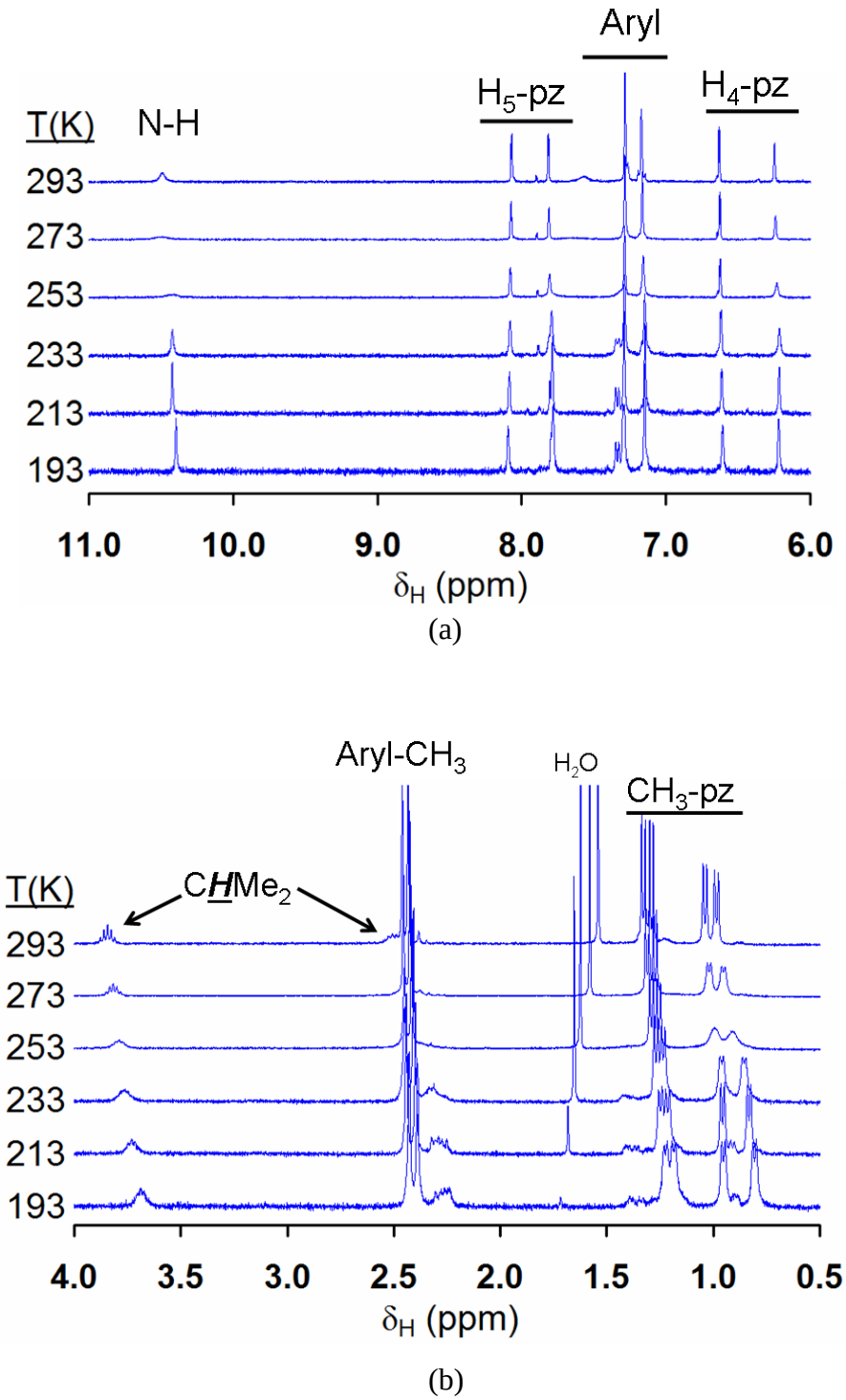

Figure 4.12. Variable (Low) temperature ^{1}H NMR spectra of **1**$^{\mathbf{iPr}}$ in CD_2Cl_2 between 193 K and 293 K. (a) downfield region, (b) upfield region (where H_2O is an impurity in the solvent).

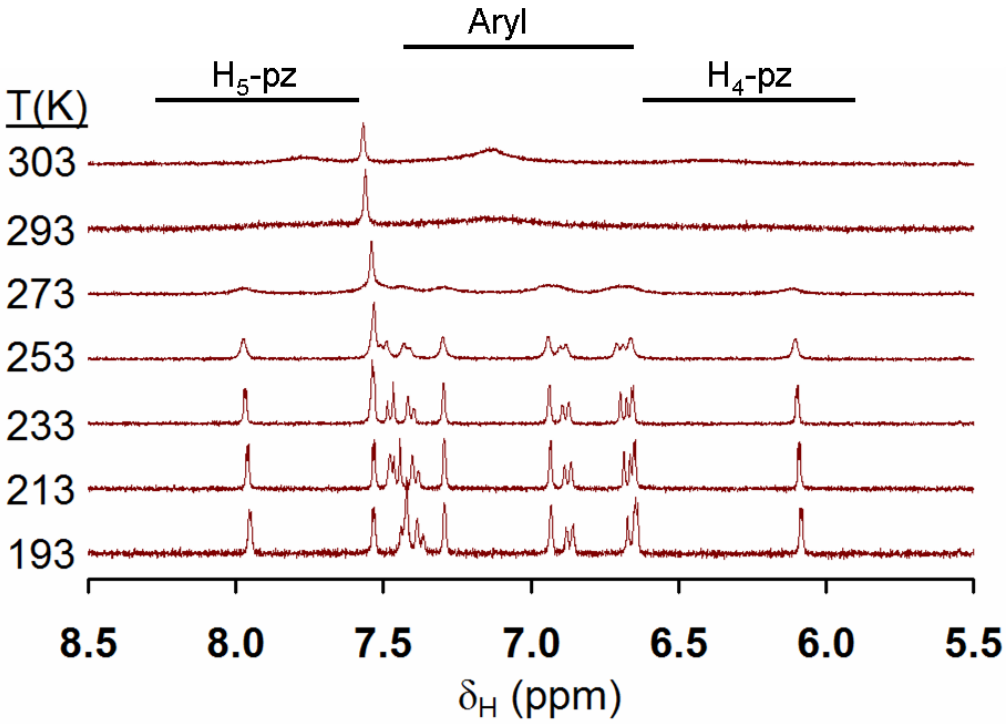

(a)

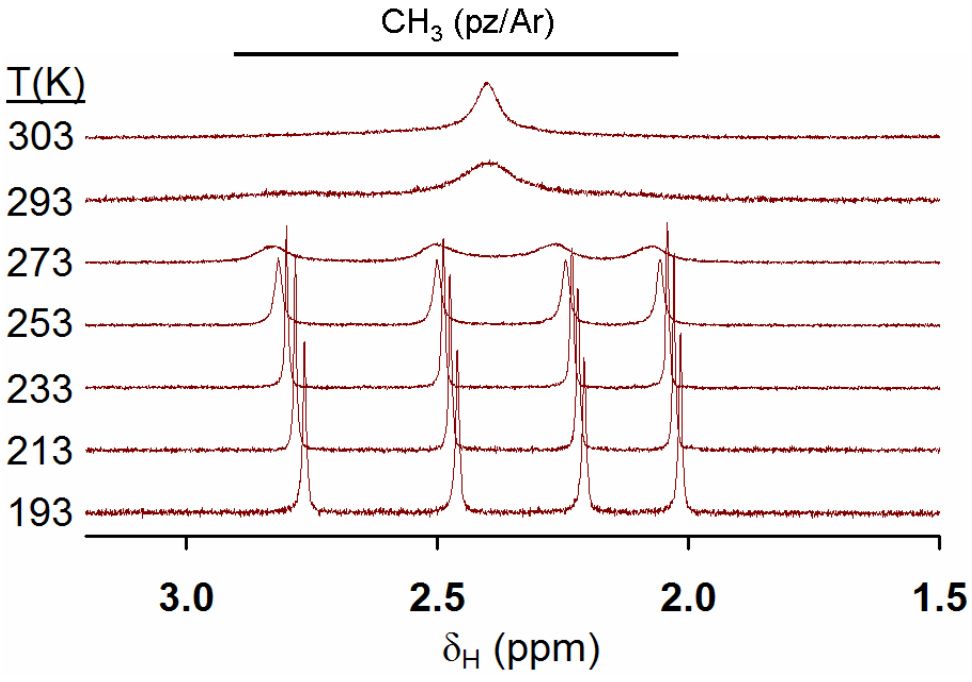

(b)

Figure 4.13. Variable temperature ^{1}H NMR spectra of **2**$^{\mathbf{Me}}$ in CD_2Cl_2 between 193 K and 293 K. (a) downfield region, (b) upfield region

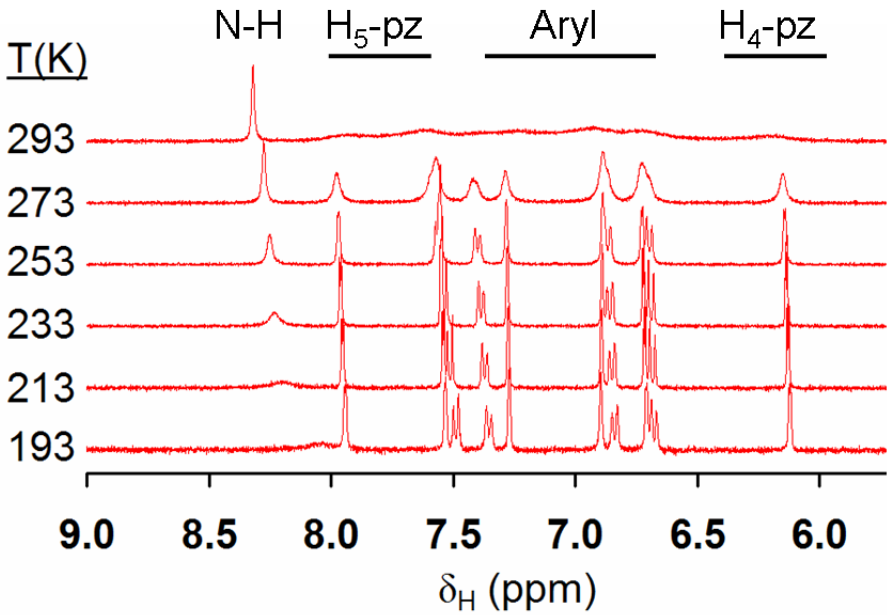

(a)

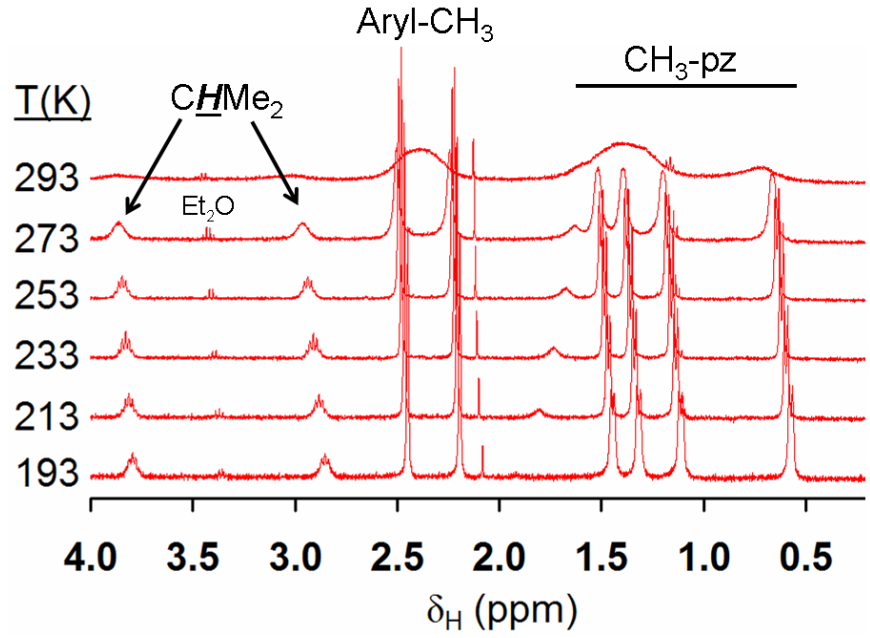

(b)

Figure 4.14. Variable temperature ^{1}H NMR spectra of **2^{iPr}** in CD_2Cl_2 between 193 K and 293 K. (a) downfield region, (b) upfield region

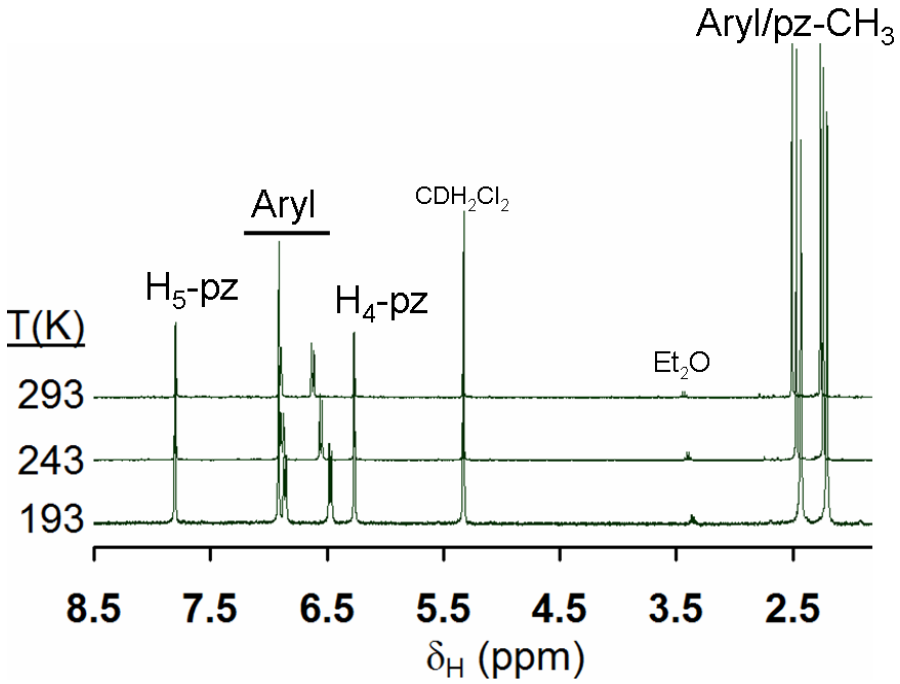

(a)

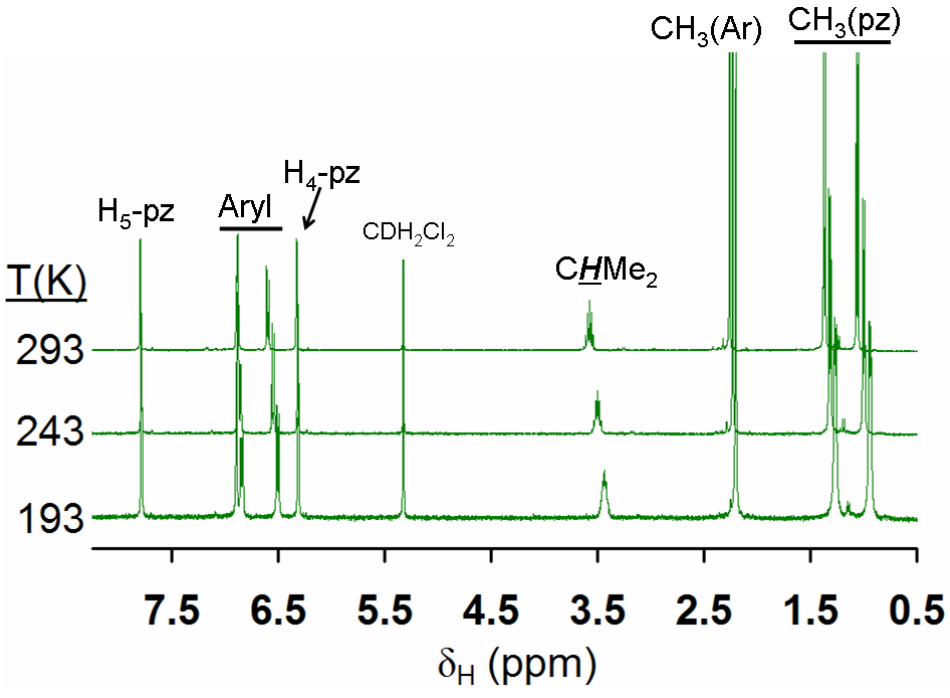

(b)

Figure 4.15. The ^{1}H NMR spectra of (a) $\mathbf{3^{Me}}$ and (b) $\mathbf{3^{iPr}}$ in CD_2Cl_2 between 193 K and 293 K.

Selected electrochemical and IR spectral data for complexes $\mathbf{1^R}$-$\mathbf{3^R}$ (R = H, Me, iPr) are given in **Table 4.2**. The current discussion of solution properties will center on the data for $\mathbf{3^R}$ because of their interesting electronic properties and disparate reactivity patterns is the focus of this work.

Compound	$\nu_{C\text{-}O}$ (cm^{-1})[a]	$E_{1/2}$ (V vs Fc/Fc^+)[a,b]
$\mathbf{1^H}$	2029, 1921, 1898; avg 1949[c]	*irr*. E_{pa} = +1.07, +0.67, +0.23
$\mathbf{1^{Me}}$	2027, 1920, 1896; avg. 1948[c]	*irr*. E_{pa} = +1.04, +0.75, +0.25
$\mathbf{1^{iPr}}$	2027, 1919, 1894; avg. 1947[c]	*irr*. E_{pa} = +1.04, +0.75, +0.20
$\mathbf{2^H}$	2040, 1950, 1930; avg. 1973	*irr*. E_{pa} =+1.17
$\mathbf{2^{Me}}$	2040, 1935, 1919; avg 1965	*irr*. E_{pa} =+1.27
$\mathbf{2^{iPr}}$	2038, 1936, 1921; avg 1965	*irr*. E_{pa} =+1.25
$\mathbf{3^H}$	2013, 1901, 1876; avg. 1930	+0.001
$\mathbf{3^{Me}}$	2009, 1903, 1879; avg. 1930	-0.011
$\mathbf{3^{iPr}}$	2008, 1898, 1876; avg. 1927	-0.015
$\mathbf{(3^H)^+}$	2034, 1927; avg. 1963	---
$\mathbf{(3^{Me})^+}$	2038, 1931; avg. 1967	---
$\mathbf{(3^{iPr})^+}$	2038, 1933; avg. 1968	---
$\mathbf{4^{Me}}$	2036, 1930, 1923; avg. 1963	not measured
$\mathbf{4^{iPr}}$	2033, 1927, 1915; avg.1958	not measured

[a]CH_2Cl_2 solution; [b]CH_2Cl_2, 100 mV/s, TBAH; [c] major species, s.

Table.4 2 IR and electrochemical data for various $Re(CO)_3$ complexes

The NMR spectra for $\mathbf{3^R}$ are simpler than expected based on the low-symmetry solid state structures owing to rapid processes that interchange supposedly symmetrically inequivalent halves of the ligands (or that invert conformations of chelate rings). That is, if the solid state structures were retained, two sets of resonances for pyrazolyl and tolyl hydrogens would be expected but only one set is observed (vide infra). In surprising contrast to $\mathbf{1^R}$, $\mathbf{2^R}$ or $\mathbf{4^R}$, the rate of the exchange process in $\mathbf{3^R}$ could not be slowed down enough to be measured by NMR(Fig 4.15) even when CD_2Cl_2 or acetone-d_6 solutions are

cooled to 193K. Given that the exchange processes can be frozen at low temperatures (Fig. 4.13-4.14) for derivatives with quarternary amino nitrogens (**1**$^{\mathbf{R}}$, **2**$^{\mathbf{R}}$ or **4**$^{\mathbf{R}}$, vide infra),† nitrogen inversion facilitates the exchange processes of **3**$^{\mathbf{R}}$. In either the solid state or solution, the IR spectrum of each **3**$^{\mathbf{R}}$ gives a characteristic pattern of three C-O stretching bands (Table 4.1) for *fac*-Re(CO)$_3$ units; the N-H stretching band is also absent. In accord with expectations based on the increasing electron density at metal centres (and greater back-bonding), the CO stretches appear at lower energy relative to **1**$^{\mathbf{R}}$ and **2**$^{\mathbf{R}}$ where average stretching frequencies decrease in the order **2**$^{\mathbf{R}}$ > **1**$^{\mathbf{R}}$ > **3**$^{\mathbf{R}}$. For **3**$^{\mathbf{R}}$, replacement of 3-pyrazolyl hydrogens for more electron donating methyl or isopropyl substituents has a surprisingly small electronic effect, as indicated by the nearly identical average CO stretching frequencies. It is likely that any potential inductive electronic effects may be offset by steric interactions that enforce longer Re-N bonds along the series **3**$^{\mathbf{H}}$ < **3**$^{\mathbf{Me}}$ < **3**$^{\mathbf{iPr}}$**.** Cyclic voltammograms of 1R, 2R and 3r are shown in Fig 4.16-4.18. The electrochemistry of each 3^{R} is distinct from their counterparts 1^{R} or 2^{R} (Table 4.1) as each 3^{R} in CH_2Cl_2 shows a quasi-reversible oxidation near 0 V versus Fc/Fc^+ (Fig 4.18, $i_{pc}/i_{pa} = 1$, but $\Delta E = E_{pa}-E_{pc}$ increases as a function of scan rate); 1^{R} and 2^{R} have irreversible oxidations ($i_{pc}/i_{pa} << 1$ and $\Delta E >> 59$ mV) at higher potentials. The oxidation potentials of 3^{Me} and 3^{iPr} are nearly equivalent and are only slightly (10-15 mV) more favourable than that of 3^{H}. Interestingly, in CH_3CN the oxidation becomes reversible(Fig 4.21) for 3^{H} and 3^{Me} but not for 3^{iPr}.† Spectrophotometic titrations with organic oxidants indicate that the oxidation is a one-electron event, as discussed later.

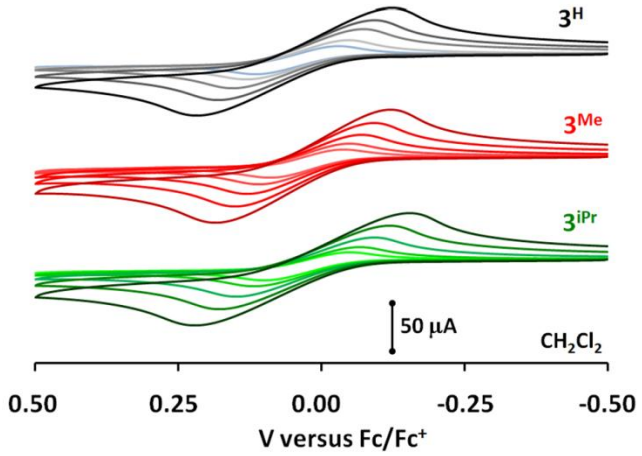

Figure 4.16. Cyclic voltammograms of *fac*-$Re(CO)_3(\mathbf{L}^{\mathbf{R}})$ ($\mathbf{3}^{\mathbf{R}}$) complexes in CH_2Cl_2 each taken with scan rates of 50 (inner), 100, 200, 400, and 800 (outer) mV/s

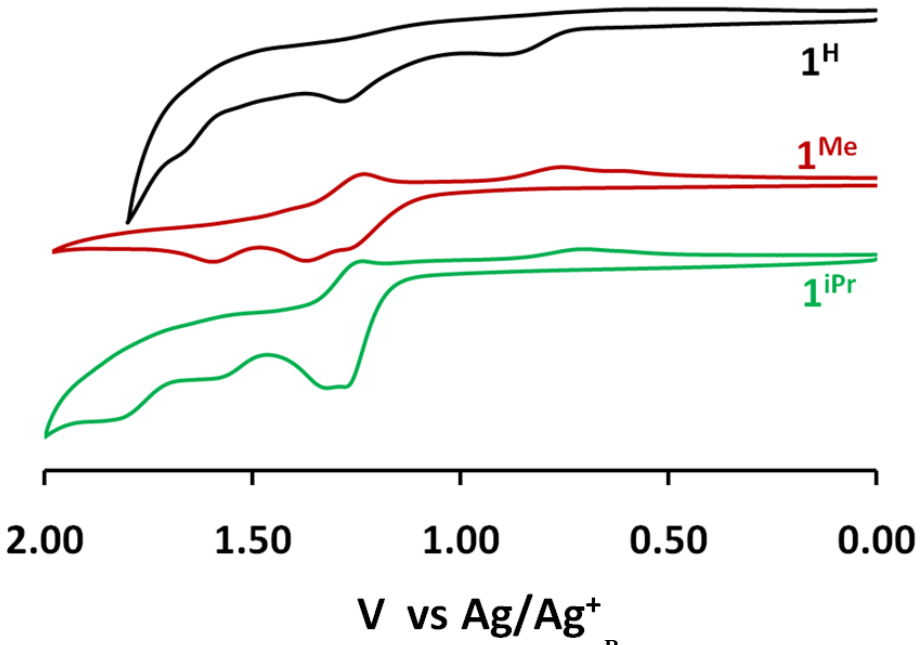

Figure. 4.17. Cyclic Voltammograms (100 mV/s) of $\mathbf{1}^{\mathbf{R}}$ in CH_2Cl_2 with NBu_4PF_6 as the supporting electrolyte.

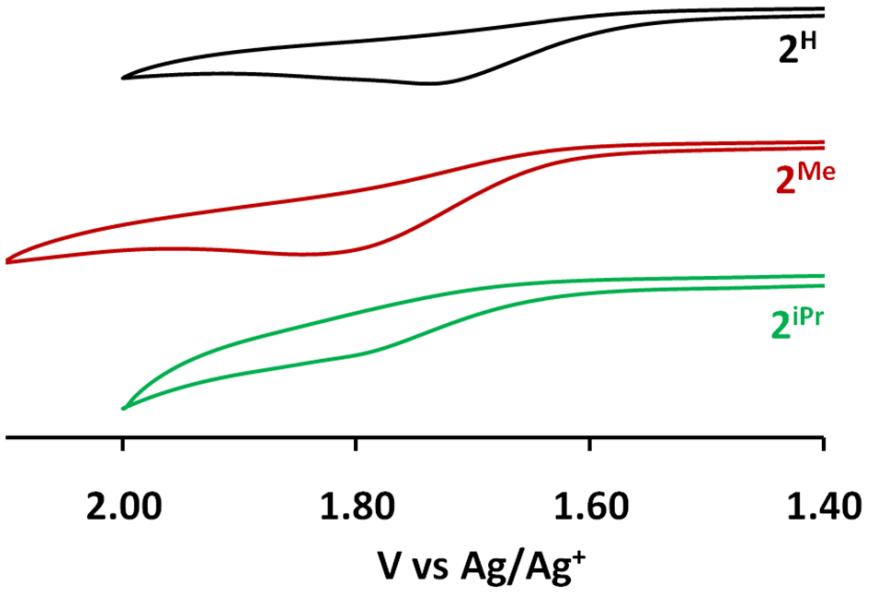

Figure. 4.18. Cyclic Voltammograms (100 mV/s) of $\mathbf{2^R}$ in CH_2Cl_2 with NBu_4PF_6 as the supporting electrolyte

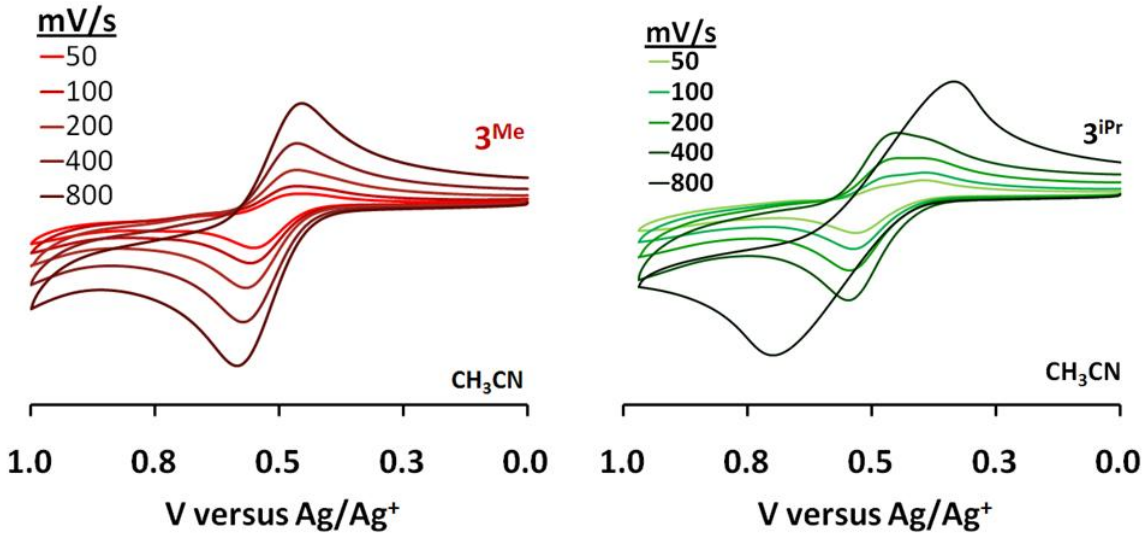

Figure. 4.19. Scan rate dependence of the cyclic voltammograms of CH_3CN solutions of $\mathbf{3^R}$ (R = Me, iPr) with NBu_4PF_6 as the supporting electrolyte

The electronic absorption spectra of $\mathbf{3^R}$ complexes in CH_2Cl_2 are found in Fig 4.20. The spectra are qualitatively similar, as might be expected, but there are subtle differences that distinguish the R = H from the R = Me, iPr derivatives. Each spectrum has two bands above about 350 nm that give rise to the yellow colour of the complexes. For $\mathbf{3^H}$ these low energy bands are more intense ($\varepsilon \sim 8000\text{-}10000\ M^{-1}cm^{-1}$) than those of either $\mathbf{3^{Me}}$ or $\mathbf{3^{iPr}}$ ($\varepsilon \sim 5000\ M^{-1}cm^{-1}$). For $\mathbf{3^H}$ the lowest energy band (400 nm, $\varepsilon \sim 8000\ M^{-1}cm^{-1}$) is less intense than the second lowest energy band (360 nm, $\varepsilon \sim 10000\ M^{-1}cm^{-1}$) while the opposite is true for either $\mathbf{3^{Me}}$ or $\mathbf{3^{iPr}}$; for the latter deconvolution is necessary to observe the second lowest energy band.

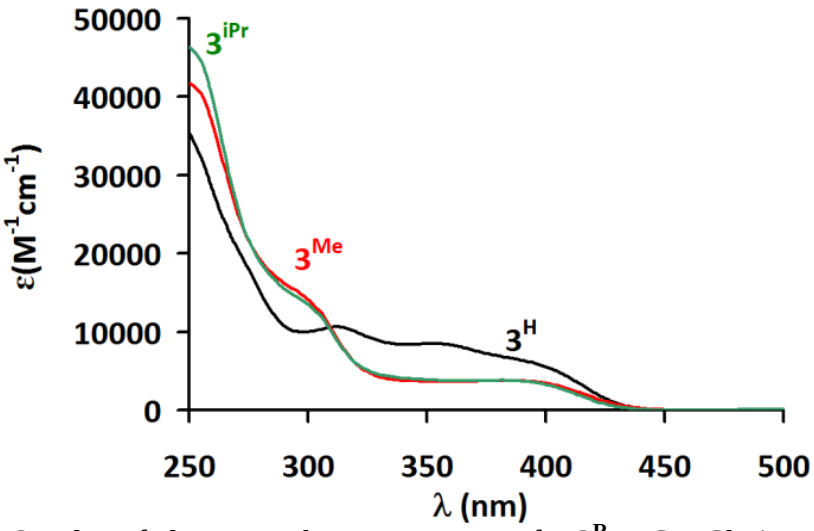

Figure 4.20. Overlay of electronic absorption spectra for $\mathbf{3^R}$ in CH_2Cl_2 (R = H, black; R = Me, red; R = iPr, green).

Since these two bands are absent in $\mathbf{1^R}$ and $\mathbf{2^R}$, they are attributed to transitions between electronic states involving an engaged dπ-pπ interaction (between the metal and available lone pair on the central amido nitrogen of the ligand). Such an assessment was bolstered by theoretical calculations where the lowest energy band enveloped transitions between the HOMO and various LUMO(+N) (N = 0-4) levels and the second-lowest energy band

involves transitions between the HOMO(-1) and the various LUMO(+N) (N = 0-4) levels. As illustrated in Fig 4.21 the HOMO is mainly a π-based obital centralized on the pincer ligand but extends onto a d-orbital of rhenium.

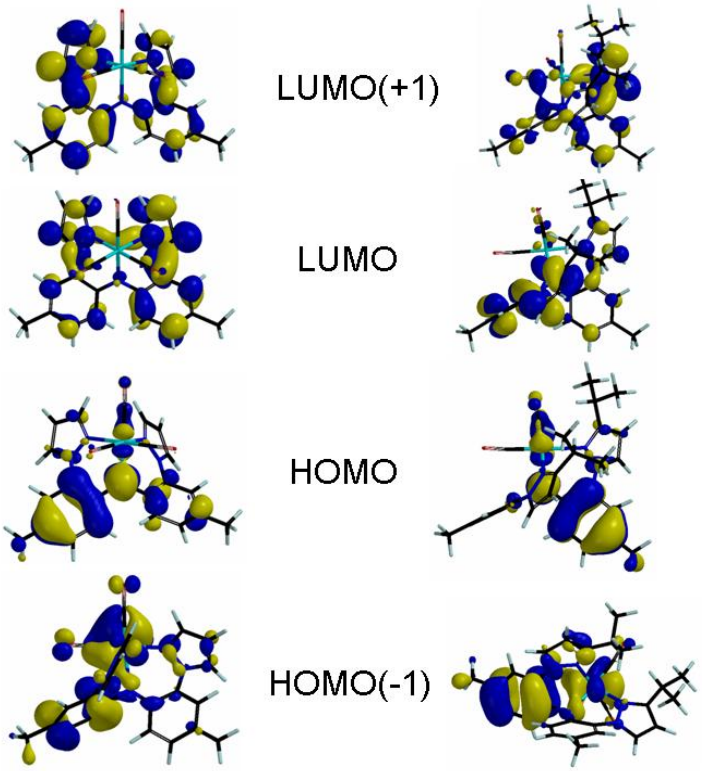

Figure 4.21. Comparison between frontier orbitals of $\mathbf{3^{H}}$ and $\mathbf{3^{iPr}}$ from theoretical calculations (B3LYP/LACVP)

The HOMO(-1) is qualitatively similar to the HOMO but with greater rhenium character. For $\mathbf{3^{H}}$, conjugation across both 2-pyrazolyl-*p*-tolyl 'arms' of the pincer ligand is evident from the atomic orbital contributions to the HOMO and to a lesser extent the HOMO(-1) but for $\mathbf{3^{Me}}$ and $\mathbf{3^{iPr}}$ the conjugation appears confined to only one 'arm' of the ligand. The LUMO and LUMO(+1) are mainly π*-orbitals of the pincer ligand while next three higher-energy virtual orbitals are those of the tricarbonyl fragment. As such these two

lowest energy bands can be considered to have metal-ligand-to-ligand charge transfer (*MLLCT*) character in accord with conventions used elesewhere.[11] The higher energy band found at 300 nm are likely due to charge transfer transitions involving the tricarbonylrhenium fragment as found in related systems[7] while the high-intensity bands found below 275 nm are likely π-π* transitions on the basis of energy and intensity considerations.

4.5. Reactivity

Given the availability of a lone pair of electrons on the central nitrogen in 3^R, the potential for these complexes to engage in nucleophilic substitution (S_N2) reactions[12] as in Scheme 4.2 was evaluated.

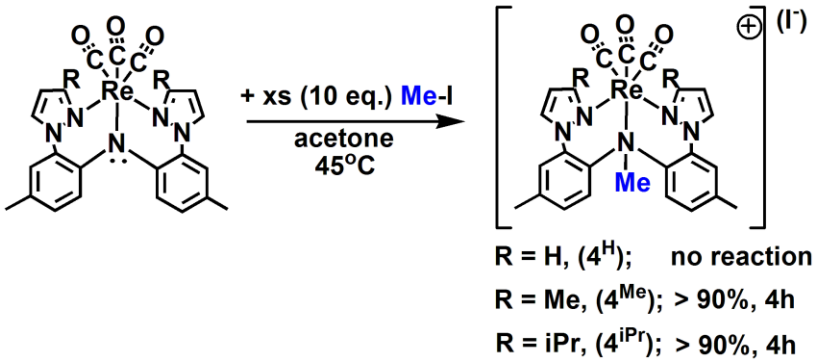

Scheme 4.2. Attempted reactions of $\mathbf{3^R}$ with MeI intended to form {*fac*-$Re(CO)_3[Me(\mathbf{L^R})]\}(I)$, $\mathbf{4^R}$ complexes

Initial stoichiometric NMR experiments performed in C_6D_6 at room temperature showed either no or trace reaction after a couple of hours. However, in hot (45°C) acetone and with a 10-fold excess of MeI, complexes 3^R (R = Me, iPr) underwent clean conversion to give {*fac*-$Re(CO)_3[Me(L^R)]\}(I)$, 4^R, over the course of about four hours detected by both

NMR and IR (Table 4.2) spectroscopy. Complex $\mathbf{3^H}$ failed to react with MeI even after days under similar reaction conditions (of temperature and reagent concentrations). The NMR spectrum of each $\mathbf{4^R}$ shows two sets of resonances for pyrazolyl and tolyl hydrogens whereas that of $\mathbf{3^R}$ shows only one set. Additionally, the solution IR spectrum (CH_2Cl_2) of $\mathbf{4^R}$ exhibited C-O stetching bands with avg. $\nu_{co} \sim 1960\ cm^{-1}$ which is comparable to that of $\mathbf{2^R}$. Single crystal X-ray diffraction of $\mathbf{4^{iPr}}$ (Fig 4.22) confirmed that the methyl group was indeed bound to the central nitrogen of the ligand rather than to a pyrazolyl nitrogen.

Also, in contrast to the $\mathbf{1^{iPr}}$ where the bromide was bound to rhenium, the iodide in $\mathbf{4^{iPr}}$ is a spectator ion and the ligand binds rhenium in a κ^3N- manner similar to that in

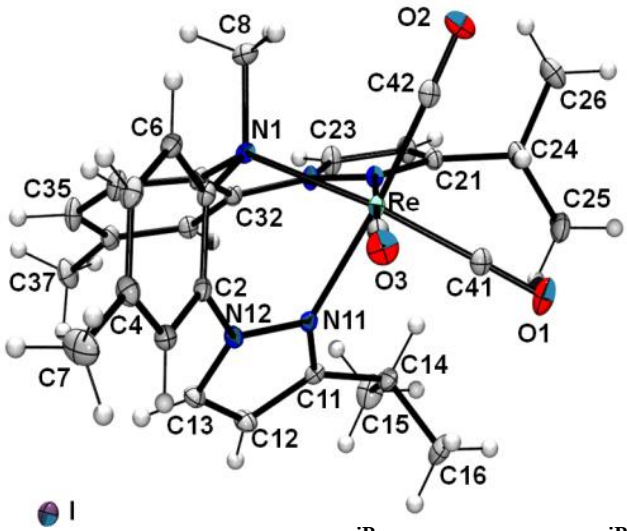

Figure 4.22 Structure of {*fac*-Re(CO)$_3$[Me($\mathbf{L^{iPr}}$)]}(I)·2CH_2Cl_2, $\mathbf{4^{iPr}}$·2CH_2Cl_2 with solvate molecules removed for clarity

2$^{\mathbf{iPr}}$. The greater steric profile of an methyl versus a hydrogen bound to nitrogen subtly impacts the cation structure by increasing the bond distances around rhenium and distorting the ligand framework (by comparing values in Table 4.1).[13]

The resonances for various 3-organopyrazolyl hydrogens for **3**$^{\mathbf{R}}$ (R = Me, iPr) and the corresponding **4**$^{\mathbf{R}}$ products are sufficiently well separated to allow for a convenient means to monitor the rates of reaction by using relative integration of signals (Fig 4.23). As illustrated in Fig 4.24, the pseudo-first order conditions ([MeI]/[**3**$^{\mathbf{R}}$] ≥ 10) gave straight-line plots with statistically identical half-lives; $t_{1/2}$ of 62 (± 3) min for **3**$^{\mathbf{Me}}$ and 65 (± 3) min for **3**$^{\mathbf{iPr}}$ where the uncertainty arises from the measurements of different types of resonances within the same experiment. In accord with Eq. 1 and the experimental conditions, the corresponding second-order rate

$$-d[\mathbf{3}^{\mathbf{R}}]/dt = k_{obs}[\mathbf{3}^{\mathbf{R}}] = k_2[\mathrm{MeI}][\mathbf{3}^{\mathbf{R}}] \quad (\mathbf{Eq.\ 1})$$

constants were found to be $k_2 = 5.7\text{x}10^{-4}$ $M^{-1}s^{-1}$ for 0.033 M **3**$^{\mathbf{Me}}$ and 0.331 M MeI and $k_2 = 8.4\text{x}10^{-4}$ $M^{-1}s^{-1}$ for 0.021 M **3**$^{\mathbf{iPr}}$ and 0.212 M MeI.

The difference in reactivity between the various 3-organopyrazolyl derivatives **3**$^{\mathbf{R}}$ and that of **3**$^{\mathbf{H}}$ can be attributed to inter-related structural and electronic factors. It was anticipated and found that the replacement of the two (very close) hydrogen atoms labeled in Figure 4.25 with any other group should (and does) drastically alter the structure and reactivity of the complexes. Given the typical inert nature of Re-ligand bonds, the spectroscopic data, and that no N-methyl pyrazolyls was detected in reactions with MeI,

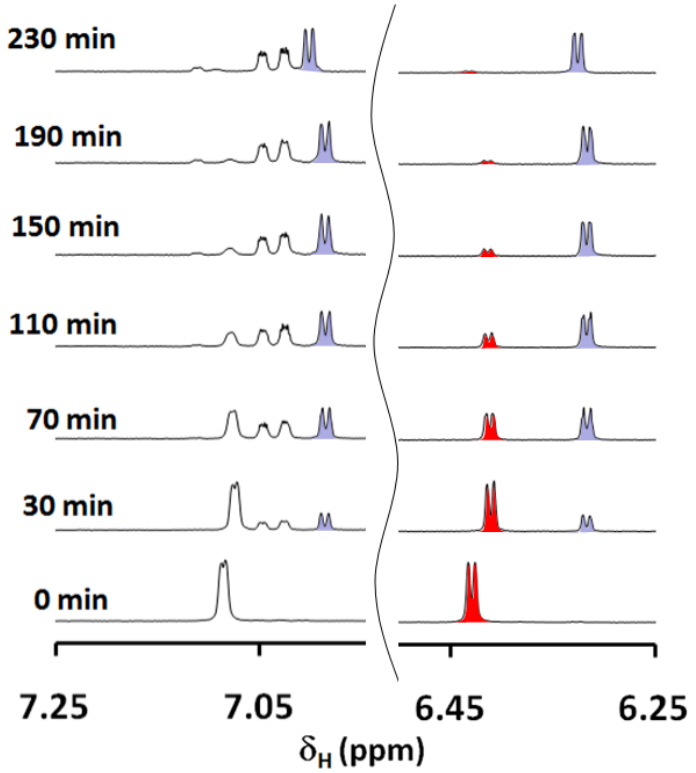

Figure 4.23. Portions of the ^{1}H NMR spectra obtained by heating a 1:10 mixture of $\mathbf{3}^{\mathbf{Me}}$: MeI, highlighting resonances for 4-pyrazolyl hydrogens of $\mathbf{3}^{\mathbf{Me}}$ (red-shaded doublet near δ_H = 6.4 ppm) and of the product $\mathbf{4}^{\mathbf{Me}}$ (two indigo-shaded doublets near δ_H = 7.0 and 6.3 ppm).

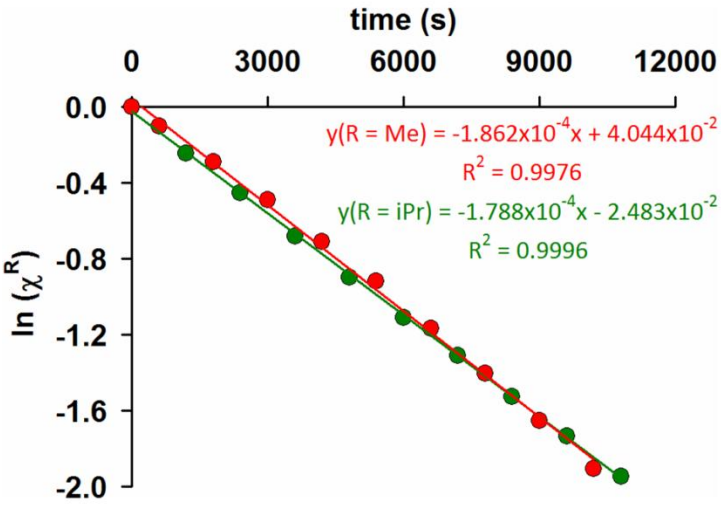

Figure 4.24. Pseudo-first order plots of ln (mol fraction of $\mathbf{3}^{\mathbf{R}}$) (R = Me, red; R = iPr, green) versus time from integration of 4-pyrazolyl hydrogen NMR resonances observed during conversions of $\mathbf{3}^{\mathbf{R}}$ to $\mathbf{4}^{\mathbf{R}}$ with MeI

it is expected that the ligands remain tridentate in acetone solutions of $\mathbf{3^H}$ and $\mathbf{3^R}$ and that pyrazolyl dissociation is unlikely the origin of increased reactivity of $\mathbf{3^R}$ versus $\mathbf{3^H}$. If the ligands are indeed tridentate, the greater reactivity of $\mathbf{3^R}$ versus $\mathbf{3^H}$ toward MeI can be rationalized by the greater the a greater (steric) accessibility of the more pyramidal nitrogen of $\mathbf{3^R}$ to incoming electrophiles than that in $\mathbf{3^H}$. The pyramidal nature of nitrogen in $\mathbf{3^R}$ has two consequences. First, the complexes $\mathbf{3^R}$ are is pre-organized in a conformation similar to that found for $\mathbf{4^R}$ (right of Fig. 4.25); the activation barrier for the conversion of $\mathbf{3^H}$ to hypothetical $\mathbf{4^H}$ should be higher due to requisite structural reorganization. Moreover, the basicity of the amido nitrogen in $\mathbf{3^R}$ is also expected to be greater owing to the greater s-character, lower degree of conjugation and the slightly higher energy HOMO versus $\mathbf{3^H}$ (Figure 4.21).

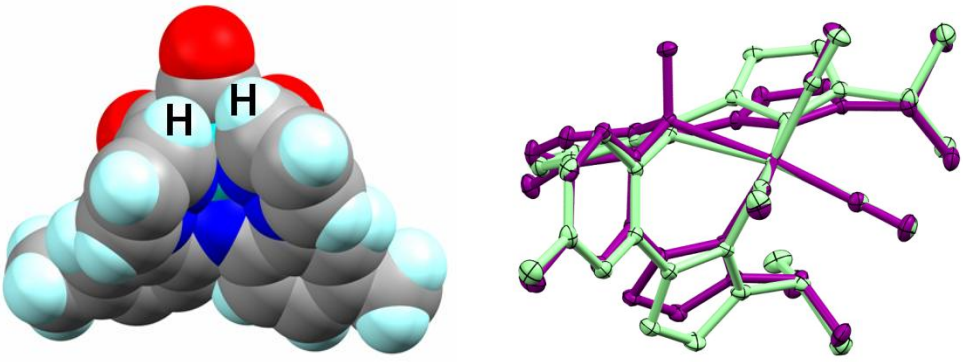

Figure 4.25. Left: Space-filling diagram of $\mathbf{3^H}$; Right: Overlay of structures for $\mathbf{3^{iPr}}$ (light green) and the cation in $\mathbf{4^{iPr}}$ (violet) referenced to common ReC_3 cores

The discrepancy in properties and reactivity between $\mathbf{3^R}$ (R = Me, iPr) and $\mathbf{3^H}$ perpetuates in the one-electron oxidized products $(\mathbf{3^{R+}})(SbCl_6^-)$. Reactions of $\mathbf{3^R}$ with the organic cation radical 9,10-dimethoxyocta-hydro-1,4:5,8-dimethanoanthracenium hexachloroantimonate $[(CRET^+)(SbCl_6^-)]$,[14] a modest oxidant ($E_{1/2,red}$ 0.58 V vs Fc/Fc^+), affords blue-green $(\mathbf{3^{R+}})(SbCl_6^-)$, see Fig 4.26 and 4.27. While $(\mathbf{3^{H+}})$ was found to be stable as a solid and only very slowly decomposed at 295K in deaerated CH_2Cl_2 ($t_{1/2}$ = 3d), $(\mathbf{3^{R(=Me\ or\ iPr)+}})(SbCl_6^-)$ decomposed much more rapidly in aerated CH_2Cl_2 ($t_{1/2}$ = 3.5 h for both); thus, solution measurements must be made on freshly prepared samples with exclusion of air. At 295 K, the EPR spectrum of each cation radical $(\mathbf{3^{R+}})$ in CH_2Cl_2 (Fig. 4.28) displays a well-resolved sextet signal due to the hyperfine interaction between the electronic spin and the $^{185/187}$Re nuclei (I = 5/2). The isotropic signal for $(\mathbf{3^{H+}})$ (g_{iso} = 2.017 a_{Re} 49.5 G) is similar but distinct from the signals for either $(\mathbf{3^{Me+}})$ (g_{av} = 2.016, a_{Re} = 33.4 G, a_N = 7.5 G) or $(\mathbf{3^{iPr+}})$ (g_{av} = 2.016, a_{Re} = 33.8 G, a_N = 7.5 G). In each case, the relatively small deviation of g-values from that for the free electron g_e = 2.0023 and the small hyperfine couplings are consistent with a ligand-centred rather than a metal-centred radical, with the spin density on rhenium being highest for $(\mathbf{3^{H+}})$.[3,15] Theoretical calculations indicate most of the spin density is located on the ligand (Fig 4.29) in accord with other experimental indicators of a ligand-centred radical such as the occurrence of intense pi-radical bands ($\pi(L) \rightarrow$ SOMO) in the 650-750 nm range of the electronic absorption specturm. Also, the average energy of the C-O stretching bands in the solution (CH_2Cl_2) IR spectra, ν_{co}(avg), increases by only 33, 37, and 41 cm^{-1} on traversing between $\mathbf{3^R}$ and $\mathbf{3^{R+}}$ for R = H, Me, and iPr, respectively (Table 4.2).

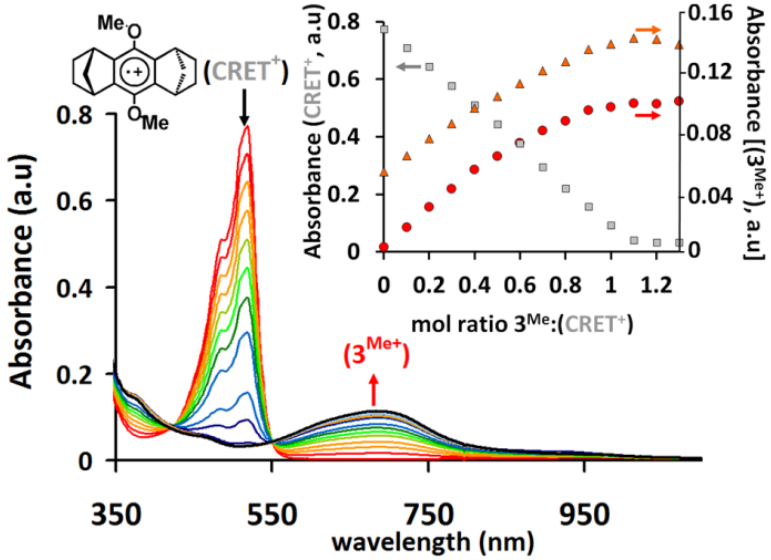

Figure 4.26. Spectroelectrochemical titiration reaction between $\mathbf{3^{Me}}$ and $(CRET^{+})(SbCl_6^{-})$ in CH_2Cl_2. Inset: Plot of absorbance versus mol ratio monitoring bands for $(CRET^{+})$ at 518 nm (grey squares) and for $(\mathbf{3^{Me+}})$ at 377 nm (orange triangles) and 687 nm (red circles

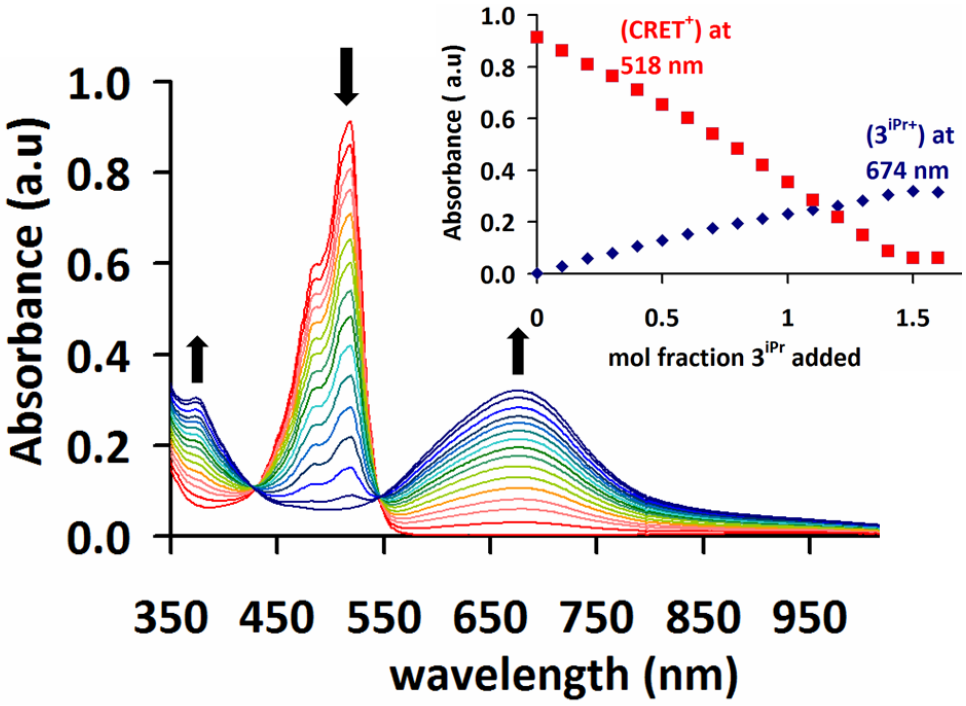

Figure 4.27. UV-visible spectra for redox titration between $(CRET^{+})(SbCl_6^{-})$ and $\mathbf{3^{iPr}}$ in aerated CH_2Cl_2, illustrating the broad pi-radical band near 674 nm. See main narrative for structure of (CRET+).

Such a relatively small increase in energy is similar to the 38 cm^{-1} increase for related PNP pincer complexes $[Re(CO)_3(PNP)]^{n+}$ (n = 0,1) (measured for KBr pellets) and is consistent with ligand-centered oxidation.[2] Rhenium-centred oxidations would be expected to have ν_{co}(avg) increase on the order of 50-100 cm^{-1}.[2,3,16]

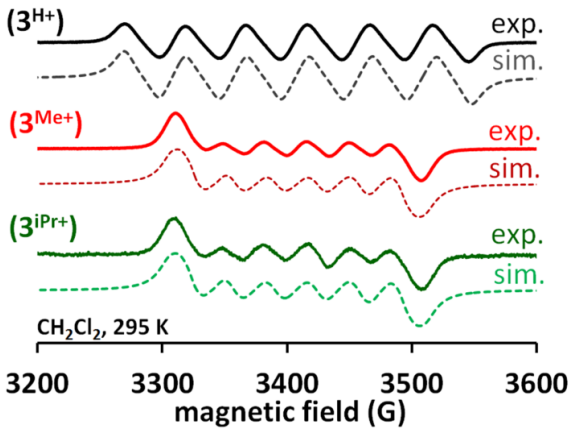

Figure 4.28. Comparison of X-Band (9.63 GHz, 295 K) EPR spectra for $(3^{R+})(SbCl_6^-)$ in CH_2Cl_2 (R = H, black; R = Me, red; R = iPr, green). Simulated spectra have dashed lines

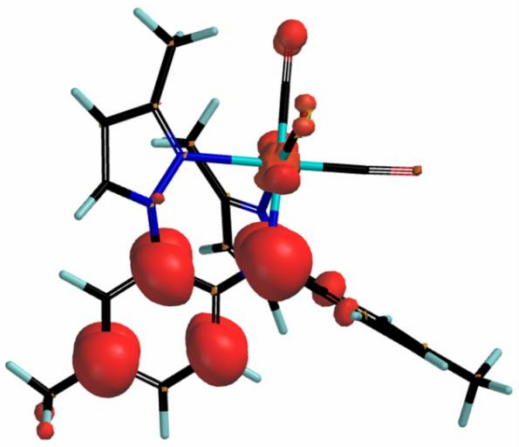

Figure 4.29. Spin density isosurface for energy minimized (BP86) structural model of (3^{Me+}) from theoretical calculations (UB3LYP/LACVP**)**

4.6. Photodecomposition

A final set poorly understood observations that highlight the incongruent reactivity patterns of $\mathbf{3^R}$ (R = Me, iPr) and $\mathbf{3^H}$ derivatives is that CH_2Cl_2 solutions of $\mathbf{3^{Me}}$ or $\mathbf{3^{iPr}}$ were light sensitive but those of $\mathbf{3^H}$ were not. Thus, CH_2Cl_2 solutions of the latter two compounds should be protected from light and measurements should be made on freshly prepared solutions. Dissolution of either $\mathbf{3^{Me}}$ or $\mathbf{3^{iPr}}$ in CH_2Cl_2 initially gives a bright yellow solution. Over the course of several hours to several days under ambient lighting conditions (32W, 4100K fluorescent bulbs and glass-filtered sunlight) the solutions turn orange and then red-violet regardless of being contained in either quartz or colorless borosilicate glass containers (Figure 4.30). The photodecomposiiton also occurred under exclusion of atmospheric moisture or oxygen. If CH_2Cl_2 solutions of $\mathbf{3^{Me}}$ or $\mathbf{3^{iPr}}$ are protected from light in foil-covered containers, they remain yellow for weeks even when exposed to air. When red-violet solutions from purposeful photoirradiation of $\mathbf{3^{iPr}}$ solutions were analyzed by electronic absorption (Figure 4.31) and EPR spectroscopy, featureless signals of an unidentified organic cation radical (λ_{max} = 475 and 540 nm; g_{iso} = 2.003) were observed. Moreoever, the ESI(+) mass spectrum (Fig. 4.32) showed peaks at m/z = 720, 743, and 758 consistent with those expected for $ReCl(CO)_3[(M)H(\mathbf{L^{iPr}})]$ (M = H, Na, K from the spectrometer) based on the similar, distinctive fragmentation pattern found for $\mathbf{1^{iPr}}$. Given the similarity in the electrochemical behavior of $\mathbf{3^R}$, the comparable energy but more intense low energy absorption bands in the electronic absorption spectrum of $\mathbf{3^H}$ versus the other two $\mathbf{3^R}$ compounds (which might be expected to render $\mathbf{3^H}$ rather more susceptible to photochemistry than $\mathbf{3^R}$ based on absorption cross-section), the difference in reactivity of

the complexes is likely steric in nature (c.f. accessibility to the central amido nitrogen) rather than being of electronic origin. We are currently continuing investigations into the intriguing photochemistry of $\mathbf{3^R}$

Figure 4.30 Photograph of ca. 2 mM CH_2Cl_2 solutions of $Re(CO)_3(\mathbf{L^R})$, $\mathbf{3^R}$, that were exposed to ambient lighting for various lengths of time in borosilicate volumetric flasks. All solutions were initially yellow; only the un-substituted $\mathbf{3^H}$ resists photodecomposition

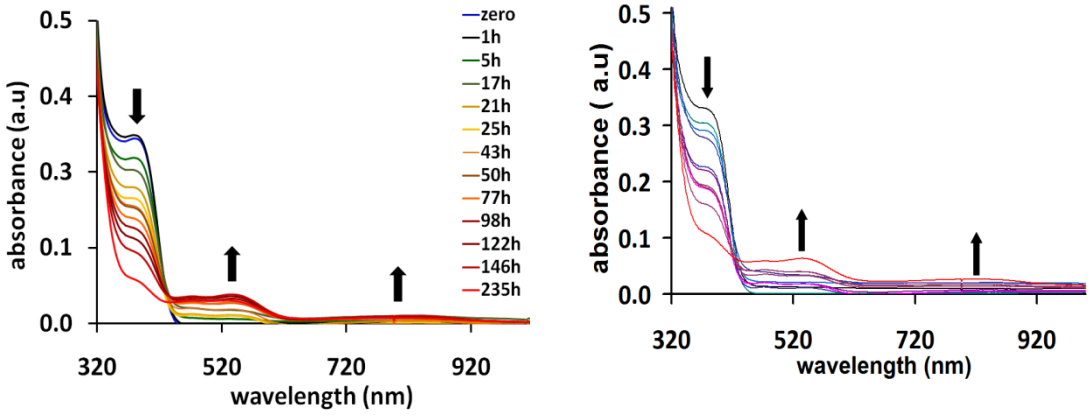

Figure 4.31. UV-Visible spectra acquired at various time intervals over the period of ten days for aliquots of a 2 mM CH_2Cl_2 solution of $\mathbf{3^{Me}}$ (left) and $\mathbf{3^{iPr}}$ (right) contained in the above volumetric flasks and that were exposed to ambient lighting

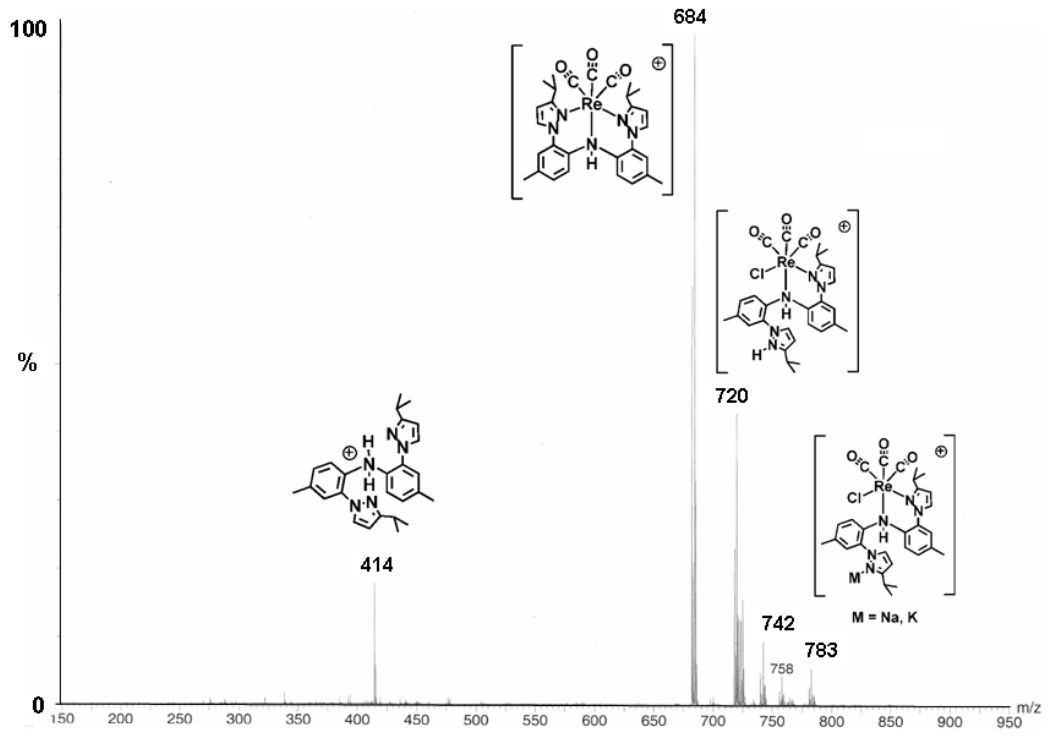

Figure 4.32. ESI(+) mass spectrum of CH_2Cl_2 solution of photodecomposed **3**$^{\mathbf{iPr}}$. Structures shown for the assignments are based on empirical formulae and are speculative, as most have not been structurally verified in cases other than m/z = 684.

4.7. Conclusions.

The purpose of this study was to investigate whether the reactivity of tricarbonylrhenium(I) complexes of di(2-(3-R-pyrazolyl)-p-tolyl)amine derivatives would be altered by substitution at the 3-pyrazolyl position; the properties of various $Re(CO)_3$ complexes of the unsusbtituted ligand H(L^R) R = H were presented previously. To this end, two new 3-alkylpyrazolyl ligands (R = Me, iPr) were prepared in good yield by straghtforward CuI-catalyzed amination reactions. The availability of the three H(**L**$^{\mathbf{R}}$) ligands (R = H, Me, and ^{i}Pr) ligands allowed a series of nine tricarbonylrhenium(I) complexes to be prepared and fully characterized both in solution and the solid state. The

most significant structural and reactivity differences were found across the series of *fac*-$Re(CO)_3(\mathbf{L^R})$ ($\mathbf{3^R}$) complexes with deprotonated, formally uninegative, NNN-ligands. The bond distances in $\mathbf{3^R}$ increased with increasing steric bulk of the 3-pyrazolyl substituents. For $\mathbf{3^H}$, a conformation with near C_s symmetry and a planar amido nitrogen was found in the solid state whereas for $\mathbf{3^{Me}}$ or $\mathbf{3^{iPr}}$, the ligands were greatly distorted with substantial pyramidalization of the amido nitrogen. This conformation is dictated by unfavorable steric interactions that would occur between 3-pyrazolyl substituents in a pseudo-C_s symmetric conformation such as in $\mathbf{3^H}$. The solution spectroscopic data demonstrate that none of the three complexes retain their static solid state geometries. Based on comparisons with other complexes, this behavior is attributed to conformational changes of intact complexes with tridentate ligands. Pyrazolyl dissociation to give bidentate ligands and perhaps a coordinatively unsaturated (or weakly-solvated)metal centers cannot be excluded in either $\mathbf{2^R}$ or $\mathbf{3^R}$ cases (which show dynamic solution behavior), but seems unlikely owing the usual kinetically inert nature of rhenium-ligand bonds, the flexibility of six-membered chelate rings, combined with the observed reactivity patterns. The relative reactivities follow the divisive pattern where $\mathbf{3^{Me}}$ and $\mathbf{3^{iPr}}$ are reactive towards MeI to afford an N-methyl (amino not pyrazolyl) derivative but $\mathbf{3^H}$ does not react with MeI under similar conditions. Moreover, CH_2Cl_2 solutions of the former two complexes are photosensitive but similar solutions of $\mathbf{3^H}$ were photo-stable. A final difference was found for the one-electron oxidized products ($\mathbf{3^{R+}}$); the room-temperature EPR spectrum of CH_2Cl_2 solutions for R = Me or ^{i}Pr gave signals indicative of a more asymmetric ligand environment than that for R = H. Moreover, solutions of ($\mathbf{3^{Me+}}$) and ($\mathbf{3^{iPr+}}$) were considerably more prone to decompostion than ($\mathbf{3^{H+}}$). The

incongruent nature of the structures and electronic spectra of the two classes of complexes combined with results of DFT calculations for the various $\mathbf{3^R}$ and $\mathbf{(3^{R+})}$ cation radicals indicate that the differences arise from a combination of the lower degree of conjugation across the ligand backbone and a a (surprising) greater accessibility to a more pyramidal amido nitrogen on the ligand. Studies are underway to further explore the chemical and photochemical potential of these and related complexes.

4.8. Experimental

Materials: Pyrazole, 3-methylpyrazole, CuI, N,N'-dimethylethylenediamine (DMED), anhydrous K_2CO_3 powder, and $(NEt_4)(OH)$ (1 M in MeOH) were purchased from commercial sources and used without further purification while $Re(CO)_5Br$,[17] di(2-bromo-*p*-tolyl)amine,[5] 3- isopropylpyrazole[6] were prepared by literature methods. Methyl iodide was distilled under vacuum before use. Solvents used in the preparations were dried by conventional methods and were distilled under nitrogen prior to use

Instrumentation

Midwest MicroLab, LLC, Indianapolis, Indiana 45250, performed all elemental analyses. ^1H and ^{13}C NMR spectra were recorded on a Varian 400 MHz spectrometer. Chemical shifts were referenced to solvent resonances at δ_H 7.27, δ_C 77.23 for $CDCl_3$; δ_H 5.32, δ_C 54.00 for CD_2Cl_2 and δ_H 2.05, δ_C 29.92 for acetone-d_6. Melting point determinations were made on samples contained in glass capillaries using an Electrothermal 9100 apparatus and are uncorrected. Infrared spectra were recorded on samples as KBr pellets and as CH_2Cl_2 solutions using a Nicolet Magna-IR 560 spectrometer. Absorption measurements were recorded on an Agilent 8453 spectrometer. Electrochemical

measurements were collected under nitrogen atmosphere at a scan rate of 100 mV/s for samples as 0.1 mM CH_2Cl_2 solutions with 0.1 M NBu_4PF_6 as the supporting electrolyte. A three-electrode cell comprised of an Ag/AgCl electrode, a platinum working electrode, and a glassy carbon counter electrode was used for the voltammetric measurements. With this set up, the ferrocene/ferrocenium couple had an $E_{1/2}$ value of +0.53 V consistent with the literature value in this solvent.[18] Mass spectrometric measurements recorded in ESI(+) or ESI(-) mode were obtained on a Micromass Q-TOF spectrometer whereas those performed by using direct-probe analyses were made on a VG 70S instrument. For the ESI(+) experiments formic acid (approximately 0.1 % v/v) was added to the mobile phase (CH_3CN). EPR measurements were obtained using a Bruker ELEXSYS E600 equipped with an ER4116DM cavity resonating at 9.63 GHz, an Oxford Instruments ITC503 temperature controller and ESR-900 helium-flow cryostat. The ESR spectra were recorded with 100kHz field modulation

Di(2-(3-methylpyrazolyl)-*p*-tolyl)amine, H(L^{Me})

A reaction vessel was charged with a mixture of 3.44 g (9.69 mmol) di(2-bromo-*p*-tolyl)amine, 2.78 g (33.9 mmol, 3.5 equiv) 3-methylpyrazole, 5.35 g (38.7 mmol, 4.0 equiv) K_2CO_3, and 0.38 mL (3.87 mmol, 40 mol %) DMED, and was deoxygenated by three evacuation and nitrogen back-fill cycles. Then, 0.18 g (0.97 mmol, 10 mol %) CuI was added as a solid under nitrogen. The reaction mixture was heated under nitrogen at 200 ^{o}C for 15 hours. After cooling to room temperature, 200 mL of H_2O was added and the mixture was extracted with three 100 mL portions of CH_2Cl_2. The combined organic layers were dried over $MgSO_4$, filtered, and solvent was removed by rotary evaporation to give an oily residue that was purified by column chromatography on silica gel. Elution

with 8:1 hexanes:ethyl acetate (R_f = 0.7) afforded 2.28 g (66 %) of H(**L^{Me}**) as a white solid. Mp, 83 - 85 ^{o}C. Anal. Calcd (obs.) for $C_{22}H_{23}N_5$: C, 73.92 (73.68); H, 6.49 (6.53); N, 19.59 (19.41). IR (KBr) ν_{NH} 3297. ^{1}H NMR: (CD_2Cl_2) 8.43 (s, 1H, NH), 7.62 (d, *J* = 2 Hz, 2H, H_5pz), 7.22 (d, *J* = 8 Hz, 2H, Ar), 7.09 (s, 2H, Ar), 7.00 (d, *J* = 8 Hz, 2H, Ar), 6.19 (d, *J* = 2 Hz, 2H, H_4pz), 2.29 (s, 12H, CH_3). ^{1}H NMR: (acetone-d_6) 8.86 (s, 1H, NH), 7.85 (d, *J* = 2 Hz, 2H, H_5pz), 7.24 (d, *J* = 8 Hz, 2H, Ar), 7.19 (s, 2H, Ar), 7.05 (d, *J* = 8 Hz, 2H, Ar), 6.24 (d, *J* = 2, 2H, H_4pz), 2.29 (s, 6H, ArCH_3), 2.28 (s, 6H, pzCH_3). ^{13}C NMR: ($CDCl_3$) 149.9, 134.6, 131.0, 130.7, 130.2, 128.8, 125.8, 118.9, 106.6, 20.7, 13.8. UV-VIS λ_{max}, nm (ε, $M^{-1}cm^{-1}$), CD_2Cl_2: 242(37149), 304(26376). Single crystals suitable for X-ray diffraction were obtained by slow evaporation of a hexane solution.

Di(2-(3-isopropylpyrazolyl)-*p*-tolyl)amine, H(L^{iPr})

In a manner similar to that described above, a mixture of 7.17 g (0.0202 mol) di(2-bromo-*p*-tolyl)amine, 7.78 g (0.0706 mol, 3.5 equiv) 3-isopropylpyrazole, 11.05 g (0.0800 mol, 4.0 equiv) K_2CO_3, and 0.79 mL (0.65 g, 7.4 mmol, 35 mol %) DMED, 0.38 g (2.0 mmol, 10 mol %) CuI afforded 5.06 g (61 %) of H(L^{iPr}) as a light yellow oil after workup and purification (SiO_2, 8:1 Hexane: ethyl acetate R_f = 0.6). Anal. Calcd (obs.) for $C_{26}H_{31}N_5$: C, 75.51 (75.61); H, 7.56 (7.48); N, 16.93 (16.78). IR (KBr) ν_{NH} 3296. ^{1}H NMR: (CD_2Cl_2) 8.82 (s, 1H, NH), 7.67 (d, *J* = 2 Hz, 2H, H_5pz), 7.18 (d, *J* = 2Hz, 2H, Ar), 7.14 (s, 2H, Ar), 6.98 (dd, *J* = 8, 2 Hz, 2H, Ar), 6.21 (d, *J* = 2 Hz, 2H, H_4pz), 2.95 (sept, *J* = 7 Hz, 2H, Me_2CH), 2.29 (s, 6H, ArCH_3), 1.22 (d, *J* = 1 Hz, 6H, iPrCH_3), 1.20 (d, *J* = 1Hz, 6H, iPrCH_3). ^{1}H NMR: (acetone-d_6) 8.70 (s, 1H, NH), 7.87 (d, *J* = 2 Hz, 2H, H_5pz), 7.23 (s, 2H, Ar), 7.20 (d, *J* = 8 Hz, 2H, Ar), 7.01 (d, *J* = 8 Hz, 2H, Ar), 6.28 (d, *J* = 2 Hz, 2H, H_4pz), 2.99 (sept, *J* = 7 Hz, 2H, Me_2CH), 2.29 (s, 6H, ArCH_3), 1.24 (d, *J* = 1

Hz, 6H, iPrCH$_3$), 1.22 (d, *J* = 1Hz, 6H, iPrCH$_3$), ^{13}C NMR: (CDCl$_3$) 160.4, 134.3, 130.9, 130.5, 129.9, 128.5, 125.6, 119.3, 103.7, 27.9, 22.9, 20.7. UV-VIS λ_{max}, nm (ε, M^{-1}cm^{-1}), CD_2Cl_2: 244(36386), 304(22429)

ReBr(CO)$_3$[H(L^{Me})], (1^{Me})

A mixture of 0.172 g (0.423 mmol) Re(CO)$_5$Br and 0.151g (0.422 mmol) of **H(L^{Me})** in 20 mL of toluene was heated at reflux 15h. The resulting precipitate was isolated by filtration, washed with two 5 mL portions Et_2O and dried under vacuum which afforded 0.22 g (75 %) **1^{Me}** as a fine white powder. Mp, 269 - 271^{o}C dec. Anal. Calcd (obs.) for $C_{25}H_{23}BrN_5O_3Re$: C, 42.44 (42.20); H, 3.28 (3.21); N, 9.90 (9.74). IR (KBr) ν_{NH} 3138; ν_{co} 2025, 1915, 1895 cm^{-1}. ^{1}H NMR: (CD_2Cl_2, 303K) three species, see text: **I**, 88% of signal integration intensity from resolved resonances in the R-CH$_3$, NH, H$_5$pz and H$_4$pz regions of spectrum; **II**, 10% of signal; **III** 2% of signal): 12.10 (br s, 1H, NH, **III**), 11.84 (br s, 1H, NH, **II**), 10.50 (br s, 1H, NH, **I**), 8.06 (d, *J* = 2 Hz, 1H, H$_5$pz, **I**), 8.03 (d, *J* = 2 Hz, 1H, H$_5$pz, **II**), 7.89 (d, *J* = 2 Hz, 1H, H$_5$pz, **II**), 7.79 (d, *J* = 2 Hz, 1H, H$_5$pz, **I**), 7.58 (d, *J* = 8 Hz, 1H, Ar, **I**), 7.33-7.24 (m, 4H, Ar, **I/II/III**), 7.21-7.02 (br m, 4H, Ar **I/II/III**), 6.60 (d, *J* = 2 Hz, 1H, H$_4$pz, **II**), 6.59 (d, *J* = 2 Hz, 1H, H$_4$pz, **I**), 6.31 (d, *J* = 2 Hz, 1H, H$_4$pz, **II**), 6.20 (d, *J* = 2 Hz, 1H, H$_4$pz, **I**), 2.74 (s, 3H, pzCH$_3$, **I**), 2.47 (s, 3H, ArCH$_3$, **I**), 2.44 (s, 3H, ArCH$_3$, **I**), 2.41-2.28 (br m, 9H, pz- and ArCH$_3$, **II**/**III**), 2.21 (s, 3H, pzCH$_3$, **II**), 1.98 (s, 3H, pzCH$_3$, **I**). ^{1}H NMR: (CD_2Cl_2, 213K) 11.70 (br s, 1H, NH, **III**), 11.48 (br s, 1H, NH, **II**), 10.29 (br s, 1H, NH, **I**), 8.17 (d, *J* = 8 Hz, 1H, Ar, **II**), 8.13 (br s, 1H, H$_5$pz, **III**), 8.08 (br s 1H, H$_5$pz, **I**), 7.99 (br s, 1H, H$_5$pz, **II**), 7.95 (br s, 1H, H$_5$pz, **III**), 7.86 (br s, 1H, H$_5$pz, **II**), 7.80 (d, *J* = 8 Hz, 1H, Ar, **I**), 7.74 (br s, 1H, H$_5$pz, **I**), 7.53 (br s, 1H, Ar, **II**), 7.41-7.01(br m, see text, Ar, **I/II/III**), 6.91 (s, 1H, Ar, **II**), 6.83 (d, J = 8 Hz,

1H, Ar, **II**), 6.61 (d, *J* = 2 Hz, 1H, H_4pz, **II**), 6.58 (d, *J* = 2 Hz, 1H, H_4pz, **I**), 6.38 (br s, 1H, H_4pz, **III**), 6.31 (d, *J* = 2 Hz, 1H, H_4pz, **II**), 6.18 (br s, 1H, H_4pz, **III**), 6.16 (br s, 1H, H_4pz, **I**), 6.07 (d, *J* = 2 Hz, 1H, H_4pz, **II**), 5.87 (1H, H_4pz, **III),** 2. 78 (s, 3H, $pzCH_3$, **II**), 2.73 (s, 3H, $pzCH_3$, **III**), 2.68 (s, 3H, $pzCH_3$, **I**), 2.62 (s, 3H, $pzCH_3$, **III**), 2.45 (s, 3H, $ArCH_3$, **II**), 2.44 (s, 3H, $ArCH_3$, **I**), 2.39 (s, 3H, $ArCH_3$, **I**), 2.33 (s, 3H, $ArCH_3$, **III**), 2.24 (s, 3H, $ArCH_3$, **III**), 2.18 (s, 3H, $ArCH_3$, **II**), 2.02 (s, 3H, $pzCH_3$, **II**), 1.83 (s, 3H, $pzCH_3$, **I**). UV-VIS λ_{max}, nm (ε, $M^{-1}cm^{-1}$), CD_2Cl_2: 231(50963), 261(34522), 289(11818). X-ray quality crystals of $\mathbf{1^{Me}}$·acetone were grown by layering an acetone solution with hexane and allowing the solvents to slowly diffuse over two days.

$ReBr(CO)_3[H(L^{iPr})]$ ($\mathbf{1^{iPr}}$)

A mixture of 0.256 g (0.630 mmol) $Re(CO)_5Br$ and 0.260g (0.727 mmol) of **$H(L^{iPr})$** in 20 mL of toluene was heated at reflux for 15 hours. The resulting precipitate was isolated by filtration, washed with two 5 mL portions Et_2O and dried under vacuum which afforded 0.34 g (71 %) as a fine white powder. Mp, 264 - 267°C dec. Anal. Calcd (obs.) $C_{29}H_{31}BrN_5O_3Re$: C, 45.61 (45.40); H, 4.09 (3.96); N, 9.17 (9.14). IR (KBr) ν_{NH} 3143; ν_{co} 2020, 1910, 1880 cm^{-1}. ^{1}H NMR: (CD_2Cl_2, 293K) two species, see text: **I**, 92% of signal integration intensity from resolved resonances in the R-CH_3, NH, H_5pz and H_4pz regions of spectrum; **II**, 8% of signal: 11.96 (br s, 1H, NH, **II**), 10.50 (br s, 1H, NH, **I**), 8.08 (d, *J* = 2.9 Hz, 1H, H_5pz, **I**), 8.06 (br m, 1H, H_5pz, **II**), 7.90 (d, *J* = 2.5 Hz, 1H, H_5pz, **II**), 7.82 (d, *J* = 2.5 Hz, 1H, H_5pz, **I**), 7.63-7.53 (br s, 6H, Ar, **II**), 7.29 (m, 3H, Ar, **I**), 7.18 (m, 3H, Ar, **I**), 6.65 (d, *J* = 2.9 Hz, 1H, H_4pz, **II**), 6.64 (d, *J* = 2.9 Hz, 1H, H_4pz, **I**), 6.37 (br m, 1H, H_4pz, **II**), 6.25 (d, *J* = 2.5 Hz, 1H, H_4pz, **I**), 3.85 (sept, *J* = 7.1 Hz, 1H, Me_2CH, **I**), 2.51 (sept, *J* = 6.7 Hz, 1H, Me_2CH, **II**), 2.46 (s, 3H, $ArCH_3$, **I**), 2.43 (s, 3H,

$ArCH_3$, **I**), 2.38 (br s, 3H, $ArCH_3$, **II**), 1.33 (d, *J* = 7 Hz, 3H, $iPrCH_3$, **I**), 1.29 (d, *J* = 7 Hz, 3H, $iPrCH_3$, **I**), 1.23 (br m, 3H, $iPrCH_3$, **II**), 1.04 (d, *J* = 7 Hz, 3H, $iPrCH_3$, **I**), 0.99 (d, *J* = 7 Hz, 3H, $iPrCH_3$, **I**), 0.88 (br m, 3H, $iPrCH_3$, **II**). UV-VIS λ_{max}, nm (ε, $M^{-1}cm^{-1}$), CD_2Cl_2: 295 (10,900), 259 (38,200), 230 (51,500). ^{13}C NMR: (CD_2Cl_2) 168.3, 161.7, 138.6, 137.5, 133.5, 130.6, 130.5, 129.4, 127.3, 125.2, 121.8, 107.2, 105.1, 31.1, 28.4, 24.3, 23.4, 23.1, 22.8, 21.3, 20.9. X-ray quality crystals were grown by layering an acetone solution with hexane and allowing the solvents to slowly diffuse over two days.

{Re(CO)$_3$[H(L^{Me})]}(PF$_6$), (2^{Me})

A mixture of 0.075 g (0.11 mmol) of **1^{Me}** and 0.04 g (0.11 mmol) of $TlPF_6$ in 10 mL dry CH_3CN was heated at reflux overnight. After cooling to room temperature TlBr was separated by filtration through Celite, and solvent was removed by rotary evaporation. The residue was washed with two 5 mL portions Et_2O and was dried under vacuum to give 0.060 g (75 %) of **2^{Me}** as a colorless to pale yellow powder Mp, 243 - 246^oC dec. Anal. Calcd (obs.) for $C_{26}H_{25}Cl_2F_6N_5O_3PRe$ (**2^{Me}**·CD_2Cl_2**)**: C, 36.41 (36.25); H, 2.94 (2.77); N, 8.17 (8.27). IR (KBr) ν_{NH} 3253; ν_{co} 2030, 1940, 1920 cm^{-1}. ^1H NMR: (CD_2Cl_2, 233 K) 7.98 (d, *J* = 3 Hz, 1H, H_5pz), 7.54 (s, 1H, NH), 7.53 (d, *J* = 3 Hz, 1H, H_5pz), 7.48 (d, *J* = 8 Hz, 1H, Ar), 7.41 (d, *J* = 8 Hz, 1H, Ar), 7.30 (s, 1H, Ar), 6.94 (s, 1H, Ar), 6.89 (d, *J* = 9 Hz, 1H, Ar), 6.69 (d, *J* = 9 Hz, 1H, Ar), 6.66 (d, *J* = 3 Hz, 1H, H_4pz), 6.10 (d, *J* = 3 Hz, 1H, H_4pz), 2.80 (s, 3H, $pzCH_3$), 2.49 (s, 3H, $ArCH_3$), 2.23 (s, 3H, $ArCH_3$, $ArCH_3$), 2.04 (s, 3H, $pzCH_3$). ^{13}C NMR: (CD_2Cl_2, 295 K) no signals were observed even after prolonged acquisition times. UV-VIS λ_{max}, nm (ε, $M^{-1}cm^{-1}$), CD_2Cl_2: 230(34154), 250 (28087), 294 (8854). X-ray quality crystals were grown by layering an acetone solution with hexane and allowing the solvents to slowly diffuse over two days

$Re(CO)_3[H(L^{iPr})]\}(PF_6)$, ($2^{iPr}$)

A mixture of 0.205 g (0.27 mmol) of **1^{iPr}** and 0.084 g (0.27 mmol) $TlPF_6$ in 20 mL dry THF was heated at reflux overnight. After cooling to room temperature, TlBr was separated by filtration through Celite and solvent was removed from the filtrate by rotary evaporation. The residue was washed with two 5 mL portions Et_2O and was dried under vacuum to give 0.198 g (84 %) of **2^{iPr}** as a white powder. Mp, 278 - 280°C dec. Anal. Calcd (obs.) for $C_{29}H_{31}F_6N_5O_3PRe$: C, 42.03 (42.26); H, 3.77 (4.02); N, 8.45 (8.12) IR (KBr) ν_{NH} 3236; ν_{co} 2035, 1940, 1911 cm^{-1}. ^1H NMR: (CD_2Cl_2, 233 K) 8.24 (s, 1H, NH), 7.97 (d, *J* = 3 Hz, 1H, H_5pz), 7.56 (d, *J* = 3Hz, 1H, H_5pz), 7.55 (d, *J* = 8 Hz, 1H, Ar), 7.40 (d, *J* = 8 Hz, 1H, Ar), 7.29 (s, 1H, Ar), 6.90 (s, 1H, Ar), 6.87 (d, *J* = 8.5 Hz, 1H, Ar), 6.73 (d, *J* = 3 Hz, 1H, H_4pz), 6.70 (d, *J* = 8.5 Hz, 1H, Ar), 6.15 (d, *J* = 3 Hz, 1H, H_4pz), 3.84 (sept, *J* = 7 Hz, 1H, Me_2CH), 2.92 (sept, *J* = 7 Hz, 1H, Me_2CH), 2.49 (s, 3H, $ArCH_3$), 2.23 (s, 3H, $ArCH_3$), 1.49 (d, *J* = 7 Hz, 3H, $iPrCH_3$), 1.36 (d, *J* = 7 Hz, 3H, $iPrCH_3$), 1.16 (d, *J* = 7 Hz, 3H, $iPrCH_3$), 0.62 (d, *J* = 7 Hz, 3H, $iPrCH_3$). ^{13}C NMR: (CD_2Cl_2, 295 K) no signals were observed even after prolonged acquisition times. UV-VIS λ_{max}, nm (ε, $M^{-1}cm^{-1}$), CD_2Cl_2: 229(31536), 249(24891), 294(5514). X-ray quality crystals were grown by layering an acetone solution with hexane and allowing the solvents to slowly diffuse over two days.

$Re(CO)_3(L^{Me})$, (3^{Me})

Method A. To a solution of 0.201 g (0.28 mmol) **1^{Me}** in 20 mL of CH_3CN was added 2.75 mL (0.283 mmol) $(NEt_4)(OH)$ solution in MeOH immediately giving a yellow solution. The mixture was stirred for 30 min then solvent was removed by rotary

evaporation. The yellow residue was washed with two 5 mL portions MeOH and was dried under vacuum to leave 0.150 g (88 %) of **3**$^{\mathbf{Me}}$ as a yellow powder. Mp, 250 - 254^{o}C dec. Anal. Calcd (obs.) for $C_{25}H_{22}N_5O_3Re$: C, 47.91 (48.01); H, 3.54 (3.58); N, 11.18 (11.23). IR (KBr) ν_{co} 2020, 1905, 1885cm^{-1}. ^{1}H NMR: (CD_2Cl_2, 293 K) 7.81 (d, *J* = 2 Hz, 2H, H_5pz),6.92 (s, 2H, Ar-H), 6.90 (part of AB d, 2H, Ar), 6.63 (part of AB d, 2H, Ar), 6.28 (d, *J* = 2 Hz, 2H, H_4pz), 2.52 (s, 6H, pzCH_3), 2.27 (s, 6H, ArCH_3). ^{1}H NMR: (acetone-d_6) 8.26 (d, *J* = 3 Hz, 2H, H_5pz), 7.10 (d, *J* = 2 Hz, 2H, Ar), 6.92 (part of AB d, *J* = 8, 2 Hz, 2H, Ar), 6.61 (part of AB d, *J* = 8 Hz, 2H, Ar), 6.44 (d, *J* = 3 Hz, 2H, H_4pz), 2.53 (s, 6H, pzCH_3), 2.23 (s, 6H, ArCH_3). ^{13}C NMR: (CD_2Cl_2) 198.2, 196.7, 155.5, 149.8, 132.2, 131.5, 129.6, 128.2, 124.2, 122.1, 108.3, 20.6 17.1. UV-VIS λ_{max}, nm (ε, $M^{-1}cm^{-1}$), CD_2Cl_2: 234(44756), 247(41711), 298(14615), 392(3687). X-ray quality crystals were grown by layering an acetone solution with hexane and allowing the solvents to slowly diffuse over two days.

Method B. A 0.32 mL aliquot of 0.509 M (NEt_4)(OH) (0.16 mmol) in MeOH was added to a solution of 0.124 g (0.160 mmol) **2**$^{\mathbf{Me}}$ in 10 mL of CH_3CN immediately giving a yellow solution. The mixture was stirred for 15 min then solvent was removed by rotary evaporation. The yellow residue was extracted with three 5 mL portions of benzene and solvent was removed by vacuum distillation to leave a mixrure of benzene-soluble **3**$^{\mathbf{Me}}$ contaminated with H(**L**$^{\mathbf{Me}}$) (NMR). The contaminant was removed by washing with minimal Et_2O (2 mL), to leave 0.030 g (30%) of **3**$^{\mathbf{Me}}$ with characterization data identical to above. Selective precipitation of **3**$^{\mathbf{Me}}$ using MeOH as in Method A, did not lead to improved yield

$Re(CO)_3(L^{iPr})$, (3^{iPr})

In a manner similar to method A of $\mathbf{3^{Me}}$, 0.091 mmol $(NEt_4)(OH)$ (1.3 mL of 0.07M solution in MeOH) and 0.073 g (0.095 mmol) gave 0.040 g (61 %) of $\mathbf{3^{iPr}}$ as a yellow powder. Mp, 240 - 243°C dec. Anal. Calcd (obs.) for $C_{29}H_{30}N_5O_3Re$: C, 51.01 (51.24); H, 4.43 (4.54); N, 10.26 (10.22). IR (KBr): ν_{co} 2010, 1900, 1875 cm^{-1}. ^1H NMR (CD_2Cl_2, 293 K) 7.80 (d, J = 3 Hz, 2H, H_5pz), 6.89 (s, 2H, Ar), 6.88 (part of AB d, 2H, Ar), 6.60 (part of AB d, 2H, Ar), 6.33 (d, *J* = 3 Hz, 2H, H_4pz), 3.57 (sept, *J* =7 Hz, 2H, Me_2CH), 2.26 (s, 6H, $ArCH_3$), 1.34 (d, *J* = 7 Hz, 6H, $iPrCH_3$), 1.02 (d, *J* = 7 Hz, 6H, $iPrCH_3$). ^1H NMR: (acetone-d_6) 8.18 (d, *J* = 3Hz, 2H, H_5pz), 7.07 (s, 2H, Ar), 6.89 (part of AB d, 2H, Ar), 6.56 (part of AB d, 2H, Ar), 6.55 (d, *J* = 2 Hz, 2H, H_4pz), 3.62 (sept, *J* =7 Hz, 1H Me_2CH), 2.22 (s, 6H, $ArCH_3$), 1.37 (d, *J* = 7 Hz, 6H, $iPrCH_3$), 1.08 (d, *J* = 7Hz, 6H, $iPrCH_3$). ^{13}C NMR: (CD_2Cl_2) 197.2, 194.5, 166.0, 150.0, 133.0, 131.5,129.5, 128.5, 124.4, 122.0, 104.6, 30.6, 23.6, 23.3, 20.6. UV-VIS λ_{max}, nm (ε, $M^{-1}cm^{-1}$), CD_2Cl_2: 234(49162), 247(46362), 305(12127), 391(3667). X-ray quality crystals were grown by layering an acetone solution with hexane and allowing the solvents to slowly diffuse over two days

General procedure for NMR-scale reactions between $\mathbf{3^R}$ and MeI

Solutions were prepared in NMR tubes by dissolving 7-9 mg $\mathbf{3^R}$ in 0.35 mL of acetone-d_6. A ten-fold excess MeI (7-9 µL, as appropriate) was injected into the solution, the NMR tube was immediately sealed and inserted into the pre-heated 45°C NMR cavity for measurements where time of insertion served as the reference point (*t* = 0 min). NMR

spectra were acquired at 10 min intervals for the first 30 min, then at 30 min intervals thereafter.

Colorless crystals of {$Re(CO)_3$[Me(**L**^{iPr})]}(I), (**4**^{iPr}) suitable for single-crystal X-ray diffraction were obtained by removing volatile components from the completed reactions by vacuum distillation, dissolving the residue in CH_2Cl_2, layering with *n*-hexane, and allowing the solvents to slowly diffuse 15 h

4^{Me} Mp, 265 - 270^{o}C dec. IR (CH_2Cl_2) ν_{co} 2036, 1930, 1923 cm^{-1}. ^{1}H NMR: (acetone-d_6, 293 K) 8.78 (d, J = 2.8 Hz, 1H, H_5pz), 8.06 (d, J = 2.8 Hz, 1H, H_5pz), 8.00 (part of AB d, J_{app} = 8.4 Hz, 1H, Ar), 7.72 (s, 1H, Ar), 7.66 (part of AB, d, J_{app} = 8.4, 2.1, 1 Hz, 1H, Ar), 7.57 (s, 1H, Ar), 7.04 (part of AB d, J_{app} = 8.4 Hz, 1H, Ar), 7.01 (d, J = 2.8 Hz, 1H, H_4pz) 6.82 (part of AB d, J_{app} = 8.4 Hz, 1H, Ar), 6.33 (d, J = 2.8 Hz, 1H, H_4pz), 3.76 (s, 3H, NCH_3), 2.92 (s, 3H, CH_3), 2.53 (s, 3H, CH_3), 2.28 (s, 3H, CH_3), 2.06 (s, 3H, CH_3). UV-VIS λ_{max}, nm (ε, M^{-1}cm^{-1}), CD_2Cl_2: 242 (52,000), 289sh (13,000), 368 (1,300)

4^{iPr}**.** Mp, 260 - 265^{o}C dec. IR (CH_2Cl_2) ν_{co} 2033, 1927, 1915 cm^{-1}. ^{1}H NMR: (acetone-d_6, 293 K) 8.79 (d, J = 3.0 Hz, 1H, H_5pz), 8.12 (d, J = 3.0 Hz, 1H, H_5pz), 8.00 (part of AB d, J_{app} = 8.4 Hz, 1H, Ar), 7.71 (s, 1H, Ar), 7.66 (part of AB, d, J_{app} = 8.4, 2.1, 1 Hz, 1H, Ar), 7.53 (s, 1H, Ar), 7.17 (d, J = 2.8 Hz, 1H, H_4pz), 7.05 (part of AB d, J_{app} = 8.4 Hz, 1H, Ar), 6.82 (part of AB d, J_{app} = 8.4 Hz, 1H, Ar), 6.49 (d, J = 2.8 Hz, 1H, H_4pz), 3.93 (sept, *J* =7 Hz, 1H, Me_2CH), 3.75 (s, 3H, NCH_3), 2.91 (sept, *J* =7 Hz, 1H, Me_2CH), 2.54 (s, 3H, $ArCH_3$), 2.28 (s, 3H, $ArCH_3$), 1.57 (d, *J* = 7 Hz, 3H, iPrCH_3), 1.49 (d, *J* = 7 Hz, 3H, iPrCH_3), 1.22 (d, *J* = 7Hz, 3H, iPrCH_3), 0.81 (d, *J* = 7 Hz, 3H, iPrCH_3). UV-VIS λ_{max}, nm (ε, M^{-1}cm^{-1}), CD_2Cl_2: 242 (50,000), 293sh (9,000), 367 (400).

4.9. Crystallographic Structure Determinations

X-ray intensity data from a colorless prism of $H(L^{Me})$, colorless block of each $ReBr(CO)_3[H(L^{Me})]\cdot$acetone ($1^{Me}\cdot$acetone), $ReBr(CO)_3[H(L^{iPr})]$ (1^{iPr}), $\{Re(CO)_3[H(L^{Me})]\}(PF_6)$, ($2^{Me}$), and$\{Re(CO)_3[H(L^{iPr})]\}(PF_6)$, ($2^{iPr}$), of a yellow block of $Re(CO)_3(L^{Me})$, (3^{Me}), and of a pale yellow block of $Re(CO)_3(L^{iPr})$, (3^{iPr}), were measured at 100(2) K with a Bruker AXS 3-circle diffractometer equipped with a SMART2[19] CCD detector using Cu(Kα) radiation. X-ray intensity data from a colorless needle of $\{Re(CO)_3[Me(L^{iPr})]\}(I)\cdot 2CH_2Cl_2$, ($4^{iPr}\cdot 2CH_2Cl_2$) were measured at 100(2) K with an Oxford Diffraction Ltd. Supernova diffractometer equipped with a 135 mm Atlas CCD detector using Cu(Kα) (or Mo(Kα) for $4^{iPr}\cdot 2CH_2Cl_2$) radiation. Raw data frame integration and Lp corrections were performed with SAINT+.[20] Final unit cell parameters were determined by least-squares refinement of 5019, and 9735 reflections from the data sets of $1^{Me}\cdot$acetone, and 1^{iPr}, respectively, of 8854, and 7055 reflections from the data sets of 2^{Me} and 2^{iPr} respectively, and of 8940, and 8003 reflections from the data sets of 3^{Me} and 3^{iPr}, respectively, and of 38198 reflections from the data set of 4^{iPr} with $I > 2\sigma(I)$ for each. Analysis of the data showed negligible crystal decay during collection in each case. Direct methods structure solutions, difference Fourier calculations and full-matrix least-squares refinements against F^2 were performed with SHELXTL.[21] Numerical absorption corrections based on the real shape of the crystals for the compounds were applied with SADABS.[20] All non-hydrogen atoms were refined with anisotropic displacement parameters. Hydrogen atoms were placed in geometrically idealized positions and included as riding atoms, except where noted below. The X-ray crystallographic

parameters and further details of data collection and structure refinements are presented in Tables 4.3 and 4.4.

	$H(L^{Me})$	1^{Me}·acetone	2^{Me}	3^{Me}
Emprical Formula	$C_{22}H_{23}N_5$	$C_{28}H_{29}BrN_5O_4Re$	$C_{25}H_{23}F_6N_5O_3PRe$	$C_{25}H_{22}N_5O_3Re$
Formula Weight	357.45	765.67	772.65	626.68
T/K	100(2)	100(2)	100(2)	100(2)
Crystal Size, mm^3	0.43x0.18x0.12	0.24x0.13x0.05	0.26x0.21x0.10	0.24x0.14x0.06
Crystal System	Orthorhombic	Triclinic	Triclinic	Monoclinic
Space Group	P bcn	P-1	P-1	C2/c
a/Å	14.6980(3)	10.8094(2)	8.63640(10)	30.8054(4)
b/Å	7.7505(2)	10.9596(2)	9.66670(10)	11.4882(2)
c/Å	33.6382(8)	13.4496(2)	16.7540(2)	13.4222(2)
α(°)	90	84.7710(10)	78.9030(10)	90
β(°)	90	85.0860(10)	82.4590(10)	94.7730(10)
γ(°)	90	60.9190(10)	78.8010(10)	90
$V/Å^3$	3831.96(16)	1385.10(4)	1340.01(3)	4733.63(12)
Z	8	2	2	8
d_c/g cm^{-3}	1.239	1.836	1.915	1.759
λ(Cu Kα), Å	1.54178	1.54178	1.54178	1.54178
μ/ mm^{-1}	0.597	10.630	10.165	10.350
Abs. Correction	multi-scan	numerical	numerical	numerical
F(000)	1520	748	752	2448
θ range (°)	2.63 to 67.97	3.30 to 67.89	2.70 to 67.70	2.88 to 68.02
Reflections collected	32005	11557	11073	19490
Reflections unique	3444	4733	4556	4198
R_{int}	0.0306	0.0150	0.0168	0.0204
T_{min}/T_{max}	0.7835/0.9318	0.1847/0.6185	0.1775/0.4297	0.1902/0.5756
Data/restraints/ parameters	3444/0/253	4046/0/363	4556/0/381	4198/0/311
GOF(F_2)	1.020	1.001	1.007	0.993
R indices[$I>2\sigma(I)$][a](all data)	0.0382 (0.0432)	0.0172 (0.0173)	0.0188 (0.0194)	0.0245 (0.0285)
*w*R indices (all data)[b]	0.0988 (0.1024)	0.0446 (0.0447)	0.0474 (0.0478)	0.0679 (0.0702)
Residuals/ eA^{-3}	0.237/-0.158	0.613/-0.548	0.714/-0.646	0.815/-0.565

[a] $R_1 = \Sigma||F_o|-|F_c||/\Sigma|F_o|$. [b] $wR_2 = \{\Sigma[w(F_o^2-F_c^2)^2]/\Sigma[w(F_o^2)^2]\}^{1/2}$

Table 4.3 Crystal and structure refinement data for $H(L^{Me})$, 1^{Me}·acetone, 2^{Me}, and 3^{Me}.

	$\mathbf{1^{iPr}}$	$\mathbf{2^{iPr}}$	$\mathbf{3^{iPr}}$	$\mathbf{4^{iPr}}\cdot 2CH_2Cl_2$
Emprical Formula	$C_{29}H_{31}BrN_5O_3Re$	$C_{29}H_{31}F_6N_5O_3PRe$	$C_{29}H_{30}N_5O_3Re$	$C_{32}H_{37}Cl_4IN_5O_3Re$
Formula Weight	763.70	828.76	682.78	994.57
T/K	100(2)	100(2)	100(2)	100(2)
Crystal Size	0.15x0.14x0.10	0.23x0.10x0.06	0.28x0.16x0.06	0.33x0.07x0.04
Crystal System	Orthorhombic	Monoclinic	Monoclinic	Triclinic
Space Group	$P2_12_12_1$	$P2_1/c$	$P2_1/c$	P-1
a/Å	13.1679(2)	9.49510(10)	15.7528(2)	10.9417(3)
b/Å	13.4486(2)	14.9707(2)	13.73050(10)	12.1830(2)
c/Å	16.2017(2)	22.1068(3)	13.76030(10)	15.7817(3)
α(°)	90	90	90	73.5426(18)
β(°)	90	100.1190(10)	114.662(1)	85.7981(19)
γ(°)	90	90	90	65.475(2)
V/Å^3	2869.16(7)	3093.56(7)	2704.79(4)	1833.16(7)
Z	4	4	4	2
d_c/g cm^{-3}	1.768	1.779	1.677	1.802
λ(Cu or Mo Kα), Å	1.54178	1.54178	1.54178	0.7107
μ/ mm^{-1}	10.234	8.854	9.110	4.487
Abs. Correction	numerical	numerical	numerical	numerical
F(000)	1496	1632	1352	968
θ range (°)	4.27 to 68.17	3.58 to 67.61	3.09 to 68.20	3.30 to 32.72
Reflections collected	23851	25065	22830	59279
Reflections unique	5079	5429	4810	12747
R_{int}	0.0216	0.0223	0.0173	0.0330
T_{min}/T_{max}	0.3090/0.4276	0.2353/0.6187	0.1847/0.6109	0.349/0.866
Data/restraints/ parameters	5079/0/362	5429/0/416	4810/0/350	12747/0/422
GOF(F_2)	0.992	0.992	0.999	1.040
R indices[$I>2\sigma(I)$][a](all data)	0.0168 (0.0170)	0.0219 (0.0252)	0.0178 (0.0182)	0.0191 (0.0241)
*w*R indices (all data)[b]	0.0428 (0.0429)	0.0541 (0.0554)	0.0462 (0.0465)	0.0456 (0.0463)
Residuals/ eA^{-3}	0.642/-0.458	0.682/-0.628	0.578/-0.606	1.006/-0.896

[a] $R_1 = \Sigma||F_o|-|F_c||/\Sigma|F_o|$. [b] $wR_2 = \{\Sigma[w(F_o^2-F_c^2)^2]/\Sigma[w(F_o^2)^2]\}^{1/2}$

Table 4.4 Crystal and structure refinement data for $\mathbf{1^{iPr}}$, $\mathbf{2^{iPr}}$, $\mathbf{3^{iPr}}$ and $\mathbf{4^{iPr}\cdot 2CH_2Cl_2}$

CHAPTER: 5

LIGAND ADDITIVITY EFFECTS ON THE ELECTROCHEMICAL PROPERTIES OF METAL COMPLEXES BEARING A REDOX-ACTIVE LIGAND.

5.1 Introduction

An emergent area of contemporary research interest centers on the development and study of metal complexes that contain redox-active ligands for potential applications that span from molecular electronics to catalysis.[1] One of the main goals of research in this area is to exploit the redox-active ligand as an "electron reservoir" to promote unusual chemical reactivity,[2] to negotiate electron/hole transfer processes in molecular wires,[3] or to identify new examples of valence tautomerism.[4] In each area, an intimate knowledge of the electrochemical properties of the metal-bound redox-active ligand and the spectroscopic properties of the reduced and oxidized forms of a complex are vital for advancement. For systematic explorations in this context, it is desirable that a given redox-active ligand is easily accessed and contains simple synthetic handles to permit tuning of the electronic or steric environment about a bound metal. We recently reported on a new class of redox-active NNN-pincer ligands based on di(2-3R-pyrazol-1-yl-*p*-aryl)amidos, Figure 5.1, that possesses such characteristics.[5,6]

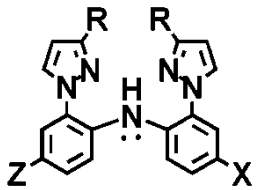

$H(^{R}ZX)$

Figure 5.1. Generic representation of NNN-pincer ligands $H(^{R}ZX)$. For this study, the ligand H(L) has R = H, Z = X = CH_3.

We demonstrated in tricarbonylrhenium(I) chemistry that one-electron oxidation gives a ligand centered-radical and that changing R groups from hydrogen to alkyls causes ligand folding and enhances ligand centered reactivity.[5] By examining the carbonylrhodium(I) chemistry,[6] we showed that the electronic properties and reactivity of the ligands are predictably tuned by varying the *para*-aryl substituents. Ligands with tolyl arms (Z and/or X = CH_3) give more electron rich carbonylrhodium(I) centers and faster oxidative addition reactions with alkyl halides than when the ligand aryl arms are trifluormethylaryls (Z and/or X = CF_3). While the trend in observed electronic properties of a series of related complexes with different substituents along the ligand periphery is understandable and predictable, the *magnitude* of changes in properties due to substitution of groups along the periphery and how this influences their place in an electrochemical activity series are not so easily predicted. One of difficulties in such predictions centers on determining the *extent* that different metal complexes, $LMX_nY_oZ_p$, with varying numbers, types, and relative stereochemistry of exogeneous ligands (X, Y, Z) can impact the electrochemical properties of a neighboring metal-bound redox-active ligand, L. Ligand additivity models offered by Bursten,[7] Pickett,[8] Lever,[9] Pombiero,[10] and others[11] detail the effects that ligands have on the electrochemical properties of a

metal-based redox couple. The tabulated, empirical electrochemical ligand parameters, E_L (or P_L), which allow for the prediction of $E_{1/2}$ values for M^n/M^{n-1} couples, have been correlated to the ligand's participation in the HOMO, its π-acceptor or π-donor abilities, and its polarizability. It follows that the $E_{1/2}$ value of an associated (metal-bound) redox-active ligand should also be modulated by both the metal and its other (non-redox-active) ligands, and that the E_L (or P_L) parameters could be used for the prediction of a ligand-centered oxidation (or reduction). To the best of our knowledge, such a correlation has not yet been extended to predicting the $E_{1/2}$ values for a redox-active ligand. Such a correlation would be important, for instance, to better understand when an exothermic electron transfer from the redox-active ligand to a bound substrate might occur during a catalytic cycle or perhaps for the design of new valence tautomers. In the chapter, we outline the synthesis of a convenient reagent for coordination chemistry of rhodium(III) complexes with a redox-active NNN-pincer ligand, namely, (NEt_4)[(di-2-pyrazo1-l-yl-*p*-tolylamido)$RhCl_3$]·H_2O, **2**·H_2O. On the basis of the results obtained from this and subsequent coordination complexes derived from **2**·H_2O, we also describe an empirical relationship between E_L parameters and the half-wave potential of a rhodium(III)-bound di(2-pyrazolyl-*p*-tolyl)amido ligand. This relationship takes into account the observed differences in $E_{1/2}$ on the stereochemistry of *mer*-LRhXYZ complexes. Although this relationship is specific for this series of rhodium(III) complexes, the described methodology should be general for other redox-active ligands and their metal complexes.

5.2.Experimental Section

5.2.1. Syntheses and Characterization of Complexes.

General Considerations. The compounds $RhCl_3 \cdot xH_2O$, $TlPF_6$, $Tl(OSO_2CF_3$ = OTf), 1.0 *M* NEt_4OH in MeOH, pyridine, 2,2'-dipyridyl, 4'-(4-methylphenyl)-2,2':6',2''-terpyridine (ttpy), PEt_3, PPh_3, and $(NO)(SbCl_6)$ were purchased from commercial sources and were used without further purification. The pincer ligand, H(L), and (L)Rh(Me)(I)(CO) were prepared as described previously.[6] The organic cation radical oxidant, 9,10-dimethoxyocta-hydro-1,4:5,8-dimethanoanthracenium hexachloroantimonate, $(CRET)(SbCl_6)$ (ε_{518} = 7300 $M^{-1}cm^{-1}$, $E_{1/2}$ = +1.09 versus Ag/AgCl), was prepared according to literature procedures.[19]

Physical Measurements. Midwest MicroLab, LLC, Indianapolis, Indiana 45250, performed all elemental analyses. ^{1}H, ^{13}C, ^{19}F and ^{31}P NMR spectra were recorded on a Varian 400 MHz spectrometer. DQCOSY and NOESY spectra were acquired on a Varian 600 MHz spectrometer. Chemical shifts were referenced to solvent resonances at δ_H 7.27, δ_C 77.23 for $CDCl_3$; δ_H 5.33, δ_C 53.84 for CD_2Cl_2; δ_H 5.99 for $C_2D_2Cl_4$; δ_H 1.94, δ_C 118.9 for CD_3CN and δ_H 2.05, δ_C 29.92 for acetone-d_6 while those for ^{19}F and ^{31}P NMR spectra were referenced against external standards of $CFCl_3$ (δ_F 0.00 ppm) and 85% H_3PO_4 (aq) (δ_P 0.00 ppm), respectively. Abbreviations for NMR and UV-Vis br (broad), sh (shoulder), m (multiplet), ps (pseudo-), s (singlet), d (doublet), t (triplet), q (quartet), p (pentet), sept (septet). Melting point determinations were made on samples contained in glass capillaries using an Electrothermal 9100 apparatus and are uncorrected. Absorption measurements were recorded on an Agilent 8453 spectrometer. Electrochemical measurements were collected under a nitrogen atmosphere for samples as 0.1 mM solutions in CH_3CN and in CH_2Cl_2, each with 0.1 M NBu_4PF_6 as the supporting

electrolyte. A three-electrode cell comprised of an Ag/AgCl electrode (separated from the reaction medium with a semipermeable polymer membrane filter), a platinum working electrode, and a glassy carbon counter electrode was used for the voltammetric measurements. Data were collected at scan rates of 50, 100, 200, 300, 400, and 500 mV/s. With this set up, the ferrocene/ferrocenium couple had an $E_{1/2}$ value of +0.53 V in CH_3CN and +0.41 V in CH_2Cl_2 at a scan rate of 200 mV/s, consistent with the literature values.[23] EPR measurements were obtained using a Bruker ELEXSYS E600 equipped with an ER4116DM cavity resonating at 9.63 GHz, an Oxford Instruments ITC503 temperature controller and ESR-900 helium-flow cryostat. The ESR spectra were recorded with 100 kHz field modulation except where noted.

[H(L)]RhCl$_3$, 1. A mixture of 0.606 g (1.84 mmol) H(**L**) and 0.484 g (1.84 mmol) $RhCl_3 \cdot xH_2O$ (for calculations it is presumed that x =3) in 30 mL absolute EtOH was heated at reflux. A red solution is formed within a few minutes, and then a golden-beige precipitate forms over the course of 1 h. After a total reflux time of 1.5 h, the mixture was cooled to room temperature. The desired insoluble product was collected by filtration where it was washed with two 5 mL portions Et_2O and then was dried under vacuum to give 0.864 g (87 %) of H(**L**)$RhCl_3$ as a golden-beige solid. Mp 272 - 274^{o}C dec. Anal. Calcd (obs.) for $C_{20}H_{19}Cl_3N_5Re$: C, 44.60 (44.68); H, 3.56 (3.76); N, 13.00 (12.56).

(NEt$_4$)[(L)RhCl$_3$], 2·H$_2$O. A 5.28 mL aliquot of a solution 0.3035 *M* (NEt_4)(OH) in MeOH (1.60 mmol) was added to a suspension of 0.863 g (1.60 mmol) of **1** in 25 mL

MeOH which immediately produced a dark green solution. After the solution had been stirred at room temperature 30 min, solvent was removed by vacuum distillation. The resulting green solid was washed with two 10 mL portions of Et_2O and was dried under vacuum to give 0.996 g (91 %) $(NEt_4)[(\mathbf{L})RhCl_3]\cdot H_2O$, (**2**·$H_2O$) as a fine green powder. Crystals of anhydrous **2** suitable for single-crystal X-ray diffraction were grown by layering a CH_2Cl_2 solution with hexanes and allowing solvents to slowly diffuse over 1d. The characterization data below are for the hydrate. Mp 261-266° C. Anal. Calcd (obs.) for $C_{28}H_{40}Cl_3N_6ORh$: C, 49.03 (48.85); H, 5.88 (5.93); N, 12.25 (11.98). ^{1}H NMR (CD_2Cl_2, 293K): δ_H 8.51 (d, *J* = 2.5 Hz, 2 H, H_3pz), 8.14 (d, *J* = 2.5 Hz, 2 H, H_5pz), 7.27 (d, *J* = 8.4 Hz, 2 H, Ar-H), 7.09 (s, 2 H, Ar), 6.76 (d, *J* = 8.4 Hz, 2 H, Ar-H), 6.61 (t, *J* = 2.5 Hz, 2 H, H_4pz), 3.17 (q, *J* = 7.3 Hz, 8 H, N*CH*$_2$CH$_3$), 2.29 (s, 6H, ArCH$_3$), 1.70 (s, 2H, H_2O), 1.18 (t, *J* = 7.3 Hz, 12 H, N-CH$_2$*CH*$_3$). UV-Vis (CH_3CN) nm (ε, $M^{-1}cm^{-1}$): 239 (41,000), 346 (9,500), 373 (4,800), 415 (5,600), 579 (770).

***trans*-(L)RhCl$_2$(py)·CHCl$_3$, *trans*-3·CHCl$_3$.** A mixture of 0.211 g (0.308 mmol) **2**·H_2O and 0.13 mL (1.6 mmol) pyridine in 20 mL chloroform was heated at reflux for 16 h and then the chloroform was removed by vacuum distillation. The resulting green solid was subject to column chromatography on neutral alumina. Elution with diethyl ether removed residual pyridine and then elution with chloroform gave *trans*-**3** in a green band near the solvent front (R_f = 0.85). After solvent was removed from the collected green band, 0.112 g (52 %) of *trans*-**3**·$CHCl_3$ was obtained as a green powder. Mp 244-247 ^{o}C (dec). Anal. Calcd (obs.) for $C_{26}H_{24}Cl_5N_6Rh$: C, 44.57 (44.79); H, 3.45 (3.48); N, 11.99 (12.03). ^{1}H NMR ($CDCl_3$): See section 5.7 Scheme 5.5 for labeling diagram, δ_H 9.24 (d,

J = 6 Hz, 2 H, $H_{2,6}$py), 8.10 (d, J = 3 Hz, 2H, H_5pz), 7.90 (t, J = 8 Hz, 1 H, H_4py), 7.45 (dd, J = 8, 6 Hz, 2 H, $H_{3,5}$py), 7.40 (d, J = 8 Hz, 2 H, H_6Ar), 7.17 (d, J = 2 Hz, 2 H, H_3Ar), 7.15 (d, J = 2 Hz, 2 H, H_3pz), 6.87 (dd, J = 8, 2 Hz, 2 H, H_5Ar), 6.51 (dd, J = 3, 2 Hz, 2 H, H_4pz), 2.31 (s, 6 H, CH_3). ^{13}C NMR ($CDCl_3$): 155.2, 143.5, 138.2, 137.4, 136.6, 134.0, 130.6, 128.7, 126.3, 124.9, 121.5, 108.6, 20.9. UV-Vis (CH_3CN) nm (ε, $M^{-1}cm^{-1}$): 238 (53,800), 337 (10,700), 370 (8,000), 404 (8,500), 579 (800). Crystals of *trans*-**3**·CH_2Cl_2 suitable for X-ray diffraction were grown by layering a CH_2Cl_2 solution with hexanes and allowing solvents to diffuse over the course of 1d. A vacuum dried sample of crystals analyzed as the dichloromethane solvate: Anal. Calcd (obs.) for $C_{26}H_{25}Cl_4N_6Rh$: C, 46.87 (46.53); H, 3.78 (3.83); N, 12.61 (12.34).

***cis*-(L)RhCl$_2$(py), *cis*-3**. A solution of 0.112 g (0.160 mmol) *trans*-**3**·$CHCl_3$ in 10 mL $C_2H_2Cl_4$ was heated at reflux 14 h. Solvent was then removed by vacuum distillation to leave a red-brown residue which was washed with two 5 mL portions Et_2O and was dried under vacuum to leave 0.099 g (88%) of a red-brown powder which is a mixture of *cis*-**3** with ca. 9% *trans*-**3** by NMR analysis. The mixture was dissolved in minimal $CHCl_3$, and subjected to flash chromatography on a short SiO_2 pad eluting first with fresh $CHCl_3$ which removed a green band of *trans*-**3** (note: *cis*-**3** decomposes slowly on SiO_2 or Al_2O_3 to form *trans*-**3** as one product, so the exposure time to these substances should be minimized). Then, flushing with ethyl acetate afforded 0.040 g (43%) of pure *cis*-**3** in the orange band near the solvent front. Mp 290 ^{o}C dec. Anal. Calcd (obs.) for $C_{25}H_{23}N_6Cl_2Rh$: C, 51.66 (51.82); H, 3.99 (4.05); N, 14.46 (14.68). ^{1}H NMR (CD_2Cl_2): See section 5.7 Scheme 5.2 for labeling diagram, δ_H 8.71 (d, J = 2 Hz, 1 H, H_3pz), 8.31

(d, J = 2.7 Hz, 1 H, H_5pz), 8.12 (d, J = 2 Hz, 1 H, H_3pz), 8.04 (d, J = 2.7 Hz, 1 H, H_5pz), 7.88 (br d, J_{app} = 4 Hz, 2 H, $H_{2,6}$py), 7.51 (t, J = 7.6 Hz, 1 H, H_4py), 7.25 (d, J = 8.8 Hz, 1 H, H_6Ar), 7.22 (br s, 1 H, H_3Ar), 7.21 (d, J = 8.6 Hz, 1 H, H_6Ar), 6.91 (br m, 3H, H_5Ar and $H_{3,5}$py), 6.74 (dd, J = 3, 2 Hz, 1 H, H_4pz), 6.65 (m, 1H, H_3Ar), 6.62 (dd, J = 3, 2 Hz, 1 H, H_4pz), 2.34 (s, 3H, CH_3), 2.07 (s, 3 H, CH_3) ppm. ^{1}H NMR ($C_2D_2Cl_4$): δ_H 8.70 (d, J = 2 Hz, 1 H, H_3pz), 8.28 (d, J = 2.7 Hz, 1 H, H_5pz), 8.12 (d, J = 2 Hz, 1 H, H_3pz), 7.98 (d, J = 2.7 Hz, 1 H, H_5pz), 7.79 (br s, 2 H), 7.49 (t, J = 7.6 Hz, 1 H, py), 7.27 (d, J = 8.5 Hz, 1 H), 7.23 (d, J = 8.9 Hz, 1 H), 7.18 (br s, 1 H, Ar), 6.89 (br m, 3H), 6.74 (dd, J = 3, 2 Hz, 1 H, H_4pz), 6.61 (m, 2H), 6.57 (dd, J = 3, 2 Hz, 1 H, H_4pz), 2.34 (s, 3H, CH_3), 2.06 (s, 3 H, CH_3) ppm. UV-Vis (MeCN) nm (ε, $M^{-1}cm^{-1}$): 246 (54,600), 336 (12,900), 388 (7,600), 522 (1,900). Crystals of *cis*-**3** suitable for X-ray diffraction were grown by layering a CH_2Cl_2 solution with toluene and allowing solvents to diffuse over the course of 1d.

***trans*-[(L)Rh(py)$_2$Cl](PF$_6$), 6**. A mixture of 0.152 g (0.222 mmol) **2**·H_2O and 0.159 g (0.454 mmol) $TlPF_6$ in 15 mL pyridine was heated at reflux for 18 h under nitrogen. After cooling, pyridine was removed by vacuum distillation to give a red powder. The red powder was taken up in $CHCl_3$ and filtered through Celite to remove residual thallium salts. The bright red solution was washed with three 15 mL portions of water to remove $(NEt_4)^+$ salts. The organic fraction was dried over $MgSO_4$, filtered, and solvent was removed by vacuum distillation. The resulting rose-red powder was washed with Et_2O and was dried under vacuum to give 0.178 g (95%) of **6**. Mp 257-260 ^oC (dec). Anal. Calcd (obs.) for $C_{30}H_{28}ClF_6N_7PRh$: C, 46.80 (46.65); H, 3.67 (3.72); N, 12.73

(12.51). ^{1}H NMR ($CDCl_3$): δ_H 8.35 (dd, *J* = 3, 1 Hz, 2 H, H_5pz), 8.28 (dd, *J* = 2, 1 Hz, 2 H, H_3pz), 7.88 (br d, J_{app} = 4 Hz, 4 H, py), 7.65 (tt, *J* = 7.6, 1.4 Hz, 2 H, py), 7.21 (part of *AB*, J_{app} = 8.5 Hz, 2 H, Ar), 7.05 (m, J_{app} = 7.6, 1.4 Hz, 4 H, py), 6.81 6.81 (br s, 2 H, Ar), 6.79 (dd, *J* = 3, 2 Hz, 2 H, H_4pz), 6.78 (part of *AB*, J_{app} = 8.5 Hz, 2 H, Ar), 2.12 (s, 6 H, Ar-CH_3) ppm. ^{1}H NMR (CD_2Cl_2): d_H 8.31 (d, *J* = 3 Hz, 4H, H_3pz and H_5pz), 7.87 (br m, 4 H, py), 7.66 (pst, J_{app} = 7.8 Hz, 1 H, py), 7.22 (part of *AB*, 2 H, Ar), 7.04 (m, 4 H, py), 6.82 (m, 6 H, s and part of *AB* of Ar), 6.80 (ps t, *J* = 3 Hz, H_4pz), 2.14 (s, 6H, CH_3). ^{13}C NMR (CD_2Cl_2): 153.6, 145.8, 140.5, 139.6, 133.0, 130.9, 129.9, 129.4, 126.1, 125.4, 125.3, 122.7, 110.6, 20.4. ^{19}F NMR (CD_2Cl_2): δ_F -73.4 (d, J_{FP} = 712 Hz). ^{31}P NMR (CD_2Cl_2): δ_P -144.4 (sept, J_{PF} = 712 Hz). UV-Vis (CH_3CN): nm (ε, $cm^{-1}M^{-1}$) 247 (59,300), 326 (15,300), 375sh (7,600), 495 (3,050). High-quality but very thin, crystalline plates can be grown by layering a CH_2Cl_2 solution with hexanes and allowing solvents to diffuse over the course of 1d.

***trans*-(L)RhCl$_2$(PEt$_3$), *trans*-4**. A mixture of 0.324 g (0.472 mmol) **2**·H_2O and 0.35 mL (2.4 mmol) PEt_3 in 20 mL $CHCl_3$ was heated at reflux for 16 h and then solvent was removed by vacuum distillation. The resulting dark brown solid was subjected to flash chromatography on a small pad of neutral alumina where elution with chloroform gave *trans*-**4** in a yellow-green band (R_f = 0.75). After evaporation of solvent from this band, 0.180 g (61 %) of *trans*-**4** was obtained as a yellow-brown powder. Mp 233-236 ^{o}C (dec). Anal. Calcd (obs.) for $C_{26}H_{33}Cl_2N_5PRh$: C, 50.34 (50.13); H, 5.36 (5.26); N, 11.29 (11.17). ^{1}H NMR ($CDCl_3$): δ_H 7.96 (dd, *J* = 2.5, 0.5 Hz, 2 H, H_5pz), 7.73 (d, *J* = 2.0 Hz, 2 H, H_3pz), 7.19 (d, *J* = 8.6 Hz, 2 H, Ar), 7.16 (bs, 2 H, Ar), 6.86 (d, *J* = 8.3 Hz, 2

H, Ar), 6.52 (t, *J* = 2.6 Hz, 2 H, H_4pz), 2.34 (m, 3 H, CH_2), 2.28 (s, 6 H, Ar-CH_3), 1.99 (m, 3 H, CH_2), 1.05 (m, 9 H, Et-CH_3) ppm. ^{1}H NMR (CD_2Cl_2): δ_H 8.03 (d, *J* = 3 Hz, 2 H, H_5pz), 7.74 (d, *J* = 2 Hz, 2 H, H_5pz), 7.17 (bs, 2 H, Ar), 7.11 (part of *AB*, J_{app} = 8 Hz, 2 H, Ar), 6.85 (part of *AB*, J_{app} = 8 Hz, 2 H, Ar), 6.59 (pst, *J* = 2.6 Hz, 2 H, H_4pz), 2.32 (br m, 9 H, PCH_2 and Ar-CH_3), 2.00 (m, 3 H, PCH_2), 1.05 (dt, *J* = 15, 7.5 Hz, 9 H, Et-CH_3) ppm. ^{13}C NMR: ($CDCl_3$) no signals were observed even after 24 h acquisition time. ^{31}P NMR (CD_2Cl_2): δ_P 7.9 (d, J = 96 Hz) ppm; ($C_2D_2Cl_4$): δ_P 6.7 (br, s) ppm. UV-Vis (CH_3CN): nm (ε, $M^{-1}cm^{-1}$) 245 (49,100), 336 (13,000), 372 (6,000), 409 (6,750), 451sh (3,500), 543 (900). Crystals of *trans*-**4** 0.18CH_2Cl_2 suitable for single-crystal X-ray diffraction were grown by layering a CH_2Cl_2 solution with hexanes and allowing solvents to diffuse over the course of 2d.

***cis*-(L)RhCl$_2$(PEt$_3$), *cis*-4**. A solution of 0.102 g (0.165 mmol) of *trans*-**4** in 10 mL tetrachloroethane was heated at reflux for 8 h and then solvent was removed by vacuum distillation to afford a red-brown solid. The solid was washed with two 10 mL portions Et_2O and dried under vacuum to give 0.075 g (73%, if pure) of a mixture of *cis*-**4** with about 10% unidentified impurities from NMR integration, Only NMR signals attributed to *cis*-**4** are reported below. ^{1}H NMR (CD_2Cl_2): δ_H 8.65 (d, *J* = 2 Hz, 1 H, H_3pz), 8.40 (d, *J* = 2 Hz, 1 H, H_3pz), 8.27 (d, *J* = 3 Hz, 1 H, H_5pz), 8.16 (d, *J* = 3 Hz, 1 H, H_5pz), 7.42 (br m, 1 H, Ar), 7.16 (br s, 1H, Ar), 7.15 (br m, 1H, Ar), 7.01 (br s, 1 H, Ar), 6.94 (br m, 1 H, Ar), 6.80 (br s, 1 H, Ar), 6.66 (dd, *J* = 3, 2 Hz, 1 H, H_4pz), 6.63 (dd, *J* = 3, 2 Hz, 1 H, H_4pz), 2.31 (br s, 6 H, $ArCH_3$), 1.57 (br m, 3 H, PCH_2), 1.25 (br m, 3 H, PCH_2), 0.68 (dt, J = 16, 7.6 Hz, 9 H, Et-CH_3) ppm. ^{1}H NMR ($C_2D_2Cl_4$, 293 K): δ_H 8.66 (d, *J* = 2 Hz, 1 H, H_3pz), 8.37 (d, *J* = 2 Hz, 1 H, H_3pz), 8.23 (d, *J* = 3 Hz, 1 H, H_5pz), 8.09

(d, J = 3 Hz, 1 H, H_5pz), 7.43 (part of *AB*, J_{app} = 8.5 Hz, 1 H, Ar), 7.20 (part of *AB*, J_{app} = 8.7 Hz, 1 H, Ar), 7.11 (s, 1H, Ar), 6.97 (br s, 1 H, Ar), 6.89 (part of *AB*, J_{app} = 8.5 Hz, 1 H, Ar), 6.80 (part of *AB*, J_{app} = 8.7 Hz, 1 H, Ar), 6.63 (dd, J = 3, 2 Hz, 1 H, H_4pz), 6.58 (dd, J = 3, 2 Hz, 1 H, H_4pz), 2.33 (br s, 3 H, $ArCH_3$), 2.27 (br s, 3 H, $ArCH_3$), 1.52 (br m, 3 H, PCH_2), 1.20 (br m, 3 H, PCH_2), 0.64 (dt, J = 16, 7.6 Hz, 9 H, Et-CH_3) ppm. ^{31}P NMR (CD_2Cl_2): δ_P 28.4 (d, J = 115 Hz) ppm; ($C_2D_2Cl_4$): δ_P 31.3 (d, J = 116 Hz) ppm.

***trans*- and *cis*-(L)RhCl$_2$(pyz), *trans*-5 and *cis*-5.** A mixture of 0.294 g (0.428 mmol) **2**·H_2O and 0.172 g (2.14 mmol) pyrazine in 20 mL $CHCl_3$ was heated at reflux for 16 h and then solvent was removed by vacuum distillation to leave a dark brown residue. The residue was washed with two 10 mL portions Et_2O and was dried.to leave 0.340 g of a dark brown solid that was a mixture containing a 45:55 ratio of *trans*-:*cis*-**5** by NMR integration using two most-downfield resonances for each isomer. The resulting dark brown solid was subjected to flash chromatography on a small pad of neutral alumina where elution with Et_2O removed pyrazine in a band near the solvent front. Then, elution with CH_2Cl_2 gave a yellow-brown band (R_f = 0.6) that contained 0.085 g (34%) *trans*-**5** as a brown-yellow powder after removing solvent by vacuum distillation. Mp > 250 ^oC. Anal. Calcd (obs.) for $C_{24}H_{22}Cl_2N_7Rh$: C, 49.50 (49.13); H, 3.81 (3.62); N, 16.84 (16.57). ^{1}H NMR (CD_2Cl_2): δ_H 9.26 (d, J = 1.7 Hz, 2 H, H_3pz), 8.76 (d, J = 2.6 Hz, 2 H, H_5pz), 8.19 (d, J = 2.2 Hz, 2 H, pyz), 7.29 (br m, 2 H, Ar), 7.22 (br s, 2 H, pyz), 7.06 (s, 2H, Ar), 6.88 (br m, 2 H, Ar), 6.60 (ps t, J = 2.2 Hz, 2 H, H_4pz), 2.34 (s, 6 H, CH_3) ppm. After *trans*-**5** was eluted, changing eluent to acetonitrile gave a red-violet band (R_f = 0.95). After evaporation of solvent from this band, washing with 2 mL Et_2O and drying

under vacuum, 0.078 g (31 %) of *cis*-**5** was obtained as a lustrous red-violet powder. Mp > 250 °C. ^{1}H NMR (CD_2Cl_2): δ_H 8.70 (d, *J* = 1 Hz, 1 H, H_3Pz), 8.32 (d, *J* =2 Hz, 1 H, H_5pz), 8.18 (d, *J* = 2.4 Hz, 2 H, pyz), 8.09 (br s, 1 H, H_5pz), 8.05 (d, *J* = 2 Hz, 1 H, H_5pz), 7.97 (br s, 2 H, pyz), 7.22 (m, 3 H, Ar), 6.92 (d, *J* = 2 Hz, 1 H, Ar), 6.75 (dd, *J* = 2, 1 Hz, 1 H, H_4pz), 6.69 (m, 2 H, Ar), 6.63 (dd, *J* = 2, 1 Hz, 1 H, H_4pz), 2.33 (s, 3 H, CH_3), 2.09 (s, 3 H, CH_3) ppm.

***trans*-[(L)Rh(PPh$_3$)(py)Cl](PF$_6$), 7**. A mixture of 0.121 g (0.173 mmol) *trans*-**3**·$CHCl_3$, 0.26 g (1.0 mmol) PPh_3, and 0.0604 g (0.173 mmol) $TlPF_6$ in 30 mL THF was heated at reflux for 14 h giving a purple solution and a colorless precipitate. After cooling to room temperature, the suspension was filtered through a Celite Pad. Solvent was removed by vacuum distillation, the residue was washed with two 10 mL portions Et_2O, and was dried under vacuum to give a green-black solid mixture. The mixture was separated by column chromatography on neutral alumina. Elution with Et_2O removed PPh_3 in a colorless band near the solvent front. Next elution with ethyl acetate removed three unidentified fractions: a green band near the solvent front, a faint yellow band (R_f = 0.8) and a pink band (R_f = 0.4). Finally elution with CH_3CN afforded a purple band (R_f - = 0.5) of that contained the desired fraction. Recrystallization by diffusion of hexanes into a dichloromethane solution, followed by filtration and the drying under vacuum gave 0.129 g (78%) of pure **7** as purple crystals. Mp 256°C dec. Anal. Calcd (obs.) for $C_{43}H_{38}ClF_6N_6P_2Rh$: C, 54.19 (54.02); H, 4.02 (3.89); N, 8.82 (8.56). ^{1}H NMR ($CDCl_3$): δ_H 8.29 (d, *J* = 2 Hz, 1 H, H_3pz), 8.23 (d, *J* = 2 Hz, 1 H, H_3pz), 7.99 (d, *J* = 3 Hz, 1 H, H_5pz), 7.76 (d, *J* = 3 Hz, 1 H, H_5pz), 7.49 (m, 2 H, py), 7.37 (m, 2 H, py), 7.18 (m, 15 H,

Ar), 6.93 (m, 4 H, Ar), 6.54 (m, 3 H, Ar), 6.14 (dd, *J* = 3, 2 Hz, 1 H, H_4pz), (dd, *J* = 3, 2 Hz, 1 H, H_4pz), 2.07 (s, 3 H, CH_3), 2.01 (s, 3 H, CH_3). ^{31}P NMR ($CDCl_3$): δ_P 21.4 (d, *J* = 114 Hz). X-ray quality crystals of **7**·CH_2Cl_2 from crystallization were taken directly from the mother liquor (prior to solvent removal and drying.

***trans*-[(L)Rh(PEt$_3$)$_2$Cl](PF$_6$), (*trans*-8$^+$)(PF$_6^-$)**. A mixture of 0.202 g (0.302 mmol) **2**·H_2O, 0.211 g (0.604 mmol) $TlPF_6$, and 0.18 mL (1.2 mmol) PEt_3 in 20 mL CH_3CN was heated at reflux for 12 h which gave a red solution and a colorless precipitate. After cooling, the mixture was filtered through Celite to remove any thallium salts. The resulting bright red solution was washed with three 15 mL portions water to remove tetraethylammonium salts. The organic fraction was dried over $MgSO_4$ and solvent was removed by vacuum distillation to give a dark red powder. This powder was purified by column chromatography on neutral alumina. First, a trace amount of *trans*-**4** was removed by elution with chloroform. Then, elution with 1:1 ethyl acetate:CH_3CN afforded the desired product in the magenta band (R_f = 0.9). After removing solvents from the magenta band, a 0.175 g (68 %) sample of (*trans*-**8**$^+$)(PF_6^-) as a red-violet powder was obtained. Mp 273-275 °C. Anal. Calcd (obs.) for $C_{32}H_{48}ClF_6N_5P_3Rh$: C, 45.32 (45.71); H, 5.70 (5.66); N, 8.26 (8.32). ^{1}H NMR ($CDCl_3$): δ_H 8.46 (d, *J* = 3 Hz, 2 H, H_3pz), 8.43 (d, *J* = 2 Hz, 2 H,H_5pz), 7.42 (d, *J* = 8 Hz, 2 H, Ar), 7.15 (s, 2H, Ar), 7.91(d, *J* = 8 Hz, 2 H, Ar), 6.79 (dd, *J* = 3, 2 Hz, 2 H, H_4pz), 2.34 (s, 6 H, Ar-CH_3), 1.31 (m, 6 H, CH_2), 1.11 (m, 6 H, CH_2), 0.65 (t, *J* = 8 Hz, 18 H, Et-CH_3) ppm. ^{1}H NMR (CD_2Cl_2): d_H 8.48 (d, *J* = 1 Hz, 2 H, H_3pz), 8.39 (d, *J* = 2 Hz, 2 H, H_5pz), 7.46 (part of *AB*, 2 H, Ar), 7.11 (s, 2 H, Ar), 6.96 (part of *AB*, 2 H, Ar), 6.77 (dd, *J* = 2, 1 Hz, 2 H,

H_4pz), 1.32 (m, 6 H, CH_2), 1.13 (m, 6 H, CH_2), 0.66 (ps p, J_{app} = 7.7 Hz, Et-CH_3) ppm. ^{13}C NMR: (CD_2Cl_2) 147.5, 142.0, 135.2, 131.4, 129.9, 128.6, 126.4, 124.0, 109.7, 20.6, 14.2 (t, J = 12.6 Hz), 6.6. ^{19}F NMR (CD_2Cl_2): δ_F -73.4 (d, J_{FP} = 710 Hz). ^{31}P NMR (CD_2Cl_2): δ_P 11.9 (d, J_{Rh-P} = 82 Hz, 2 P, PEt_3), -144.0 (sept, J_{P-F} = 710 Hz, 1 P, PF_6) ppm. UV-Vis (CH_3CN): nm (ε, cm-^{1}M^{-1}) 253 (45,400), 345 (11,200) 394 (5,300), 515 (2,400). Crystals of (*trans*-**8**$^+$)(PF_6^-)·CH_2Cl_2 suitable for single-crystal X-ray diffraction were grown by layering a dichloromethane solution with hexanes and allowing solvents to slowly diffuse over the course of 3 d.

Synthesis of [(L)RhCl(bipy)](OTf), 9. A mixture of 0.804 g (1.17 mmol) **2**·H_2O, 0.188 g (1.20 mmol) 2,2'-bipyridine, and 0.850 g (2.41 mmol) TlOTf in 15 mL CH_3CN was heated at reflux for 16 h under nitrogen. After cooling, the purple mixture was filtered through Celite and solvent was removed by vacuum distillation to give a dark brown residue which was purified by column chromatography on neutral alumina. Unidentified impurities were first removed by elution with diethyl ether. Next, elution with acetone afforded the desired product in a dark purple band (R_f = 0.73). Removal of solvent, followed by washing with Et_2O and drying under vacuum gave 0.723 g (74 %) of **9**·acetone as a grey-violet solid. Mp 228-230 ^{o}C (dec). Anal. Calcd (obs.) for $C_{34}H_{32}ClF_3N_7O_4RhS$: C, 49.20 (48.97); H, 3.89 (3.95); N, 11.81 (11.67). A sample exposed to lab atmosphere for two days analyzed as 7·acetone·0.5H_2O: Anal. Calcd (obs.) for $C_{34}H_{33}ClF_3N_7O_{4.5}RhS$: C, 48.67 (48.20); H, 3.96 (3.46); N, 11.68 (11.95). ^{1}H NMR: (CD_2Cl_2): see section 5.7, Scheme 5.6 for labeling diagram, 9.98 (d, *J* = 5.8 Hz, 1 H, H_6-py^A), 8.82 (d, *J* = 8.2 Hz, 1 H, H_3-py^A), 8.66 (d, *J* = 8.2 Hz, 1 H, H_3-py^B), 8.47 (td,

J = 8, 1 Hz, 1 H, H_4-py^A), 8.23 (d, J = 3 Hz, 1 H, H_5-pz^B), 8.09 (m, 1H, H_4-py^B), 8.06 (m, 1 H, H_6-Ar^A), 8.04 (m, 1 H, H_5-pz^B), 7.94 (t, *J* = 6.6 Hz, 1 H, H_5-py^A), 7.68 (d, J = 8.4 Hz, 1 H, H_6-py^B), 7.44 (d, J = 8.4 Hz, 1 H, H_6-Ar^B), 7.20 (s, 1 H, H_3-Ar^B), 7.12 (m, 1 H, H_5-py^B), 7.11 (m, 1 H, H_5-Ar^A), 7.01 (dd, J = 8.6, 1 Hz, 1 H, H_5-Ar^B), 6.95 (m, 2 H, H_3-Ar^A and H_3-pz^A), 6.51 (t, J = 3 Hz, 1 H, H_4-pz^A), 6.48 (m, 1 H, H_3-pz^B), 6.45 (t, 1 H, J = 3 Hz, H_4-pz^B), 2.35 (s, 3 H, CH_3tol^B), 2.30 (s, 3 H, CH_3tol^A) ppm. ^{13}C NMR (CD_2Cl_2): 156.7, 152.7, 151.3, 143.9, 143.4, 142.0, 141.6, 141.5, 141.3, 132.2, 131.8, 131.3, 131.2, 130.6, 130.1, 129.5, 129.1, 128.9, 128.6, 128.0, 127.2, 126.0, 125.6, 123.3, 122.3, 109.7, 20.8, 20.7 ppm. ^{19}F NMR (CD_2Cl_2): -80.9 ppm. UV-Vis (CH_3CN): nm (ε, $cm\text{-}^1M^{-1}$) 240 (68,300), 313 (24,200), 326sh (17,700), 356 (10,000), 386 (9,300), 444sh (3,100), 530 (2,300). Crystals of **7**·0.88hexane·$2CH_2Cl_2$ suitable for single-crystal X-ray diffraction were grown by layering a dichloromethane solution of **9**·acetone with hexanes and allowing solvents to slowly diffuse over the course of 2 d. Vacuum dried crystals of **9**·0.88hexane·$2CH_2Cl_2$ exposed to lab atmosphere for two days analyzed as **9**·$2H_2O$: Anal. Calcd (obs.) for $C_{31}H_{30}ClF_3N_7O_5RhS$: C, 46.08 (46.29); H, 3.74 (3.43); N, 12.13 (11.71).

[(L)Rh(ttpy)](OTf)$_2$, 10. A mixture of 0.608 g (0.886 mmol) **2**·H_2O, 0.287 g (0.886 mmol) ttpy, and 0.939 g (2.66 mmol) Tl(OTf) in 20 mL CH_3CN was heated at reflux for 16 h under nitrogen. After cooling to room temperature, the dark green mixture was filtered through a Celite pad to remove thallium salts. The green solution was then washed with two 15 mL portions of H_2O to remove $(NEt_4)^+$ salts. The organic fraction was dried over $MgSO_4$, filtered, and solvent was removed by vacuum distillation

to give a dark green solid which was then further purified by column chromatography on neutral alumina. Elution with Et_2O removed an unidentified yellow impurity, then with CH_3CN gave the desired product in a dark green band that moved with the solvent front. After solvent was removed by vacuum distillation, the green-black solid was washed with Et_2O and was dried under vacuum to give 0.765 g (82 %) **10** as a shiny green-black powder. Mp 290°C dec. Anal. Calcd (obs.) for $C_{44}H_{35}F_6N_8O_6RhS_2$: C, 50.20 (49.97); H, 3.35 (3.51); N, 10.64 (10.90). ^{1}H NMR (CD_3CN): see section 5.7, Scheme 5.6 for labeling diagram, δ_H 8.98 (s, 2 H, H_3-ttpy^B), 8.70 (d, J = 8.0 Hz, 2 H, H_3-ttpy^A), 8.32 (d, J = 2.8 Hz, 2 H, H_5-pz), 8.19 (d, J = 8.1 Hz, 2 H, H_4-ttpy^A), 8.09 (d, J = 8.1 Hz, 2 H, $H_{2,6}$-Ar^B), 7.72 (part of *AB*, J_{app} = 8.3 Hz, 2 H, H_6-Ar^A), 7.57 (d, J = 7.9, 2 H, $H_{3,5}$-Ar^B), 7.45 (d, J = 5.5 Hz, 2 H, H_2-ttpy^A), 7.29 (pst, J = 6.7 Hz, 2 H, H_3-ttpy^A), 7.24 (part of *AB*, J_{app} = 8.3, 2 H, H_5-Ar^A), 7.18 (s, 2 H, H_3-Ar^A), 6.76 (d, J = 2.2 Hz, 2 H, H_3-pz), 6.44 (dd, J = 2.8, 2.2 Hz, 2 H, H_4-pz), 2.52 (s, 3 H, ttpy-CH_3), 2.35 (s, 6 H, CH_3-Ar^A) ppm. ^{13}C NMR (CD_3CN): δ_C 158.6, 155.9, 155.0, 153.2, 143.6, 143.0, 142.5, 142.0, 134.5, 133.5, 131.9, 131.4, 131.2, 129.8, 129.1, 127.8, 127.4, 125.0, 124.7, 122.1 (q, J_{CF} = 321 Hz, CF_3), 110.7, 21.5 (ttpy-CH_3), 20.5 (NAr-CH_3) ppm. ^{19}F NMR (CD_2Cl_2): -80.9 ppm. UV-Vis (CH_3CN): nm (ε, $cm^{-1}M^{-1}$) 236 (76,200), 279 (31,700), 298 (36,200), 323 (35,400), 341sh (30,000), 359 (22,900), 390 (7,800), 430 (4,200), 622 (1,800). Crystals of **10**·0.5Et_2O·0.5THF·0.37H_2O suitable for single-crystal X-ray diffraction were grown by layering a THF solution with Et_2O, allowing solvents to diffuse, and then slowly evaporating the solvents from a loosely-capped vial over the course of 7 d. A sample exposed to the atmosphere for several weeks analyzed as **10**·Et_2O·6H_2O, Anal. Calcd (obs.) for $C_{48}H_{57}F_6N_8O_{13}RhS_2$: C, 46.68 (46.37); H, 4.65 (4.57); N, 9.07 (9.05).

5.2.2. Spectroscopic-scale Photochemical Conversion of *cis*-**3** to *trans*-**3**.

A red solution of 3.2 mg (5.5 μmol) *cis*-**3** in 0.6 mL CD_2Cl_2 was contained in a 5 mm O.D. NMR tube. The NMR tube was placed in a glass water bath (stirred and maintained at 30 ± 5°C) located within an aluminum foil-lined chamber. The chamber was irradiated with a 250 W incandescent lamp located approximately 50 cm from the sample. The sample was removed periodically over the course of 24 h to record the NMR spectrum. After 16 h, the solution was green and the conversion was ~50 % complete by integration. The conversion of *cis*-**3** to *trans*-**3** was also monitored by UV-Vis spectroscopy, by using a similar setup but with 50 mL of an 2.5 mM solution contained in a quartz apparatus. Periodically, the UV-Visible spectra of 3 mL aliquots were recorded. Sample spectra are found in the supporting information.

5.2.3. Chemical Oxidations.

[*trans*-(L)$RhCl_2$(py)]($SbCl_6$), (*trans*-$\mathbf{3}^+$)($SbCl_6^-$). A solution of 0.108 g (0.154 mmol) *trans*-**3**·$CHCl_3$ in 25 mL CH_2Cl_2 was added via cannula transfer to a solution of 0.0562 g (0.154 mmol) (NO)($SbCl_6$) in 25 mL CH_2Cl_2 resulting in the formation of a deep blue solution. After the solution had been stirred 15 min, solvent was removed by vacuum distillation. The blue residue was washed with two 5 mL portions Et_2O and was dried under vacuum to leave 0.112 g (79 %) (*trans*-$\mathbf{3}^+$)($SbCl_6^-$) as a blue powder. μ_{eff} (solid, 295 K) = 1.8 μ_B. Anal. Calcd (obs.) for $C_{25}H_{23}Cl_8N_6RhSb$: C, 32.79 (32.63); H, 2.53 (2.58); N, 9.18 (9.25). UV-Vis (CH_2Cl_2): nm (ε, $cm^{-1}M^{-1}$) 359 (7,000), 412sh (4,400), 517 (3,300), 606 (3,500), 752 (7,800). Crystals of (*trans*-$\mathbf{3}^+$)($SbCl_6^-$)·CH_2Cl_2 were grown by dissolving 10 mg each *trans*-**3** and (CRET)($SbCl_6$) in 3 mL CH_2Cl_2,

layering with 3 mL hexanes and allowing solvents to diffuse at room temperature over the course of 2 days.

[*cis*-(L)RhCl$_2$(py)](SbCl$_6$), (*cis*-3$^+$)(SbCl$_6^-$). A solution of 0.0464 g (76.5 μmol) (CRET)(SbCl$_6$) in 25 mL CH_2Cl_2 was added via cannula transfer to a solution of 0.0446 g (76.7 μmol) *cis*-**3** in 25 mL CH_2Cl_2 resulting in the formation of a deep blue-violet solution. After the solution had been stirred 15 min, solvent was removed by vacuum distillation. The blue-violet residue was washed with two 5 mL portions toluene and was dried under vacuum to leave 0.0575 g (82 %) (*cis*-**3**$^+$)(SbCl$_6^-$) as a blue powder. μ_{eff} (solid, 295 K) = 1.9 μ_B. Anal. Calcd (obs.) for $C_{25}H_{23}Cl_8N_6RhSb$: C, 32.79 (32.46); H, 2.53 (2.39); N, 9.18 (8.96). UV-Vis (CH_3CN): nm (ε, cm-^{1}M^{-1}) 368 (7,400), 434 (2,400), 526 (4,200), 600 (3,700), 752 (7,200). Crystals of (*cis*-**3**$^+$)(SbCl$_4^-$)·2CH_2Cl_2 suitable for single crystal X-ray diffraction were grown by dissolving 10 mg each *cis*-**3** and (CRET)(SbCl$_6$) in 3 mL CH_2Cl_2, layering with 3 mL hexanes and allowing solvents to diffuse in a -20^{o}C freezer over the period of 2 days.

***trans*-(L)RhCl(PEt$_3$)$_2$](PF$_6$)(SbCl$_6$), (*trans*-8^{2+})(PF$_6^-$)(SbCl$_6^-$).** A solution of 0.0184 g (50.5 μmol) (NO)(SbCl$_6$) in 5 mL CH_2Cl_2 was transferred by cannula under N_2 to a magnetically stirred solution of 0.043 g (50.7 μmol) **8** in 20 mL CH_2Cl_2 causing the color to immediately change from red to a dark violet-blue. After stirring 10 minutes, the solvent was removed under vacuum to leave 0.057 g (95%) of (*trans*-**8**$^{2+}$)(PF$_6^-$)(SbCl$_6^-$) as a violet-blue powder. Anal. Calcd (obs.) for $C_{32}H_{48}Cl_6F_6N_5P_3RhSb$: C, 32.50 (32.87); H, 4.09 (4.13); N, 5.92 (6.11). UV-Vis (CH_2Cl_2): 254 (59,700), 379 (7,800), 410sh (3,500), 484 (3,200), 589 (3,000), 665sh (2,800), 729 (5,400). X-ray quality crystals of

(*trans*-**6**$^{2+}$)($SbCl_6$)$_2$ were grown by dissolving 10 mg each *trans*-**8** and (CRET)($SbCl_6$) in CH_2Cl_2, layering the resulting blue solution with toluene and allowing solvents to slowly diffuse at room temperature over 2 d.

5.3. Crystallography.

X-ray intensity data from a dark green needle of (Hpy)[(**L**)$RhCl_3$]·py, complex **A**, a dark green prism of **2**, a dark-green plate of *trans*-**3**·CH_2Cl_2, a red-block of *cis*-**3**, a purple block of **7**·CH_2Cl_2, a red prism of (*trans*-**8**$^{+}$)(PF_6^-)·CH_2Cl_2, and a blue-black block of (*trans*-**8**$^{2+}$)($SbCl_6$)$_2$ were collected at 100 K with a Bruker AXS 3-circle diffractometer equipped with a SMART2[12] CCD detector using Cu(Kα) radiation. X-ray intensity data from a brown needle of *trans*-**4**·0.18CH_2Cl_2, a black plate of **9**·0.88hexane·2CH_2Cl_2, a green-brown plate of **10**·0.5Et_2O·0.5THF·0.37H_2O, a black needle of (*trans*-**3**$^{+}$)($SbCl_6^-$)·CH_2Cl_2 and a black needle of (*cis*-**3**$^{+}$)($SbCl_4^-$)·2CH_2Cl_2 were measured with an Oxford Diffraction Ltd. Supernova diffractometer equipped with a 135 mm Atlas CCD detector using Mo(Kα) radiation for *trans*-**4**·0.18CH_2Cl_2 and and (*trans*-**3**$^{+}$)($SbCl_6^-$)·CH_2Cl_2 while Cu(Kα) radiation was used for the other experiments. Raw data frame integration and Lp corrections were performed with either CrysAlis Pro (Oxford Diffraction, Ltd.)[13] or SAINT+ (Bruker).[12] Final unit cell parameters were determined by least-squares refinement of 8843, 7399, 7723, 6555, 8016, 8173, 8173, 12616, 10302, 14770, 12884, and 5663 reflections from the data sets of **A**, **2**, *trans*-**3**·CH_2Cl_2, *cis*-**3**, *trans*-**4**·0.18CH_2Cl_2, **7**·CH_2Cl_2, (*trans*-**8**$^{+}$)(PF_6^-)·CH_2Cl_2, **9**·0.88hexane·2CH_2Cl_2, **10**·0.5Et_2O·0.5THF·0.37H_2O, (*trans*-**3**$^{+}$)($SbCl_6^-$)·CH_2Cl_2, (*cis*-**3**$^{+}$)($SbCl_4^-$)·2CH_2Cl_2, and (*trans*-**8**$^{2+}$)($SbCl_6$)$_2$, respectively, with $I > 2\sigma(I)$ for each. Analysis of the data showed

negligible crystal decay during collection in each case. Direct methods structure solutions, difference Fourier calculations and full-matrix least-squares refinements against F^2 were performed with SHELXTL.[14] Numerical absorption corrections based on gaussian integration over a multifaceted crystal model were applied to the data of *trans*-**4**·0.18CH_2Cl_2, **9**·0.88hexane·2CH_2Cl_2 and **10**·0.5Et_2O 0.5THF·0.37H_2O, (*trans*-**3**$^+$)($SbCl_6^-$)·CH_2Cl_2, and (*cis*-**3**$^+$)($SbCl_4^-$)·2CH_2Cl_2, while numerical absorption corrections and based on the real shape of the crystals were applied with SADABS[12] for the remaining complexes. All non-hydrogen atoms were refined with anisotropic displacement parameters. Hydrogen atoms were placed in geometrically idealized positions and included as riding atoms. The X-ray crystallographic parameters and further details of data collection and structure refinements are given in Tables 5.1 to 5.3.

Table 5.1. Crystallographic Data Collection and Structure Refinement for (Hpy)[(**L**)$RhCl_3$]·py, complex **A**, **2**, *trans*-**3**·CH_2Cl_2, and (*trans*-**3**$^+$)($SbCl_6^-$)·CH_2Cl_2.

Compound	**A**	**2**	***trans*-3**·CH_2Cl_2	(*trans*-**3**$^+$)($SbCl_6^-$)·CH_2Cl_2
Formula	$C_{30}H_{29}Cl_3N_7Rh$	$C_{28}H_{38}Cl_3N_6Rh$	$C_{26}H_{25}Cl_4N_6Rh$	$C_{26}H_{25}Cl_{10}N_6RhSb$
Formula weight	696.86	667.90	666.23	1000.68
Crystal system	monoclinic	tetragonal	monoclinic	triclinic
Space group	P 2_1/n	I -4	P 2_1/n	P -1
Temperature [K]	100(2)	100(2)	100(2)	100.0(1)
a [Å]	9.5009(6)	20.0852(2)	10.5070(2)	10.8699(4)
b [Å]	20.9592(14)	20.0852(2)	7.99980(10)	12.7774(4)
c [Å]	14.8860(9)	14.8181(2)	32.3766(5)	13.9834(4)
α[°]	90.00	90.00	90.00	76.730(3)
β[°]	94.628(3)	90.00	91.3160(10)	72.153(3)
γ [°]	90.00	90.00	90.00	82.555(3)
V [Å^3]	2954.6(3)	5977.85(12)	2720.66(7)	1795.65(10)
Z	4	8	4	2
$D_{calcd.}$ [gcm^{-3}]	1.567	1.484	1.627	1.851
λ[Å] (Cu or Mo Kα)	1.54178	1.54178	1.54178	0.7107
μ.[mm^{-1}]	7.439	7.307	8.917	1.985
Abs. Correction	numerical	numerical	numerical	numerical
F(000)	1416	2752	1344	978
θ range [°]	3.65 to 67.61	3.11 to 67.97	2.73 to 67.88	3.53 to 29.57
Reflections collected	24159	25241	22504	40654
Independent reflections	5151 (R_{Int}=0.0197)	5216 (R_{Int}=0.0155)	4837 (R_{Int}=0.0330)	9202 (R_{Int}=0.0359)
T_min/max	0.0631/0.6240	0.2430/0.5003	0.0645/0.7168	0.718/0.955
Data/restraints/ parameters	5151/36/430	5216/0/349	4837/0/336	9202/0/399
Goodness-of-fit on F^2	0.984	1.087	1.007	1.049
$R1^a$/$wR2^b$ [I>2σ(I)]	0.0289/0.0777	0.0146/0.0380	0.0266/0.0702	0.0347/0.0694
$R1^a$ /$wR2^b$ (all data)	0.0294/0.0781	0.0146/0.0380	0.0272/0.0706	0.0484/0.0770
Largest diff. peak/hole / eÅ^{-3}	0.706/-0.465	0.325/-0.263	0.0362/0.0726	1.921/-1.510

[a] $R1 = \Sigma||F_o| - |F_c||/\Sigma|F_o|$ [b] $wR2 = [\Sigma w(|F_o| - |F_c|)^2/\Sigma w|F_o|^2]^{1/2}$.

Table 5.2. Crystallographic Data Collection and Structure Refinement for *cis*-**3**, (*cis*-**3**$^{+}$)($SbCl_4^-$)·$2CH_2Cl_2$, *trans*-**4**·$0.18CH_2Cl_2$, and *trans*-[(**L**)Rh(PPh_3)(py)(Cl)](PF_6^-)·CH_2Cl_2, **7**·CH_2Cl_2.

Compound	***cis*-3**	(*cis*-**3**$^{+}$)($SbCl_4$)·$2CH_2Cl_2$	***trans*-4**·$0.18CH_2Cl_2$	**7**·CH_2Cl_2
Formula	$C_{25}H_{23}Cl_2N_6Rh$	$C_{27}H_{27}Cl_{10}N_6RhSb$	$C_{26.18}H_{33.35}Cl_{2.35}N_5$	$C_{44}H_{40}Cl_3F_6N_6P_2Rh$
Formula weight	581.30	1014.71	635.33	1038.02
Crystal system	monoclinic	monoclinic	tetragonal	monoclinic
Space group	P 2_1/n	P 2_1/c	I 4_1/a	C 2/c
Temperature [K]	100(2)	100.2(2)	102.1	100(2)
a [Å]	9.0391(2)	16.2675(4)	31.8629(6)	36.8996(6)
b [Å]	16.3205(3)	15.4317(3)	31.8629(6)	10.0698(2)
c [Å]	16.2321(3)	15.2760(4)	10.9579(3)	25.2397(5)
α[°]	90.00	90.00	90.00	90.00
β[°]	104.9980(10)	105.369(3)	90.00	111.2950(10)
γ [°]	90.00	90.00	90.00	90.00
V [Å^3]	2313.03(8)	3697.66(15)	11124.9(4)	8738.0(3)
Z	4	4	16	8
D_{calcd}. [gcm^{-3}]	1.669	1.823	1.517	1.578
λ[Å] (Cu Kα)	1.54178	1.54178	0.7107	1.54178
μ.[mm^{-1}]	8.315	16.300	0.923	6.115
Abs. Correction	numerical	numerical	numerical	numerical
F(000)	1176	1988	5206	4208
θ range [°]	3.91 to 68.02	4.02 to 73.90	3.61 to 29.58	2.57to 67.95
Reflections collected	19213	39390	32752	36763
Independent Rflns	4140 (R_{Int}=0.0335)	7374 (R_{Int}=0.0512)	7234 (R_{Int}=0.0501)	7656 (R_{Int}=0.0273)
T_min/max	0.4112/0.7321	0.126/0.763	0.903/0.975	0.3600/0.6091
Data/restr./param.	4140/0/309	7374/9/466	7234/3/343	7656/0/561
Goodness-of-fit on F^2	1.008	1.036	1.042	1.019
$R1^a$ /$wR2^b$ [I>2σ(I)]	0.0285/0.0696	0.0379/ 0.0935	0.0340/0.0612	0.0382/0.0965
*R*1/*wR*2 (all data)	0.0362/0.0726	0.0452/ 0.0985	0.0566/0.0716	0.0417/0.0986
Largest diff. peak/hole / e Å^{-3}	0.598/-0.483	2.141/ -1.621	0.750/-0.616	1.138/-0.687

[a] $R1 = \Sigma||F_o| - |F_c||/\Sigma|F_o|$ [b] $wR2 = [\Sigma w(|F_o| - |F_c|)^2/\Sigma w|F_o|^2]^{1/2}$.

Table 5.3. Crystallographic Data Collection and Structure Refinement for (*trans*-**8**$^{+}$)(PF_6^-)·CH_2Cl_2, (*trans*-**8**$^{2+}$)($SbCl_6$)$_2$, **9**·0.88hexane·2CH_2Cl_2, **10**·0.5Et_2O·0.5THF·0.37H_2O.

Compound	(*trans*-**8**$^{+}$)(PF_6^-)·CH_2Cl_2	(*trans*-**8**$^{2+}$) ($SbCl_6$)$_2$	**9**·0.88hexane ·2CH_2Cl_2	**10**·0.5Et_2O· 0.5THF ·0.37H_2O
Formula	$C_{33}H_{50}Cl_3F_6N_5P_3Rh$	$C_{33}H_{50}Cl_3F_6N_5P_3Rh$	$C_{38.30}H_{42.37}Cl_5F_3N_7O_3RhS$	$C_{48}H_{44}F_6N_8O_{7.37}RhS_2$
Formula weight	932.95	1371.95	1018.00	1131.86
Crystal system	monoclinic	monoclinic	monoclinic	triclinic
Space group	C 2/c	P 2_1/n	P 2_1/c	P -1
Temperature [K]	100(2)	100(2)	100	101.7
a [Å]	21.7617(6)	21.7617(6)	14.9796(4)	9.1543(3)
b [Å]	67.3320(19)	67.3320(19)	32.8756(7)	11.7994(5)
c [Å]	10.8818(3)	10.8818(3)	9.1507(3)	22.4495(9)
α[°]	90.00	90.00	90.00	101.271(3)
β[°]	91.5780(10)	91.5780(10)	105.548(3)	94.018(3)
γ [°]	90.00	90.00	90.00	94.028(3)
V [Å^3]	15938.6(8)	5178.34(19)	4341.48(19)	2363.52(16)
Z	16	4	4	2
$D_{calcd.}$ [gcm^{-3}]	1.555	1.760	1.557	1.590
λ[Å] (Cu Kα)	1.54178	1.54178	1.54178	1.54178
μ.[mm^{-1}]	6.978	17.763	6.961	4.501
Abs. Correction	numerical	numerical	numerical	numerical
F(000)	7648	2692	2073	1156
θ range [°]	2.62 to 68.00	3.16 to 67.45	3.34 to 73.73	3.83 to 74.13
Reflections collected	66784	40792	23654	36987
Independent Rflns	14159 (R_{Int}=0.0271)	9134 (R_{Int}=0.0514)	8539 (R_{Int}=0.0728)	9383 (R_{Int}=0.0539)
T_min/max	0.1621/0.5421	0.1633/0.3694	0.148/0.879	0.498/0.924
Data/restr./param.	14159/0/945	9134/0/504	8539/181/555	9383/19/680
Goodness-of-fit on F^2	1.068	1.020	1.236	1.019
$R1^a$ /$wR2^b$ [I>2σ(I)]	0.0522/0.1445	0.0397/0.0903	0.1329/ 0.2990	0.0440/0.1052
*R*1/*wR*2 (all data)	0.0714/0.1695	0.0580/0.0967	0.1414/ 0.3025	0.0574/0.1143
Largest diff. peak/hole / e Å^{-3}	1.595/ -3.027	1.507/-0.767	4.384/ -1.504	1.800/ -0.696

[a] $R1 = \Sigma||F_o| - |F_c||/\Sigma|F_o|$ [b] $wR2 = [\Sigma w(|F_o| - |F_c|)^2/\Sigma w|F_o|^2]^{1/2}$.

5.4. Results

5.4.1. Syntheses. As summarized in Scheme 5.1, the reaction between the protonated pincer ligand H(**L**) and commercial rhodium(III) chloride hydrate in refluxing ethanol lead to the formation of a golden-beige insoluble solid that analyzed as [H(**L**)]$RhCl_3$, **1**. Complex **1** is insoluble in most organic solvents with the exception of Brønsted basic amines, solvents that react with **1**. For instance, dissolution of **1** in pyridine at room temperature caused deprotonation of the ligand and to give deep-green crystals of (Hpy)[(**L**)$RhCl_3$]·py, complex **A**, after vapor diffusion of Et_2O into the reaction mixture (vide infra). Inspired by this observation, we found that deprotonation of **1** with $(NEt_4)(OH)$ in MeOH afforded high yields of the deep-green complex, (NEt_4)[(**L**)$RhCl_3$]·H_2O, **2**·H_2O, an easily-handled and synthetically-useful reagent. Anhydrous **2** can be obtained after crystallization from CH_2Cl_2:hexanes and by taking precautions to avoid exposure to atmospheric moisture. Since we found the ensuing coordination chemistry of this complex to be insensitive to the presence (or absence) of the water of hydration, we chose to work with the hydrate **2**·H_2O under normal laboratory conditions rather than with anhydrous **2** under anaerobic conditions.

Scheme 5.1. Preparation of (NEt_4)[(**L**)$RhCl_3$], **2**.

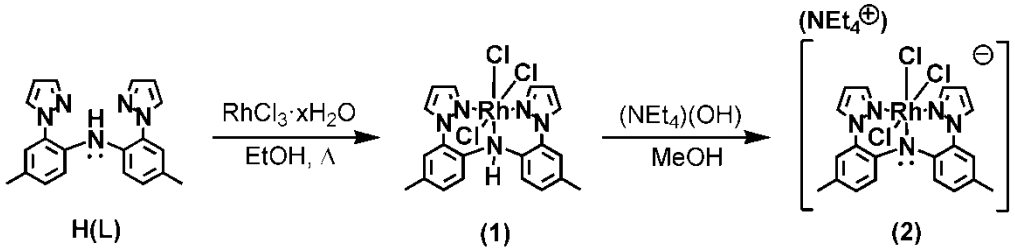

The reactions in Schemes 5.2-5.4 represent optimized routes to the various rhodium(III) complexes used in this study. Thus, heating a solution of **2**·H_2O and five equivalents

pyridine, triethylphosphine, or pyrazine in $CHCl_3$ at 60°C for 16 h, gave mixtures that contained the highest yields (ca. 40-60%) of the appropriate *trans*-(**L**)$RhCl_2$(py), *trans*-**3**, *trans*-(**L**)$RhCl_2(PEt_3)$, *trans*-**4**, or *trans*-(**L**)$RhCl_2$(pyz), *trans*-**5**, respectively, products that are easily separated from unreacted **2**·H_2O, [(**L**)Rh(py or $PEt_3)_2$Cl](Cl) and other by-products by chromatography.

Scheme 5.2. Preparation and isomerization of (**L**)$RhCl_2$(py), **3**, (**L**)$RhCl_2(PEt_3)$, **4**, and (**L**)$RhCl_2$(pyz), **5**.

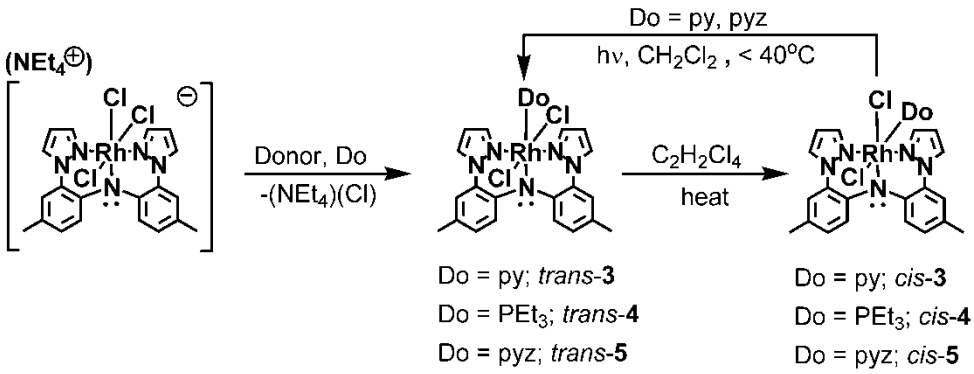

Heating solutions of either *trans*-**3**, *trans*-**4**, or *trans*-**5** in $C_2H_2Cl_4$ at 100°C caused conversion to the appropriate *cis*- isomer (right of Scheme 5.2). In the case of **3**, the isomerization proceeds cleanly but stops after a 91:9 equilibrium mixture of *cis*-**3**:*trans*-**3** is attained. For **5** the isomerization stops after a 90:10 equilibrium mixture of *cis*-**5**:*trans*-**5** is attained but there was small amounts (< 10%) of another unidentified by-product formed (Figure 5.19). The re-isomerization of *cis*-**3** or cis-**5** to the respective *trans*-isomers was achieved by irradiation of dichloromethane solutions with high-intensity visible light. With **4**, the *trans*- isomer is completely consumed upon heating to 100°C in $C_2H_2Cl_4$ but the isomerization was not clean; there are at least two other unidentified byproducts formed during the conversion. In all cases it is possible to isolate the at least

small quantities of the pure *cis*- isomer by flash chromatography,[15] which indicates a rather high activation barrier to isomerization. In fact, isomerization of **3** or **4** did not occur in lower boiling solvents such as $CHCl_3$ (bp 61°C) or THF (bp = 65°C). On the other hand, the *trans*- to *cis*- isomerization of **5** was 50 % complete in boiling $CHCl_3$ after 15 h. By examining initial rates of conversion spectroscopically (by monitoring the disappearance of the *trans*- isomer and/or the appearance of *cis*- isomer), the isomerization in $C_2H_2Cl_4$ at 100°C was found to be first order in *trans*- isomer with $t_{1/2}$ on the order of 0.25 h for *trans*-**5**, 2.0 h for *trans*-**3**, and 6.6 h for *trans*-**4**. Given the trend that the reaction is slowest for the strongest σ-donating group (PEt_3) and given the relatively high activation barrier necessary to begin isomerization, it is most likely that the reaction proceeds via a rate-limiting dissociation of *trans*- ligand rather than by dissociation of a chloride. The unique ability for *trans*-**5** to undergo isomerization in a low-boiling solvent ($CHCl_3$) compared to *trans*-**3** or *trans*-**4** is likely due to its relatively poor donating ability to rhodium(III) relative to py or PEt_3,[16] a property that is also manifested in the electrochemistry of this series of complexes (vide infra).

The reaction between **2**·H_2O, an excess of either pyridine or triethylphosphine, and one equivalent of $Tl(PF_6)$ as a halide abstracting agent in refluxing pyridine or acetonitrile (in the PEt_3 case) produced high yields of the appropriate [(**L**)$RhCl(py)_2$](PF_6), **6**, or [(**L**)$RhCl(PEt_3)_2$](PF_6), **8**, Scheme 5.3. The NEt_4Cl by-product of the reactions is easily removed by washing the organic soluble components with water.

.

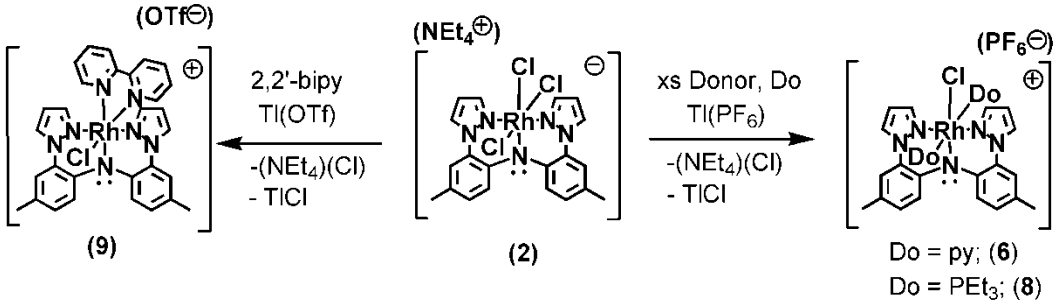

Scheme 5.3. Synthetic routes to monocationic $[(\mathbf{L})RhCl(donor)_2]^+$ species, **6**, **8**, and **9**

The reaction of *trans*-**3** with excess PPh_3 and one equivalent of $TlPF_6$ afforded $[(\mathbf{L})Rh(py)(PPh_3)Cl](PF_6)$, **7**, that has the chloride *trans*- to the amido. Single-crystal X-ray diffraction and NMR spectral data (vide infra) indicate a *trans*- disposition of monodentate Lewis donors in **6** and **8**. A *cis*- arrangement of ligands can be enforced using the chelating 2,2'-bipy as the donor (and Tl(OTf) as a halide abstracting agent) to give $[(\mathbf{L})RhCl(bipy)](OTf)$, **9**. Similarly, the reaction between $\mathbf{2}\cdot H_2O$, the tridentate ttpy ligand, and two equivalents of Tl(OTf) afforded $[(\mathbf{L})Rh(ttpy)](OTf)_2$, **10**, as in Scheme 5.4. Interestingly, attempts to prepare $[(\mathbf{L})Rh(donor)_3](PF_6)_2$ where donor = py or PEt_3 were

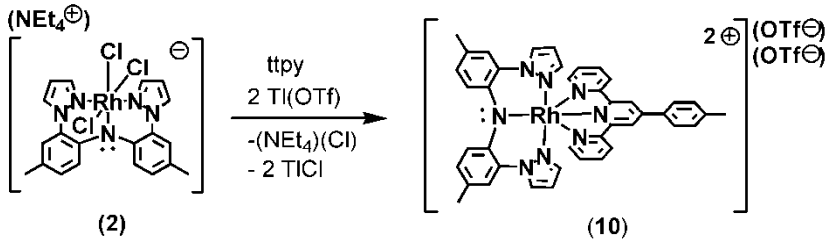

Scheme 5.4. Preparation of $[(\mathbf{L})Rh(ttpy)](OTf)_2$, **10**.

unsuccessful even when using a large excess of pyridine or PEt_3 and thallium(I) salts. Thus, the chelate effect appears to facilitate the abstraction of the third halide ligand of **2**·H_2O.

5.4.2. Structures.

Crystals of (Hpy)[(**L**)$RhCl_3$]·py (**A**), **2**, *trans*-**3**, *cis*-**3**, *trans*-**4**, and **7-10** suitable for single crystal X-ray diffraction were obtained. Views of the structures of **2**, *trans*-**3**, *cis*-**3**, **9** and **10** are given in Figure 5.2 while others are provided in the section 5.7. Selected bond distances and angles for all are given in Table 5.4. In each complex, the anionic pincer ligand has a planar amido nitrogen (indicated by the 360^o sum of the angles about nitrogen N1) and binds each octahedral rhodium(III) center in a meridional *N*,*N*,*N*-coordination mode. The average Rh-N(pyrazolyl), Rh-N_{pz}, bond distances are in the range of 2.01 to 2.03 Å, which mirrors previous findings for (**L**)Rh(Et or I)(CO)(I) and [(**L**)Rh(I)(μ-I)]$_2$ complexes.[6] The pincer amido Rh-N1 (or Rh-N_{Ar}) bond distance shows greater variability than Rh-N_{pz} and appears to depend mainly on the substituent disposed *trans*- to the amido nitrogen. Of the series of complexes listed in Table 5.3, the longest Rh-N1 bond of 2.064(2) Å is found for *trans*-**4** with the strongest σ-donor, PEt_3, that is linearly disposed from the amido group, N1-Rh1-P1 = 178.23(6) ^{o}. The shortest Rh-N1 bond of 2.000(2) Å is found for *trans*-**3** with a pyridyl *trans*- to the amido. In this derivative, the pyridyl ring and the amido fragment C1N1(Rh)C31 are nearly coplanar with a C1C31-C41C45 torsion angle of 1^o. In this geometry it is expected that the π (and π*) orbitals of the pyridyl would be in full conjugation with the filled π-orbitals on the amido fragments and rhodium (vide infra). In contrast, the chelating nature of the bipy and ttpy ligands forces the *trans*-disposed pyridyl ring of the multidentate ligand to be

twisted out of conjugation with the amido fragment C1N1(Rh)C31; the C1C31-C41C45 torsion angle is 44^{o} for **9** and is 46^{o} for **10**. In these latter cases, the Rh-N1 distances of 2.017(9) Å for **9** and 2.014(3) Å for **10** are longer than in *trans*-**3**. The corresponding Rh-N31, or Rh-N_{py}, bond distances involving the ring *trans*- to the amido decreases from 2.097(2) Å for trans-**3**, 2.064 Å for **9** and 1.969(3) Å for **10**, which likely reflects the effect of increasing charge on the complex and possibly the increasing π-acceptor character of the exogeneous ligands. The Rh-N_{py} bond distance 2.065(2) Å in *cis*-**3** is shorter than that in *trans*-**3**. The opposite trend is found for dication in **10** where the Rh-N_{py} distances involving the pyridyl rings *cis*- to

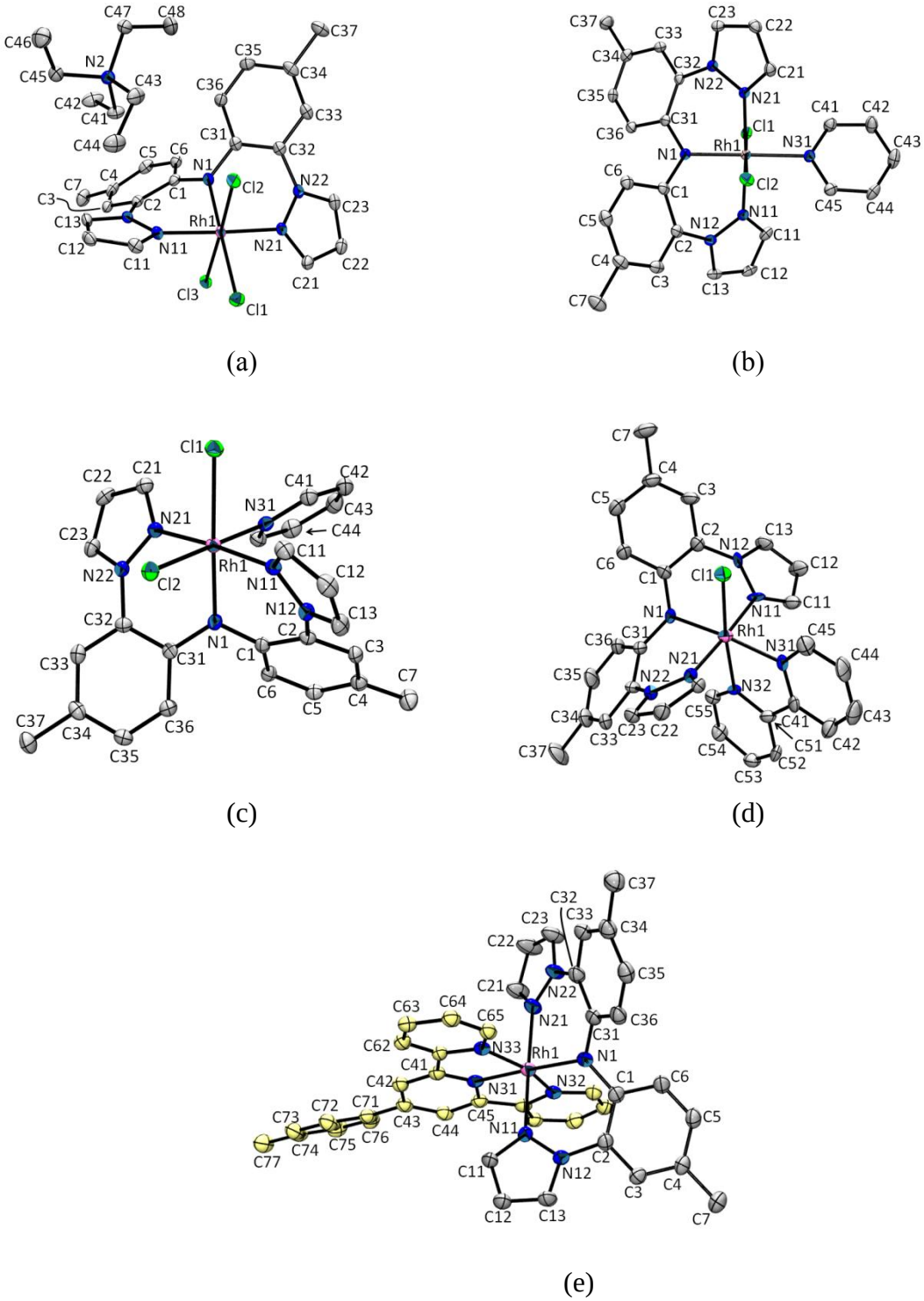

Figure 5.2. Structures of various rhodium complexes prepared in this study. Thermal ellipsoids are drawn at the 50% probability level. Hydrogen atoms, solvent molecules, and anions have been omitted for clarity.

Table 5.4. Selected bond distances (Å) and angles (^{o}) for the new rhodium(III) pincer complexes.[a]

	Complexes								
Distances(Å)	**A**	**2**	***trans*-3**	***cis*-3**	***trans*-4**	**7**	**8**	**9**	**10**
Re-N_{Ar}	2.010(2)	2.017(1)	2.000(2)	2.013(2)	2.064(2)	2.023(3)	2.042(4)	2.017(9)	2.014(3)
Re-N_{pz}[a]	2.010(2)	2.013(2)	2.016(2)	2.015(2)	2.033(2)	2.018(3)	2.026(4)	2.023(9)	2.016(3)
Re-N_{py}[a]			2.097(2)	2.065(2)		2.140(3)		2.066(9)	2.033(3)
Re-P					2.346(1)	2.3484(8)	2.413(1)		
Re-Cl_{ax}[b]	2.3551(7)	2.3481(4)	2.3418(5)	2.3398(7)	2.3481(6)			2.332(3)	
Re-Cl_{eq}[c]	2.4056(6)	2.3937(4)		2.3903(7)		2.3713(7)	2.379(2)		
Angles(^{o})									
N11-Re-N1	87.77(9)	88.41(6)	88.00(8)	88.99(10)	84.25(8)	88.22(10)	88.7(2)	88.5(4)	89.23(11)
N21-Re-N1	90.25(9)	87.60(6)	87.94(8)	87.43(10)	83.63(8)	89.52(10)	88.8(2)	88.7(4)	88.54(11)
N31-Rh-N1			179.21(7)	87.89(10)		88.88(10)		175.3(4)	178.02(11)
N31-Rh-N32								80.3(4)	80.25(12)
N32-Rh-N33									160.39(11)
pz-aryl	29.5	32.0	31.9	33.7	40.9	30.4	34.9	30.2	26.8
RhN-NC_{ipso}[d]	6.4	6.9	8.1	8.1	5.9	10.8	13.6	2.6	7.2

[a]In cases where more than one of the same type of atom or crystallographically-independent molecule is present, an average value is reported. [b]*cis*-to amido N1 atom. [c]*trans*- to amido N1 atom. [d]absolute value of torsion angle.

the amido (2.060(3), 2.069(3) Å) are much longer than the pyridyl ring *trans*- to the amido. The cation in **9** displays statistically identical Rh-N_{py} bond distances of 2.067(9) and 2.065(9) Å. The Rh-Cl bond distances across the entire series of complexes display a strong *trans*- influence with the chloride situated *cis*- to the amido being much shorter than a chloride *trans*- to the amido, regardless of the charge on the complex.

5.4.3. Solution Characterization.

The ^{1}H, ^{13}C, and ^{31}P NMR spectra are in general agreement with expectations based on the idealized symmetry and solid-state structures of the complexes. With the exception of **7**, which had several regions of overlapping multiplet resonances in the

aromatic regions that hindered analysis, full assignments of resonances in the ^{1}H NMR spectra could be made by analysis of 1D spectrum and 2D (DQCOSY and NOESY) spectra. Full details and discussion of data are provided in the section 5.7

The rhodium(III) complexes of the di(2-pyrazolyl-*p*-tolyl)amido ligand are intensely-colored species like the previously reported carbonylrhodium(I) (d^8), organorhodium(III) (low spin d^6), or even the tricarbonylrhenium(I) (low-spin d^6) pincer counterparts.[5] Table 5.5 summarizes data from electronic

Table 5.5. Summary of electronic absorption spectra data for complexes **2-10** in CH_2Cl_2.

compound	λ, nm (ε, $M^{-1}cm^{-1}$)
2:	241 (55,700), 348 (13,800), 382 (7,600), 416 (8,700), 590 (1,500), 720 sh (500)
trans-**3**·CH_2Cl_2**:**	239 (63,800), 339 (12,600), 376 (9,900), 405 (10,400), 592 (1,040)
cis-**3:**	246 (56,600), 339 (13,700), 362sh (9,000), 388 (8,900), 519 (2,400)
trans-**4:**	244 (56,700), 286 (18,100), 339 (13,600), 378 (6,500), 412 (8000), 455 (3,900), 570 (900)
cis-**4:**	248 (61,900), 345 (12,300), 398 (7,600), 512 (2,700), 658 (1,150), 725 sh (980)
trans-**5:**	241 (51, 000), 337 (9,200), 379 (6,400), 407 (8,100), 500 sh (1,700), 600 (810)
cis-**5:**	243 (37,500), 334 (9,100), 371 (5,100), 393 (5,600), 503 (1,200)
6:	248 (60,700), 328 (14,500), 365sh (8,100), 499 (2,900)
7:	245 (92, 000), 326 (17,900), 391 (9,800), 502 (2,100)
8:	253 (54,900), 344 (14,300), 385 (7,100), 510 (3,000)
9:	242 (69,900), 327 (14,900), 364sh (8,500), 390 (8,900), 443 (2800), 510sh (3,000), 555 (1100)
10:	240 (53,600), 312 (22,400), 320 (22,700), 345 (19,900), 362 (20,900), 430 (2500), 645 (1300)

spectroscopic measurements of **2-10** in CH_2Cl_2; the data acquired in CH_3CN are found in the Experimental sections of the main text and section 5.7. All complexes exhibit high-intensity bands below 300 nm ($\varepsilon > 10^4\ M^{-1}cm^{-1}$) that are likely π-π^* transitions, on the

basis of energy and intensity considerations. Each complex also exhibits a medium-intensity band (ε ca. 10,000 - 20,000 $M^{-1}cm^{-1}$) centred in a narrow range of 320 - 350 nm that is likely an n-π* transition given its rather invariant energy range and intensity across the series of complexes as well as its similarity with the band found for solutions of the free ligand, H(**L**) (λ_{max} = 320 nm, ε = 22,500 $M^{-1}cm^{-1}$). The lower energy, visible bands (λ_{max} > 350 nm) are likely for ligand-to-metal charge transfer (LMCT) and/or ligand-to-ligand charge transfer (LLCT) transitions, as suggested by a comparison of their energies and intensities relative to related complexes[17] and by theoretical calculations. The frontier orbitals for two representative complexes *trans*-**3** and *trans*-**4** are shown in Figure 5.3. The HOMO for all complexes is π_L orbital (pi-lone-pair orbital, as per Kasha's convention[18]) on the pincer ligand with a small pi-antibonding contribution

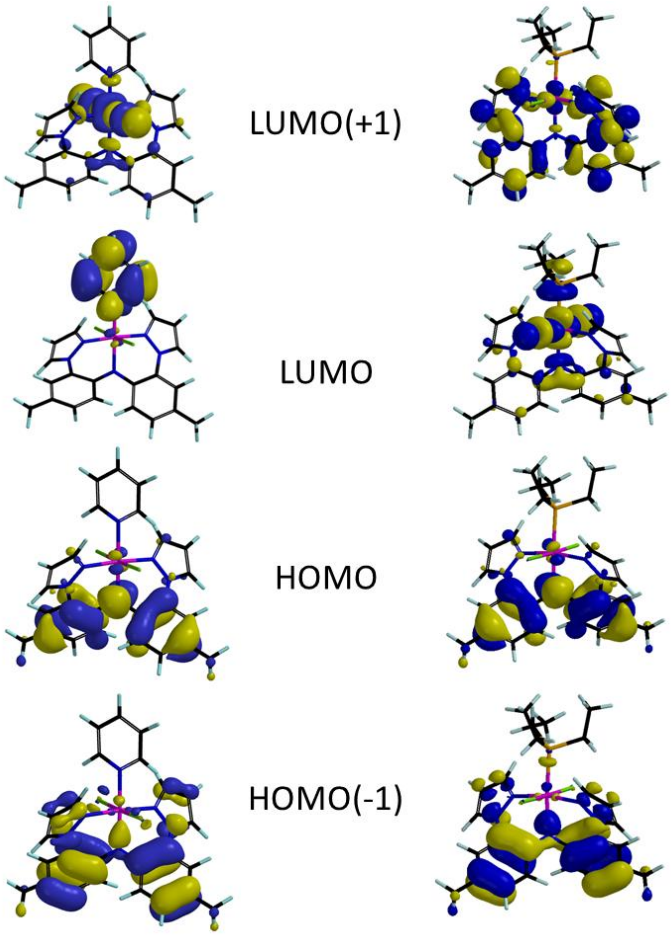

Figure 5.3. Frontier orbitals for *trans*-**3** and *trans*-**4** from DFT calculations (B3LYP/LACVP).

from a metal d-orbital. For pyridyl or poly(pyridyl)-containing complexes **3**, **6**, 7, **9**, and **10**, the π* orbitals on pyridyl rings constitute the LUMO. Thus, the lowest energy band (HOMO-LUMO transition) for each of these four complexes is LLCT in character. For the other complexes such as **2**, **4**, and **8**, the LUMO is a π* orbital with pronounced metal character. In these latter cases, the lowest energy transition is LMCT in nature. For all complexes, the subsequent higher energy visible bands involve transitions between different HOMO(-M) (M = 0-3) and LUMO(+N) (N = 0-4) levels that represent the gamut of various LMCT or LLCT transitions involving pincer and non-pincer ligand orbitals, as summarized in the section 5.7. The *d-d* transitions are not observed as these

expectedly weak-intensity transitions are likely obscured by the other, more intense bands.

5.4.4. Cyclic Voltammetry.

The electrochemistry of the various complexes was investigated and a summary of findings from cyclic voltammetry experiments is given in Table 5.6. A representative set of voltammograms for *trans*-**3** is given in Figure 5.4. Each complex shows a quasi-reversible ($E_{p,a}$-$E_{p,c}$ > 59

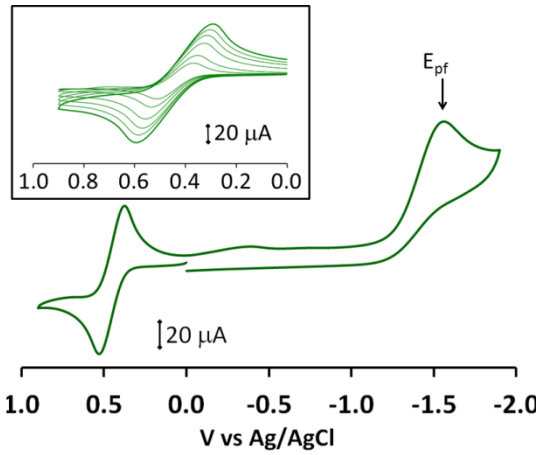

Figure 5.4. Cyclic voltammogram (300 mV/s) obtained for *trans*-**3** in CH_2Cl_2 with NBu_4PF_6 as a supporting electrolyte. Inset: Oxidation waves obtained at 50 (innermost plot), 100, 200, 300, 400, and 500 (outermost plot) mV/s. The vertical arrow near -1.6 V in the voltammogram is the E_{pf} cited in Table 5.

mV and increases with scan rate, see inset of Fig. 5.4), one-electron, ligand-based oxidation wave at potentials that depend mainly on the overall charge of the complex and to a lesser extent on the nature of the exogenous (non-pincer) ligands. That is, **2**·H_2O, with an anionic complex, has the lowest oxidation potential at +0.27 Vs Ag/AgCl. The charge-neutral rhodium(III) complexes **3**-**5** are at least +0.1 V more stable than **2**·H_2O with respect to oxidation where *trans*-**4,** with a strong σ-donating PEt_3 group, exhibits a lower oxidation potential (+0.38 V) than *trans*-**3** (+0.44 V) or *trans*-**5** (+0.50 V) with

pyridyl and pyrazine donors, respectively. (See section 5.7, Figure 5.26) Interestingly, *trans*-**3** has a lower oxidation potential than *cis*-**3** (+0.55 V) which is a reflection of the lower thermodynamic stability of the former versus the latter

Table 5.6. Summary of electrochemical data for complexes **2**-**10**.

	oxidation	*reduction*
compound	$E_{1/2}$[b] (ΔE, mV)[c]	$E_{1/2}$ (ΔE, mV)[c]
2·H_2O	+0.27 (182)	not observed
trans-**3**	+0.44 (231)	E_{pf} = -1.56 (irrev.)
cis-**3**	+0.55 (177)	E_{pf} =-1.20 (irrev.)
trans-**4**	+0.38 (135)	E_{pf} = -1.57 (irrev.)
cis-**4**	+0.54 (104)	E_{pf} =-0.88 (irrev.)
	+0.73 (113)	E_{pf} =-1.33 (irrev.)
trans-**5**	+0.50(152)	E_{pf} = -1.46 (irrev.)
cis-**5**	+0.59(150)	E_{pf} = -1.51 (irrev.)
6	+0.81 (227)	E_{pf} = -1.56 (irrev.)
7	+0.75 (124)	E_{pf} = -1.40 (irrev.)
8	+0.80 (140)	E_{pf} = -1.53 (irrev.)
9	+0.74 (182)	-1.12 (152), E_{pf} =-1.45 (irrev.)
10	+0.91(152)	-0.77 (145), E_{pf} =-1.30 (irrev.)

[a]samples as 0.1m*M* solutions in CH_2Cl_2 with 0.1*M* NBu_4PF_6 as a supporting electrolyte. [b]Average value from scan rates of 50, 100, 200, 300, 400, and 500 mV/s, V versus Ag/AgCl ($E_{1/2}$ for ferrocene under these conditions = 0.41 V). [c]for a scan rate of 200 mV/s.

from isomerization studies and computational findings. The chelating dipyridyl derivative **9** is detectably more electron-rich (E_{ox} = + 0.74 V) than **6** (E_{ox} = + 0.81 V) with two *trans*- disposed pyridine rings. The dicationic ttpy derivative in **10** is the most difficult to oxidize (+ 0.91 V) of the series, as might be expected based from coulombic considerations. Each complex also shows an irreversible, presumably, metal-based reduction at E_{pf} values equal to or more negative than -1.2 V versus Ag/AgCl. A quasi-reversible, one-electron, polypyridyl-based reduction wave is found at -1.12 V for **9** and -0.77 V for **10**. The HOMO-LUMO energy gaps of 1.86 eV (or 667 nm) for **9** and 1.68 eV (or 738 nm) for **10** from electrochemical experiments are close to those obtained from

UV-visible spectroscopic experiments (692 nm for **9** and 747 nm for **10**) by using the onsets of the low energy transitions, which lends support to the LLCT assignment of the lowest-energy visible band in the electronic spectrum.

5.4.5. Chemical Oxidations.

Given the electrochemical quasi-reversibility of the oxidation waves for the complexes reported above, the chemical oxidations of *trans*-**3**, *cis*-**3**, and **8** were investigated to probe the nature of the resulting doublets. In each case, the one-electron oxidation gave paramagnetic complexes (μ_{eff} ca. 1.8 μ_B) that were ligand-centered radicals based on structural and spectroscopic studies. The experimental findings were also supported by the results of theoretical calculations. Spectrophotometric redox titrations were performed by adding substoichiometric amounts of *trans*-**3**, *cis*-**3**, or **8** in CH_2Cl_2 to solutions of the moderately strong organic cation radical oxidant, 9,10-dimethoxyocta-hydro-1,4:5,8-dimethanoanthracenium hexachloroantimonate, (CRET)($SbCl_6$) (ε_{518} = 7300 $M^{-1}cm^{-1}$, $E_{1/2}$ = +1.09 versus Ag/AgCl).[19] As shown for *trans*-**3** in Figure 5.5, the characteristic π- radical bands at λ = 752, 606, 517 nm for HOMO(-N) (N = 0-3) to SOMO transitions of the oxidized (metal-bound) ligand grow at the expense of the band at λ_{max} = 518 for (CRET)($SbCl_6$) until an equimolar ratio of oxidant:*trans*-**3** is reached, verifying the one-electron nature of the oxidation. Similar results were found for the other two complexes.

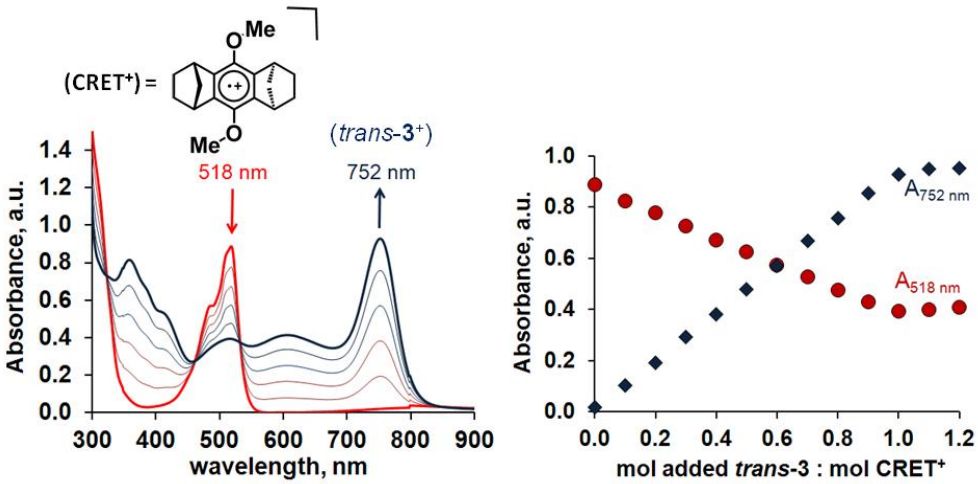

Figure 5.5. Spectrophotometric redox titration of trans-**3** with (CRET)($SbCl_6$) in CH_2Cl_2.

Synthetic scale oxidations used either (CRET)($SbCl_6$) or (NO)($SbCl_6$) as the oxidant. EPR spectra for ambient temperature and frozen (5 K) CH_2Cl_2 solutions of the bulk powders showed isotropic signals with g-factors of 2.010 for each (*trans*-**3**)$^+$ and (*cis*-**3**)$^+$ and of 2.013 for (*trans*-**8**)$^{2+}$. These g-factor values are near the free electron value and are indicative of ligand centered radical; the oxidized species are unlikely to be mainly metal-centered radicals since low-spin Rh(IV) is typically EPR silent at ambient temperature.[20]

X-ray quality crystals of each oxidized derivative could be grown by diffusing hexanes or toluene into small-scale reaction mixtures in CH_2Cl_2. Figure 5.6 shows overlays of the structures of the isomers of **3** and their oxidized forms, (**3**)$^+$ while the associated metrical data are found in Table 5.7. The structural overlay, of **8**$^+$ and **8**$^{2+}$ along with metrical data and discussion is given in the section 5.7. One of the main differences between the structures of the reduced and oxidized forms of the complexes is manifested in changes in the coordination environment about rhodium. In particular, the distances along the N_{Ar}-Rh-X (X = Cl1 or N31) vector decrease upon oxidation. Such changes would be

expected if an antibonding orbital (from dπ-pπ interactions) were to become depopulated upon oxidation. The HOMO of *trans*-**3** left of Figure 5.3 and the SOMO of (*trans*-**3**)$^+$ and similar MO diagrams for the other complexes indeed show such interactions. However, the HOMO of each non-oxidized complex is mainly a ligand-centered orbital. Within the ligand, there are pi-antibonding interactions between atoms corresponding to bonds A, A' C, C', F and F' and pi-bonding interactions corresponding to bonds B, B', G and G', as per the labeling diagram to the right of Fig. 5.6. Thus, the depopulation of the HOMO by oxidation should lead to a shortening of the former bonds and a

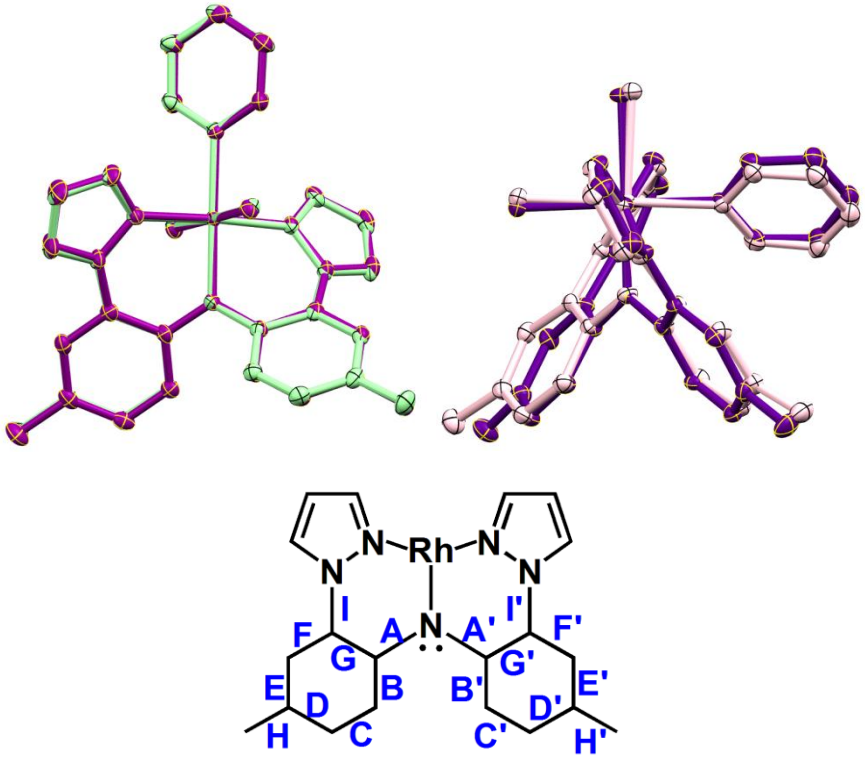

Figure 5.6. Left: Thermal ellipsoid plots (50% probability level) of *trans*-**3**, pale green, and (*trans*-**3**)$^+$, magenta, overlaid at the least-squares minimum mean position of five common atoms Rh, N_{pz}, and N_{py} and N_{Ar}; Center: Similar plot of *cis*-**3**, pale pink, and (*cis*-**3**)$^+$, violet, but overlaid at four atoms Rh, N_{pz}, and N_{Ar}; Right: Labeling diagram used for ligand bonds in Table 5.7.

Table 5.7. Comparison of bond distances and angles in isomers of **3** and $(\mathbf{3})^{+}$.

	Bond distances (Å)					
	trans-**3**	$(trans\text{-}\mathbf{3})^{+}$	Δ^{b}	*cis*-**3**	$(cis\text{-}\mathbf{3})^{+}$	Δ^{b}
Rh-Cl1	2.3425(5)	2.3318(8)	*-0.0107*	2.3903(7)	2.3446(9)	*-0.0457*
Rh-Cl2	2.3411(5)	2.3413(8)	*+0.0002*	2.3398(7)	2.3266(9)	*-0.0132*
Rh-N1	2.000(2)	1.985(2)	*-0.015*	2.013(2)	2.000(3)	*-0.013*
Rh-N11	2.012(2)	2.007(2)	*-0.005*	2.014(2)	2.024(3)	*+0.010*
Rh-N21	2.020(2)	2.019(2)	*-0.001*	2.015(2)	2.016(3)	*+0.001*
Rh-N31	2.097(2)	2.071(2)	*-0.026*	2.065(2)	2.073(3)	*+0.008*
Ligand Bond label[a]						
A	1.386(3)	1.384(4)	*-0.002*	1.384(4)	1.389(5)	*+0.005*
A’	1.386(3)	1.386(4)	*0.000*	1.393(4)	1.391(5)	*-0.002*
B	1.404(3)	1.410(4)	*+0.006*	1.401(4)	1.407(5)	*+0.006*
B’	1.414(3)	1.406(4)	*-0.008*	1.406(4)	1.403(6)	*-0.003*
C	1.381(3)	1.377(4)	*-0.004*	1.382(4)	1.381(6)	*-0.001*
C’	1.378(3)	1.374(4)	*-0.004*	1.385(4)	1.385(6)	*0.000*
D	1.391(3)	1.402(5)	*+0.009*	1.395(4)	1.398(6)	*+0.003*
D’	1.399(4)	1.396(4)	*-0.004*	1.398(4)	1.399(6)	*+0.001*
E	1.384(3)	1.385(4)	*+0.001*	1.383(4)	1.396(6)	*+0.013*
E’	1.387(4)	1.393(4)	*+0.005*	1.387(4)	1.389(6)	*+0.002*
F	1.396(3)	1.389(4)	*-0.007*	1.401(4)	1.387(5)	*-0.014*
F’	1.393(3)	1.385(4)	*-0.008*	1.393(4)	1.398(5)	*+0.005*
G	1.408(3)	1.413(4)	*+0.005*	1.405(4)	1.416(5)	*+0.011*
G’	1.402(3)	1.420(4)	*+0.018*	1.407(4)	1.408(5)	*+0.001*
H	1.509(3)	1.505(4)	*-0.004*	1.509(4)	1.502(6)	*-0.007*
H’	1.506(3)	1.502(4)	*+0.004*	1.498(4)	1.501(6)	*+0.003*
I	1.432(3)	1.421(4)	*-0.011*	1.431(4)	1.426(5)	*-0.005*
I’	1.433(3)	1.416(4)	*-0.017*	1.426(4)	1.419(5)	*-0.007*
Dihedral and torsion angles(°)						
Pz-tol	29.71	26.22	*-3.49*	32.05	27.60	*-4.45*
Pz-tol’	34.06	33.35	*-0.71*	35.29	29.83	*-5.46*
Tol-tol	69.04	64.27	*-4.77*	64.21	62.27	*-1.94*
|RhN-NC|	4.18	0.11	*-4.07*	2.99	7.15	*-4.16*
|(RhN-NC)’|	12.04	9.47	*-2.54*	13.12	15.60	*+2.48*

[a] see right of Figure 6 for labeling diagram of ligand bonds. [b] Δ = oxidized distance – non-oxidized distance

lengthening in the latter bonds (B, B’, G and G’). In general, such changes are observed but in many cases these changes upon oxidation are at the border-line of being or are not statistically significant. The most significant changes in ligand bonds of *trans*-**3** upon oxidation are found for bond F’ (shortened by 0.008 Å) and bond G’ (lengthened by 0.018 Å); the shortening of bonds C and C’ (Table 5.7) are at the borderline of statistical significance. Similarly for *cis*-**3**, bond F’ (shortened by 0.014 Å) and bond G’ (lengthened by 0.011 Å) show significant changes upon oxidation. For **8**, bonds C and F’

show significant shortening, but changes in other ligand bond distances are statistically insignificant. Concomitant with bond distance changes upon oxidation, there is a detectable reduction in dihedral angles involving the aromatic and heterocyclic rings, leading to an overall increase in ligand planarity. Thus, the dihedral angle between mean planes of the pyrazolyl-ring and the tolyl-group to which it is bound reduces by 2-4^{o} upon oxidation. The dihedral angle between mean planes of tolyl group arms either remains unchanged (compared to the average of three independent units of **8**) or reduces by up to 4^{o} (for *trans*-**3**) upon oxidation. Such changes in the ligand framework lead to subtle, but difficult-to-rationalize, differences in the (RhN-NC) torsion angles, the so-called 'pyrazolyl ring-twisting' that describes the "fit" of the ligand to the metal center.[21]

5.5. Discussion.

The electrochemistry associated with the rhodium(III) complexes of the ligand, $\mathbf{L}^{-}$, reported here is ligand-centered where the oxidation potential was found to span a remarkable range of 700 mV. In the development of an empirical model for the electrochemical data we noted that the effects of complex charge were predominant. For charge-neutral or a given set of complexes with the same ionic charge, ligand effects were either less than or equally as important to the range of observed $E_{1/2}$ values which could vary as much as 200 mV depending on the ligand set. Finally, for a given complex, differences in isomers (*trans*- versus *cis*-) lead to differences in $E_{1/2}$ values on the order of 100 mV or less where the *cis*- isomer was found to be more resistant to oxidation than a *trans*- isomer. It was recognized that the tabulated E_L (or P_L) parameters were from electrochemical data acquired in CH_3CN. We found that some of the complexes reported

here react with CH_3CN (the anionic and some charge-neutral derivatives) with chloride displacement, thus we chose to work with the electrochemical data in CH_2Cl_2 where we have confidence in the integrity of our complexes. Rather than re-determine the E_L parameters in CH_2Cl_2, we used the tabulated values or optimized values when ranges were reported, where it was hoped (and found) that differences due to solvent effects would be minor in most cases and could be accounted for in the data treatment.[22] Based on the above observations, the expression for $E_{1/2}$ values of the ($\mathbf{L}^0/\mathbf{L}^+$) couple was expected to follow the form of Eq. 1 where A is a

$$E_{1/2} = A + qQ + \Sigma E_L + \delta D \quad (1)$$

baseline constant for the given metal, the redox-active ligand, electrochemical setup (solvent, electrode, electrolyte concentration, etc.), Q was the overall charge on the complex, q is the coefficient describing the charge dependence of the complex, ΣE_L the sum of the E_L parameters, and δD would be an expression for the symmetry of the complex that would be a perturbation of the other variables. By first ignoring the latter term, a plot of $E_{1/2}$ - ΣE_L (vs NHE) versus charge Q should give a straight line with q as the slope and A as the intercept. To arrive at the symmetry dependence it was noted that for this system the *cis*- isomers of $LRhX_2Z$ had higher oxidation potentials that the *trans*-isomers and that the deviation from the average value is about 50 mV (giving a difference between isomers on the order of 100 mV). Moreover, it was also noted that complexes with C_2 point group symmetry generally needed no or little correction for agreement between predicted and experimental $E_{1/2}$ values; derivatives of the form **L**RhXYZ ($X \neq Y \neq Z$) needed the largest correction.

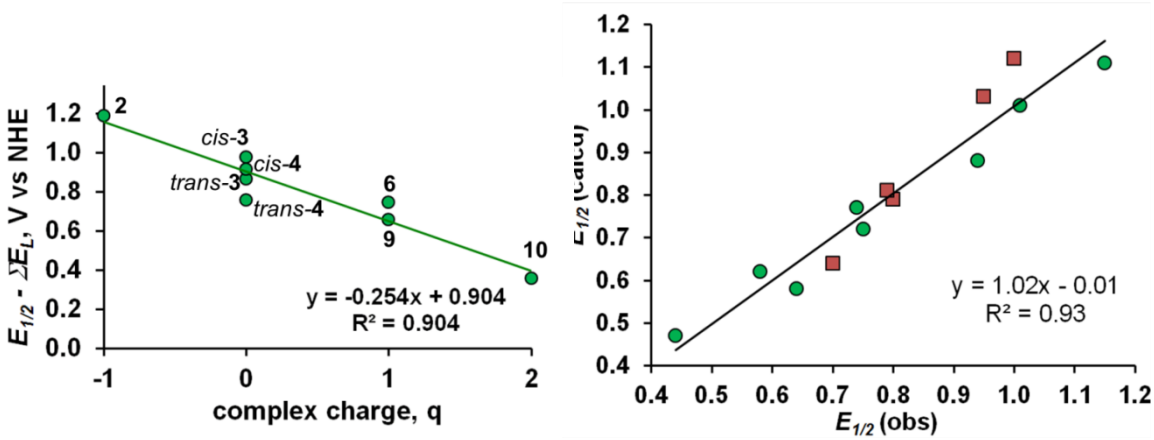

(a) (b)

Figure 5.7. (a) Plot of charge and ligand dependence on the oxidation potential of [**L**RhXYZ]^q complexes (b) Correlation between experimental oxidation potential and that predicted from Eq. 2 for basis complexes (green circles) and non-basis complexes (red squares).

Across a series of related complexes (such as **3** and **4**), the substituent, Z, *trans*- to the amido had the largest impact on $E_{1/2}$ values; the substituents, X and Y, *cis*- to the amido had lesser impact on $E_{1/2}$ (cis-**3** vs cis-**4** or **5** vs **6**). After trial and error fitting geometric terms, the full expression (Equation 2) was found that includes symmetry considerations.

$$E_{1/2} = 0.904 - 0.254Q + \Sigma E_L - (\delta_{xyz}/10)[2*E_L^{trans} - (-1)^g(E_L^{cisX} + E_L^{cisY})] \qquad (2)$$

Here, $\delta_{xyz} = 0$ if X=Y=Z and $\delta_{xyz} = 1$ if X≠Z or X≠Y. The power term, g, is the degeneracy of groups *cis*- to amido (g = 2 if X=Y, = 1 if X≠Y Table 6.8 collects the predicted and experimental $E_{1/2}$ values for both basis and non-basis complexes while the correlation between predicted and observed values for both basis (green circles) and non-basis (red circles) is found in Figure 5.7b. Given the expected

Table 5.8. Summary of predicted and experimental values of oxidation potentials in V vs NHE.

	Complex	$E_{1/2}$ (obs)	$E_{1/2}$ (calcd)	$\Delta E_{1/2}$ (obs-calcd)
Non-basis	*trans*-(**L**)$RhCl_2$(pyrazine)	+0.70	+0.64	0.06
	cis-(**L**)$RhCl_2$(pyrazine)	+0.79	+0.79	0
	trans-[(**L**)$Rh(PEt_3)_2Cl]^+$	+1.00	+1.12	-0.12
	[(**L**)$Rh(PPh_3)(py)(Cl)]^+$	+0.95	+1.03	-0.08
	(**L**)Rh(Me)(I)(CO)	+0.79	+0.81	-0.02
basis complexes	**2**	+0.47	+0.47	-0.03
	trans-**3**	+0.64	+0.58	+0.06
	cis-**3**	+0.75	+0.72	+0.03
	trans-**4**	+0.58	+0.62	-0.04
	cis-**4**	+0.74	+0.77	-0.03
	6	+1.01	+1.01	0
	9	+0.94	+0.88	+0.06
	10	+1.15	+1.11	+0.04

differences in E_L values due to variation in solvent (tabulated values are from experiments in CH_3CN versus current experiments that were performed in CH_2Cl_2) and to metal dependencies, there is a satisfying agreement between the predicted and actual values of $E_{1/2}$ for the non-basis (and entire set of) complexes. Better agreement may be anticipated if a more rigorous theoretical basis for the symmetry dependence is found in the future. Nonetheless, if one ignores the symmetry terms in Equation 2, the resulting expression is adequate for crude predictions of $E_{1/2}$. Such predictions on this and other systems may be useful in designing future systems capable of intra-ligand electron transfer reactions.

5.6.Conclusions.

The discovery of the convenient new reagent $(NEt_4)[(\mathbf{L})RhCl_3]\cdot H_2O$ has been central to the development of new rhodium(III) coordination chemistry involving the redox active di(2-pyrazolyl-p-tolyl)amido pincer ligand, **L**. In the various rhodium

complexes, the ligand-centered oxidation was found to vary up to 700 mV by appropriate choice of exogeneous ligand substitutions at the rhodium(III) center. That is, the other non-pincer ligands can (de)stabilize the "RhXYZ" fragment to varying extents based on their σ- and π- donor/acceptor properties. In doing so, the energy match between the pincer ligand and metal frontier orbitals differs. By changing the the efficacy of the dπ-pπ interaction between metal and amido pincer fragments, the $E_{1/2}$ of the ligand-centered oxidation is indirectly affected. It will be of interest to determine the generality of this indirect method for tuning redox potentials of non-innocent ligands and whether such findings can be exploited for controlling intramolecular electron transfer in chemical reactions or for the discovery of new valence tautomers.

5.7. Further Discussion of Syntheses and Characterization

In our early observations of the reactions of **2**·H_2O with various Lewis base donors, mixtures were obtained whose ultimate composition depended on the type of donor, the stoichiometry, and the reaction time. For instance, heating **2**·H_2O in neat pyridine at reflux (bp 115 ^oC) for 10 minutes gave a mixture of unreacted **2**·H_2O, green *trans*-(**L**)$RhCl_2$(py), *trans*-**3**, red-brown *cis*-(**L**)$RhCl_2$(py), *cis*-**3**, and rose-red *trans*-[(**L**)$RhCl(py)_2$](Cl), **5**, where unreacted **2**·H_2O and *trans*-**3** predominated the mixture. However, longer reaction times gave a greater quantity of [(**L**)$RhCl(py)_2$](Cl) at the expense of the other rhodium products. Similar reactions using **2**·H_2O and an excess PEt_3 in refluxing THF gave mixtures of unreacted **2** with yellow-brown *trans*-(**L**)$RhCl_2(PEt_3)$, *trans*-**4**, and violet-red *trans*-[(**L**)$RhCl(PEt_3)_2$](Cl) as the only other rhodium-containing products – no *cis*-**4** was detected. With pyrazine as a base, both

isomers of (**L**)$RhCl_2$(pyz) were detected, but the other by-products have not yet been identified.

For the pyridine derivative, the *trans*-3 to *cis*-3 isomerization is evident from 1H NMR spectroscopy (vide infra) and by the drastic color change from green to red. The isomer cis-3 decomposes at a modest rate on Al_2O_3 but slightly slower on SiO_2, a slow enough rate to permit the isolation of small quantities (50-100 mg) of the pure complex. The color changes associated with the isomerizations of the PEt_3 or pyz derivatives are more subtle. Therefore, the conversion is best monitored by NMR spectroscopy (vide infra). Unlike the isomerization of trans-3 or trans-5 the isomerization of trans-4 to cis-4 is accompanied by significant decomposition products that are difficult to separate from the desired product. The isomer cis-4 decomposes rapidly on SiO_2 or Al_2O_3 and appears to share similar solubility as the decomposition products, which has stymied all attempts to obtain large quantities (> 100 mg) of pure *cis*-**4** for further synthetic studies.

5.7.1. Crystal Structures.

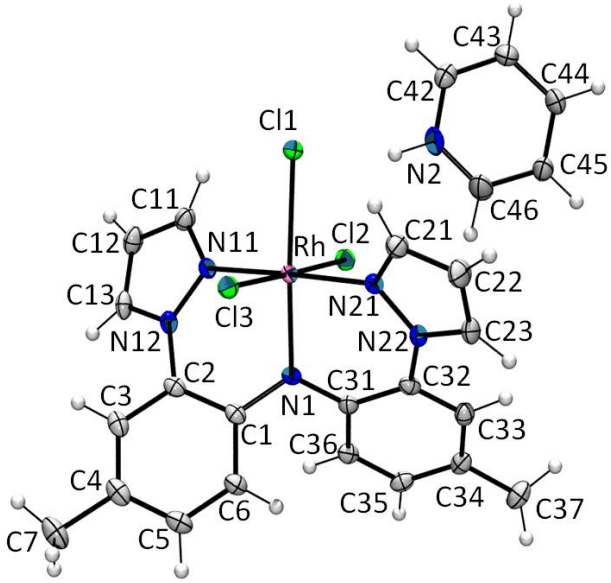

Figure 5.8. Structure and labeling of complex **A**. Solvate pyridines have been removed for clarity. Thermal ellipsoids shown at the 50% probability level.

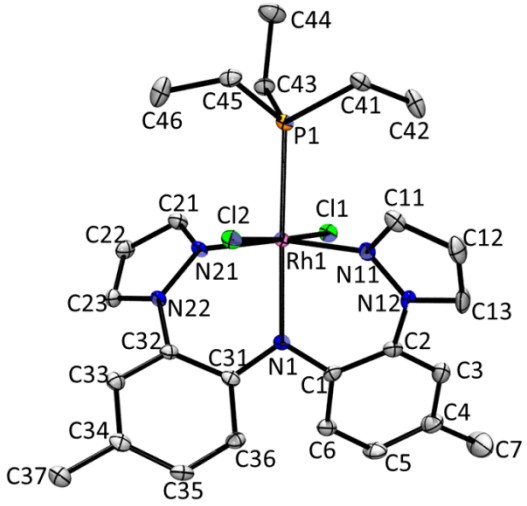

Figure 5.9. Structure and labeling of trans-**4**. Hydrogens have been removed for clarity. Thermal ellipsoids shown at the 50% probability level.

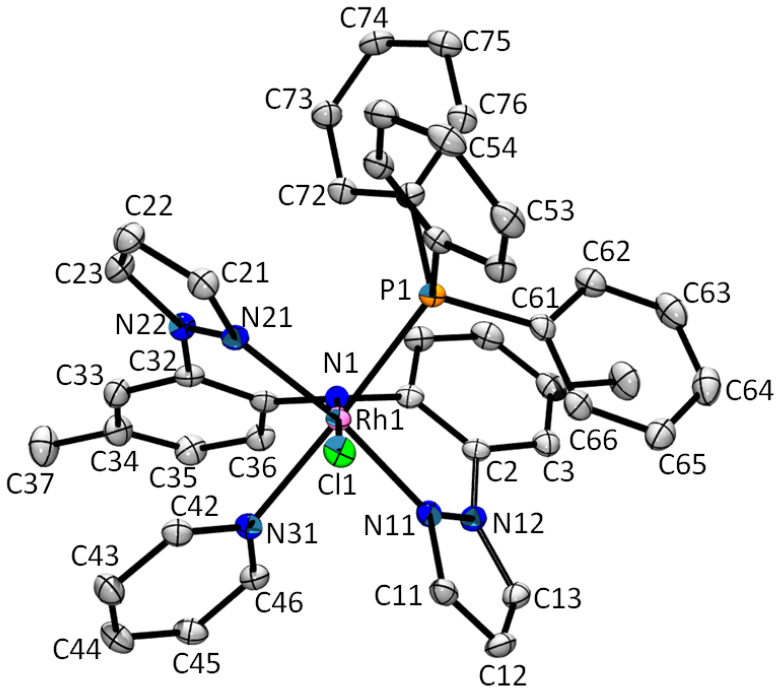

Figure 5.10. Structure and labeling of **7**. Hydrogens have been removed for clarity. Thermal ellipsoids shown at the 50% probability level

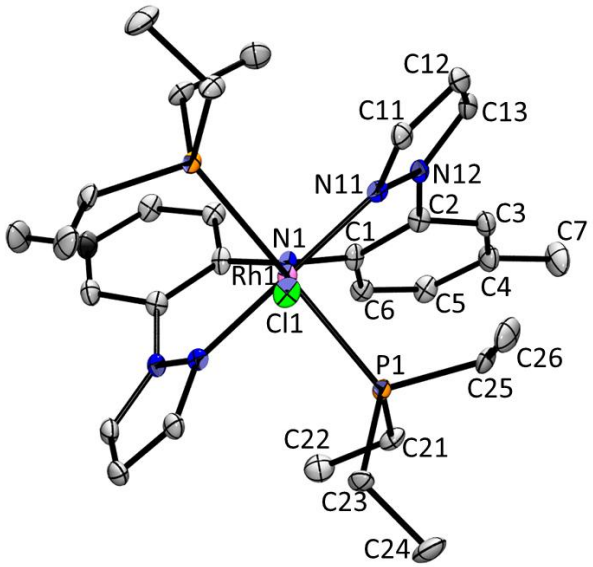

Figure 5.11 Structure and labeling of (*trans*-**8**$^{+}$). Hydrogens have been removed for clarity. Thermal ellipsoids shown at the 50% probability level.

5.7.2.NMR Spectroscopy.

The rhodium-bound pincer ligand is non-planar nature due to substantial ring-puckering in its two six-membered chelate rings and to tolyl-tolyl dihedral angles that range between 64^{o} and 71^{o}. Therefore, the rhodium complexes in **2**·H_2O, *trans*-**3**, *trans*-**4**, **6**, **8** and **10** each have only C_2-symmetry (ignoring ethyl groups of **4** and **8**). As such, the ^{1}H and ^{13}C NMR spectra of these complexes in CD_2Cl_2 exhibit one set of signals for pyrazolyl or tolyl hydrogen and carbon nuclei. The spectrum of complex **10** in all solvents is uncomplicated and gives the expected signals. However, the spectrum for each of the other five C_2-symmetric complexes are sometimes unexpectedly broad in certain chlorinated solvents ($CDCl_2$, CD_2Cl_2, or $C_2D_2Cl_4$) due to either dynamic processes associated with aryl-aryl ring twisting for **2**, *trans*-**3**, and *trans*-**4** or to ion-pairing effects for **6** and **8**. The downfield portions of the ^{1}H NMR spectra of **2** in CD_2Cl_2 acquired in the temperature range of 193 to 293 K is given in Figure 5.12. At 193 K the expected signals are observed and on increasing temperature the resonances for tolyl hydrogens broaden significantly; those for the pyrazolyl hydrogens experience shifts but do not broaden appreciably.

The ^{1}H NMR spectra of pure **4** or **8** in CD_2Cl_2 gives the expected sets of signals. It is noted that for complexes such as **4** or **8**, with PEt_3 bound to rhodium, two sets of second-order multiplet resonances for methylene hydrogens are observed in the ^{1}H NMR spectra owing to the prochiral nature of the CH_2 groups and the coupling to rhodium (I = ½); the resonance for ethyl-CH_3 hydrogens is a doublet of triplets due to coupling with hydrogen and rhodium nuclei. When the solvent is changed to $CDCl_3$ the ^{1}H NMR

spectrum of either pure **4** or **8** show that most of the tolyl and triethylphosphine hydrogen resonances are broad (sometimes to the extent that they are not observed).

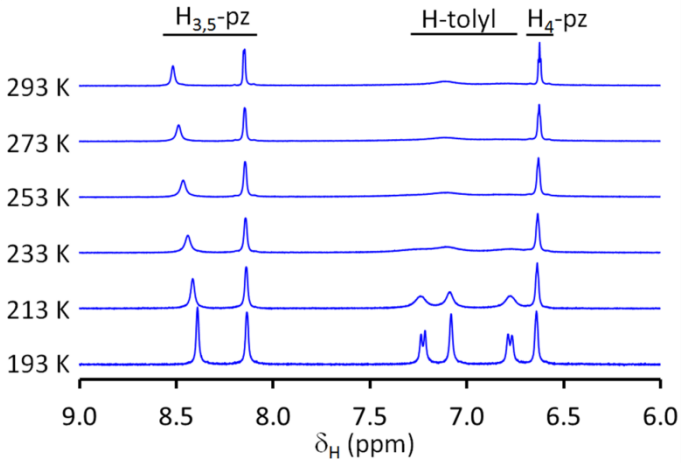

Figure 5.13 The downfield region of the ^{1}H NMR spectrum of **2** in CD_2Cl_2 acquired at different temperatures.

The exact origin of the line broadening remains unclear but likely involves ion-pairing. As exemplified for **8** in Figure 5.14, the addition of NBu_4PF_6 to the $CDCl_3$ solution increases the dielectric constant and the resonances become sharper like those in CD_2Cl_2.

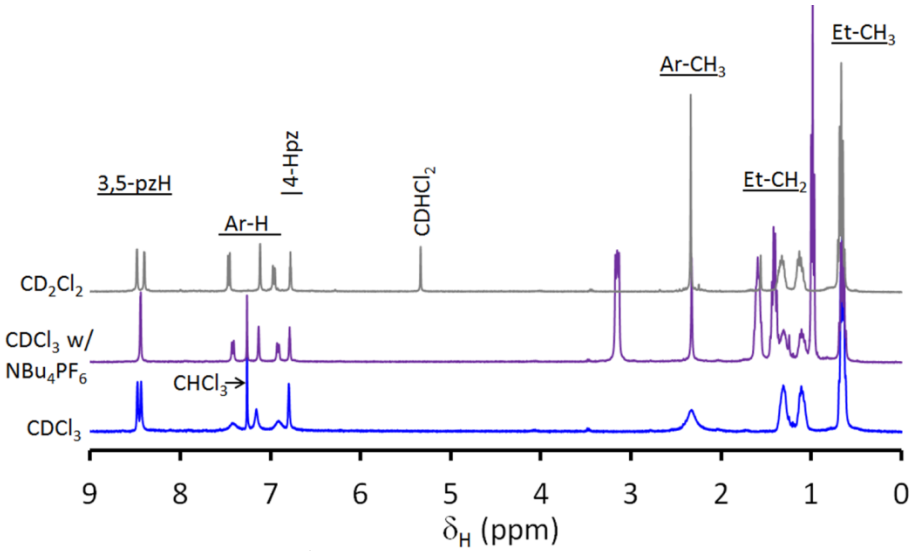

Figure 5.14. ^{1}H NMR spectrum of **8** in different solvents.

Full assignments for proton resonances for C_2 symmetric complexes in CD_2Cl_2 could be made by examination of 1D as well as 2D $^1H,^1H$ COSY and $^1H,^1H$ NOESY spectra. A portion of the COSY spectrum for *trans*-**3** is given in Figure 5.15 while the labeling diagrams for *trans*-**3** and **10** are found in Scheme 5.5.

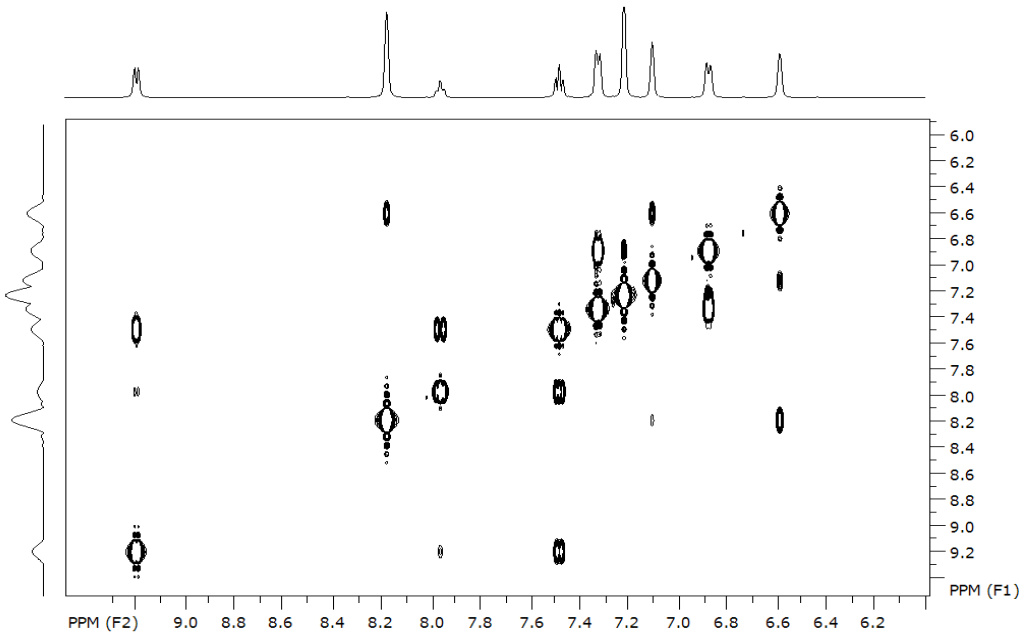

Figure 5.15. Down field portion of the COSY spectrum of *trans*-**3**·CH_2Cl_2 in CD_2Cl_2

Complexes *cis*-**3**, *cis*-**4**, and **9**, with two different groups situated *cis*- to the amido nitrogen of the pincer ligand, possess only C_1-symmetry. The dissimilar *cis*- substituents differentiate the arms of the pincer ligand and two sets of resonances for each of the pyrazolyl and tolyl groups are found in the spectrum, exemplified for the 2D COSY spectrum of *cis*-**3** in Figure 5.16 or for the 1D ^1H NMR spectrum in the top of Figure 5.17. The assignments and labeling diagram for *cis*-**4** and **9** are given in Scheme 5.6.

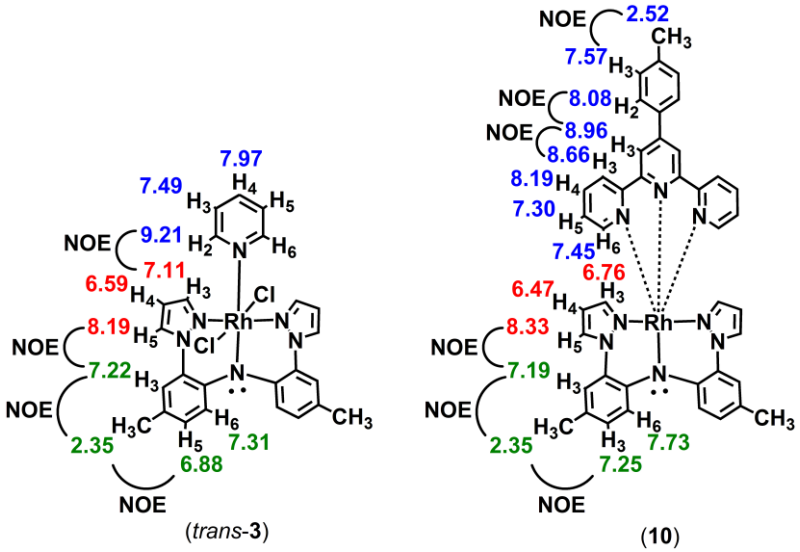

Scheme 5.5. Labeling Diagrams for NMR spectral data of *trans*-**3** and **10**.

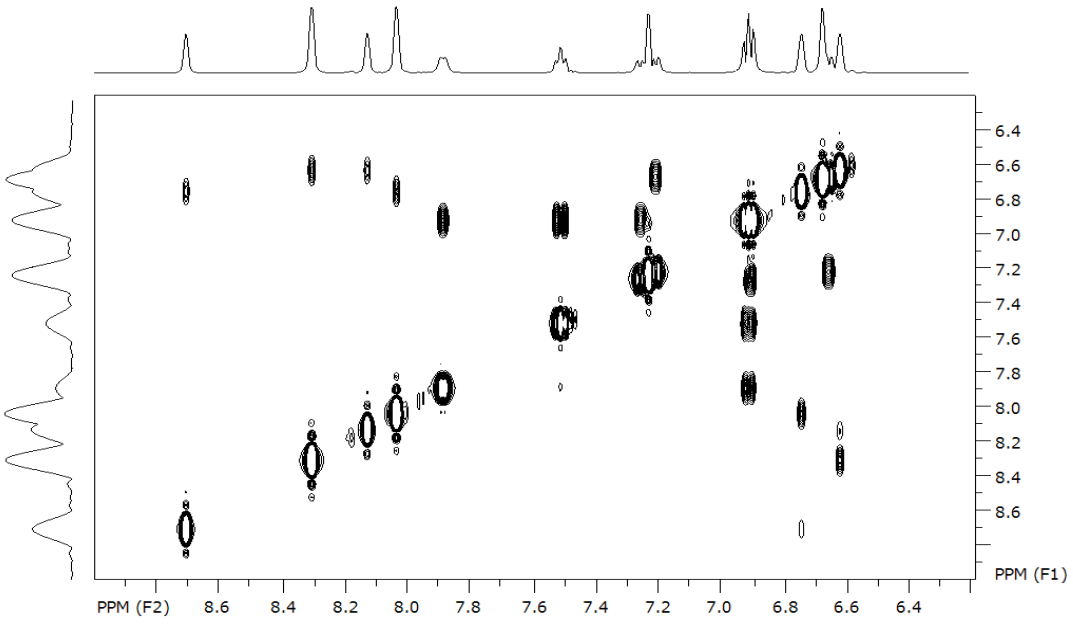

Figure 5.16. Down field portion of the COSY spectrum of *cis*-**3**·CH_2Cl_2 in CD_2Cl_2.

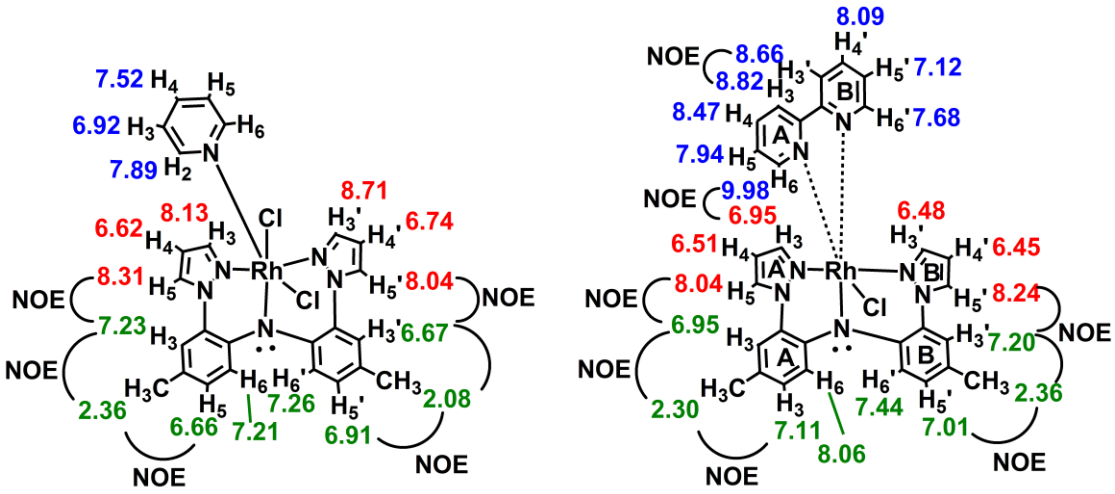

Scheme 5.6. Labeling Diagrams for NMR spectral data of *cis*-**3** and **9**.

5.7.3. Thermal Isomerization Reactions.

For **3**, there is sufficient resolution in the most downfield (H_5-pyrazolyl hydrogen) resonances to allow successful monitoring of the conversion of *trans*-**3** to *cis*-**3**, as in Figure 5.17, It was found that heating tetrachloroethane solutions of *trans*-**3** at 100^{o}C gave equilibrium mixtures of *trans*-**3** and *cis*-**3** after 7h, where *cis*-**3** was the major component (91%). By monitoring the relative integration of ^{1}H NMR resonances for the H_5-pyrazolyl hydrogens of each *trans*-**3** and *cis*-**3**, the initial rates of reactions over the first two half-lives ($t_{1/2}$ = 2 h) that were recorded for several solutions indicated that the isomerization reaction was first-order in *trans*-**3** with a rate constant of 9.8 x 10^{-5} s^{-1}.

Unlike the isomerization of *trans*-**3**, the isomerization of *trans*-**4** is accompanied by decomposition reactions that complicate analyses. For instance, the conversion from *trans*-**4** to *cis*-**4** could not be monitored reliably by using the downfield pyrazolyl hydrogen resonances (δ_H = 8.67, 8.38 ppm for *cis*-**4**, 7.96 ppm for *trans*-**4**) because these

resonances happen to overlap others for unidentified decomposition products, as shown below. Instead, ^{31}P NMR spectroscopy was a more useful diagnostic tool. Figure 5.18 shows the ^{31}P NMR spectra acquired for a solution (initially) of *trans*-**4**, after heating at 100^{o}C over various periods of time. Over the course of 12 h, a sharp doublet resonance at ca. 29 ppm for *cis*-**4** grows in at

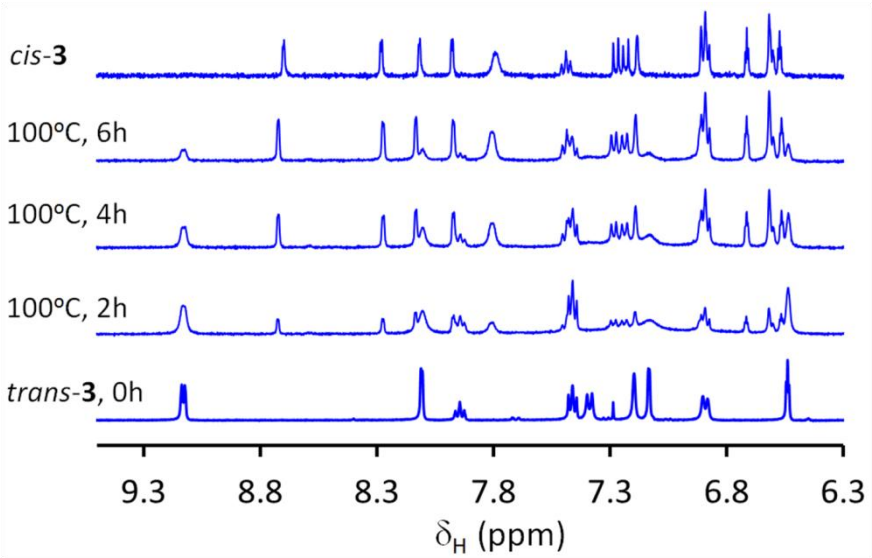

Figure 5.17. Downfield region of the ^{1}H NMR spectra showing the conversion of *trans*-**3** (bottom) to *cis*-**3** (top) in $C_2D_2Cl_4$ at 100^{o}C over time

the expense of the broad resonance at ca. 7 ppm for *trans*-**4**. After *cis*-**4** is formed, a weak-intensity resonance near 50 ppm is detectable. This latter resonance is tentatively assigned to $P(O)Et_3$ due to its chemical shift and to the apparent absence of coupling to ^{103}Rh (I = ½, 100%). After 8 h, other doublet signals near 40 ppm (J_{Rh-P} =117 Hz) and 6 ppm (J_{Rh-P} =100 Hz) for unidentified decomposition products are also observed. These decomposition products likely contain phosphorus *trans*- to a chloride from the magnitude of the coupling constants [24]

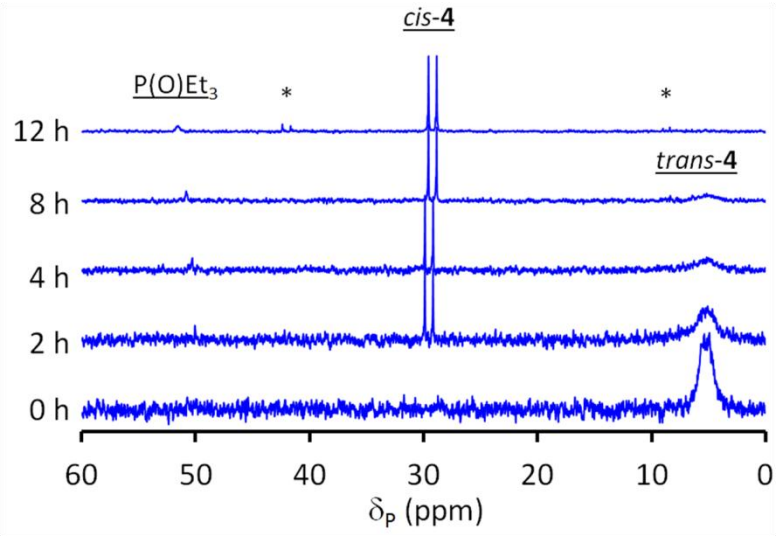

Figure 5.18 An overlay of ^{13}P NMR spectra acquired over 12 h that shows the conversion of *trans*-**4** (bottom) to *cis*-**4** (top) after heating in $C_2D_2Cl_4$ at 100^{o}C. The doublets for unknown decomposition products are demarcated with asterisks (*).

These doublet resonances are clearly different than that of **6** which occurs at δ_P 12 ppm ($J_{Rh\text{-}P}$ =82 Hz, P *trans*- to P[24]) but the species responsible for these resonances remain unknown. By monitoring the integration of the resonance for *trans*-**4** versus the total integration of all ^{31}P NMR signals (including those attributed to $P(O)Et_3$) for the first 10 h, a first-order rate constant of 2.9 x 10^{-5} s^{-1} was found.

The thermal isomerization of *trans*-**5** in $C_2D_2Cl_4$ at 100^{o}C was essentially complete within 1 h. Figure 5.19 shows an overlay of ^{1}H NMR spectra for a sample heated at 100^{o}C for various periods of time. The resonances for *trans*-**5** decrease and those for *cis*-**5** increase in intensity over the first 30 min, until the relative integrations reach a constant 1:9 ratio favoring the *cis*- isomer. The weak intensity resonances between 7.5 and 7.7 ppm in the middle spectra of Figure 5.19, indicate that the isomerization is also accompanied by the formation of a minor by-product (circles in

Figure 5.19) and free pyrazine (δ_H = 8.58 ppm). The pure compounds **5** can be separated from the "impurities" via chromatography. The by-product is probably a five coordinate intermediate (vide infra) but its true nature remains unknown. By ignoring this species, the relative integrations of *cis*- and *trans*- isomers give an estimate of $t_{1/2}$ of

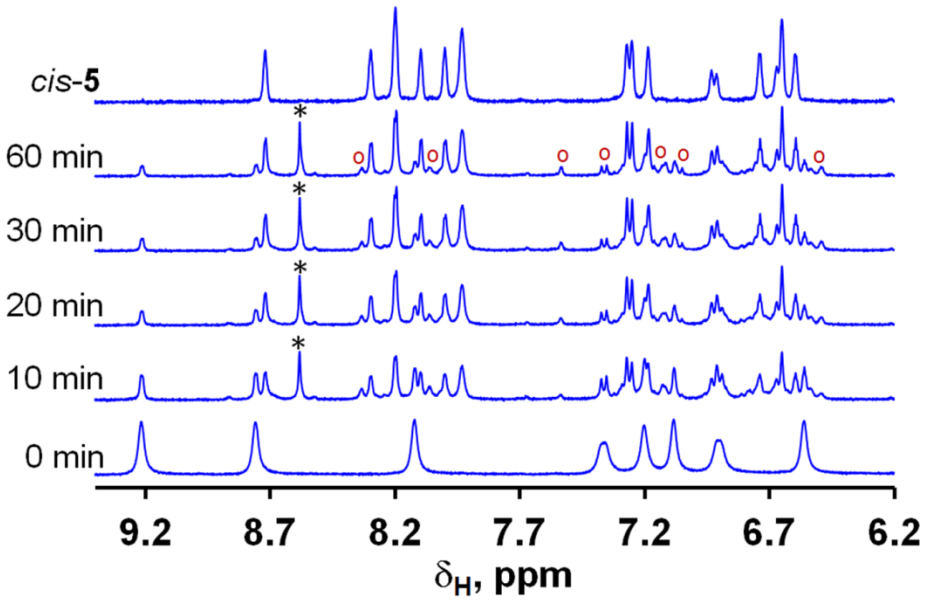

Figure 5.19. Downfield portion of the ^{1}H NMR spectra of *trans*-**5** in $C_2D_2Cl_4$ (bottom) after heating for various periods of time at 100^{o}C. The asterisk demarcates the resonance for free pyrazine in $C_2D_2Cl_4$. The red circles demarcate the intermediate/by-product formed during isomerization. The ^{1}H NMR spectrum of *cis*-**5** in $C_2D_2Cl_4$ is also shown for reference (top).

about 15 min and a first order rate constant of $4.6x10^{-2}$ s^{-1}. The nearly isoergonic nature of the isomers in each **3** and **5** is also revealed by the modest equilibrium constants (K_{373} ~ 9) for the conversion of the respective *trans*- to *cis*- isomer.

It is noteworthy to reiterate that neither *trans*-**3** nor *trans*-**4** underwent isomerization in low-boiling solvents such as THF (bp = 65°C) or $CHCl_3$ (bp = 61°C) which implicates a rate-determining dissociative step for isomerization. High activation barriers for the isomerization reactions are also implied by the ability to separate mixtures of isomers at room temperature. The complex *trans*-**5** does undergo isomerization in boiling $CHCl_3$ and faster overall isomerization in TCE at 100°C versus the other two related complexes. It is noted that the rates of isomerization under common conditions decrease as the relative σ-donating ability[25] of the *trans*- ligand increases: pyrazine < pyridine < PEt_3, implying dissociation of the charge-neutral Lewis base as the rate limiting step. Free pyrazine is indeed observed in the isomerization of *trans*-**5**. Thus, of the two possible dissociative mechanisms for the isomerization provided in Scheme 5.7 we favor that in (a) as being predominant. In this pathway, five-coordinate intermediates **I** or **II** might give rise to the minor species seen in the NMR spectra of *trans*-**5** during heating. We cannot exclude the possibility of chloride dissociation as in Scheme 5.7b, especially considering that species of the type $[(\mathbf{L})Rh(X= py \text{ or } PEt_3)_2Cl]^+$ are observed in reactions between $\mathbf{2}\cdot H_2O$ and excess base, X. Such species would be the direct result of ligand addition to intermediate ***V***. In fact, this latter mechanism (Scheme 5.7b) may be predominant for very strong σ-donors, which may explain why *cis*-**4** is more readily decomposed than either *cis*-**3** or *cis*-**5**.

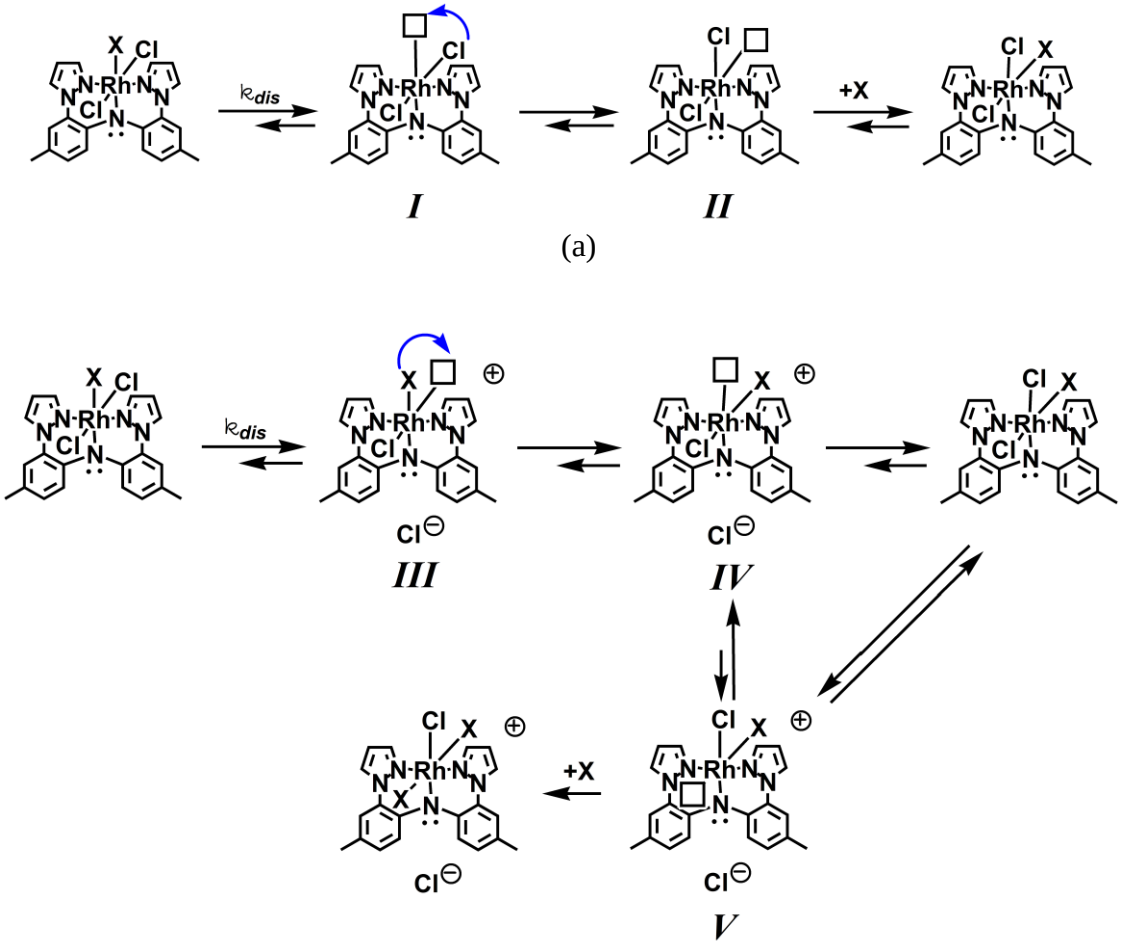

Scheme 5.7. Proposed mechanisms for the isomerization of *trans*-**3** (X = py) or *trans*-**4** (X = PEt_3)

5.7.4. Photochemical Conversion of *cis*-3 to *trans*-3.

It was found that irradiation of red dichloromethane solutions of *cis*-**3** with visible light from a 250 *W* incandescent bulb caused a color change to green, similar to that of *trans*-**3**. The formation of *trans*-**3** was verified by monitoring the photo-induced changes by ^{1}H NMR spectroscopy as shown in the left of Figure 5.20 The conversion of *cis*-**3** to *trans*-**3** at 35^{o}C in an all-glass apparatus and using this illumination source is about 50% complete after 16 h. The conversion was also monitored by

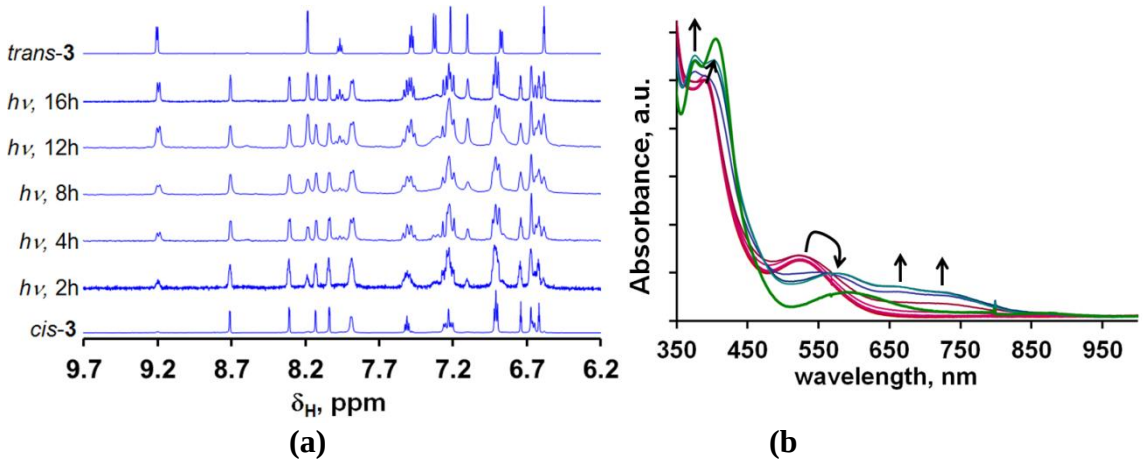

Figure 5.20. (a) ^{1}H NMR spectral data for a CD_2Cl_2 solution that was originally 2 m*M* in *cis*-**3** after various periods of illumination with visible light. The spectra of pure *cis*-**3** (bottom) and *trans*-**3** (top) from separate experiments are given for reference. (b) Overlay of visible spectra of a CH_2Cl_2 solution initially 2.78×10^{-5} *M cis*-**3** after various periods of visible light irradiation. The green spectrum is that anticipated for a solution 2.78×10^{-5} *M* in *trans*-**3**, as a reference.

UV-Visible spectroscopy using about 100-fold diluted solutions compared to the NMR experiment, and a quartz apparatus with the same illumination source. Under these conditions, the original solution was red and had the characteristic spectrum for *cis*-**3** (thick red line, Fig 5.20b). After time the solution changed to blue-green and the spectra gave the appearance of a mixture of *trans*-**3** and another colored species tentatively assigned as an oxidized species on the basis of the bands near 740 and 660 nm which resemble those characteristic for pi-radicals. These pi-radical bands are at different position and intensity that either (*cis*-$\mathbf{3}^{+}$) or (*trans*-$\mathbf{3}^{+}$); it was not possible to mimic the spectra of the photo-oxidized species by summing spectra for varying amounts of *trans*-**3** and known radicals (*cis*-$\mathbf{3}^{+}$) or (*trans*-$\mathbf{3}^{+}$). Thus, the nature of the species obtained under these conditions remains unknown. The use of the glass apparatus appears to slow the rate of photo-damage but does not eliminate the production of the colored byproduct.

Similar observations were found for the conversion of *cis*-**5** to *trans*-**5**, Figure 5.21. It is curious that paramagnetic species do not seem to be produced in NMR experiments.

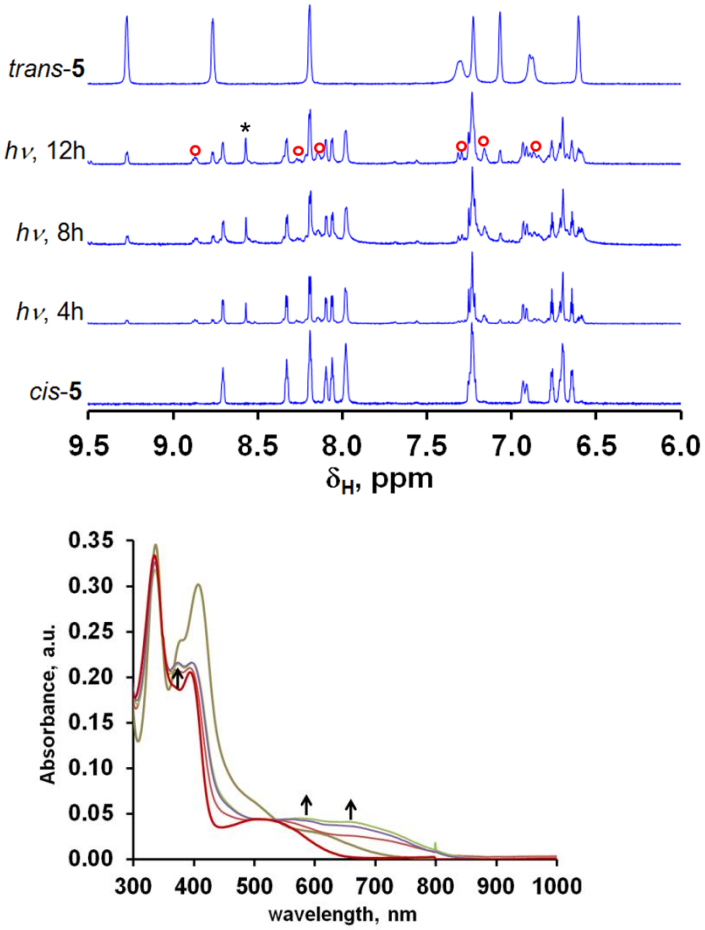

Figure 5.21. (a) ^{1}H NMR spectral data for a CD_2Cl_2 solution that was originally 2 m*M* in cis-**5** after various periods of illumination with visible light. The spectrum of pure *trans*-**5** (top) from a separate experiment is given for reference. The asterisk demarcates the resonance for free pyrazine and the red circles demarcate the intermediate/by-product formed during isomerization. (b) Overlay of visible spectra of a CH_2Cl_2 solution initially 3.67×10^{-5} *M cis*-**5** (thick magenta line) after various periods of visible light irradiation. The spectrum with the tan-colored line is that anticipated for a solution 3.67×10^{-5} *M* in *trans*-**5**, as a reference

5.7.5.Chemical Oxidations.

As discussed above, the stoichiometry of oxidations were established through redox titrations with (CRET)($SbCl_6$). Figure 5.22 shows the spectral data from the titration performed by adding substoichiometric amounts of *cis*-**3** to a solution of the organic oxidant. Treating a CH_2Cl_2 solution of the red-violet [(**L**)Rh(PEt_3)$_2$Cl](PF_6), (*trans*-**8**$^+$)(PF_6), with one equivalent of the oxidizing agent (NO)($SbCl_6$) immediately produced a violet-blue solution of the [(**L**)Rh(PEt_3)$_2$Cl]$^{2+}$, (*trans*-**8**$^{2+}$), cation. Crystals were deposited after a layer of toluene had been allowed to diffuse into the CH_2Cl_2

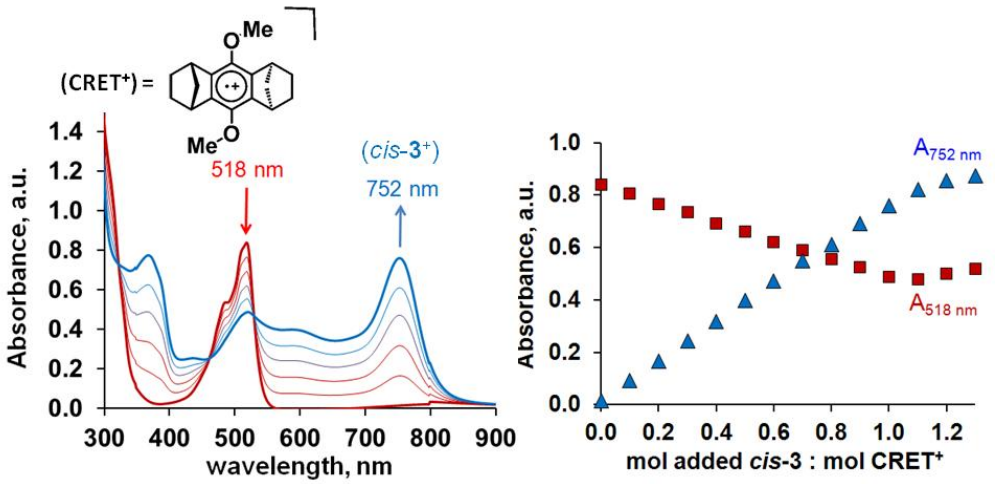

Figure 5.22 Spectrophotometric redox titration of *cis*-**3** with CRET($SbCl_6$).

solution. One crystal was selected for an X-ray diffraction study and was shown to be the $SbCl_6$ salt, [(**L**)Rh(PEt_3)$_2$Cl]($SbCl_6$)$_2$. The bulk sample analyzed as the mixed PF_6/$SbCl_6$ salt, as expected. Thus, the selection of a crystal of the $SbCl_6$ salt over a PF_6 salt or a genuine mixed PF_6/$SbCl_6$ salt is likely fortuitous. A comparison of structures of [(**L**)Rh(PEt_3)$_2$Cl]$^{2+}$ and one of the three crystallographically-independent units of

[(**L**)Rh(PEt_3)$_2$Cl]$^+$ (that possessed the same chirality as that in (*trans*-**8**$^{2+}$) is found in Figure 5.23. Selected bond distances and angles for [(**L**)Rh(PEt_3)$_2$Cl]$^{n+}$ (n = 1, 2) are listed in Table 5.9. One of the main differences in the structures between the reduced and oxidized form of the cations is manifested in changes in the coordination environment about rhodium.

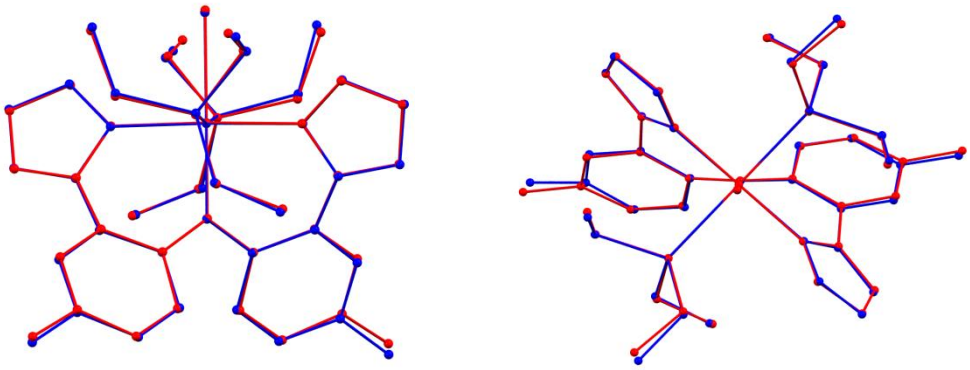

Figure 5.23. Views of structures of complexes in **6** (red) and **9** (blue) overlaid by least-squares minimum mean position of five common atoms $N_{Ar}RhP_2C1$.

In particular, the distances along the N-Rh-Cl vector decrease upon oxidation (Rh-Cl (avg.) = 2.3786(23) Å and Rh-N_{Ar} (avg.) = 2.042(8) Å for **6** versus Rh-Cl = 2.3433(13) Å and Rh-N_{Ar} = 2.019(4) Å for **9**). Such a bond shortening upon oxidation might be expected from the depopulation of the HOMO of (*trans*-**8**$^+$) which has a pi-antibonding interaction between pincer ligand π_L orbital and a metal d-orbital, (see SOMO of (*trans*-**8**$^{2+}$), right of Figure 5.24). Similarly, there is a pi antibonding interaction between atoms of the ligand corresponding to bonds A, A' C, C', F and F' in Scheme 5.8. Thus depopulation of the HOMO by oxidation should lead to a shortening of these bonds. Indeed, bonds C and F' show a significant shortening upon oxidation but changes in other

bond distances are statistically insignificant. The distances involving the Rh-N_{pz} unit in the cation and dication remain statistically identical with Rh-N_{pz} (avg.) = 2.032(6) Å for (*trans*-**8**$^{2+}$) and Rh-N_{pz} (avg.) = 2.026(6) Å for (*trans*-**8**$^{+}$)].

	Bond distances (Å)				
	$[Rh(PEt_3)_2Cl(\mathbf{L_1})]^{+a}$				$[Rh(PEt_3)_2Cl(\mathbf{L_1})]^{2+}$
	I	**II**	**III**	Avg.	
Rh-Cl	2.3809(16)	2.3810(12)	2.3738(12)	2.3786(23)	2.3433(13)
Rh-N1	2.023(5)	2.061(4)	2.041(4)	2.042(8)	2.019(4)
Rh-P1	2.4052(13)	2.4106(9)	2.4218(9)	2.4125(18)	2.4279(14)
Rh-P2	2.4052(13)	2.4106(9)	2.4218(9)	2.4125(18)	2.4336(14)
Rh-N11	2.025(4)	2.025(3)	2.028(3)	2.026(6)	2.035(4)
Rh-N21	2.024(4)	2.025(3)	2.028(3)	2.026(6)	2.029(4)
Ligand Bond label[b]					
A	1.397(6)	1.382(4)	1.385(4)	1.388(8)	1.381(7)
A’	1.400(6)	1.382(4)	1.385(4)	1.389(8)	1.384(7)
B	1.413(7)	1.410(5)	1.412(6)	1.412(6)	1.415(7)
B’	1.420(7)	1.410(5)	1.412(6)	1.414(6)	1.420(7)
C	1.374(7)	1.382(6)	1.376(6)	1.377(6)	1.352(8)
C’	1.378(7)	1.382(6)	1.376(6)	1.379(7)	1.372(8)
D	1.399(7)	1.401(6)	1.399(6)	1.400(7)	1.387(8)
D’	1.391(7)	1.401(6)	1.399(6)	1.397(7)	1.406(8)
E	1.377(7)	1.383(6)	1.388(6)	1.383(7)	1.385(8)
E’	1.377(7)	1.383(6)	1.388(6)	1.383(7)	1.387(8)
F	1.407(7)	1.388(6)	1.394(6)	1.396(7)	1.395(7)
F’	1.403(7)	1.388(6)	1.394(6)	1.395(7)	1.379(8)
G	1.396(7)	1.410(5)	1.404(5)	1.403(7)	1.415(7)
G’	1.397(7)	1.410(5)	1.404(5)	1.404(7)	1.410(8)
H	1.502(6)	1.514(6)	1.510(6)	1.509(6)	1.510(8)
H’	1.507(6)	1.514(6)	1.510(6)	1.510(6)	1.505(8)
I	1.431(6)	1.428(5)	1.432(5)	1.430(9)	1.422(7)
I’	1.432(6)	1.428(5)	1.432(5)	1.431(9)	1.423(7)
Dihedral and torsion angles					
Pz-tol	32.4	37.5	34.2	34.7	33.0
Pz-tol’	33.8	37.5	34.2	35.2	30.4
Tol-tol	66.6	62.8	70.5	66.6	67.2
RhN-NC	13.8(9)	17.4(5)	10.4(5)	14(4)	14.5(7)
(RhN-NC)’	12.4(8)	17.4(5)	10.4(5)	13(4)	16.4(6)

[a] three independent molecules in unit cell,.labeled **I**, **II**, or **III**. See labeling in Scheme 5.

Table 5.9. Selected bond distances (Å) and angles (^{o}) for $[Rh(PEt_3)_2Cl(\mathbf{L_1})]^{n+}$ (n = 1, 2). Labeling is per the diagram on the right of Scheme 5.8

These results combined with those previously noted for rhodium(I) chemistry,[6] indicate that the Rh-N_{pz} bond distances are insensitive to the formal oxidation state of rhodium or to the other ligands bound to the metal. This observation was initially surprising given that for other metals, such as in iron chemistry, the M-N_{pz} distances in poly(pyrazolyl) ligands are sensitive to both spin-state and formal oxidation state.[26] However, the lack of contribution from pyrazolyl-centered group orbitals in the HOMO of **6** (or of carbonylrhodium(I) derivative) helps to rationalize this observation. Interestingly, the interatomic distances involving the RhP_2 fragment increase upon oxidation (Rh-P (avg.) = 2.4308(20) Å in (*trans*-**8**$^{2+}$) versus Rh-P (avg.) = 2.4125(18) Å in (*trans*-**8**$^{+}$)) which is difficult to rationalize.

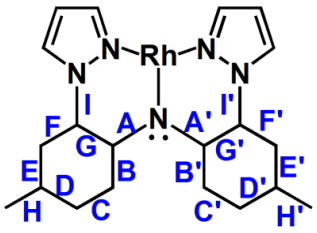

Scheme 5.8. Labeling diagram used for ligand bonds in Table 5.9

A comparison and of the electronic absorption spectrum of (*trans*-**8**$^{+}$) and (*trans*-**8**$^{2+}$) is given in Figure 5.24. Similar to that previously observed in [(**L**)Re$(CO)_3$]$^{+}$,[5] the electronic absorption spectrum of the violet-blue dication in (*trans*-**8**$^{2+}$) exhibits characteristic π-radical bands at 560, 680, and 730 nm in the visible spectrum for HOMO(-N) (N = 0-3,5) to SOMO (right of Fig. 5.24) transitions, bands which are absent

in the spectrum of red-orange (*trans*-**8**$^{+}$). The remaining charge transfer bands in (*trans*-**8**$^{2+}$) are shifted to higher energy compared to those in (*trans*-**8**$^{+}$).

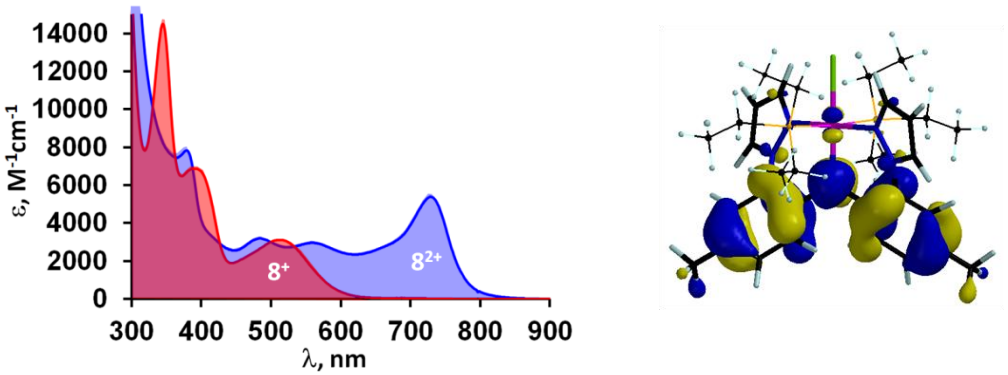

Figure 5.24. Overlay of electronic absorption spectra of each **6** and **9** in CH_2Cl_2. Right: SOMO of the dication

5.7.6. EPR spectroscopy.

Bulk samples of (*trans*-**3**$^{+}$)($SbCl_6$) and (*cis*-**3**$^{+}$)(($SbCl_6$) as frozen (5K) CH_2Cl_2 solutions or [(*trans*-**8**$^{2+}$)](PF_6)($SbCl_6$) as a frozen (12 K) CH_3CN:toluene glass were subject to X-band EPR spectroscopy. The EPR spectra for the former two complexes are given in the top of Figure 5.25 while representative experimental and simulated EPR spectra for [(*trans*-**8**$^{2+}$)] are provided on the bottom left of Figure 5.25. The EPR spectra of all three samples are nearly identical, so the discussion is limited to that of (*trans*-**8**$^{2+}$). The EPR spectra acquired with 100 mW field modulation shows a nearly isotropic signal centered at g = 2.018 with a small interaction with a single I = ½ nucleus with a hyperfine splitting, a, of 14 mT. The observed coupling of the unpaired electron is due to weak

interaction with the 100% abundant $I = ½$ ^{103}Rh nucleus. It is less likely that this interaction involves only one of the two symmetry-equivalent $I = ½$ ^{31}P nuclei or a single 1.1 % abundant $I = ½$ ^{13}C nuclei with unusually high spin density

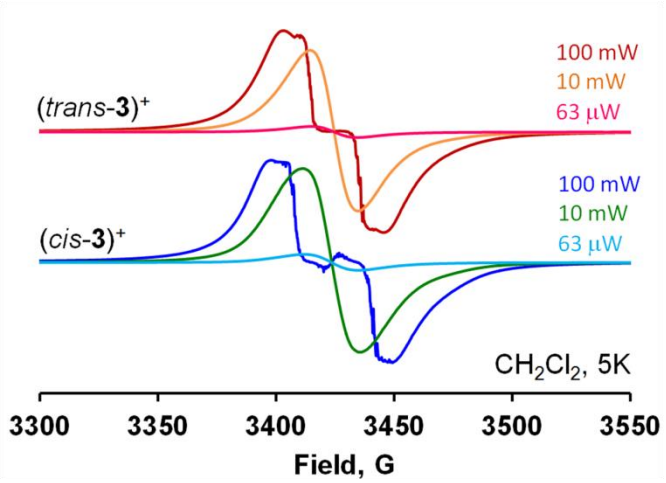

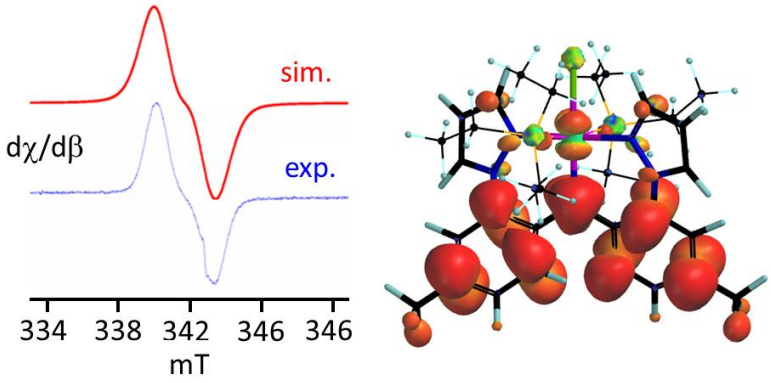

Figure 5.25. Top: EPR spectra of (*trans*-**3**$^{+}$)($SbCl_6$) and (*cis*-**3**$^{+}$)(($SbCl_6$) at acquired at various field modulations. Left: Experimental (blue, bottom) and simulated (red, top) X-Band EPR spectrum of (*trans*-**8**$^{2+}$) as a frozen (12 K) CH_3CN:toluene glass. Right: Spin-density isosurface map of the dication

With smaller field modulations (10 mW and 63 μW) the spectra are isotropic. Density functional calculations indicate that most of the unpaired spin density in each complex resides on the ligand ^{14}N (I = 1, 99.6% abundant) and ^{13}C (I = 1/2, 1.1% abundant) nuclei, and to a lesser extent on (in order) rhodium, phosphorus, and chlorine., as can be seen from the spin-density iso-surface map for (*trans*-**8**$^{2+}$) shown on the right of Figure 5.28. Again, it should be noted that the oxidized species is probably not mainly a metal-centered radical as low-spin Rh(IV) is typically EPR silent at ambient temperature.[27]

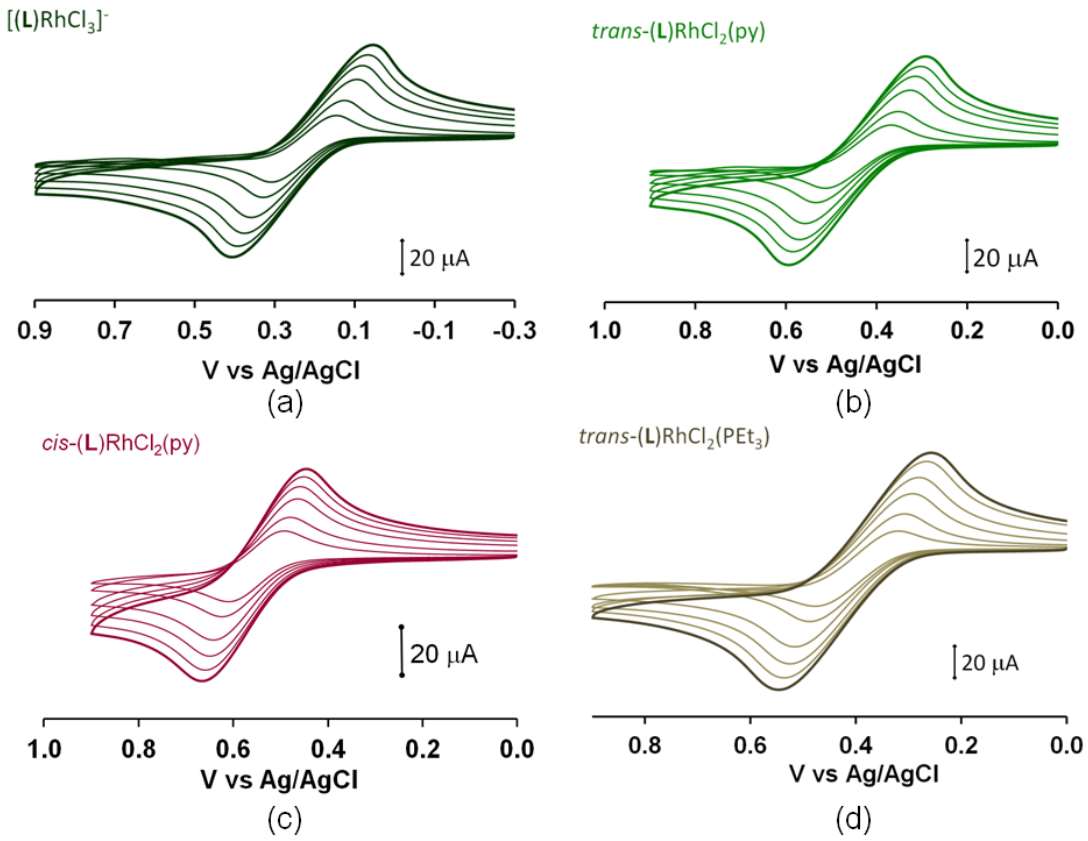

Figure 5.26 Voltammograms for various (pincer)rhodium(III) complexes in CH_2Cl_2 at scan rates of 50, 100, 200, 300, 400, 500 (outer) mVs^{-1}

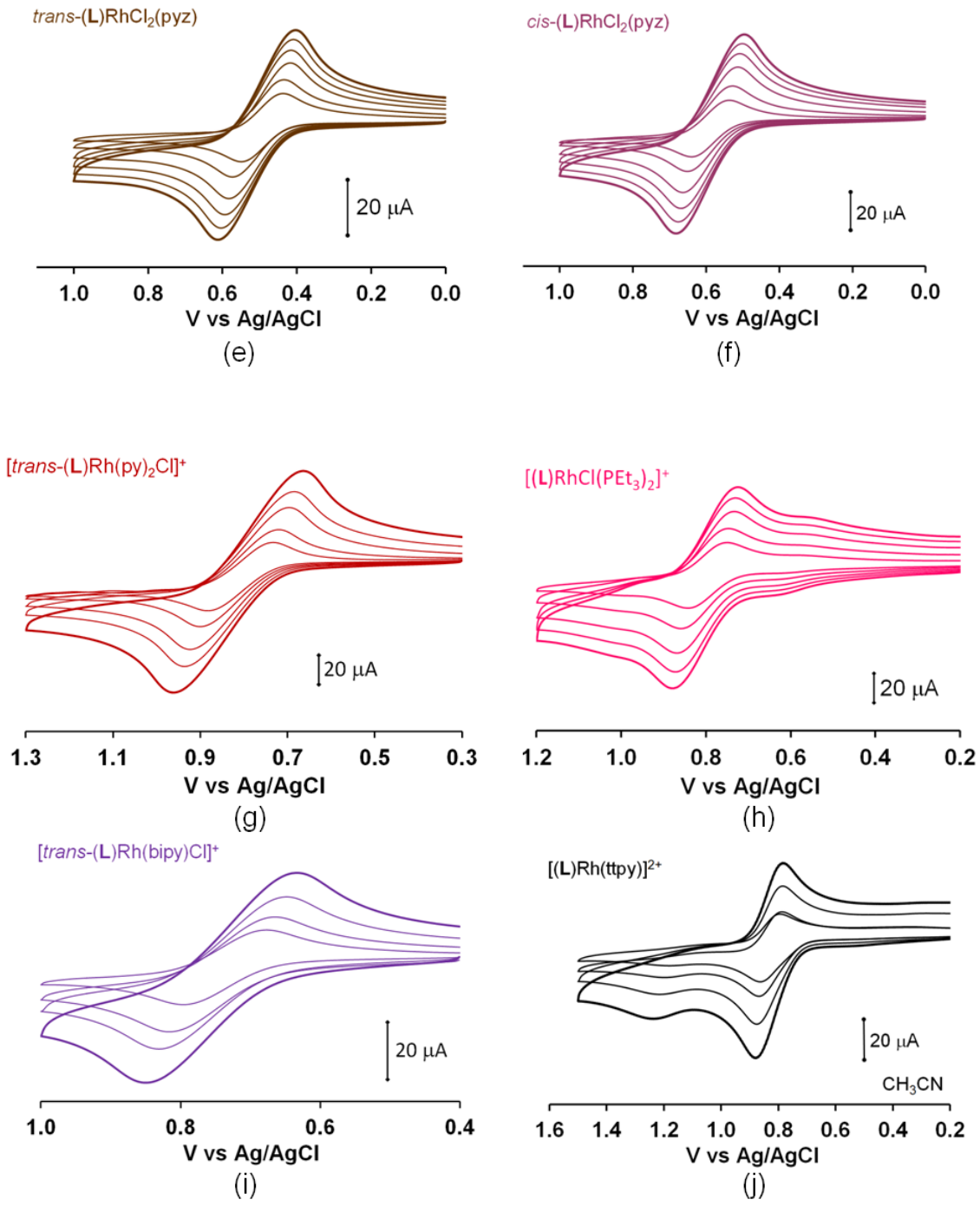

Figure 5.26, Cont'd. Voltammograms for various (pincer)rhodium(III) complexes in CH_2Cl_2 at scan rates of 50, 100, 200, 300, 400, 500 (outer) mVs^{-1}. For (i) scan rates of 50, 100, 200, and 400 (outer) mVs^{-1}. For ttpy, the voltammograms in (j) are in CH_3CN at scan rates of 50, 100, 200, and 400 (outer) mVs^{-1}.

CHAPTER 6

PREPARATION, PROPERTIES, AND REACTIVITY OF CARBONYLRHODIUM(I) COMPLEXES OF DI(2-PYRAZOLYLARYL) AMIDO- PINCER LIGANDS

6.1. Introduction

Since the seminal report by Moulton and Shaw ofrhodium(I) and other metal complexes of uni-negative, meridonially-coordinating 'pincer' ligandswith PCP- donors in 1976,[1]the chemistry of rhodium(I) pincer complexes has remained affixed among the more popular contemporary investigations given the historical importance of low-valent rhodium complexes in the Monsanto process for the production of acetic acid from methanol.Part of the appeal of pincer complexes arises from their relatively high stability and unusual chemistry that can be promoted by judicious ligand designs.[2]Early reports by van Koten's group concerning metal complexes of NCN- pincer variants demonstrated that exciting new chemistry was attainable by varying donor groups.[3] In particular, van Koten's observations regarding rhodium NCN- pincer complexes[4]presaged numerous contemporary discoveries that other rhodium pincer complexes are competent for the activation of normally robust C-X (X=halide), C-H, N-C, N-H, and H-H bonds.[5]Notable rhodium pincer complexes that show unusual chemistry typically have an anchoring amido nitrogen with two flanking phosphorus donors such as in (PNP)Rh derivatives by the groups of Liang,[6] Ozerov,[7] Mayer and Kaska,[8]Milstein,[9] or Caulton.[10]Other fascinating chemistry is found by replacing one or more of the donor groups with

different atoms, as in (PCP)Rh derivatives,[11,12] the (PSiP)Rh derivatives of Turculet,[13] or the various (SPS)Rh derivatives of the Cauzzi[14] and LeFloch groups.[15] More exotic donors are found in the (NBN)Rh derivatives of Nakamura,[16] the (CNC)Rh derivative with flanked olefin donors described by Grützmacher[17]or that with N-heterocyclic carbene donors as in Kunz's 1,8-bis(imidazolin-2-yliden-1-yl)carbazolide (bimca) derivatives.[18] There has been growing interest in the development of late transition metal complexes of pincer ligands that possess an NNN donor set (Chart 1) since nitrogen donors tend to be more resistant to oxidative degradation versus phosphine donors and because it is thought that the dichotomy between hard Lewis donors and soft rhodium(I) center could lead to enhanced or unexpected reaction chemistry relative to derivatives with soft Lewis donors. Although many examples of metal complexes of NNN pincer ligands are known,[19-30]studies of their low-valent rhodium chemistry are relatively limited. For instance, of the twelve representative classes of ligand **A**-**L** in Chart 1, low-valent rhodium chemistry has only been described for five (**A**,[19]**B**,[20]**C**,[21]**D**,[22] and **F**[24]). Of these, the oxidative addition reactionsof (**C**)Rh(CO) and (**F**)Rh(CO) have been addressed where it was found that the electron-rich character of the NNN-ligand substantially increased the rate of iodomethane oxidative addition relative to the traditional Monsanto catalyst $[Rh(CO)_2(I)_2]^-$.

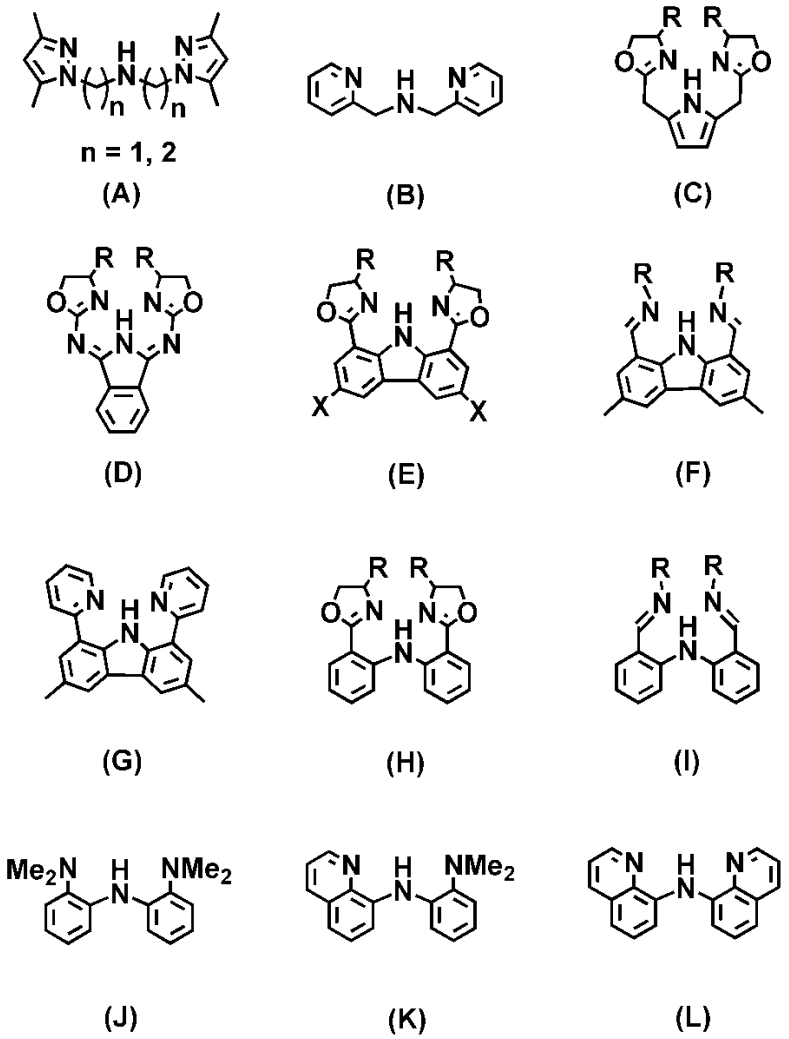

Chart 6.1. Selected examples of NNN-pincer ligands in the literature

Unfortunately, the effect of different R groups on the rates of oxidative addition of iodomethane or of other alkyl halides or the implementation of complexes such as (**F**)Rh(CO) in catalytic reactions have not yet been reported.

We recently reported a set of three new di(2-(3R-pyrazolyl-1-yl)-4-tolyl)amine NNN-pincer ligands, H(^{R}MeMe) (R = H, Me, i-Pr),whose notation is defined in Fig. 6.1.[31] In those reports we documented some unusual ligand-centered chemistry of

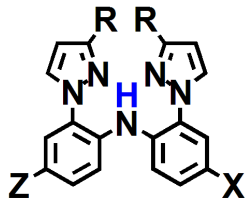

H(^{R}ZX)

Figure.6.1. General representation and notation of the NNN-pincer ligands used in this work. When R = H, the superscript R is omitted.

fac-tricarbonylrhenium(I) complexes that arose from the unconventional coordination geometry of the pincer ligand enforced by both the *fac*-Re(CO)$_3$ moiety and the steric bulk of the R groups at the 3-position of the pyrazolyl (Fig. 6.1). We were interested to begin investigation of rhodium(I) derivatives of these new pincer ligands because metal-centered chemistry was anticipated for potential square planar complexes. Specifically, we wanted to get a sense of how the reactivity of the new complexes toward iodoalkanes would compare to other rhodium(I) pincers and of the extent that the reactivity could be attenuated by making changes to the groups decorating the new ligand scaffold. In this report, we describe an important advance in ligand syntheses that provides a simple,convergent means to prepare (2-pyrazolyl)aryl-containing ligands that have different pincer 'arms'. Also, we provide a full account of the preparation and properties of six carbonylrhodium(I) complexes; (MeMe)Rh(CO), **1**, (^{Me}MeMe)Rh(CO), **2**, (^{iPr}MeMe)Rh(CO), **3**, (MeH)Rh(CO), **4**, (MeCF$_3$)Rh(CO), **5**, and (CF$_3$CF$_3$)Rh(CO), **6**. The oxidative addition reactions involving**1**-**6** and iodoalkanes and, in one case iodine, were probed to delineate the effects of ligand sterics and electronics on the kinetics and thermodynamic outcomes of OA reactions. These results provide a benchmark for our future work with related pincer variants.

6.2. Experimental

6.2.1. Materials.

Pyrazole, CuI, N,N'-dimethylethylenediamine (DMED), anhydrous M_2CO_3 powders (M = K, Cs), 1-bromo-2-fluoro-4-trifluoromethylbenzene, 1-bromo-2-fluorobenzene, NaH, and Li(*n*-Bu) (1.6*M* in hexanes) were purchased from commercial sources and used without further purification while $[(CO)_2Rh(\mu\text{-}Cl)]_2$,[32] $Rh(CO)_2(acac)$,[33] H(MeMe),[31b] H(^{Me}MeMe),[31a] and H(^{iPr}MeMe),[31a] H(pzAn^X) (pzAn^X = 2-(pyrazolyl)-*p*-X-aniline;X = CF_3, CH_3)[34] were prepared by literature methods. Commercial methyl- and ethyl iodide were dried over $CaCl_2$ and distilled under vacuum before use. Solvents used in the preparations were dried by conventional methods and were distilled under nitrogen prior to use.

6.2.2. Physical measurements.

Midwest MicroLab, LLC, Indianapolis, Indiana 45250, performed all elemental analyses. ^1H, ^{13}C and ^{19}F NMR spectra were recorded on a Varian 400 MHz spectrometer. Chemical shifts were referenced to solvent resonances at δ_H 7.26 and δ_C 77.23 for $CDCl_3$, δ_H5.32 and δ_C53.84 for CD_2Cl_2, δ_H 2.05 andδ_C 29.92 for acetone-d_6. Infrared spectra were recorded on samples as either KBr pellets or as acetone solutions with cells having KBr windows using a Nicolet Magna-IR 560 spectrometer.Melting point determinations were made on samples contained in glass capillaries using an Electrothermal 9100 apparatus and are uncorrected. Mass spectrometric measurements recorded in ESI(+) mode were obtained on a Micromass Q-TOF spectrometer whereas those performed by using direct-probe analyses were made on a VG 70S instrument. For

the ESI(+) experiments, formic acid (approximately 0.1 % v/v) was added to the mobile phase (CH_3CN).

6.2.3. Synthesis of 2-Bromoarylpyrazole Precursors.

6.2.3.1. Synthesis of 1-(2-bromophenyl)-1H-pyrazole, BrPhpz.

A solution of 3.53 g (0.0518 mol) pyrazole in 20 mL of dry DMF was slowly transferred to a suspension of 1.24 g (0.0518 mol) NaH in 30 mL of dry DMF to control the rate of hydrogen evolution. After complete addition the solution was stirred for 15 min and then 7.56 g (0.0432 mol) of 1-bromo-2-fluorobenzene in 10 mL of dry DMF was added by cannula transfer and the mixture was heated at reflux for 30 min. After cooling to room temperature 200 mL of water was added and the mixture was extracted with three 50 mL portions of CH_2Cl_2. The combined organic layers were then washed with five 50 mL portions water and the organic phase was dried over $MgSO_4$ and was filtered. The solvent was removed by vacuum distillation to leave an oily residue. The oily residue was subjected to column chromatography on silica gel where the desired product (R_f = 0.6 on SiO_2 plate) was isolated as an colorless oil (8.34 g, 86 %) using 6:1 hexane: ethyl acetate as an eluent. ^{1}HNMR ($CDCl_3$): δ_H7.82 (dd, J = 2.4, 0.6 Hz, 1H), 7.76 (dd, J = 1.8, 0.4 Hz, 1H), 7.71 (m, 1H), 7.52 (m, 1H), 7.42 (m, 1H), 7.28 (m, 1H), 6.47 (dd, J = 2.4, 1.8 Hz, 1H) ppm. ^{13}CNMR ($CDCl_3$): δ_C141.0, 140.0, 133.9, 131.4, 129.7, 128.5, 128.4, 118.7, 106.6 ppm.

6.2.3.2. Synthesis of 2-bromo-5-trifluoromethylphenyl-1H-pyrazole,Br-CF_3Phpz.

Similar to above, the reaction between 4.20 g (0.0617 mol) pyrazole, 1.63 g (0.0679 mol) NaH and 15.0 g (0.0618 mol) of 1-bromo-2-fluoro-4-trifluoromethylbenzene gave an oily residue after work-up that was subjected to column chromatography on silica gel. The desired product (R_f = 0.75 on SiO_2 plate) was separated from a more polar, but unidentified, impurity (R_f = 0.5 on SiO_2 plate) using 6:1 hexane:ethyl acetate as an eluent. Removal of solvents under vacuum afforded 10.16 g (57 % based on pyrazole) of Br-CF_3Phpz as a colorless oil. ^{1}H NMR: ($CDCl_3$): δ_H 7.90 (d, *J* = 2 Hz, 1H, H_5pz), 7.83(m, 2H, Ar), 7.78 (d, *J* = 2 Hz, 1H, H_3pz), 7.52 (part of *AB*, J_{app} = 8, 2 Hz, 1H, Ar), 6.51 (t, *J* = 2 Hz, 1H, H_4pz) ppm. ^{13}C NMR ($CDCl_3$): δ_C141.7, 140.4, 134.8, 131.4, 131.1 (q, $^2J_{C-F}$= 33 Hz), 126.1 (q, $^3J_{C-F}$= 3 Hz), 125.4 (q, $^3J_{C-F}$= 3 Hz), 123.4 (q, $^1J_{C-F}$= 272 Hz), 122.1 (q, $^4J_{C-F}$ = 2 Hz), 107.4 (C_4pz) ppm. ^{19}F NMR ($CDCl_3$): δ_F -62.8 ppm.

6.2.4. Synthesis of New Pincer Ligands.

6.2.4.1. Synthesis of N-(4-methyl-2-(1H-pyrazol-1-yl)phenyl)-2-(1H-pyrazol-1-yl)benzenamine, H(MeH).

A Schlenk flask was charged with 2.238 g (0.0129 mol) H(pzAn^{Me}), 3.455 g (0.0155 mol, 1.2 eq) BrPhpz, 5.047 g (0.0155 mol, 1.2 eq) Cs_2CO_3 and was deoxygenated by three evacuation and nitrogen back-fill cycles. Then 30 mL of dioxane and 0.492 g (2.581 mmol, 20 mo l%) CuI were added under nitrogen blanket. The reaction mixture was heated at reflux for 15 h under nitrogen. After cooling to room temperature, dioxane was removed by vacuum distillation. The solid product mixture was extracted with four 20 mL portions of Et_2O and then Et_2O was removed by vacuum distillation to afford a residue that was further purified by column chromatography on silica gel. After elution

with 6:1 hexane: ethyl acetate (R_f = 0.4) and removal of solvents the desired product was obtained as a white solid. Yield: 2.957g , 73 %. M.p.: 63-65 ^{0}C Anal. Calcd.for $C_{19}H_{17}N_5$: C, 72.37; H, 5.43; N, 22.21.Found: C,72.21; H, 5.64; N, 22.11. ^{1}H NMR (acetone-d_6): δ_H9.11 (s), 7.92 (m, 2 H), 7.76 (dd, J = 2.0, 1.7 Hz, 1H), 7.72 (d, J = 2 Hz, 1H), 7.37 (m, 3 H), 7.26 (m, 1 H), 7.33 (m, 1 H), 7.12 (dd, J = 8.3, 1.3 Hz, 1 H), 6.94 (m, 1 H), 6.49 (t, J = 2.1 Hz, 1 H), 6.46 (t, J = 2.1 Hz, 1 H), 2.32(s, 3 H) ppm.^{13} C NMR(acetone-d_6): δ_c141.13, 141.08, 140.6, 138.5, 134.7, 131.94, 131.85, 130.9, 130.7, 129.4, 129.0, 126.4, 125.9, 121.0, 120.5, 118.3, 107.32, 107.27, 20.5 ppm.

6.2.4.2. Synthesis of N-(4-(trifluoromethyl)-2-(1H-pyrazol-1-yl)phenyl)-4-methyl-2-(1H-pyrazol-1-yl)benzenamine,H(MeCF_3).

A Schlenk flask was charged with 0.784 g (4.53 mmol) H(pzAn^{Me}), 1.581 g (5.43 mmol, 1.2 eq) Br-CF_3Phpz, 1.770 g (5.43 mmol, 1.2 eq) Cs_2CO_3 and was deoxygenated by three evacuation and nitrogen back-fill cycles. Then, 15 mL of dry dioxane and 0.173 g (0.905 mmol, 20 mol %) CuI were added under a nitrogen blanket. The reaction mixture was heated at reflux for 15 hunder nitrogen. After cooling to room temperature, dioxane is removed by vacuum distillation. The solid product mixture was extracted with four 20 mL portions of Et_2O (until filtrate was nearly colorless) and then Et_2O was removed by vacuum distillation to afford a residue that was further purified by column chromatography on silica gel. After elution with 6:1 hexanes:ethyl acetate (R_f = 0.38) and removal of solvents by vacuum distillation, the desired product was obtained as a beige solid. Recrystallization by cooling hot supersaturated hexane solutions to room temperature over the course of several hours afforded 1.432 g (83 %) of H(MeCF_3)as colorless needles. M.p.:79 - 82°C.Anal.Calcd.for $C_{20}H_{16}F_3N_5$: C, 62.66; H, 4.21; N,

18.27. Found: C, 62.69; H, 4.29; N, 18.41. ^{1}H NMR ($CDCl_3$): δ_H9.03 (br s, 1H, NH), 7.78 (dd, 1H, *J* = 2, 1 Hz, H_5pz-ArCF_3), 7.76 (dd, 1H, *J* = 2, 1 Hz, H_3pz-ArCF_3), 7.70 (dd, *J* = 2, 1 Hz, 1H, H_5pz-tolyl), 7.67 (dd, 1H, *J* = 2, 1 Hz, H_3pz-tolyl), 7.50 (d, *J* = 2 Hz, 1H, H-ArCF_3), 7.40 (part of *AB*, J_{app} = 8 Hz, 1H, ArCF_3), 7.38 (part of *AB*, J_{app} = 8, 1 Hz, 1H, ArCF_3), 7.31 (part of *AB*, J_{app} = 8 Hz, 1H, tolyl), 7.25 (d, *J* = 1 Hz, 1H, tolyl), 7.13 (part of *AB*, J_{app} = 8, 2 Hz, 1H, ArCF_3), 6.51 (t, *J* = 2 Hz, 1H, H_4pz-ArCF_3), 6.40 (t, *J* = 2 Hz, 1H, H_4pz-tolyl), 2.36 (s, 3H, CH_3) ppm. ^{13}C NMR ($CDCl_3$): δ_C141.4, 141.2, 140.7, 133.7, 132.4, 131.9, 130.2, 129.8, 128.9, 127.9, 125.9, 125.5 (q, $^{3}J_{C\text{-}F}$= 4 Hz), 124.2 (q, $^{1}J_{C\text{-}F}$= 271 Hz, CF_3), 122.3 (q, $^{3}J_{C\text{-}F}$= 4 Hz), 122.2, 120.9 (q, $^{2}J_{C\text{-}F}$= 33 Hz), 115.4, 107.3 (C_4pz-ArCF_3), 106.9 (C_4pz-tolyl), 20.8 ppm. ^{19}F NMR ($CDCl_3$): δ_F-61.4 ppm.

6.2.4.3. Synthesis ofbis(4-(trifluoromethyl)-2-(1H-pyrazol-1-yl)phenyl)amine, H(CF_3CF_3).

Similar to above,a deoxygenated mixture of 0.652 g (2.87 mmol) H(pzAn^{CF3}), 1.002 g (3.44 mmol, 1.2 eq) Br-CF_3Phpz, 1.122 g (3.44mmol, 1.2 eq) Cs_2CO_3, and 0.110 g (0.578 mmol, 20 mol %) CuI in 15 mL of dioxanewas heated at reflux for 15 hunder nitrogen. After cooling to room temperature, dioxane was removed by vacuum distillation. The solid product mixture was extracted with four 20 mL portions of Et_2O (or until filtrate was nearly colorless) and then Et_2O was removed by vacuum distillation to afford a residue that was further purified by column chromatography on silica gel. Elution of the column with 6:1 hexanes:ethyl acetate (R_f = 0.47) and removal of solvents by vacuum distillation gave the desired product as a tan solid. After recrystallization by cooling hot supersaturated hexane solutions to room temperature over the course of several hours afforded 1.125 g (90 %) of H(CF_3CF_3) as white needles. M.p.: 89 - 91°C.

Anal.Calcd.for $C_{20}H_{13}F_6N_5$: C, 54.94; H, 3.10; N, 16.01. Found: C, 54.94; H, 3.10; N, 15.96. ^{1}H NMR ($CDCl_3$): δ_H 9.76 (br s, 1H, NH), 7.77 (d, J = 3 Hz, 2H, H_5pz), 7.76 (d, J = 2 Hz, 2H, H_3pz), 7.60 (s, 2H, Ar), 7.58 (part of *AB*, J_{app} = 8 Hz, 2H, Ar), 7.50 (part of *AB*, J_{app} = 8 Hz, 2H, Ar), 6.51 (dd, J = 3, 2 Hz, 2H, H_4pz) ppm. ^{13}C NMR ($CDCl_3$): δ_C 141.4, 139.0, 138.9, 130.1, 125.4 (q, $^3J_{C-F}$= 4 Hz), 123.8 (q, $^1J_{C-F}$= 271 Hz, CF_3), 123.6 (q, $^2J_{C-F}$= 34 Hz), 122.6 (q, $^3J_{C-F}$= 4 Hz), 118.5, 107.6 (C_4pz) ppm. ^{19}F NMR ($CDCl_3$): δ_F -61.9 ppm.

6.2.5. Synthesis of Carbonylhodium(I) Complexes.

6.2.5.1. Synthesis of(MeMe)Rh(CO), **1**.

*Method A:*A mixture of 0.2079 g (0.632 mmol) H(MeMe) and 0.1629 g (0.632 mmol) $Rh(CO)_2$(acac) in 15 mL of dry, deoxygenated acetone was heated at reflux for 30 hoursunder nitrogen. After cooling to room temperature, the volatile components were removedunder vacuum to give 0.2398 g (83 %) of pure **1** as a yellow,crystallinesolid. *Method B:* A 2.6 mmol portion of Li(n-Bu) (1.6 mL of a 1.6 *M*solution in hexanes) was added to a solution of 0.847 g (2.57 mmol) of H(MeMe) in 15 mL THF at -78^{o}C. The resultant yellow solution was stirred at -78^{o}C for 30 minutes and a solution of 0.500 g (1.29 mmol) $[(CO)_2Rh(\mu\text{-}Cl)]_2$ in 15 mL THF was subsequently added via cannula transfer. After the resulting red-brown solution had been stirred at -78^{o}C for an additional 30 min, the cold bath was removed and stirring was continued an additional 14 h. Solvent was then removed under vacuum to leave a brown solid. The brown solid was washed with hot pentane to remove any H(MeMe) and the filtrate was reserved (vide infra). The solid was then extracted with dry toluene and the solvent was removed under

vacuum to give 0.373 g (32%) of **1** as a yellow powder. The original pentane extract contained an additional fraction 0.140 g (12%) of **1** which slowly crystallized on standing. The combined yield of **1** from the toluene and pentane extracts was 0.513 g (44 %).M.p.: 280-283 ^{o}C(dec.) Anal. Calcd.for$C_{21}H_{18}N_5ORh$: C, 54.91; H, 3.96; N, 15.25. Found: C, 55.26; H, 4.02; N, 15.03.^{1}HNMR (acetone-d_6): δ_H 8.45 (d, *J* = 2 Hz, 2H, H_3pz), 7.83 (d, *J* = 2 Hz, 2H, H_5pz), 7.30 (s, 2H, Ar), 6.95 (part of *AB*, 2H, Ar), 6.88 (part of *AB*, 2H, Ar), 6.67 (t, *J* = 2, 2H, H_4pz), 2.26 (s, 6H, $ArCH_3$). ^{13}C NMR (acetone-d_5): δ_C 193.1 (d, $^{1}J_{Rh\text{-}C}$= 72 Hz, CO), 146.6 (d,$^{3}J_{Rh\text{-}C}$ = 3 Hz), 143.5, 130.5, 130.1 (d,$^{3}J_{Rh\text{-}C}$ = 1Hz), 129.7, 127.5, 123.6, 123.4, 108.7 (d,$^{3}J_{Rh\text{-}C}$ = 2Hz, C_4pz), 20.4. IR (ν_{CO}, cm^{-1}): 1952 (KBr pellet); 1955 (acetone). LRMS (Direct Probe, *m*/*z*) (int.) [assign.]: 459 (52) $[LRh(CO)]^{\cdot+}$,431 (100) $[LRh]^{\cdot+}$, 329 (40) $[HL]^{+}$. X-ray quality crystals were obtained by layering a benzene solution with pentane and allowing solvents to slowly diffuse over 12 h. Alternatively, slow evaporation of saturated pentane solution of **1** was a successful approach.

6.2.5.2. Synthesis of(^{Me}MeMe)Rh(CO),**2**.

Method A: Heating mixture of 0.179 g (0.499 mmol) H(^{Me}MeMe) and 0.129 g (0.499 mmol) $Rh(CO)_2$(acac) in 15 mL acetone for 30 h, then removing volatiles under vacuum gave 0.243 g (87 %) of pure **2** as a yellow crystalline solid. *Method B*: In a manner similar to that described for **1**, 0.619 g (1.70 mmol) H(^{Me}MeMe), 1.76 mmol Li^{n}Bu (1.10 mL, 1.6 *M* in hexanes) and 0.337 g (1.73 mmol) $[(CO)_2Rh(\mu\text{-}Cl)]_2$ in 30 mL THF gave 0.171 g (20 %) of **2** as a yellow powder after work-up.M.p.: 260-262^{o}C (dec.)Anal. Calcd. (obsd.) for $C_{23}H_{22}N_5ORh$: C, 56.68; H, 4.55; N, 14.37. Found: C, 56.52; H, 4.56;

N, 14.15. ^{1}H NMR (acetone-d_6): δ_H8.23 (d, J = 2 Hz, 2H, H_5pz), 7.29 (s, 2H, Ar), 6.82 (both parts of *AB*, 4H, Ar), 6.53 (d, J = 2, 2H, H_4pz), 2.48 (s, 6H, pzCH_3), 2.26 (s, 6H, ArCH_3) ppm. ^{13}C NMR (acetone-d_5): δ_C193.6 (d, $^{1}J_{Rh\text{-}C}$= 70 Hz, Rh-CO), 153.5 (d, $^{2}J_{Rh\text{-}C}$ = 2 Hz), 142.7, 132.2, 131.1 (d, $^{3}J_{Rh\text{-}C}$ = 1 Hz), 129.4, 127.0, 122.8, 122.3, 109.8 (d, $^{3}J_{Rh\text{-}C}$ = 2 Hz, C_4pz), 20.5, 17.2 ppm. IR (ν_{CO}, cm^{-1}): 1952 (KBr pellet); 1951 (acetone). LRMS (Direct Probe, *m*/*z*) (int.) [assign.]: 487 (28) $[LRh(CO)]^{\cdot+}$,459 (100) $[LRh]^{\cdot+}$, 444 (16) $[LRh - CH_3]^{\cdot+}$, 357 (8) $[HL]^{+}$.

6.2.5.3. Synthesisof (^{iPr}MeMe)Rh(CO),**3**.

Under nitrogen, a 0.75 mmol sample of Li(*n*-Bu) (0.47 mL of 1.6 *M* solution in hexane) was added dropwise by syringe to a solution of 0.31 g (0.75 mmol) H(^{iPr}MeMe) in 15 mL toluene at -78^{o}C. After stirring at -78^{o}C for 10 min, a solution of 0.146 g (0.375 mmol) $[(CO)_2Rh(\mu\text{-}Cl)]_2$ in 15 mL toluene was added dropwise via cannula transfer. After complete addition, the mixture was stirred at -78^{o}C for 4 h then the cold bath was removed. After the mixture was stirred an additional 15 h, the volatile components were removed by vacuum distillation to leave a brown solid. The solid was extracted using five 20 mL portions of pentane and filtering from the brown insoluble solid (until the extracts were colorless). The desired yellow product slowly crystallized from the pentane extracts on standing. Several crops of pure crystalline **3** were collected after four cycles of decanting the mother liquor, concentrating the solution by rotary evaporation to half volume, and crystallization. The crystals were dried under vacuum to give a total of 0.152 g (37% based on H(^{iPr}MeMe)). M.p.: 227-230 ^{o}C (dec.) Anal. Calcd.for $C_{27}H_{30}N_5ORh$: C, 59.67; H, 5.56; N, 12.89. Found: C, 59.80; H, 5.71; N, 12.85.^{1}HNMR

(acetone-d_6): δ_H8.28(d, *J* = 3 Hz, 2H, H_5pz), 7.29 (s, 2H, Ar), 6.83 (part of *AB*, 2H, Ar), 6.79 (part of *AB*, 2H, Ar), 6.63 (d, *J* = 3 Hz, 2H, H_4pz), 3.56 (sept, *J* = 7 Hz, 2H, $CHMe_2$), 2.25 (s, 6H, $ArCH_3$). 1.32 (d, *J* = 7 Hz, 6H, i-$PrCH_3$). 1.30 (d, *J* = 7 Hz, 6H,i-$PrCH_3$) ppm. ^{13}C NMR (acetone-d_5): δ_C193.5 (d, $^1J_{Rh\text{-}C}$= 70 Hz, Rh-CO), 163.8 (d,$^2J_{Rh\text{-}C}$ = 2 Hz), 142.7, 132.8, 131.2, 129.4, 126.9, 122.8, 121.8, 106.1 (d,$^3J_{Rh\text{-}C}$ = 2Hz, C_4pz), 23.8, 23.3, 20.5 ppm.IR (ν_{CO}, cm^{-1}): 1948 (KBr pellet); 1948 (acetone). LRMS (Direct Probe, *m*/*z*) (int.) [assign.]: 543 (31) $[LRh(CO)]^{\cdot+}$,515 (100) $[LRh]^{\cdot+}$, 413 (12) $[HL]^+$.*Attempted Preparations by Method A*: Reactions between H(^{iPr}MeMe) and $Rh(CO)_2$(acac) were only 45-50% complete after 3 days according NMR-scale reactions. Moreover, the similar solubilities of the rhodium-containing reagent and product hindered separation and only allowed isolation of trace quantities of pure **3** by this route even from half-gram scales of reagents.

6.2.5.4. Synthesisof (MeH)Rh(CO),**4**.

Heating mixture of 0.236 g (0.749 mmol) H(MeH) and 0.193 g (0.749 mmol) $Rh(CO)_2$(acac) in 20 mL acetone for 60 h, then removing volatiles under vacuum gave 0.282 g (84 %) of pure (MeH)Rh(CO) as a yellow crystalline solid. M.p.: 220-225^{o}C (dec.). Anal.Calcd.for $C_{20}H_{16}N_5ORh$: C, 53.95; H, 3.62; N, 15.73. Found: C, 54.05; H, 3.71;N, ;15.63. ^{1}H NMR (acetone-d_6): δ_H8.47 (d, J = 2.8 Hz, 1 H), 8.45 (d, J = 2.8 Hz, 1H), 7.84 (m, 2 H), 7.44 (m, 2 H), 7.32 (m, 1 H), 7.03 (m, 2 H), 6.97 (m, 1 H), 6.91 (m, 1 H), 6.76 - 6.67 (m, 3 H), 2.27 (s, 3 H). ^{13} C NMR (acetone-d_6): δ_C192.56 (d, $J_{Rh\text{-}CO}$ = 71 Hz), 146.72 (d, J = 2.7 Hz), 146.60 (d, J = 2.8 Hz), 146.21, 143.15, 130.62, 130.61, 130.44 (d, J = 1.2 Hz), 130.41 (d, J = 1.2 Hz), 129.82, 128,84, 128.18, 123.76, 123.72,

123.53, 123.15, 117.88, 108.86 (d, J = 2.2 Hz), 108.81 (d, J = 2.2 Hz), 20.43. IR (ν_{CO} ,cm^{-1}) : 1954 (KBr pellet). 1956 (acetone).

6.2.5.5. Synthesisof ($MeCF_3$)Rh(CO),**5**.

*Method A:*Heating mixture of 0.133 g (0.347 mmol) H($MeCF_3$) and 0.0896 g (0.347 mmol) $Rh(CO)_2(acac)$ in 15 mL acetone for 72 h, then removing volatiles under vacuum left a brown solid. The pentane soluble product was extracted from the brown solid by extractions with three 8 mL portions of pentane. Pentane was removed from the collected filtrates to give 0.162 g (91 %) of pure **5** as a yellow solid.*Method B*: In a manner similar to complex **1**, a mixture of 1.098 g (2.87 mmol) H($MeCF_3$), 2.9 mmol (1.8 mL of a 1.6 *M* solution in hexane) Li(*n*-Bu), and 0.557 g (1.43 mmol) of $[(CO)_2Rh(\mu\text{-}Cl)]_2$ in 15 mL THF gave 0.618 g (42 %) of **5** as a yellow powder after organic work-up (extraction and crystallization). M.p.: 210-214 ^oC (dec.).Anal.Calcd.for $C_{21}H_{15}N_5F_3ORh$: C, 49.13; H, 2.95; N, 13.65. Found: C, 49.45; H, 3.04; N, 13.67.^{1}HNMR (acetone-d_6):δ_H8.64(d, *J* = 2 Hz, 1H, H_3pz-$ArCF_3$), 8.52(d, *J* = 2 Hz, 1H, H_3pz-tolyl), 7.89 (m, 1H, H_5pz-$ArCF_3$), 7.86 (m, 1H, H_5pz-tolyl), 7.76 (m, 1H, H_3-$ArCF_3$), 7.40(m, 1H, H_3-tolyl), 7.28 (part of *AB*, 1H, $ArCF_3$), 7.10 (part of *AB*, 1H, $ArCF_3$), 7.00 (*AB* m, 2H, tolyl), 6.74 (dd, *J* = 2, 1Hz, 1 H, H_4pz-$ArCF_3$), 6.70 (dd, *J* = 2, 1Hz, 1H, H_4pz-tolyl), 2.30 (s, 3H, $ArCH_3$) ppm.^{13}C NMR (acetone-d_6): δ_C192.4 (d, $^1J_{Rh\text{-}C}$= 72 Hz, CO), 150.0, 147.2 (d,$^3J_{Rh\text{-}C}$ = 3Hz), 147.0 (d,$^3J_{Rh\text{-}C}$ = 3Hz), 141.8, 131.3, 131.2, 131.1, 131.0, 130.4, 130.1, 129.5 (d,$^3J_{Rh\text{-}C}$ = 1Hz), 125.8 (q, $^1J_{C\text{-}F}$= 272 Hz, CF_3), 125.4 (q, $^3J_{C\text{-}F}$= 4 Hz), 124.5, 124.0, 122.3, 121.0 (q, $^3J_{C\text{-}F}$= 4 Hz), 117.5 (q, $^2J_{C\text{-}F}$= 33 Hz), 109.3 (d,$^3J_{Rh\text{-}C}$ = 2Hz, C_4pz), 109.0 (d,$^3J_{Rh\text{-}C}$ = 2 Hz, C_4pz), 20.5 ppm. ^{19}F NMR (acetone-

d_6): δ_F-61.21 ppm.IR (ν_{CO}, cm^{-1}): 1958 (KBr pellet); 1962 (acetone). LRMS (Direct Probe, *m*/*z*) (int.) [assign.]: 513 (11) $[LRh(CO)]^{\cdot+}$,485 (26) $[LRh]^{\cdot+}$, 383 (100) $[HL]^+$.

6.2.5.6. Synthesis of $(CF_3CF_3)Rh(CO)$,**6**.

Method A: A mixture of 0.119 g (0.272 mmol) $H(CF_3CF_3)$ and 0.0701 g (0.272 mmol) $Rh(CO)_2(acac)$ in 15 mLacetone was heated at reflux under nitrogen for 20 hoursto give 0.145 g (94 %) of pure **6**as a yellow crystalline solid after removing solvent and H(acac) by vacuum distillation. *Method B:* In a manner similar to that for compound **1**, 0.908 g (2.08 mmol) $H(CF_3CF_3)$, 2.1 mmol Li^nBu(1.3 mL,1.6 *M* in hexanes) and 0.404 g (1.04 mmol) $[(CO)_2Rh(\mu\text{-}Cl)]_2$in 30 mL THF gave 0.613 g (52 %) of **6** as a yellow powder after work-up. M.p.: 250-254 ^oC(dec.) Anal. Calcd.for $C_{21}H_{12}N_5F_6ORh$: C, 44.47; H, 2.14; N, 12.35. Found: C, 44.97; H, 2.32; N, 11.95. ^{1}HNMR (acetone-d_6):δ_H 8.71 (d, *J* = 2 Hz, 2H, H_3pz), 7.93 (m, 2H, Ar-H), 7.87 (d, *J* = 2 Hz, 2H, H_5pz), 7.40 (part of *AB*, 1H, Ar-H), 7.26 (part of *AB*, 1H, Ar-H), 7.24 (s, 1H, Ar-H), 6.77 (t, *J* = 2, 2H, H_4pz) ppm.^{13}C NMR (acetone-d_6): δ_C 192.0 (d, $^1J_{Rh\text{-}C}$= 72 Hz, CO), 148.7, 147.6 (d,$^3J_{Rh\text{-}C}$ = 3 Hz), 131.9, 130.7, 125.8 (q, $^3J_{CF}$= 3 Hz), 125.2 (q, $^1J_{C\text{-}F}$= 272 Hz, CF_3), 123.9, 121.4 (q, $^3J_{C\text{-}F}$= 4 Hz), 120.3 (q, $^2J_{CF}$= 33 Hz), 109.5(d,$^3J_{Rh\text{-}C}$ = 2Hz, C_4pz) ppm. ^{19}F NMR (acetone-d_6): δ_F-61.64 ppm.IR (ν_{CO}, cm^{-1}): 1962 (KBr pellet); 1968 (acetone). LRMS (Direct Probe, *m*/*z*) (int.) [assign.]: 567 (38) $[LRh(CO)]^{\cdot+}$,539 (100) $[LRh]^{\cdot+}$, 437 (8) $[HL]^+$.

6.2.6. Oxidative Addition Reactions with 1-6.

6.2.6.1. Spectroscopic Experiments (Kinetics Study):General Considerations.

Typical procedure for NMR scale experiments is as follows. About 4-6 mg of rhodium(I) complex, (^{R}ZX)Rh(CO), was added to a pre-weighed NMR tube and the mass of tube and sample are recorded. Next, 0.35 mL of acetone-d_6 was added to dissolve the rhodium complex. The tube was inserted into the spectrometer was allowed to equilibrate at the desired temperature (313-323 K) for 15 min. The tube was ejected from the spectrometer and an appropriate amount (5-10 μL, ≥ 10 mol equiv) of MeI or EtI was added by syringeand rapidly returned to the heated spectrometer (representing the reference time of zero seconds). The NMR spectra were recorded after 5 min, then after 10 min intervals thereafter. While no problems were encountered in obtaining ^{13}C NMR spectra for reactions involving MeI, the spectra from reactions using EtI did not give useful signal-to-noise ratios due to extensive decomposition that occurred during overnight acquisitions (exacerbated by the long reaction times). Therefore, ^{13}C NMR data are only reported for MeI cases. Only representative data for reactions involving (MeMe)Rh(CO) are given below, those for the remaining derivatives can be found in the main text..

(MeMe)Rh(Me)(CO)(I), 7_{Me}. ^{1}HNMR (acetone-d_6): δ_H 8.55(d, J = 3 Hz, 2H, H_3pz), 8.07 (d, J = 2 Hz, 1H, H_5pz), 7.90 (d, J = 2 Hz, 1H, H_5pz), 7.43 (s, 1H, Ar), 7.33 (s, 1H, Ar), 7.16 (part of *AB*, J_{app} = 8 Hz, 1H, Ar), 7.05(part of *AB*, J_{app} = 8 Hz, 1H, Ar), 6.93 (part of *AB*, J_{app} = 8, 2 Hz, 1H, Ar), 6.86(part of *AB*, J_{app} = 8, 2 Hz, 1H, Ar), 6.77 (t, J = 3 Hz, 1H, H_4pz),6.76 (t, J = 3 Hz,1H, H_4pz), 2.28 (s, 3H, $ArCH_3$), 2.27 (s, 3H, $ArCH_3$), 1.26(d, $^{2}J_{Rh-H}$ = 2 Hz, 3H, Rh-CH_3)ppm. ^{13}C NMR (acetone-d_6): δ_C 187.4 (d, $^{1}J_{Rh-C}$= 55 Hz, Rh-CO), 149.1, 145.2 (d, $^{3}J_{Rh-C}$= 1 Hz), 145.1, 142.3, 132.8, 131.8, 131.6, 130.4, 129.6, 129.1, 128.9, 128.8, 128.6, 126.2, 125.1, 122.9, 122.7, 109.8 (C_4pz), 109.3(C_4pz),

20.6, 20.5, 9.9 ($J_{Rh\text{-}C}$ = 20 Hz, $RhCH_3$)ppm. IR (acetone, ν_{CO}, cm^{-1}): 2063. LRMS (ESI(+), *m*/*z*) (int.) [assign.]: 446 (13) $[LRh(Me)]^+$, 474 (100) $[LRh(Me)(CO)]^+$, 487 (20) $[LRh(Me)(CH_3CN)]^+$, 515 (67) $[LRh(Me)(CO)(CH_3CN)]^+$, 601 (3) $[LRh(Me)(CO)(I)]^{\cdot+}$, 927 (1) $[L_2Rh_2(Me)_2Cl]^+$, 955 (2) $[L_2Rh_2(Me)_2(CO)Cl]^+$, 983 (7) $[L_2Rh_2(Me)_2(CO)_2Cl]^+$, 1019 (2) $[L_2Rh_2(Me)_2I]^+$, 1047 (2) $[L_2Rh_2(Me)_2(CO)I]^+$, 1075 (15) $[L_2Rh_2(Me)_2(CO)_2I]^+$.

(MeMe)Rh(Et)(CO)(I), 7_{Et}. ^{1}HNMR (acetone-d_6): δ_H8.53 (m, 2H, H_3pz), 8.06 (d, *J* = 2 Hz, 1H, H_5pz), 7.97 (d, *J* = 2 Hz, 1H, H_5pz), 7.46 (s, 1H, Ar), 7.28 (s, 1H, Ar), 7.19(part of *AB*, J_{app} = 8 Hz, 1H, Ar), 7.04 (part of *AB*, J_{app} = 8 Hz, 1H, Ar), 6.95 (part of *AB*, 1H, Ar), 6.84 (part of *AB*, 1H, Ar), 6.77 (t, *J* = 2 Hz, 1H, H_4pz), 6.75 (t,*J* = 2 Hz,1H, H_4pz), 2.44 (m,1H, CH_2), 2.31 (s, 3H, Ar-CH_3),2.27 (s, 3H, ArCH_3), 2.23 (m,1H, CH_2), 0.65 (td, $^2J_{C\text{-}H}$ = 8 Hz, $^3J_{Rh\text{-}H}$ = 1 Hz, 3H, EtCH_3) ppm.IR (acetone, ν_{CO}, cm^{-1}): 2055. HRMS [ESI(+), *m*/*z*] Calcd. (Obs) for $C_{25}H_{27}N_5Rh$, $[LRh(Et)(CO)]^+$, 516.1271 (516.1276). LRMS (ESI(+), *m*/*z*) (int.) [assign.]: 432 (6) $[LRh(H)]^+$, 446 (58) $[LRh(Et)]^+$, 472 (14) $[LRh(CH_3CN)]^+$, 488 (100) $[LRh(Et)(CO)]^+$, 501 (35) $[LRh(Et)(CH_3CN)]^+$, 529 (4) $[LRh(Et)(CO)(CH_3CN)]^+$, 615 (1) $[LRh(Et)(CO)(I)]^{\cdot+}$, 927 (0.2) $[L_2Rh_2(Et)_2Cl]^+$, 955 (0.5) $[L_2Rh_2(Et)_2(CO)Cl]^+$, 1011 (5) $[L_2Rh_2(Et)_2(CO)_2Cl]^+$, 1019 (0.1) $[L_2Rh_2(Et)_2I]^+$, 1047 (0.5) $[L_2Rh_2(Et)_2(CO)I]^+$, 1103 (9) $[L_2Rh_2(Et)_2(CO)_2I]^+$.

(^{Me}MeMe)Rh(Me)(CO)(I),8_{Me}. ^{1}H NMR (acetone-d_6): δ_H 8.42(d, *J* = 3 Hz, 1H, H_5pz), 8.38 (d, *J* = 3 Hz, 1H, H_5pz), 7.29 (s, 1H, Ar), 7.18 (s, 1H, Ar), 7.04 (part of AB, J_{app} = 8 Hz, 1H, Ar), 6.96 (part of AB, J_{app} = 8 Hz, 1H, Ar), 6.90 (part of AB J_{app} = 8, 2 Hz, 1H, Ar), 6.82 (part of AB J_{app} = 8, 2 Hz, 1H, Ar), 6.61 (d, *J* = 2 Hz, 1H, H_4pz), 6.59

(d, J = 2 Hz, 1H, H_4pz), 2.92 (s, 3H, pz-CH_3), 2.59 (s, 3H, pzCH_3), 2.27 (s, 3H, ArCH_3), 2.26 (s, 3H, ArCH_3), 1.36 (d, $^2J_{Rh\text{-}H}$ = 2 Hz, 3H, Rh-CH_3) ppm. ^{13}C NMR (acetone-d_6): The solubility is too low to obtain a spectrum in reasonable acquisition times (< 2 d). IR (acetone, γ_{CO}, cm^{-1}): 2056.

(^{Me}MeMe)Rh(Et)(CO)(I), $\mathbf{8_{Et}}$. ^{1}H NMR (acetone-d_6): δ_H 8.41 (d, J = 3 Hz, 1H, H_5pz), 8.35 (d, J = 3 Hz, 1H, H_5pz), 7.33 (s, 1H, Ar), 7.14 (s, 1H, Ar), 7.06 (part of AB, J_{app} = 8 Hz, 1H, Ar), 6.98 (part of AB, J_{app} = 8 Hz, 1H, Ar), 6.92 (part of AB J_{app} = 8, 2 Hz, 1H, Ar), 6.82 (part of AB J_{app} = 8, 2 Hz, 1H, Ar), 6.61 (d, J = 3 Hz, 1H, H_4pz), 6.57 (d, J = 3 Hz, 1H, H_4pz), 2.91 (s, 3H, pzCH_3), 2.66 (s, 3H, pzCH_3), 2.56 (m, 1H, one of RhCH_2), 2.29 (s, 3H, ArCH_3), 2.26 (s, 3H, ArCH_3), 2.25 (m, 1H, one of RhCH_2), 0.68 (td, $J_{C\text{-}H}$= 7 Hz, $^3J_{Rh\text{-}H}$ = 1 Hz, 3H, Et-CH_3) ppm. IR (acetone, γ_{CO}, cm^{-1}): 2051. LRMS (ESI(+), m/z) (int.) [assign.]: 459 (4) $[LRh]^{\cdot+}$, 488 (6) $[LRh(Et)]^+$, 501 (14) $[HLRh(CH_3CN)]^+$, 516 (52) $[LRh(Et)(CO)]^+$, 521 (35) $[HLRh(HCO_3)]^+$, 529 (22) $[LRh(Et)(CH_3CN)]^+$, 557 (100) $[LRh(Et)(CO)(CH_3CN)]^+$, 562 (51) $[HLRh(HCO_3)(CH_3CN)]^+$, 586 (14) $[LRh(I)]^+$, 598 (16) $[LRh[C(O)Et](CH_3CN)_2]^+$, 627 (22) $[LRh(I)(CH_3CN)]^+$, 643 (1) $[LRh(Et)(CO)(I)]^{\cdot+}$, 668 (21) $[LRh(I)(CH_3CN)_2]^+$, 713 (2) $[LRh(I)_2]^{\cdot+}$, 742 (7) $[HLRh(I)_2(CO)]^+$, 1058 (0.3) $[L_2Rh_2(Et)(Cl)_2(CH_3CN)]^+$, 1109 (0.5) $[L_2Rh_2(Et)(Cl)(I)]^+$.

(^{iPr}MeMe)Rh(Me)(CO)(I),$\mathbf{9_{Me}}$. ^{1}H NMR (acetone-d_6): δ_H 8.45 (d, J = 3 Hz, 1H, H_5pz), 8.41 (d, J = 3 Hz, 1H, H_5pz), 7.32 (s, 1H, Ar), 7.21 (s, 1H, Ar), 7.01 (part of *AB*, J_{app} = 8 Hz, 1H, Ar), 6.93 (part of *AB*, J_{app} = 8 Hz, 1H, Ar), 6.89 (part of *AB*, J_{app} = 8, 2 Hz, 1H, Ar), 6.80 (part of *AB*, J_{app} = 8, 2 Hz, 1H, Ar), 6.75 (d, J = 3 Hz, 1H, H_4pz), 6.72

(d, J = 3 Hz, 1H, H_4pz), 4.25 (sept, J = 7 Hz, 1H, $CHMe_2$), 3.26 (sept, J = 7 Hz, 1H, $CHMe_2$), 2.27 (s, 3H, $ArCH_3$), 2.19 (s, 3H, $ArCH_3$), 1.4-1.2 (m, 15H, $iPrCH_3$ and Rh-CH_3) ppm. ^{13}C NMR (acetone-d_6): δ_C 190.2 (d, $^1J_{Rh\text{-}C}$= 54 Hz, Rh-CO), 166.7 (d,$^3J_{Rh\text{-}C}$ = 1 Hz), 164.0 (d,$^3J_{Rh\text{-}C}$ = 1 Hz), 146.0, 142.4, 134.7, 134.0, 133.6, 131.8, 129.3, 128.7, 128.5, 128.2, 125.8, 124.4, 122.8, 122.6, 107.3 (d,$^3J_{Rh\text{-}C}$ = 1 Hz, C_4pz), 107.2 (d,$^3J_{Rh\text{-}C}$ = 1 Hz, C_4pz), 31.2, 30.3, 24.9, 24.6, 23.7, 23.4, 20.7, 20.6, 9.2 (d, $J_{Rh\text{-}C}$ = 21 Hz) ppm. IR (acetone, ν_{CO}, cm^{-1}): 2051.

(^{iPr}MeMe)Rh(Et)(CO)(I), 9_{Et}. ^{1}H NMR (acetone-d_6): δ_H 8.45 (d, J = 3 Hz, 1H, H_5pz), 8.37 (d, J = 3 Hz, 1H, H_5pz), 7.38 (s, 1H, Ar), 7.17 (s, 1H, Ar), 7.03 (part of *AB*, J_{app} = 8 Hz, 1H, Ar), 6.95 (part of *AB*, J_{app} = 8 Hz, 1H, Ar), 6.90 (part of *AB*, 1H, Ar), 6.81 (part of *AB*, 1H, Ar), 6.74 (d, J = 3 Hz, 1H, H_4pz), 6.72 (d, J = 3 Hz, 1H, H_4pz), 4.31 (sept, J = 7 Hz, 1H, $CHMe_2$), 3.31 (sept, J = 7 Hz, 1H, $CHMe_2$), 2.60 (m, 1H, one of $RhCH_2$), 2.29 (s, 3H, $ArCH_3$), 2.27 (s, 3H, $ArCH_3$), 2.14 (m, 1H, one of $RhCH_2$), 1.43 (d, J = 7 Hz, 3H, $iPrCH_3$), 1.42 (d, J = 7 Hz, 3H, $iPrCH_3$), 1.32 (d, J = 7 Hz, 6H, $iPrCH_3$), 0.71 (td, $J_{C\text{-}H}$ = 7 Hz, $^3J_{Rh\text{-}H}$ = 1 Hz, 3H, $EtCH_3$) ppm. IR (acetone, γ_{CO}, cm^{-1}): 2047.

(MeH)Rh(Me)(CO)(I), 10_{Me}. Two isomers are observed in a 10:9 ratio by averaging relative integrations of well resolved resonances for H_5-pz (δ_H 8.08 and 7.92 ppm for minor and major isomers, respectively) and Rh-CH_3 (δ_H 1.28 and 1.26 ppm for major and minor isomers, respectively). The remaining resonances are difficult to assign due to their overlapping nature and similarity in signal intensity. IR (ν_{CO} ,cm^{-1}) : 2060 (KBr). 2064 (acetone)

($MeCF_3$)Rh(Me)(CO)(I), 11_{Me}. ^{1}H NMR (acetone-d_6): Two isomers are observed in 3:1.8 ratio (63%:37% composition) by averaging relative integrations of well resolved resonances for $RhCH_3$, H_5pz, and two sets of aryl hydrogens. *Major isomer:* δ_H 8.74 (d, *J* = 2 Hz, 1H, H_3pzArCF_3), 8.61 (d, *J* = 2 Hz, 1H, H_3pztolyl), 8.11 (d, *J* = 2 Hz, 1H, H_5pzArCF_3), 8.00 (d, J = 2 Hz, 1H, H_5pz-tolyl), 7.82 (s, 1H, Ar-H^F), 7.52 (s, 1H, tolyl), 7.28 (part of *AB*, 1H, ArCF_3), 7.26 (part of *AB*, 1H, ArCF_3), 7.24 (part of *AB*, 1H, tolyl), 7.03 (part of *AB*, 1H, tolyl), 6.84 (t, *J* = 2 Hz, 1H, H_4pzArCF_3), 6.78 (t, *J* = 2 Hz, 1H, H_4pz-tolyl), 2.32 (s, 3H, CH_3), 1.34 (d, J_{Rh-H} = 2 Hz, 3H, $RhCH_3$) ppm; *Minor isomer*: δ_H 8.74 (d, *J* = 2 Hz, 1H, H_3pzArCF_3), 8.61 (d, *J* = 2 Hz, 1H, H_3pz-tolyl), 8.14 (d, *J* = 2 Hz, 1H, H_5pzArCF_3), 7.97 (d, *J* = 2 Hz, 1H, H_5pz-tolyl), 7.92 (s, 1H, ArH^F), 7.41 (s, 1H, tolyl), 7.39 (part of *AB*, 1H, ArCF_3), 7.34 (part of *AB*, 1H, ArCF_3), 7.12 (part of *AB*, 1H, tolyl), 6.97 (part of *AB*, 1H, tolyl), 6.82 (t, *J* = 3 Hz, 1H, H_4pzArCF_3), 6.79 (t, *J* = 2 Hz, 1H, H_4pz-tolyl), 2.31 (s, 3H, CH_3), 1.27 (d, J_{Rh-H} = 2 Hz, 3H, $RhCH_3$) ppm. ^{13}C NMR (acetone-d_6): δ_C 186.9 (d, $^1J_{Rh-C}$= 56 Hz, Rh-CO), 186.8, (d, $^1J_{Rh-C}$= 56 Hz, Rh-CO), 151.9, 149.8, 149.6, 148.9, 145.9, 145.8, 143.4, 140.7, 133.4, 132.8, 132.5, 132.5, 132.4, 132.2, 131.3, 131.2, 130.0, 129.9, 129.3, 127.04, 127.01, 125.8, 125.6 (q, $^1J_{C-F}$= 270 Hz, CF_3), 125.0 (q, $^3J_{C-F}$= 4 Hz), 124.5, 124.3 (q, $^3J_{C-F}$= 4 Hz), 123.4, 123.2, 120.3 (q, $^3J_{C-F}$= 4 Hz), 120.2 (q, $^3J_{C-F}$= 4 Hz), 119.2 (q, $^2J_{C-F}$= 33 Hz), 118.7 (q, $^2J_{C-F}$= 33 Hz), 110.4, 110.1, 109.5, 109.8, 20.7, 20.6, 10.4 ($^1J_{Rh-C}$ = 20 Hz, $RhCH_3$), 10.1 ($^1J_{Rh-C}$ = 20 Hz, $RhCH_3$) ppm. ^{19}F NMR (benzene-d_6): δ_F -60.51 (minor), -60.44 (major) ppm. IR (acetone, γ_{CO}, cm^{-1}): 2069.

($MeCF_3$)Rh(Et)(CO)(I),11$_{Et}$. ^{1}H NMR (acetone-d_6): Two isomers observed in 2.35:1 ratio (70%:30% composition) by averaging relative integrations of well resolved resonances for ethyl-CH_3, H_4pz, and one set of aryl hydrogens. *Major isomer:* δ_H 8.71 (d, *J* = 2 Hz, 1H, H_3pz$ArCF_3$), 8.61 (d, *J* = 2 Hz, 1H, H_3pztolyl), 8.10 (d, *J* = 2 Hz, 1H, H_5pz$ArCF_3$), 8.07 (d, J = 2 Hz, 1H, H_5pz-tolyl), 7.76 (s, 1H, Ar-H^F), 7.55 (s, 1H, tolyl), 7.27 (part of *AB*, 1H, $ArCF_3$), 7.25 (parts of *AB*, 2H, $ArCF_3$ and tolyl), 7.24 (part of *AB*, 1H, tolyl), 7.03 (part of *AB*, 1H, tolyl), 6.84 (t, *J* = 2 Hz, 1H, H_4pz$ArCF_3$), 6.78 (t, *J* = 2 Hz, 1H, H_4pz-tolyl), 2.56 (m, 1H, one of $RhCH_2$), 2.36 (s, 3H, CH_3), 2.27 (m, 1H, one of $RhCH_2$), 0.71 (td, J_{C-H} = 7 Hz, $^3J_{Rh-H}$ = 1 Hz, 3H, Et-CH_3) ppm; *Minor isomer*: δ_H 8.73 (d, *J* = 2 Hz, 1H, H_3pz$ArCF_3$), 8.60 (d, *J* = 2 Hz, 1H, H_3pz-tolyl), 8.13 (d, *J* = 2 Hz, 1H, H_5pz$ArCF_3$), 8.05 (d, *J* = 2 Hz, 1H, H_5pz-tolyl), 7.97 (s, 1H, ArH^F), 7.36 (s, 1H, tolyl), 7.42 (part of *AB*, 1H, $ArCF_3$), 7.35 (part of *AB*, 1H, $ArCF_3$), 7.12 (part of *AB*, 1H, tolyl), 6.95 (part of *AB*, 1H, tolyl), 6.82 (t, *J* = 3 Hz, 1H, H_4pz$ArCF_3$), 6.81 (t, *J* = 2 Hz, 1H, H_4pz-tolyl), 2.44 (m, 1H, one of $RhCH_2$), 2.32 (s, 3H, CH_3), 2.22 (m, one of Rh-CH_2), 0.64 (td, J_{C-H} = 7 Hz, $^3J_{Rh-H}$ = 1 Hz, 3H, Et-CH_3) ppm. ^{19}F NMR (acetone-d_6): δ_F -61.65 (minor), -61.38 (major) ppm. IR (acetone, ν_{CO}, cm^{-1}): 2063.

(CF_3CF_3)Rh(Me)(CO)(I), 12$_{Me}$. ^{1}H NMR (acetone-d_6): δ_H 8.81 (d, *J* = 3 Hz, 2H, H_3pz), 8.18 (d, *J* = 2 Hz, 1H, H_5pz), 8.07 (d, *J* = 2 Hz, 1H, H_5pz), 8.02 (s, 1H, Ar), 7.92 (s, 1H, Ar), 7.52 (part of *AB*, 1H, Ar), 7.46 (part of *AB*, 1H, Ar), 7.39 (part of *AB*, 1H, Ar), 7.38 (part of *AB*, 1H, Ar), 6.88 (dd, *J* = 3, 2 Hz, 1H, H_4pz), 6.86 (dd, *J* = 3, 2 Hz, 1H, H_4pz), 1.36 (d, $^2J_{Rh-H}$ = 2 Hz, 3H, $RhCH_3$) ppm. ^{13}C NMR (acetone-d_6): δ_C 186.5, (d, $^1J_{Rh-C}$= 56 Hz, Rh-CO), 150.7, 150.2 (d, $^3J_{Rh-C}$ = 1 Hz), 147.6 (d, $^3J_{Rh-C}$ = 1 Hz), 146.4 (d,

$^{3}J_{Rh\text{-}C}$ = 1 Hz), 133.4, 133.3, 133.0, 130.9, 127.0, 125.7, 125.5 (q, $^{3}J_{C\text{-}F}$= 4 Hz), 125.4 (q, $^{1}J_{C\text{-}F}$= 272 Hz, CF_3), 125.3 (q, $^{1}J_{C\text{-}F}$= 272 Hz, CF_3), 124.8 (q, $^{3}J_{C\text{-}F}$= 4 Hz), 121.6 (q, $^{2}J_{C\text{-}F}$= 33 Hz), 121.2 (q, $^{2}J_{C\text{-}F}$= 33 Hz), 120.8 (q, $^{3}J_{C\text{-}F}$= 4 Hz), 120.5 (q, $^{3}J_{C\text{-}F}$= 4 Hz), 110.6 (d, $^{3}J_{Rh\text{-}C}$ = 1 Hz, C_4pz), 110.1 (d, $^{3}J_{Rh\text{-}C}$ = 1 Hz, C_4pz), 10.5 ($J_{Rh\text{-}C}$= 20 Hz, $RhCH_3$) ppm. ^{19}F NMR (acetone-d_6): δ_F -61.75, -61.62 ppm. IR (acetone, ν_{CO}, cm^{-1}): 2075.

(CF_3CF_3)Rh(Et)(CO)(I),12$_{Et}$. ^{1}H NMR (acetone-d_6): δ_H 8.80 (dd, *J* = 3, 1 Hz, 1H, H_3pz), 8.78 (dd, *J* = 3, 1 Hz, 1H, H_3pz), 8.16 (d, *J* = 2 Hz, 1H, H_5pz), 8.14 (d, *J* = 2 Hz, 1H, H_5pz), 8.05 (m, 1H, Ar), 7.84 (m, 1H, Ar), 7.54 (part of *AB*, 1H, Ar), 7.47 (part of *AB*, 1H, Ar), 7.36 (*AB*, 2H, Ar), 6.88 (dd, *J* = 3, 2 Hz, 1H, H_4pz), 6.85 (dd, *J* = 3, 2 Hz, 1H, H_4pz), 2.54 (m, 1H, one of $RhCH_2$), 2.27 (m, 1H, m, 1H, one of $RhCH_2$), 0.70 (td, $J_{C\text{-}H}$ = 8 Hz, $^{3}J_{Rh\text{-}H}$ = 2 Hz, 3H, Et-CH_3) ppm. ^{19}F NMR (acetone-d_6): δ_F -61.91, -61.75 ppm. IR (acetone, ν_{CO}, cm^{-1}): 2070.

Preparative (Synthetic-Scale) Experiments

6.2.6.2. Synthesis of(MeMe)Rh(Me)(CO)(I),**7$_{Me}$.**

A 0.15 mL (2.4 mmol) aliquot of CH_3I was added by syringe to a yellow solution of 0.109 g (0.238 mmol) **1**in 15 mL acetone. After the resulting red solution had been stirred at room temperature for 10 min,volatiles were removed under vacuum to give 0.109 g (76 %) of **7$_{Me}$** as red-orange microcrystalline powder. M.p.: 245-250 ^{o}C, (dec). Anal. Calcd for $C_{22}H_{21}N_5IORh$: C, 43.95; H, 3.52; N, 11.65. Found: C, 44.13; H, 3.29; N, 11.92.^{1}H NMR (CD_2Cl_2): δ_H8.13 (d, *J* = 2 Hz, 1H, H_5pz), 8.12 (d, *J* = 2 Hz, 1H, H_5pz), 8.02 (d, *J* = 1 Hz, 1H, H_3pz), 7.52 (d, *J* = 1 Hz, 1H, H_3pz), 7.22-7.12 (overlapping s's and part of *AB*,

4H, Ar), 6.92 (part of *AB*, 2H, Ar),6.66 (d, *J* = 2 Hz, 1H, H_4pz), 6.65 (d, *J* = 2 Hz, 1H, H_4pz), 2.34 (s, 3H, $ArCH_3$),2.30 (s, 3H, $ArCH_3$), 1.25 (d, $^2J_{Rh\text{-}H}$ = 2 Hz, 3H, Rh-CH_3).IR (ν_{CO}, cm^{-1}): 2060 (KBr pellet).

6.2.6.3 Synthesis of(MeMe)$Rh(I)_2(CO)$, 7_I.

A solution of 0.0262 g (0.103 mmol) I_2 in 15 mL acetone was added drop-wise via cannula to a solution of 0.0474 g (0.103 mmol) **1** in 10 mL acetone. After the resulting green-brown solution had been stirred at room temperature for 12 h, acetone was removed under vacuum to give 0.0739 g (100 %) of $\mathbf{7_I}$ as dark yellow-brown powder. M.p.: > 300 ^{0}C. Anal.Calcd.for$C_{21}H_{18}N_5OI_2Rh$: C, 35.37; H, 2.54; N, 9.82. Found: C, 35.55; H, 2.61; N, 10.13.^{1}HNMR (acetone-d_6): 8.62(d, *J* = 3 Hz, 2H, H_3pz), 8.08 (d, *J* = 3 Hz, 2H, H_5pz), 7.40 (s, 2H, Ar), 7.16 (part of *AB*, J_{app} = 8 Hz, 2H, Ar), 6.93 (part of *AB*, J_{app} = 8, 1 Hz, 2H, Ar), 6.81 (t, *J* = 3, 2H, H_4pz), 2.30 (s, 6H, $ArCH_3$).^{13}C NMR (acetone-d_5): 206.1 (d, $^1J_{Rh\text{-}C}$= 40 Hz, Rh-CO), 149.9 (d,$^3J_{Rh\text{-}C}$ = 1 Hz), 145.1, 132.9, 132.5, 129.3, 129.1, 126.0, 122.7, 109.9 (d,$^3J_{Rh\text{-}C}$ = 1 Hz, C_4pz), 20.6. ^{1}HNMR (CD_2Cl_2): 8.16 (d, *J* = 3 Hz, 2H, H_3pz), 7.89 (d, *J* = 2 Hz, 2H, H_5pz), 7.21 (part of *AB*, J_{app} = 8 Hz, 2H, Ar), 7.17 (s, 2H, Ar), 6.95 (part of *AB*, J_{app} = 8, 1 Hz, 2H, Ar), 6.67 (dd, *J* = 3, 2 Hz, 2H, H_4pz), 2.34 (s, 6H, $ArCH_3$).IR (ν_{CO}, cm^{-1}): 2080 (KBr pellet); 2078 (acetone). HRMS [ESI(+), *m*/*z*] Calcd. (Obs) for $C_{21}H_{18}I_2N_5ORh$, $[LRh(I)_2(CO)]^{\cdot+}$, 712.8656 (712.8652). LRMS (ESI(+), *m*/*z*) (int.) [assign.]: 713 (26) $[LRh(I)_2(CO)]^{\cdot+}$, 714 (100) $[HLRh(I)_2(CO)]^+$,726 (12) $[LRh(I)(CH_3CN)]^+$.

(^{Me}MeMe)Rh(Me)(CO)(I),8$_{Me}$. A 0.10 mL (1.5 mmol) aliquot of CH_3I was added by syringe to a yellow solution of 0.074 g (0.15 mmol) **2** in 15 mL dry benzene. After stirring at room temperature 16 h, volatiles were removed from the resulting red solution by vacuum distillation, the solid was washed with Et_2O, and dried under vacuum to give 0.095 g (85%) of (^{Me}MeMe)Rh(Me)(CO)(I) as a red-orange crystalline powder. Larger X-ray quality crystals (43.1 mg, 73%) of **7$_{Me}$** were prepared by allowing a solution of 46.0 mg **2** and 58.0 µL CH_3I in 3 mL to stand undisturbed 2 d at room temperature (22^{o}C) in acetone. Mp: 205-207 ^{o}C, (dec). Anal.Calcd. (obsd.) for $C_{24}H_{25}N_5OIRh$: C, 45.81 (45.79); H, 4.00 (4.01); N, 11.13 (11.07). ^{1}H NMR (CD_2Cl_2): δ_H 8.03 (d, *J* = 3 Hz, 1H, H_5pz), 8.01 (d, *J* = 3 Hz, 1H, H_5pz), 7.08-7.03 (overlapping signals, two singlets and part of *AB*, 4H, Ar), 6.88 (part of *AB*, 2H, Ar), 6.45 (d, *J* = 3 Hz, 1H, H_4pz), 6.44 (d, *J* = 3 Hz, 1H, H_4pz), 2.89 (s, 3H, pz-CH_3), 2.56 (s, 3H, pzCH_3), 2.32 (s, 3H, ArCH_3), 2.29 (s, 3H, ArCH_3), 1.35 (d, $^2J_{Rh\text{-}H}$ = 2 Hz, 3H, Rh-CH_3) ppm. IR (ν_{CO}, cm^{-1}): 2045 (KBr pellet). LRMS (ESI(+), *m*/*z*) (int.) [assign.]: 474 (17) $[LRh(Me)]^+$, 502 (100) $[LRh(Me)(CO)]^+$, 515 (94) $[LRh(Me)(CH_3CN)]^+$, 543 (31) $[LRh(Me)(CO)(CH_3CN)]^+$, 548 (10) $[LRh(Me)(Et_2O)]^+$, 630 (4) $[HLRh(Me)(CO)(I)]^+$, 734 (2) $[LRh(I)(Et_2O)_2]^+$, 742 (1.7) $[HLRh(I)_2(CO)]^+$, 1045 (1) $[L_2Rh_2I]^+$, 1088 (3) $[L_2Rh_2(Me)(CO)(I)]^+$, 1131 (0.5) $[L_2Rh_2(Me)_2(CO)_2I]^+$. After letting a CD_2Cl_2 solution of **7$_{Me}$** decompose for two weeks (also monitored by NMR, vide infra), LRMS (ESI(+), *m*/*z*) (int.) [assign.]: 474 (1) $[LRh(Me)]^+$, 475 (2) $[HLRh(Me)]^+$, 487 (2) $[LRh(CO)]^+$, 488 (5) $[HLRh(CO)]^+$, 501 (7) $[HLRh(CH_3CN)]^+$, 515 (38) $[LRh(Me)(CH_3CN)]^+$, 529 (3) $[HLRh(CO)(CH_3CN)]^+$, 543 (5) $[LRh(Me)(CO)(CH_3CN)]^+$, 550 (11) $[HLRh(formate)_2]^{\cdot+}$, 556 (7) $[LRh(Me)(CH_3CN)_2]^+$, 564 (2) $[LRh(CO)(acetate)(H_2O)]^+$ or $[HLRh(formate)(acetate)]^+$,

569 (10) $[LRh(Me)(acetate)(H_2O)_2]^{\cdot+}$, 595 (100) [*unassigned*], see later section on the decomposition of $\mathbf{7_{Me}}$.

6.2.6.4 Synthesis of*mer, trans*-$[(MeMe)Rh(Me)(\mu\text{-}I)]_2$, $\mathbf{13_{Me}}$.

A mixture of 0.0420 g (91.4μmol) **1** and 57.0 μL (91.6 mmol) CH_3I was left undisturbed for 2d at room temperature in a capped vial during which time small needles of insoluble product deposited. After 2 days the solution was decanted and the needles were washed with Et_2O and were dried under vacuum to give 0.0483 g(92 %) of $\mathbf{13_{Me}}$ as a red crystalline solid. M.p.: > 300 ^oC. Anal.Calcd.for$C_{21}H_{21}N_5IRh$: C, 44.00; H, 3.69; N, 12.22. Found: C, 44.03; H, 3.74; N, 11.99. HRMS [ESI(+), *m*/*z*] Calcd. (Obs) for $C_{42}H_{42}IN_{10}Rh_2$, $[L_2Rh_2(Me)_2(I)]^{\cdot+}$, 1019.0749 (1019.0731). LRMS (ESI(+), *m*/*z*) (int.) [assign.]: 446 (25) $[LRh(Me)]^+$, 487 (100) $[LRh(Me)(CH_3CN)]^+$, 528 (6) $[LRh(Me)(CH_3CN)_2]^+$, 573 (27) $[LRh(Me)(I)]^{\cdot+}$, 727 (1.5) $[HLRh(I)_2(CH_3CN)]^+$, 927 (0.7) $[L_2Rh_2(Me)_2Cl]^+$, 968 (0.7) $[L_2Rh_2(Me)_2(CH_3CN)Cl]^+$, 1019 (5) $[L_2Rh_2(Me)_2I]^+$, 1060 (6) $[L_2Rh_2(Me)_2(CH_3CN)(I)]^+$,1101 (2) $[L_2Rh_2(Me)_2(CH_3CN)_2(I)]^+$, 1131 (0.7) $[L_2Rh_2(Me)(I)_2]^{\cdot+}$, 1146 (0.7) $[L_2Rh_2(Me)_2(I)_2]^{\cdot+}$, 1172 (1.1) $[L_2Rh_2(Me)_2(CH_3CN)(I)_2]^{\cdot+}$, 1187 (0.6) $[L_2Rh_2(Me)_2(CH_3CN)_2(I)_2]^{\cdot+}$. An X-ray-quality single crystal was selected from another similar preparation, but before decanting the mother liquor. This crystal showed about 9.37% replacement of iodide for each of the methyls, or equivalently represents a mixture of 90.63% $\mathbf{13_{Me}}$ and 9.37% $\mathbf{13_I}$. Given the combustion analysis data, this crystal is likely not representative of the bulk.

6.2.6.5. Synthesis of*mer, trans*-$[(MeMe)Rh(I)(\mu\text{-}I)]_2$, $\mathbf{13_I}\cdot Et_2O$.

A solution of 0.0524 g (0.206 mmol) I_2 in 15 mL THF was added to a solution of 0.0948 g (0.206 mmol) **1** in 5 mL THF. The resulting red-brown solution was heated at reflux for 12 h. After cooling to room temperature, the precipitate was collected by filtration, washed with 5 mL each THF and Et_2O and then was dried under vacuum to give 0.110 g (74 %) of $\mathbf{13_I}\cdot Et_2O$ as an orange-brown solid. M.p.: >300 ^oC. Anal.Calcd.for$C_{44}H_{46}N_{10}I_4ORh_2$, $\mathbf{13_I}\cdot Et_2O$: C, 36.59; H, 3.21; N, 9.70. Found: C, 36.34; H, 2.98; N, 9.27. LRMS (ESI(+), *m*/*z*) (int.) [assign.]: 466 (12) $[LRh(Cl)]^+$, 476 (3) $[LRh(formate)]^+$, 517 (10) $[LRh(formate)(CH_3CN)]^+$, 531 (21) $[LRh(CH_3CO_2)(CH_3CN)]^+$, 548 (9) $[LRh(formate)(CH_3CN)_2]^+$, 558 (55) $[LRh(I)]^+$, 599 (60) $[LRh(I)(CH_3CN)]^+$, 640 (100) $[LRh(I)(CH_3CN)_2]^+$,686 (5) $[HLRh(I)_2]^+$, 726 (43) $[LRh(I)_2(CH_3CN)]^{\cdot+}$, 1243 (1) $[L_2Rh_2(I)_3]^+$, 1261 (0.3) $[L_2Rh_2(I)_3(H_2O)]^+$, 1284 (2) $[L_2Rh_2(I)_3(CH_3CN)]^+$, 1325 (1) $[L_2Rh_2(I)_3(CH_3CN)_2]^+$. X-ray quality crystals were obtained by vapor diffusion of Et_2O into a room-temperature solution that was obtained by mixing 0.103 mmol of each **1** and I_2 in 2 mL THF.

6.3. Single crystal X-ray crystallography

X-ray intensity data from a yellow needle of **1**and a yellow block of **5** were collected at 273 K with a Bruker AXS 3-circle diffractometer equipped with a SMART2[35] CCD detector using Mo(Kα) for the former and Cu(Kα) radiation for the latter.X-ray intensity data from a yellow needle of $\mathbf{2}\cdot C_6H_6$, a yellow prism of **3**, a yellow prism of $\mathbf{4}\cdot C_6H_6$,a brown prism of $\mathbf{7_{Et}}$, a brown prism of $\mathbf{7_I}\cdot$1.5acetone, an orange prism of $\mathbf{8_{Me}\cdot C_6H_6}$, a brown prism of $\mathbf{13_{Me}}\cdot$acetone, and a brown needle of $\mathbf{13_I}\cdot Et_2O$ were measuredwith an Oxford Diffraction Ltd. Supernova diffractometer equipped with a 135 mm Atlas CCD detector using Mo(Kα) for all except **3**and $\mathbf{4}\cdot C_6H_6$which used Mo(Kα) radiation. Raw

data frame integration and Lp corrections were performed with either CrysAlis Pro (Oxford Diffraction, Ltd.)[36]or SAINT+ (Bruker).[35]Final unit cell parameters were determined by least-squares refinement of 9874, 13022, 10797, 9932, 9989, 28084, 20898, 11437, 15332, and 9630 reflections from the data sets of **1**, **2**·C_6H_6, **3**, **4**·C_6H_6, **5**, $\mathbf{7_{Et}}$, $\mathbf{7_I}$·1.5acetone, $\mathbf{8_{Me}}$·C_6H_6, $\mathbf{13_{Me}}$·acetone, $\mathbf{13_I}$·Et_2O, respectively, with $I > 2\sigma(I)$ for each. Analysis of the data showed negligible crystal decay during collection in each case. Direct methods structure solutions, difference Fourier calculations and full-matrix least-squares refinements against F^2 were performed with SHELXTL.[37]Numerical absorption corrections and based on the real shape of the crystals were applied with SADABSfor **1** and **5**.[35] Empirical absorption corrections were applied to the data of **2**·C_6H_6 and $\mathbf{8_{Me}}$·C_6H_6using spherical harmonics implemented in the SCALE3 ABSPACK multi-scan method.[38] Numerical absorption corrections based on gaussian integration over a multifaceted crystal model were applied to the data of the remaining complexes. All non-hydrogen atoms were refined with anisotropic displacement parameters. Hydrogen atoms were placed in geometrically idealized positions and included as riding atoms. The X-ray crystallographic parameters and further details of data collection and structure refinements are presented in Tables 6.1-6.4. The crystal of **5** is a quasi-merohedral pseudo-orthorhombic TWIN with 27% contribution of a (-1 0 0 0 -1 0 0 0 1) component where the CF_3 and CH_3 groups in both symmetrically independent molecules are interchangeably superimposed. The CF_3 group has an apparent rotational disorder; however, given the low population against the superimposed Me-group, we treated this group adequately with an anisotropic representation and avoided over-modeling by splitting it into two different orientations.

Table 6.1. Crystallographic Data Collection and Structure Refinement for **1**,**2**, and **3**.

Compound	**1**	**2**·C_6H_6	**3**
Formula	$C_{21}H_{18}N_5ORh$	$C_{29}H_{28}N_5ORh$	$C_{27}H_{30}N_5ORh$
Formula weight	459.31	565.47	543.47
Crystal system	orthorhombic	triclinic	triclinic
Space group	Pnna	P -1	P -1
Temp. [K]	100(2)	100.0	100(2)
a [Å]	9.7817(7)	10.0029(3)	12.4341(5)
b [Å]	26.5319(18)	10.9129(4)	13.6245(7)
c [Å]	14.2307(10)	12.7569(4)	14.8775(6)
α [°]	90	74.557(3)	84.671(4)
β [°]	90	72.389(3)	86.420(3)
γ [°]	90	87.204(3)	76.703(4)
V [Å^3]	3693.3(4)	1278.60(7)	2440.01(18)
Z	8	2	4
$D_{calcd.}$ [gcm^{-3}]	1.652	1.469	1.479
λ [Å] (Mo or Cu Kα)	0.71073	0.71073	1.5418
μ.[mm^{-1}]	0.947	0.699	5.888
Abs. Correction	numerical	multi-scan	numerical
F(000)	1856	580	1120
2θ range [°]	3.08 to 64.18	6.78 to 59.16	6.68 to 147.62
Reflections collected	61457	22593	23525
Independent reflections	6291[R(int) = 0.0384]	6410[R(int) = 0.0324]	9614[R(int) = 0.0318]
T_min/max	0.6906/0.9255	0.95436/1.00000	0.598/0.815
Data/restraints/ parameters	6291/0/259	6410/0/329	9614/0/625
Goodness-of-fit on F^2	0.998	1.071	1.022
*R*1/*wR2*[$I>2\sigma(I)$][a]	0.0237/0.0565	0.0278/0.0569	0.0254/0.0646
*R*1/*wR2* (all data)[a]	0.0320/0.0609	0.0343/0.0604	0.0303/0.0673
Largest diff. peak/hole / e Å^{-3}	0.901/-0.392	0.657/-0.440	0.710/-0.537

[a] $R = \Sigma||F_o|-||F_c||/\Sigma|F_o|$. [d] $wR = [\Sigma w(|F_o^2|-|F_c^2|)^2/\Sigma w|F_o^2|^2]^{1/2}$

Table 6.2 . Crystallographic Data Collection and Structure Refinement for **4**·C_6H_6,**5**, and $\mathbf{7_{Et}}$.

Compound	**4**·C_6H_6	**5**	$\mathbf{7_{Et}}$
Formula	C26 H22 N5 O Rh	$C_{21}H_{15}F_3N_5ORh$	$C_{23}H_{23}IN_5ORh$
Formula weight	523.40	513.29	615.27
Crystal system	triclinic	monoclinic	monoclinic
Space group	P -1	$P2_1/n$	$P2_1/n$
Temp. [K]	101.0	100.4	100.0
a [Å]	9.0197(3)	9.9482(3)	7.44834(10)
b [Å]	10.0599(3)	26.7919(9)	18.3451(3)
c [Å]	12.7565(4)	14.5872(5)	16.7515(2)
α [°]	83.830(2)	90.00	90.00
β [°]	81.875(3)	90.2190(10)	92.4100(12)
γ[°]	77.668(3)	90.00	90.00
V [$Å^3$]	1115.86(6)	3887.9(2)	2286.90(6)
Z	2	8	4
$D_{calcd.}$ [gcm^{-3}]	1.558	1.754	1.787
λ [Å] (Mo or Cu Kα)	0.7107	1.54178	0.7107
μ.[mm^{-1}]	0.795	7.585	2.122
Abs. Correction	numerical	numerical	numerical
F(000)	532	2048	1208
2θ range [°]	6.84 to 59.16	6.06 to 136.24	7.06 to 59.06
Reflections collected	25073	7008	60084
Independent reflections	5708[R(int) = 0.0322]	6843[R(int) = 0.0000]	6156[R(int) = 0.0332]
T_min/max	0.917/0.975	0.2826/0.3998	0.616/0.746
Data/restraints/ parameters	5708/0/299	6843/24/621	6156/0/283
Goodness-of-fit on F^2	1.075	1.034	1.053
*R*1/*wR2*[$I>2\sigma(I)$][a]	0.0382/0.0907	0.0404/0.0976	0.0190/0.0390
*R*1/*wR2* (all data)[a]	0.0446/0.0950	0.0415/0.0981	0.0235/0.0410
Largest diff. peak/hole / e $Å^{-3}$	1.758/-1.519	0.824/-0.826	0.467/-0.602

[a]$R = \Sigma||F_o|-||F_c||/\Sigma|F_o|$. [d]$wR= [\Sigma w(|F_o^2|-|F_c^2|)^2/\Sigma w|F_o^2|^2]^{1/2}$

Table 6.3.. Crystallographic Data Collection and Structure Refinement for $\mathbf{7_I}$·1.5acetone and $\mathbf{8_{Me}}$·C_6H_6.

Compound	$\mathbf{7_I}$·1.5acetone	$\mathbf{8_{Me}}$·C_6H_6
Formula	$C_{25.5}H_{27}I_2N_5O_{2.5}Rh$	$C_{30}H_{31}IN_5ORh$
Formula weight	800.23	707.41
Crystal system	triclinic	monoclinic
Space group	P -1	$P2_1/c$
Temp. [K]	100.3	100.3
a [Å]	13.0548(4)	9.4775(2)
b [Å]	13.9045(4)	22.6275(5)
c [Å]	15.7643(4)	13.5609(4)
α [°]	83.791(2)	90.00
β [°]	79.004(2)	100.519(3)
γ [°]	85.109(2)	90.00
V [Å^3]	2786.41(13)	2859.30(12)
Z	4	4
$D_{calcd.}$ [gcm^{-3}]	1.908	1.643
λ [Å] (Mo or Cu Kα)	0.7107	0.7107
μ.[mm^{-1}]	2.862	1.709
Abs. Correction	numerical	multi-scan
F(000)	1544	1408
2θ range [°]	6.6 to 59.22	6.84 to 59.1
Reflections collected	53463	32496
Independent reflections	14130[R(int) = 0.0334]	7333[R(int) = 0.0406]
T_min/max	0.608/0.898	0.85935/1.00000
Data/restraints/ parameters	14130/0/659	7333/0/348
Goodness-of-fit on F^2	1.059	1.113
$R1/wR2[I>2\sigma(I)]$[a]	0.0268/0.0509	0.0333/0.0633
$R1/wR2$ (all data)[a]	0.0380/0.0564	0.0499/0.0745
Largest diff. peak/hole / e Å^{-3}	1.559/-1.098	1.543/-0.799

[a]$R = \Sigma||F_o|-||F_c||/\Sigma|F_o|$. [d]$wR = [\Sigma w(|F_o^2|-|F_c^2|)^2/\Sigma w|F_o^2|^2]^{1/2}$

Table 6.4.. Crystallographic Data Collection and Structure Refinement for **13_{Me}**·acetone, and **13_{I}**·Et_2O.

Compound	**13_{Me}**·acetone	**13_{I}**·Et_2O
Formula	$C_{44.81}H_{47.44}I_{2.19}N_{10}ORh_2$	$C_{44}H_{46}I_4N_{10}ORh_2$
Formula weight	1225.52	1444.33
Crystal system	monoclinic	monoclinic
Space group	$P2_1/n$	$P2_1/n$
Temp. [K]	100.0	100.7
a [Å]	15.7695(3)	16.2250(5)
b [Å]	8.12639(17)	8.4566(2)
c [Å]	20.1709(4)	19.2983(6)
α [°]	90.00	90.00
β [°]	93.007(2)	93.683(3)
γ [°]	90.00	90.00
V [$Å^3$]	2581.33(9)	2642.42(13)
Z	2	2
$D_{calcd.}$ [gcm^{-3}]	1.577	1.815
λ [Å] (Mo or Cu Kα)	0.7107	0.7107
μ.[mm^{-1}]	1.988	3.002
Abs. Correction	numerical	numerical
F(000)	1200	1380
2θ range [°]	6.72 to 59.08	6.78 to 59.06
Reflections collected	32699	40194
Independent reflections	6684[R(int) = 0.0296]	6940[R(int) = 0.0585]
T_min/max	0.607/0.926	0.731/0.975
Data/restraints/ parameters	6684/6/302	6940/7/300
Goodness-of-fit on F^2	1.107	1.049
*R*1/*wR*2[$I>2\sigma(I)$][a]	0.0283/0.0859	0.0497/0.1218
*R*1/*wR*2 (all data)[a]	0.0340/0.0896	0.0787/0.1380
Largest diff. peak/hole / e $Å^{-3}$	1.349/-0.452	1.696/-1.114

[a]$R = \Sigma||F_o|-||F_c||/\Sigma|F_o|$. [d]$wR= [\Sigma w(|F_o^2|-|F_c^2|)^2/\Sigma w|F_o^2|^2]^{1/2}$

6.4. Results and discussion

6.4.1. Syntheses

The synthetic routes to the six NNN-pincer ligands used in this study are given in Scheme 6.1. The syntheses of the di[(2-3R-pyrazolyl)-p-tolyl]amine ligands (R = H, Me, ^{i}Pr), H(^{R}MeMe), have been detailed elsewhere.[34] Briefly, H(^{R}MeMe) can be prepared in about 65% yield (after two steps) by first bromination of the commercially-available ditolylamine followed by a CuI-catalyzed amination reaction with the appropriate 3R-pyrazole.[39]After significant synthetic effort, an optimized convergent route to

Scheme 6.1. Summary of preparative routes to the NNN-pincer ligands used in this work.

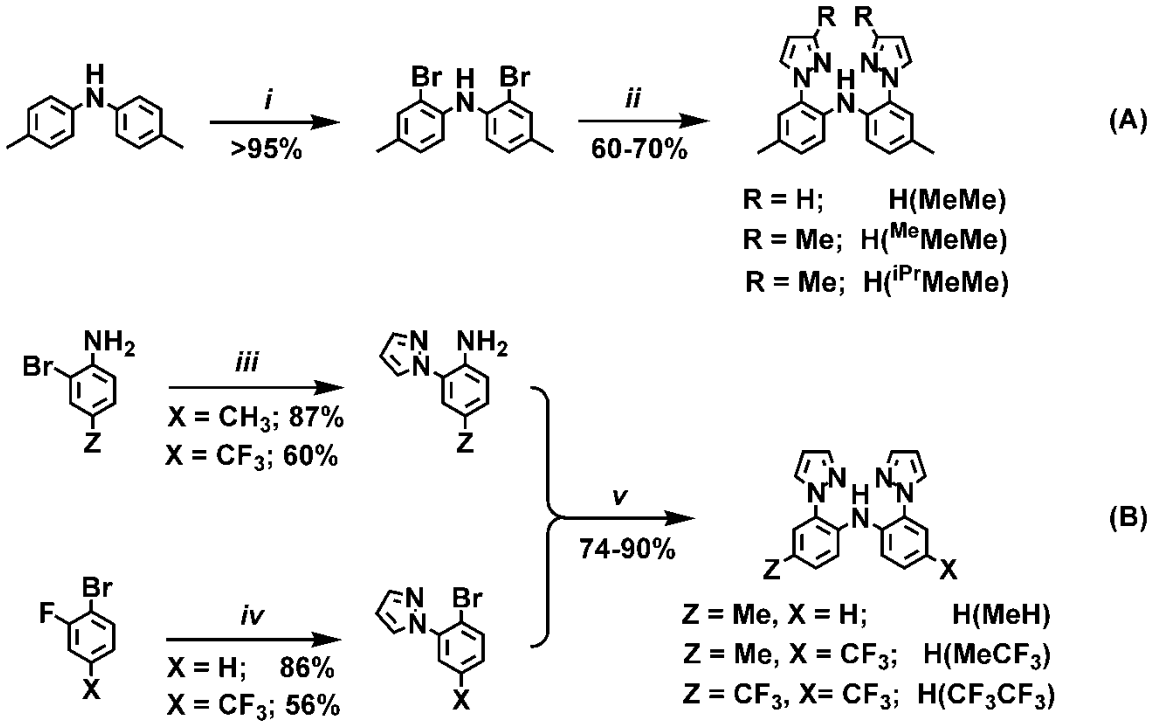

Key: *i*) Br_2, 1:1 CH_2Cl_2:MeOH 0^{o}C; *ii*) 3.5 equiv. Hpz, xs K_2CO_3, cat. CuI, cat.DMED, xylenes, reflux 24 h; *iii*) 1.1 Hpz, 1.2 Cs_2CO_3, cat. CuI, DMF; *iv*) NaH, Hpz, DMF, Δ 30 min.; *v*) cat. CuI, 1.2 Cs_2CO_3, dioxane, Δ 16 h.

ligands decorated with two different pyrazolylaryl arms , H(MeH) and H($MeCF_3$), and a ligand with two trifluoromethylaryls, H(CF_3CF_3),was discovered (Scheme 6.1B) that permitted fine-tuning of the electronic properties of the ligands. In this approach, each 'arm' of the appropriate ligand was constructed separately before being assembled together in a final step that employs a CuI-catalyzed amination reaction. That is, the appropriate commercially-available *para*-X-anilines (X = CF_3 or CH_3) were quantitatively *ortho*-brominated with NBS in CH_3CN at 0^oC, then a CuI-catalyzed amination reaction of the 2-bromo-4-X-anilines and pyrazole gave the corresponding 2-pyrazolyl-4-X-aniline "arm" in good yield.[40] The second 'arm' of the pincer ligand is prepared by a nucleophilic substitution reaction between sodium pyrazolide (prepared in-situ from NaH and Hpz) and commercially-available 1-bromo-2-fluorobenzeneor 1-bromo-2-fluoro-4-(trifluoromethyl)benzene in DMF. In the final step, the two separate arms are attached by a second, convenient amination reaction that employed 20 mol % CuI as a catalyst, 1.2 equiv Cs_2CO_3 as a base, and dioxane as a solvent. The use of this CuI catalyst system circumvented the need for expensive palladium catalysts and chelating phosphine co-catalysts (Xanthphos, DPEPhos, etc.) that gave lower yields of H($MeCF_3$) and H(CF_3CF_3) after longer periods of time. The possibility of using a lower catalyst loading was not investigated due to the success of the reactions and the low cost of CuI. Alternative preparative routes using various Ullman-type conditions (Cu^0 powder, Ph_2O, high temp > 200^oC) were low-yielding (15-25%) and gave significant amounts of 2,2'-pz_2biaryls as by-products. Furthermore, a direct route to H($MeCF_3$) and H(CF_3CF_3) similar to that for H(^{R}MeMe) was hampered by a number of factors, including: i) diarylamines with *para*-trifluoromethyl- substituents were neither

commercially-available nor well-known; ii) once in hand, the final coupling reaction between di(2-bromoaryl)amines and pyrazole (in xylene with K_2CO_3 and DMED) was often very sluggish, incomplete, and accompanied by unexpected decomposition or by-products including those derived from C-F activation.[41]

Since the deprotonated, anionic NNN-pincer ligands $(^{R}ZX)^{-}$ are six-electron donors in the ionic formalism (or five electron donors in the covalent formalism), square planar, sixteen-electron complexes of the type $(^{R}ZX)Rh(CO)$ were the anticipated products from known carbonylrhodium(I) reagents. Scheme 6.2 outlines the two successful synthetic routes that were used for the preparation of the six new carbonylrhodium(I) complexes, **1**-**6**.

Scheme 6.2. Preparation of carbonylrhodium(I) pincer complexes. (* yield from NMR spectroscopic measurement, not isolated).

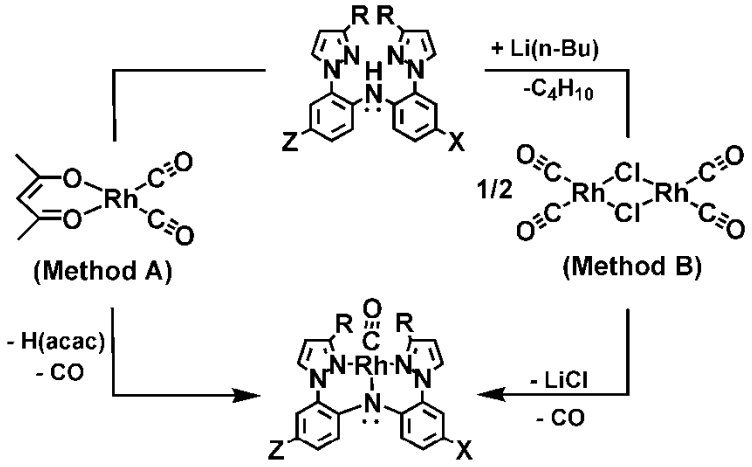

(L)Rh(CO) L = (^{R}ZX), (#)	Method A	Method B	ν_{CO} (cm^{-1}) acetone
MeMe, (1)	95%	42%	1955
^{Me}MeMe, (2)	75%	25%	1951
^{iPr}MeMe, (3)	45%*	37%	1948
MeH, (4)	84%	na	1956
$MeCF_3$, (5)	91%	42%	1962
CF_3CF_3, (6)	76%	32%	1968

na, not attempted

First, **1**-**6** could be obtained by an acetylacetone elimination route between the desired ligand and $Rh(CO)_2(acac)$. The metathetical reactions between $[Rh(CO)_2(\mu\text{-}Cl)]_2$ and "Li(^{R}ZX)" (prepared in-situ from the ligand and Li(n-Bu) at low temperature in THF, or in toluene for **3**) were also used to access all but **4**, which was not attempted. For complexes **1**, **2**, **5**, and **6**, the acetylacetone elimination route is superiorto the metathesis route because the former goes to completion (by NMR monitoring) and the separation of the desired products and byproducts is simpler; neither was true for **3**. For complex **3**, low yields were obtained by either route; however, the metathetical reactionusing toluene as a solvent gave the best isolated yield because the product mixture was the easiest to separate by fractional precipitation from pentane. The low isolated yield of **3** by eitherroute can be attributed to a number of factors. First, the acetylacetone elimination reaction is only about 45% complete after three days, and after such time significant free ligand, unreacted $Rh(CO)_2(acac)$, and unidentified decomposition products are also found. Secondly, the high solubilityof H(^{iPr}MeMe), **3**, and byproducts in most organic solvents complicates the separation of the complex from mixtures obtained by either route. Thirdly, the "Li(^{R}ZX)" saltsappear to be temperature-sensitive in THF and to a lesser extent in toluene, indicated by the loss of their characteristic cyan luminescence upon UV irradiation(254 nm, see Supporting Information) when solutions are warmedabove about -20^{o}C, which may contribute to the generally lower isolated yields of rhodium(I) products from the metathetical reactions.

Once isolated, the yellow complexes **1**-**6** appear air-stable as solids. Aerated solutions (hydrocarbon, ethereal, halocarbons, acetone or CH_3CN) of **1**-**6** are initially yellow but slowly darken and leave brown mirrors on the glassware. This decomposition

occurs slowly over the course of week or two for solutions in nonpolar hydrocarbons (pentane, hexane, benzene) but occurs more quickly with increasing polarity of other solvents (a few minutes for CH_3CN solutions). Thus, spectroscopic data were acquired using freshly prepared *yellow* solutions of **1-6** that were protected from the atmosphere when possible.

6.4.2. Description of crystal structures

Complexes **1-5** were characterized by single crystal X-ray diffractionthat verified the anticipated monomeric nature of the complexes and the square planar geometry of donor atoms about rhodium. The molecular structures are given in **Figures 6.2-6.6.**

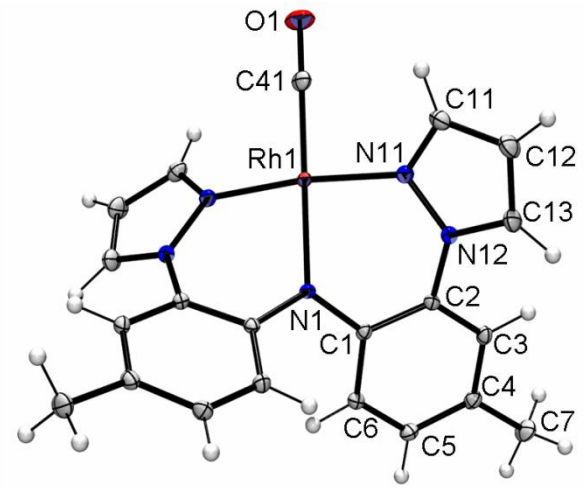

Figure.6.2. Structure of (MeMe)Rh(CO), **1**.Selected bond distances (Å): Rh1-N1, 2.036(2); Rh1-N11, 2.024(1); Rh1-C41, 1.832(2); C41-O1, 1.148(3); Selected bond angles (^{o}): N1-Rh1-C41 180.0; N11-Rh1-N11', 173.08(7); N11-Rh1-N1, 86.54(3); C41-Rh1-N11, 93.46(3).

In each structurally characterized complex, the RhN_3C kernel adopts a distorted square planar geometry (sum of angles about rhodium = 360º) where the two acute N11-Rh-N1

and N21-Rh-N1 angles (Fig. 6.3) give rise to non-linear ligating *trans*- pyrazolyl nitrogens, with N_{pz}-Rh-N_{pz} angles that range between 169.0(1)^{o} for **3** to 173.8(2)^{o} for **5**.

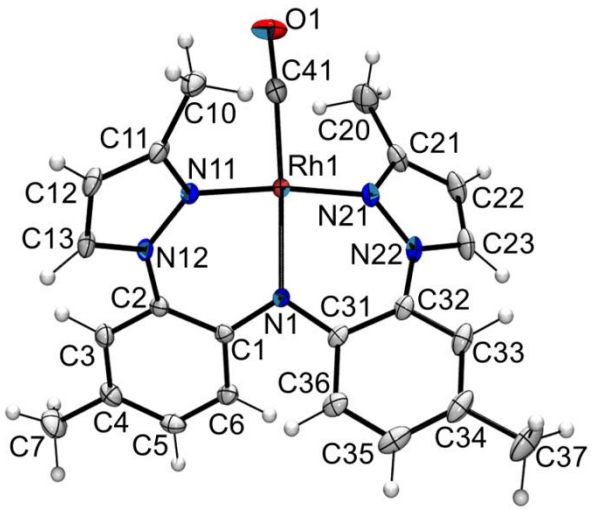

Figure.6.3. Structure of (^{Me}MeMe)Rh(CO) inthe crystal of **2**·C_6H_6.Selected bond distances (Å):. Rh1-N1, 2.039(2); Rh1-N11, 2.039(2); Rh1-N21, 2.032(2); Rh1-C41, 1.813(2); C41-O1, 1.154(3); Selected bond angles (^{o}): N1-Rh1-C41 176.0(1); N11-Rh1-N21 173.2(1);N1-Rh1-N11, 86.7(1); N21-Rh1-N1, 86.6(1); C41-Rh1-N11, 94.9(1); C41-Rh1-N21, 91.9(1).

The rhodium-nitrogen(pyrazolyl), Rh-N_{pz}, bond distances increase slightly with increasing steric bulk of the 3-pyrazolyl substituent. Thus, the average Rh-N_{pz} distances of 2.025(1) Å and 2.028(6) Å (for two independent units) in each **1** and **5,** respectively, are comparable to or shorter than 2.035(2) Å for **2** which in turn is shorter than that of 2.055(2) Å in **3**. All of the Rh-N_{pz} bond distances in **1**-**5** are comparable to those found in $[EtN(CH_2pz^*)_2]Rh(CO)]^+$ (pz* = 3,5-dimethylpyrazolyl, avg 2.019(3) Å),[42] $\{[O(CH_2pz^*)_2]Rh(CO)\}^+$ (avg. 2.037(4) Å),[43] or $\{[S(CH_2CH_2pz^*)_2]Rh(CO)\}^+$ (avg 2.044(2) Å).[44] The remaining bond distances for the rhodium-amido (Rh-N1 ranging from 2.027(2) Å in **1** and 2.050(4) Å in **5**) and rhodium carbonyl (Rh-C41 ranging from

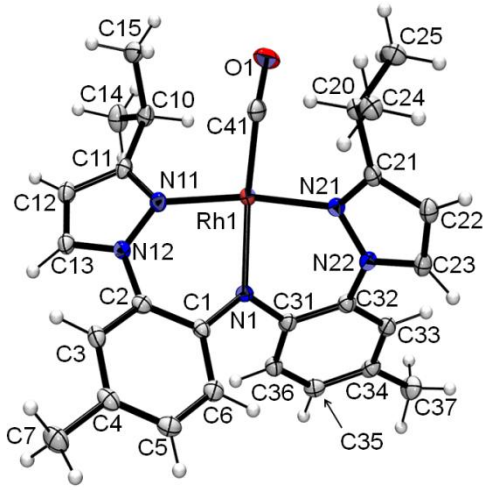

Figure 6.4. Molecular structure and atom labeling for one of the crystallographically-independent units in the crystal of **3**

Selected bond distances (Å):. Rh1-N1, 2.0301(17); Rh1-N11, 2.0457(17); Rh1-N21, 2.0516(18); Rh1-C41, 1.820(2); C41-O1, 1.155(3); Selected bond angles (°): N1-Rh1-C41 175.94(9); N11-Rh1-N21 169.93(7); N1-Rh1-N11, 85.56(7); N21-Rh1-N1, 84.78(7); C41-Rh1-N11, 93.81(8); C41-Rh1-N21, 96.03(9)

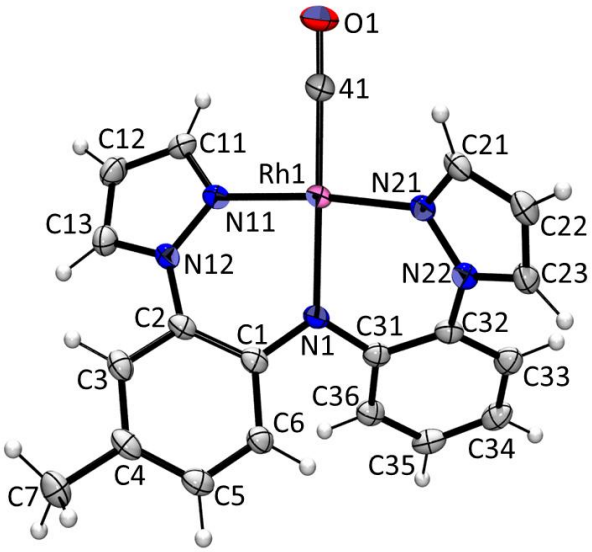

Figure 6.5. Molecular structure and atom labeling for one of the crystallographically-independent units in the crystal of **4** in the structure of **4**·C_6H_6

Selected bond distances (Å): Rh1-N1, 2.044(2); Rh1-N11, 2.014(2); Rh1-N21, 2.021(2); Rh1-C41, 1.828(3); C41-O1, 1.147(4); Selected bond angles (°): N1-Rh1-C41 178.36(11); N11-Rh1-N21, 173.36(9); N11-Rh1-N1, 87.23(9); N21-Rh1-N1, 87.28(9); C41-Rh1-N11, 91.71(11); C41-Rh1-N21, 93.86(11).

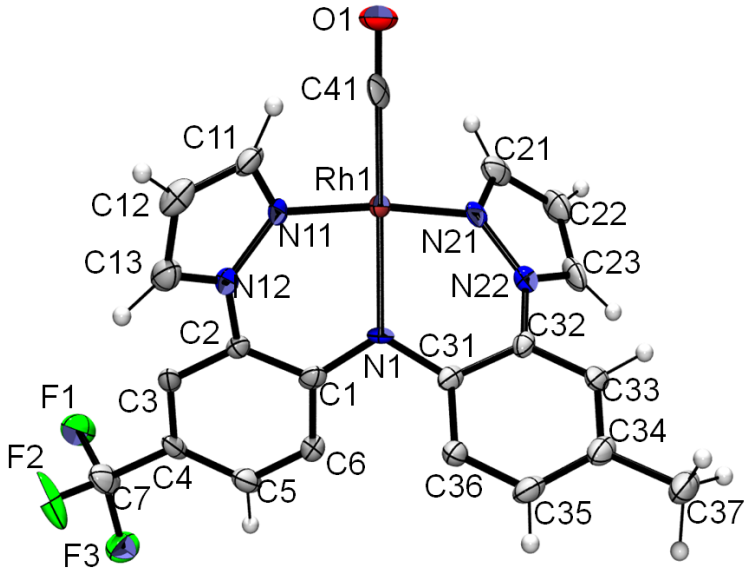

Figure 6.6. Molecular structure and atom labeling for one of the crystallographically-independent units in the crystal of **5**.

Selected bond distances (Å):. Rh1-N1, 2.049(4); Rh1-N11, 2.030(5); Rh1-N21, 2.026(5); Rh1-C41, 1.819(5); C41-O1, 1.158(6); Selected bond angles (^{o}): N1-Rh1-C41 179.4(3); N11-Rh1-N21 173.62(16); N1-Rh1-N11, 86.8(2); N21-Rh1-N1, 86.8(2); C41-Rh1-N11, 93.2(3); C41-Rh1-N21, 93.2(3

1.812(6) Å in **5** to 1.834(2) Å in **3** and C41-O1 ranging from 1.147(2) Å in **3** to 1.170(8) Å in **5**) fragments in line with other carbonylrhodium(I) complexes of amido-anchored pincer complexes.[19-22,24,45]

6.4.3. IR Spectroscopic Data

As expectedfor the series of complexes **1**, **4**, **5** and **6**, the frequency for the C-O stretching band in the IR spectrum of each complex increased with the extent that the electron-donating methyls were replaced by either hydrogen or by electron-withdrawing trifluoromethyl groups (ν_{CO} 1952 cm^{-1} for **1**, 1954 cm^{-1} for **4**, 1958 cm^{-1} for **5**, and 1962

cm^{-1} for **6** as KBr pellets).Although the number of data points is rather limited, there is a strong correlation between the energy of the C-O stretching frequency and the average of the σ_p Hammett parameter[46]of *para*-X-aryl substituents (σ_p = -0.17 for Me and 0.53 for CF_3): $\nu_{CO}=13.984[(\Sigma\sigma_p)/2] + 1954.9$, $R^2 = 0.987$ (see Fig. 6.7).By comparisonof

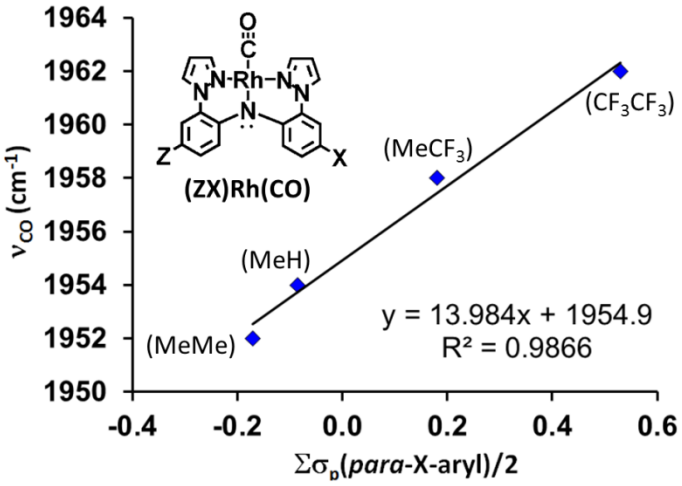

Figure 6.7. Correlation between the C-O stretching frequency and the average of the σ_p Hammett parameters (σ_p =0 for H, -0.17 for Me, and 0.53 for CF_3) of *para*-X-aryl substituents in various (ZX)Rh(CO) pincer complexes.

C-O stretching frequencies for **1**-**6** with those of other pincer complexes with various donor sets, it is apparent that the electronic nature of the amido nitrogen anchor *trans*- to the carbonyl rather than the type of flanking Lewis donors in pincer complexes dictates the energy of the C-O stretching vibrations, as might be expected. That is, the ν_{CO} range of 1948-1968 cm^{-1} for **1**-**6**is comparable to the frequency of 1967 cm^{-1} found in cationic carbonylrhodium(I) complexes with bis(carbene)-based pincers of the type 2,6-bis(alkylimidazol-2-ylidene)-pyridine[47]and is between those frequencies found for carbonylrhodium(I) complexes of carbazole-based pincers 1,8-bis(imidazolin-2-yliden-1-yl)carbazolide (CNC-bimca, 1916 cm^{-1})[18]or 1,8-di(phenylimino)-3,6-

dimethylcarbazolides (R = Ph in Chart 1 **F**, 1980 cm^{-1})[24].These ν_{CO} values for **1**-**6** are also comparable to 1957cm^{-1}found for the charge-neutral $Rh(PEt_3)_2(CO)I$,[48] to 1961 cm^{-1} for $Rh(Cp)(CO)(PPh_3)$.[49]

6.4.4.. Spectroscopic Studies of Oxidative Addition Reactions

Given the electron-rich nature of **1**-**6**,oxidative addition reactions with MeI, EtI, and, in one case, I_2 were investigated to determine whether any reaction would occur, and if so, to discern to what extent, if at all, the reaction rates or the nature of the products were affected by the different *para*-X-aryl or 3-R-pyrazolylsubstituents. Indeed, IR and NMR spectroscopic studies verified that oxidative addition reactions occurred in all cases, as illustrated in Scheme 6.3. That is, the original IR band centered in theν_{CO} range of 1948-1968 $cm^{-1}$of each spectrum of **1**-**6** in acetone was replaced by a new band in the range 2047-2078 cm^{-1} for the appropriate (^{R}ZX)Rh(E = Me or Et)(CO)(I) complexes $\mathbf{7_E}$-$\mathbf{12_E}$, as per Scheme 6.3. The original set of hydrogen resonances were replaced cleanly with new sets of NMR signals after reaction with alkyl iodides, as exemplified for the formation of

Scheme 6.3.Summary of oxidative addition reactions of **1**-**6** to form $\mathbf{7_E}$-$\mathbf{12_E}$.

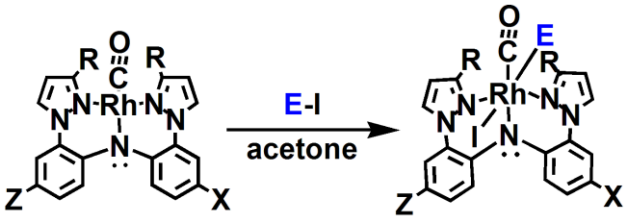

(L)Rh(E)(CO)(I)			ν_{C-O} (cm^{-1})
Ligand	E	(#)	(acetone)
MeMe	Me	(7_{Me})	2063
	Et	(7_{Et})	2054
	I	(7_{I})	2078
^{Me}MeMe	Me	(8_{Me})	2057
	Et	(8_{Et})	2052
^{iPr}MeMe	Me	(9_{Me})	2051
	Et	(9_{Et})	2047
MeH	Me	(10_{Me})	2069
	Et	(10_{Et})	2067
$MeCF_3$	Me	(11_{Me})	2069
	Et	(11_{Et})	2067
CF_3CF_3	Me	(12_{Me})	2075
	Et	(12_{Et})	2070

$\mathbf{7_{Et}}$ in Fig.6.8.It is likely that all complexes share the configuration with alkyl and iodide groups *trans*- to one another, as shown in Scheme 6.3, given: *i*) the solid-state structural studies of three derivatives ($\mathbf{7_{Et}}$, $\mathbf{7_I}$, and $\mathbf{8_{Me}}$,vide infra),*ii*)the similarity in IR and NMR spectroscopic datafor all complexes (for instance, a *cis*– configuration is expected to lead to drastically different ν_{CO} stretching frequencies due the *trans*- effect), and *iii*) because, kinetically, oxidative addition of alkyl halides to square planar d^8complexes typically lead to *trans*- disposition of added fragments.[50]The different non-pincer (alkyland iodide) ligands differentiate the "arms" of the non-planar pincer ligandand gives low (C_1)

symmetry to the complexes. For a *trans*- disposition of alkyland iodide ligands as indicated in Scheme 6.3, one pincer arm is proximal to the iodide group while

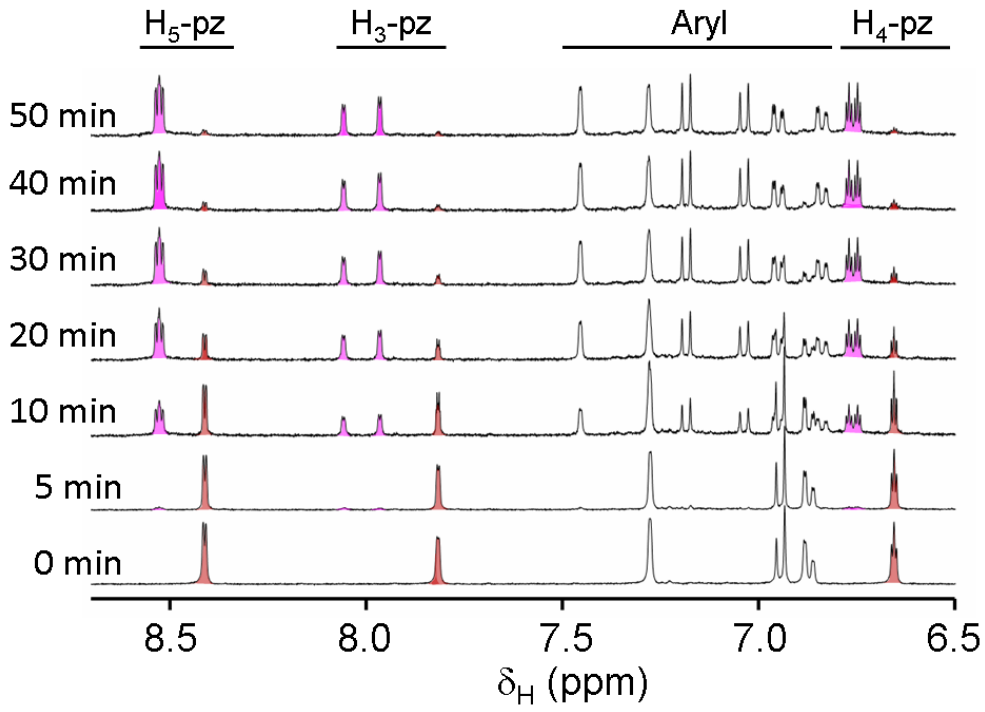

Figure.6.8. The downfield region of the ^{1}H NMR spectra during heating a 1:10 mixture of **1** : EtI in acetone-d_6 at 45^{o}C to form $\mathbf{7_{Et}}$. The resonances for pyrazolyl hydrogens are shaded.

the second pincer arm is closer to the alkyl group E. Thus, two sets of pyrazolyl and aryl hydrogen resonances are found in the NMR spectrum for the rhodium(III) complexes $\mathbf{7_E}$-$\mathbf{9_E}$ and $\mathbf{12_E}$ (E = Me, Et). The NMR spectra for complexes $\mathbf{10_E}$and $\mathbf{11_E}$ (E = Me, Et) with different pincer arms(a *p*-tolyl and either a phenyl or a *p*-trifluoromethylaryl, respectively) are more complicatedbecause two isomers are present in each. The isomers can be distinguished by the position of the pincer arms relative to the iodide ligand. One possible isomer places the iodide ligand in van der Waals contact with the tolyl arm of the diarylamido anchor while the second isomer places the halide in contact with the

other (phenyl or trifluoromethylaryl) arm, as shown in Fig. 6.9. Molecular mechanics and semi-empirical (PM3) equilibrium geometry calculations indicate that the isomer

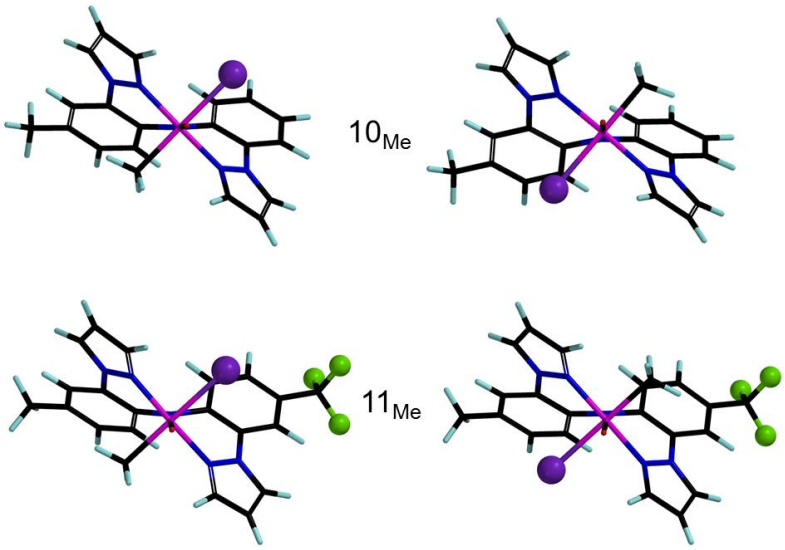

Figure.6.9. Two low-energy isomers of $\mathbf{10_{Me}}$(top) and $\mathbf{11_{Me}}$ (bottom) from PM3 calculations. The isomers on the left with the iodide (purple ball) closer to phenyl or trifluoromethylarylare slightly lower energy than the isomers on the right.

with the iodide ligand in van der Waals contact with the less electron-rich *p*-trifluoromethylaryl ring, left of Fig. 6.9, is lower energy than the isomer with the iodide group in contact with the more electron-rich tolyl group, right of Fig. 6.9. Integration of well-resolved signals in the 3/5-Hpz and Rh-alkyl regions of the ^{1}H NMR spectrum of $\mathbf{10_E}$and$\mathbf{11_E}$ (E = Me, Et) indicate a 10:9 relative ratio of isomers for $\mathbf{10_E}$and a7:3 ratio for $\mathbf{11_E}$. Thus, empirically, the two isomers (or pathways to them) are nearly equal in energy but the very different electronic properties between CF_3 and CH_3 groups in $\mathbf{11_E}$ versus the H and CH_3 groups in $\mathbf{10_E}$gives a greater preference for one isomer over the other.

6.4.5. Kinetic Studies of Oxidative Addition Reactions

The data for rate constant determinations at various temperatures were obtained by relative integration of well-resolved signals for **1**-**5** and their corresponding oxidative

addition product $\mathbf{7_{Et}}$-$\mathbf{12_{Et}}$ in two regions of the spectrum- the H_5-pyrazolyl region and the H_4-pyrazolyl region, (as in Fig. 6.8). Linear plots were obtained for *ln* [**1**-**6**] vs time, see Figure 6.10 for sample data from one experiment involving **1**. Each reaction was performed a minimum of three times

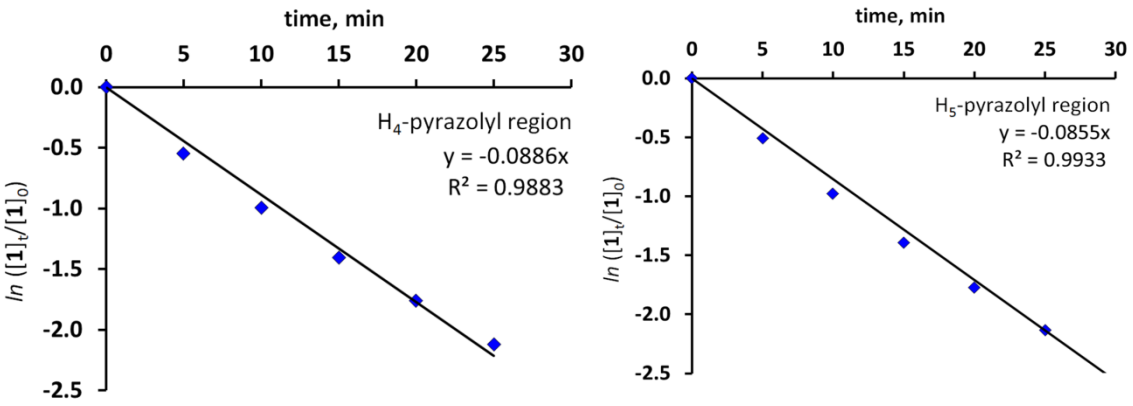

Figure 6.10. Plots showing of the disappearance of **1** over time from relative integration of resonances for **1** and $\mathbf{7_{Et}}$ in the H_4-pyrazolyl region (left) and the H_5-pyrazolyl region (right) of the ^{1}H NMR spectrum of a mixture of **1** and EtI in acetone-d_6 at 45^{o}C

(experiments with **1**, **4**, **5**, and **6** were performed four times). The reported k_{obs} and k_2 of Table 6.5 are the average of all values obtained from each region of the spectrum in each experiment (i.e from six or eight data points and associated calculations). For Eyring analyses, a minimum of three different experiments were performed at various spectrometer temperatures between 35^{o}C and 50^{o}C, depending on the relative rates of the reactions, see Table 6.6 and Figure 6.11. For convenience, slower reactions were generally perfomed at higher temperatures (i.e., 40, 45, and 50 ^{o}C for **3**) where as faster

reactions could also be performed at lower temperatures (35, 40, 45, and 50^{o}C for **1**) over a reasonable period of time (several hours).

(^{R}ZX)Rh(CO) Complex	[Rh], *M*	[EtI], *M*	k_2 (318K), $M^{-1}s^{-1}$	$\Delta^{\ddagger}H^{o}$, kJ mol^{-1}	$\Delta^{\ddagger}S^{o}$, J K^{-1} mol^{-1}	$\Delta^{\ddagger}G^{o}_{318}$, kJ mol^{-1}
1	0.031	0.31	8.0×10^{-3}	59	-9.8×10^{1}	90
2	0.030	0.30	1.6×10^{-3}	54	-1.3×10^{2}	95
3	0.025	0.25	1.4×10^{-3}	52	-1.4×10^{2}	97
4	0.034	0.34	7.9×10^{-3}	54	-1.2×10^{2}	91
5	0.025	0.25	2.5×10^{-3}	49	-1.4×10^{2}	94
6	0.026	0.26	8.2×10^{-4}	50	-1.5×10^{2}	98

Table 6.5. Summary of kinetic data for reactions between (^{R}ZX)Rh(CO) and iodoethane in acetone-d_6

The reactions between 0.03 *M***1**-**6** in acetone-d_6 and 10-fold excess iodomethane were instantaneously complete (at least within seconds) at 295 K. By performing similar reactions at 295 K but in the less polar solvent benzene, the oxidative addition reaction of MeI to **1** was instantaneously complete but those reactions involving complexes with trifluoromethyl- pincer substituents(**5** and **6**) were slow enough to measure pseudo-first order rate constants.

	average k_2, ($M^{-1}s^{-1}$)			
Compound	35 °C	40 °C	45 °C	50 °C
(MeMe)Rh(CO), **1**	$4.027x10^{-3}$	$6.429x10^{-3}$	$7.981x10^{-3}$	$12.84x10^{-3}$
(^{Me}MeMe)Rh(CO), **2**	---	$0.9892x10^{-3}$	$1.567x10^{-3}$	$1.943x10^{-3}$
(^{iPr}MeMe)Rh(CO), **3**	---	$0.9333x10^{-3}$	$1.371x10^{-3}$	$1.378x10^{-3}$
(MeH)Rh(CO), **4**		$5.165x10^{-3}$	$7.946x10^{-3}$	$10.091x10^{-3}$
($MeCF_3$)Rh(CO), **5**	---	$1.457x10^{-3}$	$2.458x10^{-3}$	$2.774x10^{-3}$
(CF_3CF_3)Rh(CO), **6**	$0.4187x10^{-3}$	$0.5942\ x10^{-3}$	$0.8219x10^{-3}$	$1.068x10^{-3}$

Table 6.6. Temperature dependence of average second order rate constants, k_2, for reactions between EtI and complexes **1**-**6**

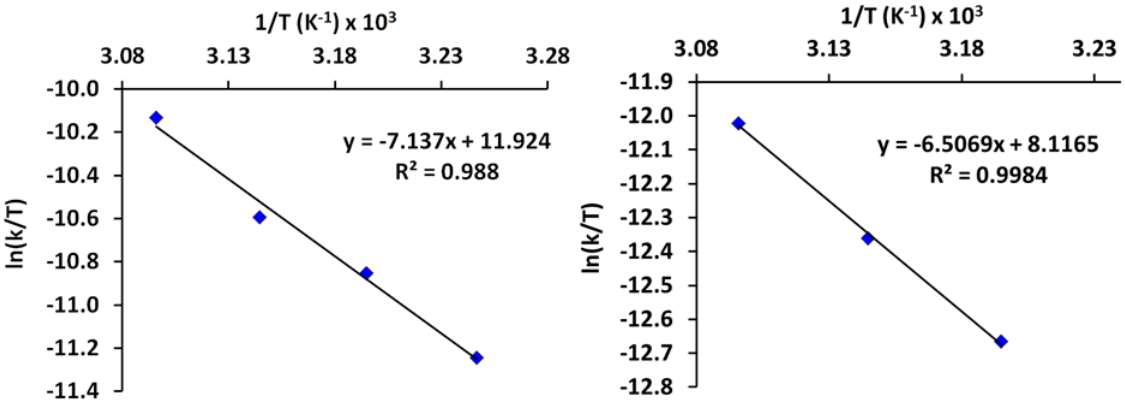

Figure 6.11. Reprentative Eyring plots for reactions between EtI and **1(left)2 (right)** in acetone-d_6

In these latter two cases, the pseudo-first order half-life, $t_{1/2}$, was on the order of 1 min for **5** and 26 min for **6**. Qualitatively, the instantaneous reactions in acetone parallel a similar

observation reported for (CNC-bimca)Rh(CO)which was found by stopped-flow spectroscopic measurements to exhibit the highest rate forthe oxidative addition of CH_3I by a rhodium(I) complex (k_2 = 3.4 X $10^{-3}M^{-1}s^{-1}$, 196 K in THF).[18]The rapidity of the oxidative addition of **1**-**6** with iodomethane prompted examination of reactions with iodoethane. It is known [49-51] that the rate of oxidation addition of iodoethaneto rhodium(I) complexes is generally about 100 to 1000 times slower than those reactions involving iodomethane because theadded steric bulk hinders the S_N2-attack by rhodium(I). This strategy permitted successful evaluation of rate constants and activation parameters for reactions involving the entire series of complexes **1**-**6**, as summarized in Table6.5. At 318K, linear plots of *ln* [(^{R}ZX)Rh(CO)] versus time were obtained which showed that the reactions were first order in each **1**-**6**. Moreover, plots of k_{obs} versus [EtI] were linear, indicating the reaction to be first order in EtI and, therefore, second order overall as in Equation 1.Theactivation parameters for the

$$\text{rate} = k_2[(^R\text{ZX})\text{Rh(CO)}][\text{EtI}] \qquad (1)$$

reactions between EtI andeach carbonylrhodium(I) complex were obtained by Eyring analyses of data from experiments performed at various temperatures between 303 and 323 K. As typical for rhodium(I) chemistry, the activation entropies are all large and negative,characteristic of a highly-organized transition statefor oxidative addition reactions that proceed by an S_N2 mechanism.[51]Such a mechanism is also suggested from comparison of rate constants of reactions involving **1**-**3**. Complex **1** is the least electron-rich of the three from IR data, yet the reaction with EtI is the fastest. Complex **3** is the most electron-rich owing to the presence of i-Pr pyrazolyl substituents but it reacts slowest of the three complexes owing to steric bulk. Sequential substitution of methyl

groups in **1** for hydrogen (in **4**) or electron-withdrawing trifluoromethyl groups (in **5** and **6**) results in predictably slower reactions. There is a good linear correlation between $logk_2$ and the average of the Hammett parameter, σ_p, for the *p*-X-aryl substituents, $logk_2 = -1.494(\Sigma\sigma_p/2) - 2.3013$ ($R^2 = 0.987$; see Fig. 6.12, which signifies that remote electronic effects can provide a powerful means to fine-tune reactivity in these systems without interfering with the steric profile near the metal center.

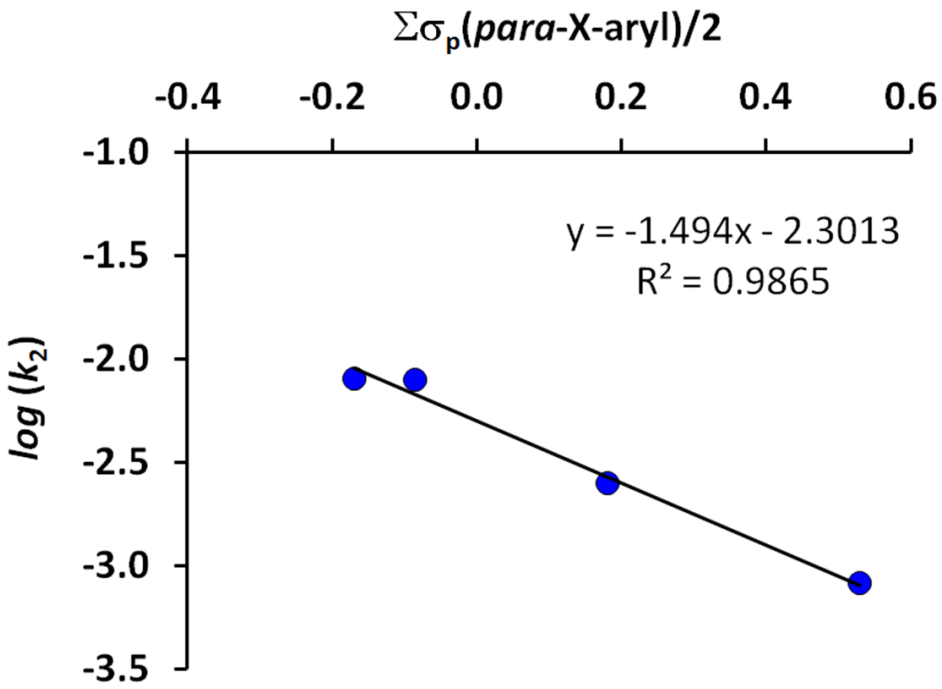

Figue 6.12. Correlation between Hammett σ_p parameter for para-X-aryl substituents of pincer ligands and log (second order rate constant k_2) for oxidative addition reactions with EtI in acetone at 45°C

6.4.6. Synthetic Studies of Oxidative Addition Reactions.

During attempts to isolate bulk quantities of $\mathbf{7_E}$-$\mathbf{12_E}$ (E = Me, Et, or I, as appropriate) for further reaction chemistry it was discovered that these complexes were

metastable. In fact, we have only been successful at isolating complexes $\mathbf{7_{Me}}$, $\mathbf{7_{I}}$, and $\mathbf{8_{Me}}$ as *analytically pure* solids from synthetic-scale (decigram to gram scale) reactions performed in acetone or benzene. All other complexes in Scheme 6.3 give mixtures from preparative-scale reactions in benzene or acetone owing to various competitive decomposition reactions that appear to be accelerated by excess CH_3I, donor solvents, and by solvent removal. The ability to isolate $\mathbf{7_{Me}}$, $\mathbf{7_{I}}$, and $\mathbf{8_{Me}}$ in bulk, pure form is due to the combination of the rapidity of their preparative oxidative addition reactions andthe relatively slow rates of their decomposition reactions. Thus, mixing benzene solutions of **1**or **2** and iodomethane or of **1** and iodine for a minimum amount of time required for complete reaction as monitored by IR or NMR spectroscopy, followed by removing volatiles under vacuum gave quantitative yields of the desired rhodium(III) species as red-orange or orange air-stable powders. Complex $\mathbf{8_{Me}}$ exhibits relatively low solubility in benzene or acetone compared to the other new complexes and precipitates as X-ray quality crystals from unstirred solutions. The other two isolable complexes are soluble in CH_2Cl_2 and acetone, however, solutions begin to deposit insoluble decomposition products (vide infra) over the course of several hours at room temperature. It is possible to isolate a few X-ray quality crystals of various other 'metastable' complexes if the rate of crystallization competes with the rate of decomposition. Thus, a few X-ray quality crystals of $\mathbf{7_{Et}}$and $\mathbf{7_{I}}$ were obtained along with copious decomposition products (vide infra) by allowing a layer of hexane to diffuse into a CH_2Cl_2 solution of $\mathbf{7_{Et}}$ or by slow evaporation of an acetone solution of $\mathbf{7_{I}}$, over the course of a day. The structures of $\mathbf{7_{Et}}$, $\mathbf{7_{I}}$, and $\mathbf{9_{Me}}$ are found in Figures 6.13-6.15 respectively.

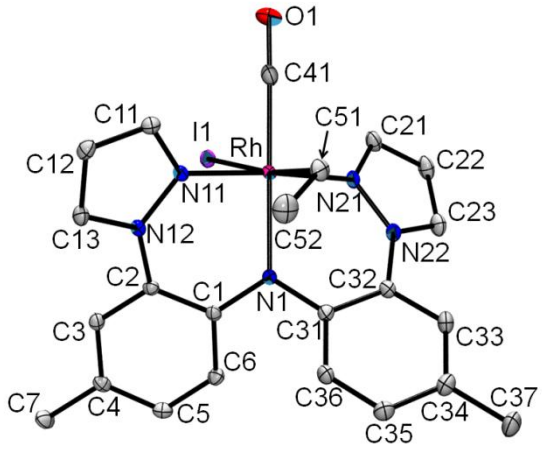

Figure.6.13. Structure of (MeMe)Rh(Et)(CO)(I), $\mathbf{7_{Et}}$, with hydrogens removed for clarity. Selected bond distances (Å):. Rh1-N1, 2.035(1); Rh1-N11, 2.011(1); Rh1-N21, 2.030(1); Rh1-C51, 2.110(2);Rh1-C41, 1.890(2); C41-O1, 1.126(2); Rh1-I1, 2.8708(2); Selected bond angles (^{o}): N1-Rh1-C41 179.41(7); N11-Rh1-N21 175.25(6); I1-Rh1-C51, 173.17(5); N1-Rh1-N11, 88.96(5); N21-Rh1-N1, 86.62(6); C41-Rh1-I1, 83.67(6); C41-Rh1-C51, 89.50(7).

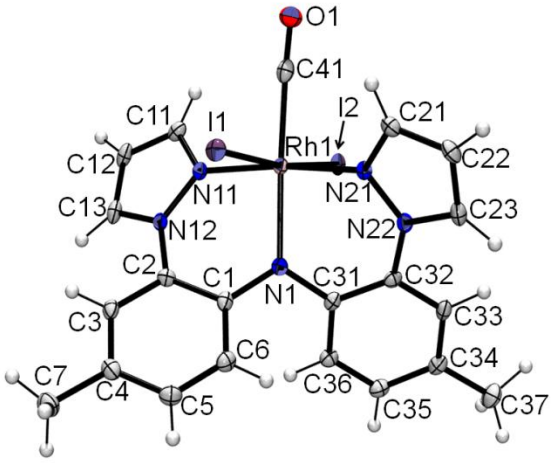

Figure.6.14. Structure of (MeMe)Rh(I)$_2$(CO), $\mathbf{7_I}$.Selected bond distances (Å):. Rh1-N1, 2.024(2); Rh1-N11, 2.020(2); Rh1-N21, 2.023(2); Rh1-C41, 1.916(3); C41-O1, 1.102(4); Rh1-I1, 2.6907(3); Rh1-I2, 2.6784(3); Selected bond angles (^{o}): N1-Rh1-C41 176.8(1); N11-Rh1-N21 174.4(1);N1-Rh1-N11, 86.8(1); N21-Rh1-N1, 87.7(1); C41-Rh1-I1, 89.0(1); C41-Rh1-I2, 83.9(1); I1-Rh1-I2, 172.83(1).

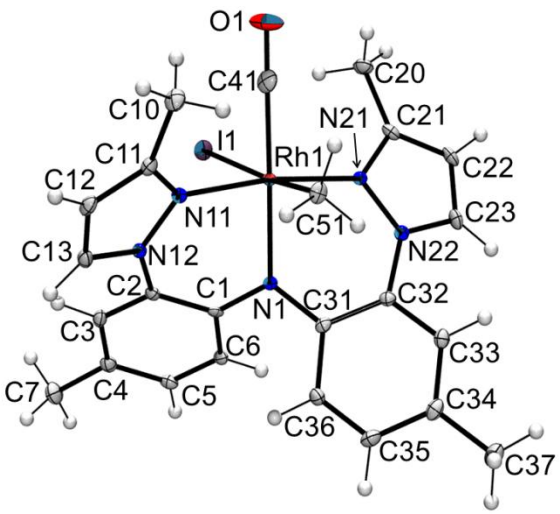

Figure.6.15. Structure of (^{Me}MeMe)Rh(Me)(CO)(I) in the crystal of $\mathbf{8_{Me}\cdot C_6H_6}$.Selected bond distances (Å):. Rh1-N1, 2.035(2); Rh1-N11, 2.052(3); Rh1-N21, 2.046(3); Rh1-C41, 1.892(3); C41-O1, 1.126(4); Rh1-C51, 2.093(3), Rh1-I1, 2.8604(3); Selected bond angles (^{o}): N1-Rh1-C41 179.7(1); N11-Rh1-N21 172.9(1);N1-Rh1-N11, 86.6(1); N21-Rh1-N1, 86.6(1); C51-Rh1-I1, 175.6(1); C41-Rh1-C51, 90.4(1).

Each structure verified the *trans*- disposition of the added iodide and/or alkyl ligands. The biggest difference between common fragments in the structures of **1,** $\mathbf{7_{Et}}$ and $\mathbf{7_I}$ involve the metal-carbonyl moieties. The Rh-C41 bond of 1.890(2) Å in $\mathbf{7_{Et}}$ and of 1.916(3) Å in $\mathbf{7_I}$ is each longer than that of 1.832(2) Åin **1**. The C-O bond distance of 1.126(4) Å in $\mathbf{7_{Et}}$ and 1.102(4) Å in $\mathbf{7_I}$ are also shorter than that of 1.148(3) Å in **1**. These structural differencescan be explained by the expected relative capability for a rhodium(III) versus a rhodium(I) center to engage in back-bonding to the carbonyl group. The greater electron σ-donating character of an alkyl versus iodide groups, first evident in IR spectra of $\mathbf{7_{Et}}$ and $\mathbf{7_I}$, is also manifest in the discrepancy in the bond distances of the rhodium-carbonyl fragment in $\mathbf{7_{Et}}$ versus $\mathbf{7_I}$. Surprisingly, the Rh-N bonds and associated angles about the metal-pincer moiety in the three complexes **1,** $\mathbf{7_{Et}}$, and $\mathbf{7_I}$ are remarkably similar withRh1-N1,2.035(1), 2.024(2), and 2.036(2) Åfor $\mathbf{7_{Et}}$,$\mathbf{7_I}$,and **1**,

respectively.Likewise, the average Rh-N_{pz}distances of 2.021(1), 2.022(2),and 2.024(1) Å for $\mathbf{7_{Et}}$,$\mathbf{7_{I}}$,and **1,** respectively,are essentially equivalent. The bond distances involving the carbonyl moiety in $\mathbf{8_{Me}}$ (Rh1-C41, 1.892(3) Å, C41-O1, 1.126(4)Å) are in accord with a lower degree of metal-carbonyl back-bonding compared to that in **2** (Rh1-C41, 1.813(2) Å, C41-O1, 1.154(3) Å). The Rh1-N1 amido bond distance in $\mathbf{8_{Me}}$ of 2.035(2) Å is statistically-indistinguishable from that in **2** of2.039(2) Å. In contrast, there is a significant difference in average Rh-N_{pz} bond distances between those in $\mathbf{8_{Me}}$, 2.049(3) Å, and in **2,** 2.036(2) Å. Presumably unfavorable steric interactions between 3-methylpyrazolyl substituents and axial methyl and iodo groups are important enough to cause Rh-N_{pz} bond lengthening in the rhodium(III) complex relative to the rhodium(I) center in **2**.

Complexes $\mathbf{7_E}$, $\mathbf{10_E}$, $\mathbf{11_E}$ and $\mathbf{12_E}$ (with un-substituted pyrazolyl groups on the pincer ligand) decompose over the course of several hours with CO dissociation to give highly insoluble iodide-bridged dimers, exemplified for the conversion of $\mathbf{7_E}$ to crystallographically-verified cases of dimeric $\mathbf{13_E}$ (E = Me, I) in Scheme 6.4. Views of the structure of $\mathbf{13_I}$and $\mathbf{13_{Me}}$are found in Fig. 6.16 and 6.17.

Scheme 6.4.Unexpected decomposition reactions of $\mathbf{7_E}$ to form dimeric species $\mathbf{13_E}$.

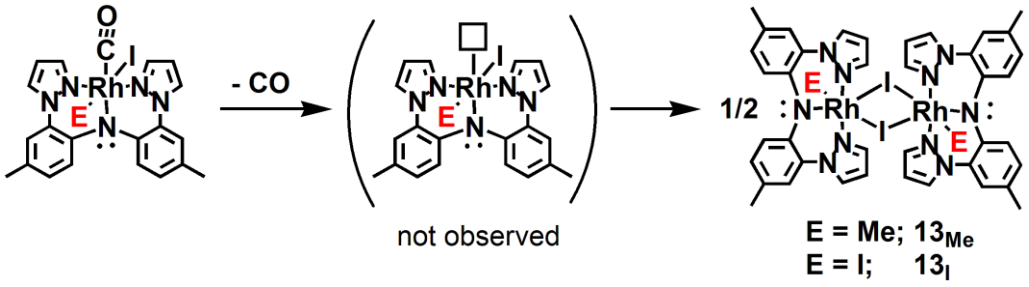

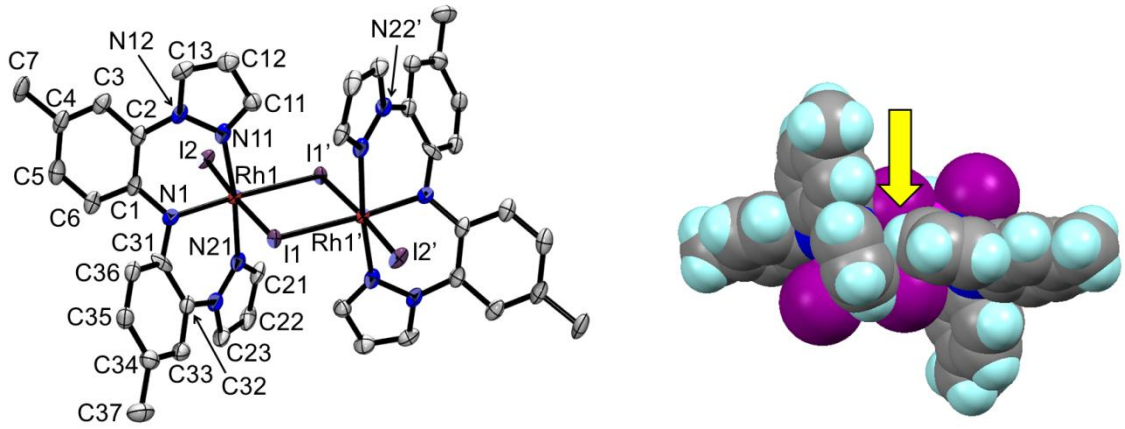

Figure.6.16.Left: Structure of [(MeMe)Rh(I)(μ-I)]$_2$, **13$_I$**, with atom labeling and hydrogens removed for clarity. Selected bond distances (Å): Rh1-N1, 2.006(5); Rh1-N11, 2.018(5); Rh1-N21, 2.034(5); Rh1-I1', 2.6812(6); Rh1-I1, 2.7215(6); Rh1-I2, 2.6478(6); Selected bond angles (^{o}): N1-Rh1-I1' 176.2(2); N11-Rh1-N21, 173.5(2); N11-Rh1-N1, 87.1(2); N21-Rh1-N1, 86.8(2); I1-Rh1-I2, 174.03(2); I1-Rh1-I1', 83.77(2); I2-Rh1-I1', 90.3(2); Right: Space-filling structural representation with arrow denoting potential steric interactions between pyrazolyl rings.

The rhodium-amido nitrogen bond distance in **13$_I$**, Rh1-N1 2.006(5) Å, is significantly shorter than those found in **1**, 2.036(2) Å, **7$_{Et}$**, 2.035(1) Å, or **7$_I$**, 2.024(2) Å Again, the average Rh-N$_{pz}$ 2.026(5) Å in **13$_I$** is invariant across this series of complexes. Also, the terminal Rh1-I2 bond distance of 2.6478(6) Å in **13$_I$** is slightly shorter than the range of Rh-I distancesfound among the two crystallographically-independent units in **7$_I$** of 2.6768(3) to 2.6984(3) Å. Thecentrosymmetric Rh_2I_2 metallacycle of **13$_I$** has two shorter 2.6812(6) Å Rh-I bonds and two longer 2.7215(6) Å Rh-I bondssimilar to other complexes with an Rh_2I_2core.[52]The non-bonded Rh···Rh and I···I distances within the metallacycle of **13$_I$**are 4.0222(7) and 3.6071(6) Å, respectively. The longer Rh-I bonds of the metallacycle in **13$_I$** are *trans*- to the terminal Rh1-I2 or Rh1'-I2' bonds. A similar geometry with longer Rh-I bonds of the metallacycle being situated *trans*- to terminal

ligands persists in the structure of $\mathbf{13_{Me}}$. It is noted that the structure of $\mathbf{13_{Me}}$ displays about a 9% substitution of methyls for iodides or could be considered a 91:9 co-crystal of $\mathbf{13_{Me}}$:$\mathbf{13_{I}}$. Thus, the decomposition pathway is likely more complicated than. simple CO dissociation and subsequent oligomerization, as depicted in Scheme 6.4

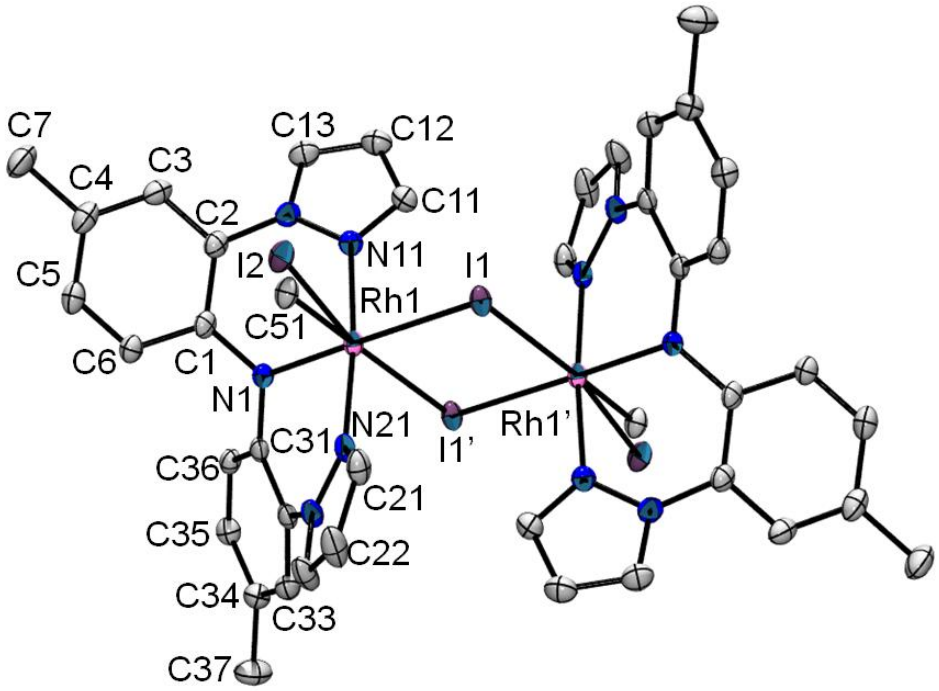

Figure 6.17. Molecular structure and atom labeling for superimposed components of dimeric species in the crystal of $\mathbf{13_{Me}}$·acetone. Solvent and hydrogen atoms have been omitted for clarity. The crystal was found to have two components, nominally $\mathbf{13_{Me}}$ and $\mathbf{13_{I}}$where the population of atoms C51 : I2 refined to a ratio of 90.6% : 9.4%.

Selected bond distances (Å): Rh1-N1, 2.013(2); Rh1-N11, 2.025(3); Rh1-N21, 2.019(2); Rh1-I1, 2.6942(3); Rh1-I1', 2.9040(3); Rh1-C51, 2.061(5); Rh1-I2, 2.598(3); Selected bond angles (°): N1-Rh1-I1 178.54(7); C51-Rh1-I1', 174.72(11); N11-Rh1-N21, 174.02(9); N11-Rh1-N1, 87.11(10); N21-Rh1-N1, 87.28(10); C51-Rh1-I1, 91.13(12); C51-Rh1-N1, 90.31(14); C51-Rh1-N11, 91.01(15); C51-Rh1-N21, 86.95(15); I1-Rh1-I2, 85.98(6); I1-Rh1-I1', 84.687(8); I2-Rh1-I1', 169.34(6). The non-bonded Rh⋯Rh and I⋯I distances within the metallacycle of $\mathbf{13_{Me}}$are 4.1402(3) and 3.7740(3) Å, respectively.

6.4.7. Electrospray Mass Spectrometry Studies of Decomposition Products.

The electrospray ionization mass spectra, ESI (+) MS, for various complexes ($7_{\mathbf{E = Me, Et, I}}$, $\mathbf{8}_{\mathbf{E = Me, Et}}$, $\mathbf{13}_{\mathbf{E= Me, I}}$) were acquired for added characterization and as an attempt to provide further insight into the nature of the solution decomposition of $\mathbf{7}_{\mathbf{E}}$ and $\mathbf{8}_{\mathbf{E}}$. The results of these studies suggest that insoluble dimeric species are the ultimate decomposition products of pincer complexes $7_{\mathbf{E=Me,Et}}$ with un-substituted pyrazolyl donors whereas soluble, monomeric species are the likely the ultimate decomposition products of pincer complexes $\mathbf{8}_{\mathbf{E=Me,Et}}$ with 3-methylpyrazolyl donors. The spectrum of $\mathbf{7}_{\mathbf{I}}$ as a CH_3CN solution showed only three main signals at *m*/z = 713 for $[(MeMe)RhI_2(CO)]^{\cdot+}$, *m*/*z* = 714 (100% relative intensity) for $[H(MeMe)RhI_2(CO)]^+$, and at *m*/*z* = 726 for $[(MeMe)RhI(CH_3CN)]^+$. All the othercomplexes showed more complex fragmentation patterns with peaks in the region between ca. *m*/*z* = 450 to 750 for monomeric cations and between ca. *m*/*z* = 925 to 1400 for dimeric cations, as exemplified for $\mathbf{7}_{\mathbf{Me}}$ in Figure 6.18. The 100% relative intensity signal for complexes other than $\mathbf{7}_{\mathbf{I}}$ were for monomeric cations- either $[LRh(alkyl)(CO)]^+$, $[LRh(alkyl)(CH_3CN)_{x=1,2}]^+$, or $[LRh(alkyl)(CO)(CH_3CN)]^+$ depending on the complex or experimental run (some spectra were acquired multiple times using different samples of a given complex). Thus, dissociation of one iodide is a predominant fragmentation pattern in each complex, CO loss is also common for all, and rhodium-alkyl fragmentation is more prevalent in $\mathbf{8}_{\mathbf{E =Me,Et}}$ than in $\mathbf{7}_{\mathbf{E =Me,Et}}$. The data also suggest that the new pincer ligands are capable of

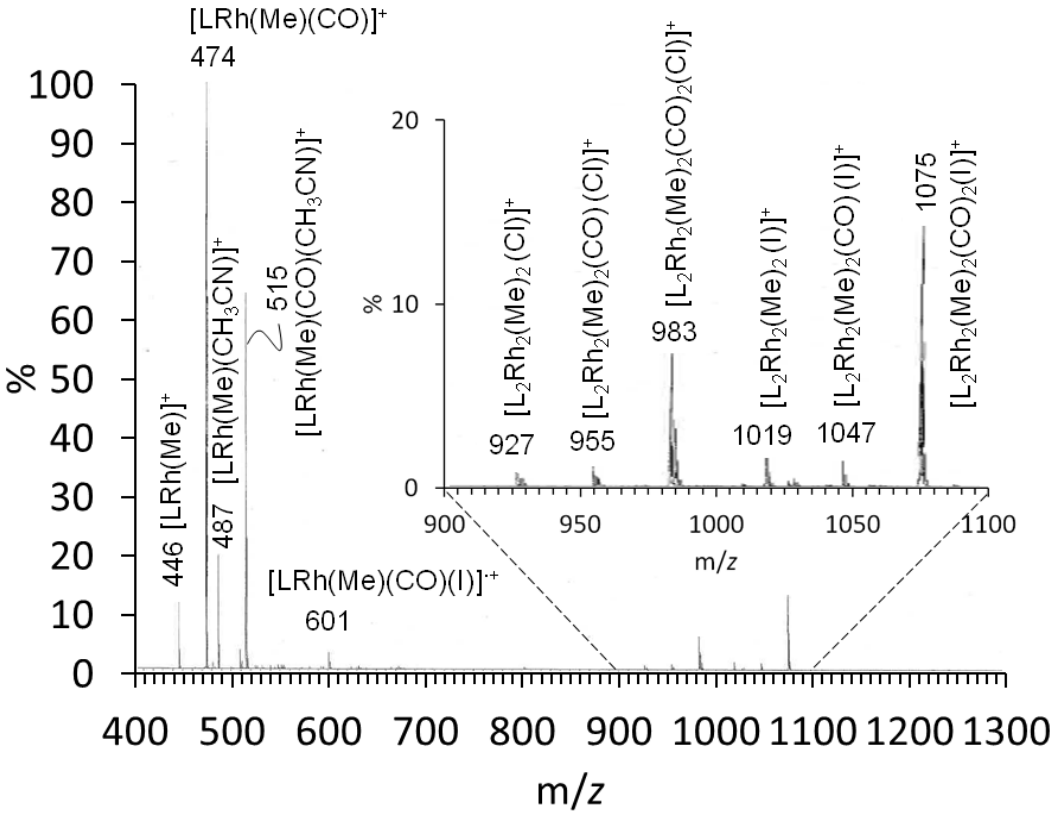

Figure.6.18. ESI(+) mass spectrum for a CH_3CN solution of (MeMe)Rh(Me)(CO)(I), $\mathbf{7_{Me}}$.(the chloride comes from the common anion impurity in the ESI(+) experiment rather than from the sample).

supporting coordinatively-unsaturated rhodium(III) species such as $[LRh(alkyl)]^+$, at least under these experimental conditions. The observation of peaks in the *m*/*z* range above 950 in the mass spectra of $\mathbf{8_{E\ =Me,Et}}$ demonstrate that dimeric cations can still form after/with loss of an initial iodide or carbonyl ligand despite the added steric bulk on the pyrazolyls in $\mathbf{8_{E\ =Me,Et}}$. This result was initially surprising since inspection of the structure of the related $\mathbf{13_E}$ suggested that unfavorable steric interactions between 3-organopyrazolyl groups (as indicated by the yellow arrow in the right of Fig. 6.16, for instance) might preclude association. When CD_2Cl_2 solutions of $\mathbf{8_E}$ were allowed to decompose over the period of two weeks, peaks for dimeric species derived from

fragmentation of $\mathbf{8_E}$ (and $\mathbf{9_E}$) were no longer present in the ESI(+) spectrum. Instead, peaks for new monomeric ions were observedthat were clearly different than those expected based on the ESI(+) mass spectra of the insoluble decomposition products of$\mathbf{7_E}$, formed under similar conditions. Unfortunately, the identity of the ultimate product(s) of decomposition of $\mathbf{8_E}$ remains uncertain despite multiple attempts at monitoring the decomposition reaction by both ^{1}H NMR spectroscopic and ESI(+) mass spectral studies .

6.5. Concluding remarks

A convergent method to prepare pyrazolyl-containing pincer ligands is reported that uses CuI as an inexpensive amination catalyst rather than the more typical palladium or bulky phosphine catalyst systems. This synthetic methodology affords ready access to pincer scaffolds with different aryl 'arms' and permits systematic investigations of the roles that electronics and sterics can have on their coordination chemistry. For rhodium chemistry described here, we have demonstrated that it was possible to isolate carbonylrhodium(I) complexes using two different synthetic routes. The rates of oxidative addition reactions involving these new carbonylrhodium(I) pincer complexes varied in a regular manner with different steric requirements of 3-pyrazolyl substituents or the electronic donating character of the *para*-X-aryl pincer substituents. Thus, replacing *para*- methyl groups of the tolyl pincer 'arms' with trifluoromethyls gave less electron-rich rhodium(I) centers, as gauged by increasing ν_{CO} IR stretching frequencies, and ultimately slowed the rates of oxidative addition reactions with alkyl iodides. The replacement of hydrogen at the 3-position of the pyrazolyls (closest to the metal center) with methyl or isopropyl groups resulted in more electron-rich rhodium(I) centers along series MeMe $<^{Me}$MeMe $<^{iPr}$MeMe due to inductive effects. However, oxidative addition

reactions with alkyl iodides became progressively slower with increasing steric bulk of 3-pyrazolyl substituents. The resultant rhodium(III) complexes were found to be unstable and decomposed with loss of CO regardless of substitution pattern on the pincer ligand. The one difference in the decomposition products is that those with unsubstituted pyrazolyls were insoluble dimeric species that were doubly iodide-bridged while those with 3-organopyrazolyl derivatives were soluble and likely monomeric in nature from ESI(+) mass spectral studies. The different stabilities of the rhodium(III) complexes of the new NNN- pincers reported here and those of related NNN- or NCN pincer ligands underscores the importance of ligand donor atoms and of chelate ring size on the reactivities of metal pincer complexes. Given the synthetic advances reported here and those reported elsewhere for accessing new pyrazole variants [53], the full potential of the new pincer ligands and their metal complexes in stoichiometric and catalytic reactions are currently being investigated in our laboratory and results will be reported in due course.

CHAPTER 7

RHODIUM COMPLEXES OF A NEW PYRAZOLYL-CONTAINING PNN-PINCER LIGAND: COMPARISON OF PROPERTIES AND TRANSFER HYDROGENATION CAPABILITIES VERSUS NNN-PINCER RELATIVES

7.1 Introduction:

As evident by the number of reviews and a recent RSC journal special issue devoted to metal pincer complexes, there is growing interest the development of new variants of uninegative, meridionally-coordinating pincer ligands and their complexes for a variety of applications from molecular electronics to catalysis.[1] Chapter 6 described the preparation, properties, and reactivity of (NNN)Rh(CO) complexes (Fig.7. 1, left) towards oxidative addition reactions with alkyl iodides and iodine.[2] It was found that complexes of the type (NNN)Rh(E = alkyl or I)(CO)(I) were formed in-situ but their isolation was problematic due to facile decomposition reactions that gave insoluble iodide-bridged dimers $[(NNN)Rh(E)(\mu\text{-}I)]_2$ (Fig. 7.1, right). Since initial reports by Moulton and Shaw[3] combined with those offered by the van Koten[4] groups demonstrated that that simple changes in the central anchor or peripheral flanking donors of a given pincer ligand could lead to rich and unexpected chemistry, we were hopeful that changing one flanking pyrazolyl donor for a more sterically-demanding diphenylphosphine group

would permit isolation of soluble rhodium(III) complexes that could be used for further synthesis or even homogeneous catalysis. In this chapter, we report on the synthesis of a new pincer ligand with a PNN donor set and the successful isolation of soluble organorhodium(III) complexes including five-coordinate, sixteen-electron complexes of the type (PNN)Rh(I)[C(O)R]. We also highlight the successful implementation of these rhodium pincer complexes in catalytic transfer hydrogenation reactions.

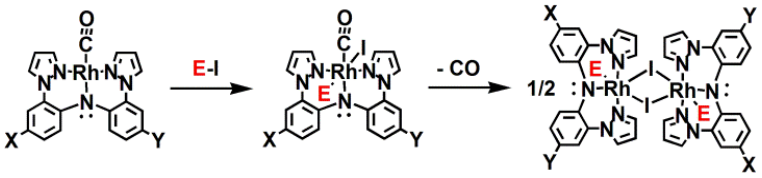

Figure7.1. Summary of rhodium chemistry of di(2-pyrazolylaryl)amido NNN 'pincer' ligands (E = alkyl or I)

7.2. Results and Discussion

The synthetic routes to the new pincer ligand and its carbonylrhodium(I) complex are outlined in Scheme 7.1. A CuI-catalyzed amination reaction between 2-pyrazolyl-4-toluidine, H(pzAn^{Me}),[5] and diiodobenzene affords 2-iodo-N-(4-methyl-2-(1H-pyrazol-1-yl)phenyl)benzenamine, H(N^{IPh}-pzAn^{Me}), a precursor (top right of Scheme 1) that is used in the final step of the ligand construction. A Pd^{0}-catalyzed coupling reaction between H(N^{IPh}-pzAn^{Me}) and diphenylphosphine affords the pincer ligand with a PNN- donor set (the crystal structure of H(PNN) is found in the section 7.5). It is noted that the sequence of reactions to the PNN- ligand in Scheme 7.1 was the only successful method of several that were attempted. For instance, the reactions between Li(n-Bu) and H(N^{IPh}-pzAn^{Me}) or its bromophenyl counterpart, and subsequent addition of PPh_2Cl gave diphenylphosphine substitution exclusively at the 5-pyrazolyl carbon rather than at the expected aryl

position. The unexpected substitution of acidic hydrogens of pyrazolyl via alkyllithium reagents is not unique to this pincer system.[6] Also, attempts to reverse the sequence of coupling steps (i.e., introducing the diphenylphosphine before the pyrazolyl flanker) were unsuccessful despite trying a variety of different amination catalysts or reaction conditions.

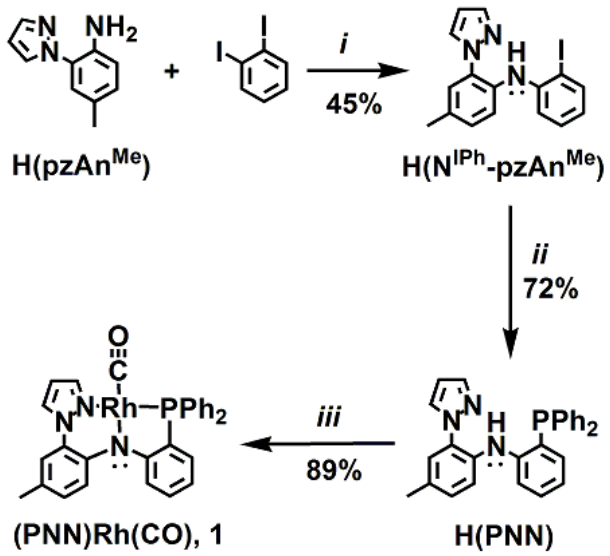

Scheme 7.1. Key: *i*) cat. CuI, 1.2 Cs_2CO_3, dioxane, Δ 16 h; *ii*) $HPPh_2$, $Pd(PPh_3)_4$, NEt_3, toluene, 40 h; *iii*) $Rh(CO)_2(acac)$, acetone, Δ 15 min

The reaction between $Rh(CO)_2(acac)$ and the PNN- pincer ligand in acetone afforded a high yield of the desired carbonylrhodium(I) complex (PNN)Rh(CO), **1**. The related (NNN)Rh(CO) derivative (left of Fig. 7.1 where X = CH_3 and Y = H), complex **2**, was prepared previously.[2] Complex **1**, like **2**, appears air-stable as a solid. Both are soluble in most organic solvents except alkanes and alcohols where each complex is moderately soluble. In contrast to **2**, which was slightly air sensitive in solution and had to be protected from the atmosphere, **1** is air-stable in solution and no special precautions

were required for its handling. The IR spectral data for **1** and **2** both in the solid state and solution indicate that the NNN- pincer ligand affords only a slightly more electron-rich rhodium centre than the PNN- pincer ligand. For instance, the C-O stretching frequency, ν_{CO} = 1954 cm^{-1}, for **2** is slightly lower energy than ν_{CO} =1957 for **1** due to increased back-bonding in the former. The C-O stretching frequency for **1** is comparable to 1960 cm^{-1} reported for the related PNP derivative of Kaska with a diarylamido anchor and two PPh_2 flankers.[7] These comparable results corroborate our previous findings that the *para*-aryl substituents (rather than flanking donors) dictate the electronic properties of the metal complexes of diarylamido-anchored pincers. Although all attempts to obtain crystals of **1** suitable for X-ray diffraction have been stymied by its propensity to form microcrystalline needles, the NMR spectral data of **1** are in accord with the structural formulation depicted in Scheme 1. The ^{13}C NMR spectrum of **1** shows a doublet-of-doublet signal at δ_C = 193 ppm (J_{Rh-C} = 67 Hz and J_{P-C} = 18 Hz) for the rhodium-bound carbonyl; that for **2** showed a doublet resonance at δ_C =193 ppm (J_{Rh-C} = 71 Hz). The similarity of chemical shift and coupling constant between **1** and **2**, suggests that **1** has a square planar coordination geometry about rhodium with *trans*- disposed amido and carbonyl groups like that in structurally-characterized **2**. The ^{31}P NMR spectrum of **1** shows a doublet resonance at δ_P = 61 ppm ($^1J_{P-Rh}$ = 167 Hz) which is shifted downfield from the singlet resonance at δ_P = -20 ppm for H(PNN) and the doublet resonance at δ_P = 41.8 ppm ($^1J_{P-Rh}$ = 135.1 Hz) reported for Kaska's PNP derivative.[7] It was found that **1** and **2** were sufficiently effective nucleophiles to participate in oxidative addition (OA) reactions with MeI (BDE = 239 kJ/mol), EtI (BDE = 234 kJ/mol), and 4-$BrCH_2C_6H_5Br$

(BDE 241 kJ/mol) but were ineffective for reactions with iodobenzene (BDE = 272 kJ/mol), or CH_3Br (BDE 294 kJ/mol).[8] Scheme 7.2 summarizes the OA reactions between **1** and alkyl halides.

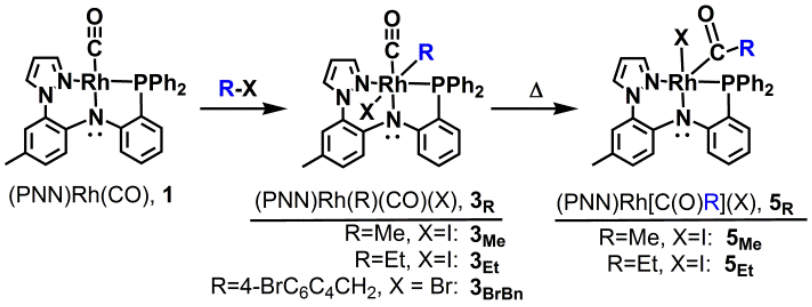

Scheme 7.2. Summary of rhodium chemistry of di(2-pyrazolyl-aryl)amido NNN 'pincer' ligands

It was possible to isolate bulk samples of pure (PNN)Rh(4-$CH_2C_6H_4Br$)(CO)(Br), **3**BrBn, and characterize this compound by single-crystal X-ray diffraction (Fig. 7.2). While the bond distances and angles are unremarkable, the meridional coordination of the PNN- pincer ligand and the *trans*- disposition of the bromide and 4-bromobenzyl groups were confirmed by the structure. The structure of **3**BrBn is of an isomer where the bromide is closer to the arylphosphine arm than the pyrazolyltolyl arm. Although an isomer where the bromide is situated next to the pyrazolyltolyl arm is conceivable, it was not observed even in solution presumably due to steric interactions between the bromophenyl and PPh_2 groups. As a contrast, a 5:4 ratio of isomers is observed in the NMR spectra of the sterically less-demanding, NNN- pincer derivative, $\mathbf{4}_{BrBn}$, as detailed in the section 7.6.. Unlike $\mathbf{3}_{BrBn}$ it was not possible to isolate pure bulk samples of (PNN)Rh(Me or Et)(CO)(Br), $\mathbf{3}_{Me}$ or $\mathbf{3}_{Et}$, because these complexes undergo facile

migratory insertion reactions to give (PNN)Rh[C(O)Me](I), $\mathbf{5_{Me}}$, and (PNN)Rh[C(O)Et](I), $\mathbf{5_{Et}}$. We have been unable to coax $\mathbf{3}_{\text{BrBn}}$ into a migratory insertion reaction.

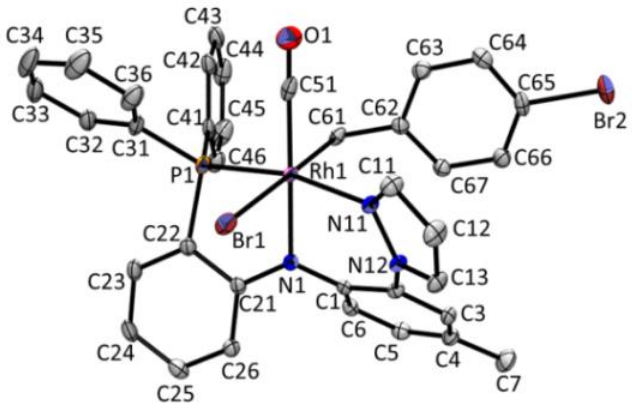

Figure 7.2. Structure of the rhodium complex in (PNN)Rh(4-$CH_2C_6H_4Br$)(CO)(Br)·acetone, $\mathbf{3_{BrBn}}$·acetone. Selected bond distances (Å): Rh1-Br1, 2.6373(3); Rh1-P1, 2.2636(5); Rh1-N1, 2.0518(16); Rh1-N11, 2.1040(17); Rh1-C51, 1.910(2); Rh1-C61, 2.148(2); C51-O1, 1.091(3); Selected bond angles (°): N1-Rh1-C51 178.84(8); P1-Rh1-N11, 167.66(5); Br1-Rh1-C61, 179.00(5); N11-Rh1-N1, 86.49(6); P1-Rh1-N1, 82.90(5); Br1-Rh1-N1, 89.60(5), C61-Rh1-N1, 90.32(7). Hydrogens atoms and acetone molecule have been omitted for clarity

The structure of 5_{Me} is shown in Fig 7.3. As with 3_{BrBn}, the ligand binds in the expected *mer*- coordination mode but in 5_{Me} the metal centre is five-coordinate with a square pyramidal geometry about rhodium. The carbon of the acyl group occupies the axial position while the iodide and amido nitrogen are *trans*-to one another in the basal plane. In contrast to the trigonal planar amido nitrogen in 3_{BrBn} where the sum of angles about N1 was 358°, the amido nitrogen in 5_{Me} is slightly more pyramidal with a sum of angles about N1 of 353°. It was previously observed that pyramidalization of the amido nitrogen can lead to enhanced reactivity at this atom.[9]

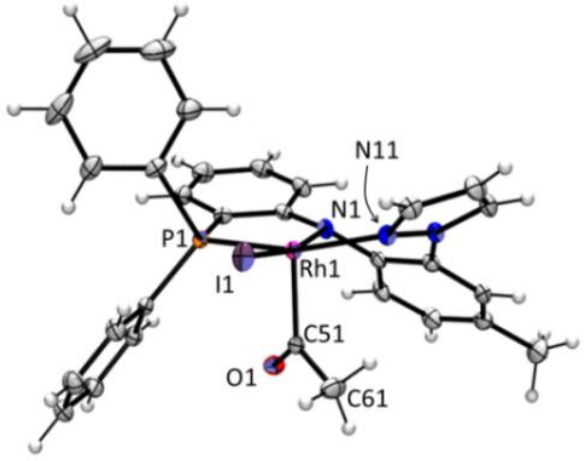

Figure 7.3. Structure of (PNN)Rh[C(O)Me](I), 5_{Me}. Selected bond distances (Å): Rh1-I1, 2.6636(2); Rh1-P1, 2.2303(5); Rh1-N1, 2.0352(18); Rh1-N11, 2.1165(17); Rh1-C51, 1.963(2); C51-C61, 1.514(3); C51-O1, 1.196(3); Selected bond angles (°): P1-Rh1-N11, 165.38(5); I1-Rh1-N1, 169.82(5); N11-Rh1-N1, 87.13(7); P1-Rh1-N1, 85.44(5); N1-Rh1-C51 89.62(8); I1-Rh1-P1, 92.305(15); I1-Rh1-N11, 92.81(5); C51-Rh1-N11, 100.79(8); C51-Rh1-P1, 91.74(6); C51-Rh1-I1, 100.38(6)

Given the favourable juxtaposition of the *cis*- disposed amido lone pair and the vacant coordination site on rhodium, we have begun exploration into the ability of 5_{Me} to act as a bifunctional catalyst. Transfer hydrogenation of ketones by sacrificial hydrogen donors such as *iso*-propanol or formic acid is a well-studied reaction in which a coordinatively-unsaturated metal centre and a bound Lewis basic ligand are thought to cooperatively arbitrate the organic transformation for many different metal systems.[10] Thus, we chose to begin this survey by comparing the activity of 5_{Me} and some related rhodium pincer complexes in the transfer hydrogenation reaction of acetophenone using *iso*-propanol as a hydrogen donor (Scheme 7.3). Table 7.1 summarizes the results of this initial investigation. Of the species

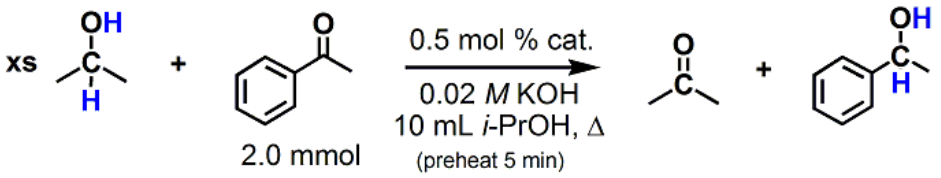

Scheme 7.3. Transfer hydrogenation of acetophenone with ^{i}PrOH

tested, the rhodium(III) complexes outperformed the rhodium(I) derivatives while the (NNN)Rh^{III} pincer complexes underwent faster, more complete reactions than the corresponding (PNN)Rh^{III} derivatives. This latter behaviour may have been anticipated by the lower steric profile and greater basicity of the NNN- pincer versus the PNN- ligand. In each case, the reaction mixture changed colour, which combined with the similar reactivity of $\mathbf{3_{Me}}$ and $\mathbf{5_{Me}}$ or $\mathbf{4_{Me}}$ and $\mathbf{4_{BnBr}}$, indicate that the initial rhodium pincer complexes are pre-catalysts. The turnover numbers (TON, mol product/mol cat) and

turnover frequencies (TOF, mol product/(mol cat.·h)) found for the reactions involving the current rhodium(III) pincer complexes are comparable to (if not greater than) those values reported for similar reactions with other rhodium(III) complexes[11] with the lone exception being Grützmacher's incredible CNC- bis(tropylium)amido pincer system (TON = 1,000,000 in EtOH).[12] In light of this latter report, it is anticipated that the identification of the catalytically- active species and judicious modifications of the pincer scaffold could lead to drastically improved catalytic performance.

	conversion % [b]		*TON*[c]	*TOF*[d]
catalyst	2 h	5 h	after 5h	
(PNN)Rh(CO), **1**	8(1)	18(1)	36(2)	7
(NNN)Rh(CO), **2**	12(1)	23(8)	46(16)	9
[e](PNN)Rh(Me)(CO)(I), $\mathbf{3_{Me}}$	41(3)	74(4)	148(8)	30
(PNN)Rh(BnBr)(CO)(Br), $\mathbf{3_{BnBr}}$	67(3)	93(1)	186(2)	37
[f](NNN)Rh(Me)(CO)(I), $\mathbf{4_{Me}}$	73(3)	97(1)	194(2)	39
[g](NNN)Rh(BnBr)(CO)(Br), $\mathbf{4_{BnBr}}$	88(1)	96(2)	192(2)	38
(PNN)Rh[C(O)Me](I), $\mathbf{5_{Me}}$	35(5)	69(7)	138(14)	28
(PNN)Rh[C(O)Et](I), $\mathbf{5_{Et}}$	47(2)	75(2)	150(2)	30
None	5(2)	9(1)	---	---

Table 7.1. Results from transfer hydrogenation experiments[a].

[a]Conditions: Under N_2, see Scheme 3. [b] by NMR integration, average values of three runs with (±) range in parentheses. [c]mol product/mol catalyst after 5h; [d]TON/5h; [e]94% pure with 6% 5_{Me} by NMR, see text. [f]see structure centre of Fig. 1; X = Me, Y = H, E = Me. [g] mixture with dimer, similar to right of Fig. 1

7.3. Conclusions

We have outlined a new synthetic protocol that allows access to a pincer ligand with a PNN donor set. The rhodium(I) complex (PNN)Rh(CO) shares similar electronic

properties with its NNN- counterpart but is more stable toward decomposition reactions. After oxidative addition with iodomethane and subsequent migratory insertion, it was possible to isolate a coordinatively-unsaturated 16-electron rhodium(III) complexes (PNN)Rh[C(O)(Me or Et)](I); the NNN counterpart decomposes to give an insoluble carbonyl-free dimer instead of undergoing insertion. The rhodium(III) pincer complexes all give rise to better performance in hydrogen transfer reactions than related rhodium(I) derivatives.

7.4. Experimental

Materials.

CuI, anhydrous Cs_2CO_3, 4-bromobenzylbromide, 1,2-diiodobenzene, NEt_3, $HPPh_2$, and Li(*n*-Bu) (1.6 *M* in hexanes) were purchased from commercial sources and used without further purification while $Pd(PPh_3)_4$,[13] $Rh(CO)_2(acac)$,[14] (MeH)Rh(CO) (**2**, see left of Fig 7.1,where X = Me, Y = H),[15] (MeH)Rh(R = Me, Et)(CO)(I) $\mathbf{4_R}$,[15] $H(pzAn^{Me})$ ($pzAn^{Me}$ = 2-(pyrazolyl)-*p*-toluidine)[16] was prepared by literature methods. Commercial methyl- and ethyl iodide were dried over $CaCl_2$ and distilled under vacuum before use. Solvents used in the preparations were dried by conventional methods and were distilled under nitrogen prior to use.

Physical measurements.

Midwest MicroLab, LLC, Indianapolis, Indiana 45250, performed all elemental analyses. ^1H, ^{13}C and ^{31}P NMR spectra were recorded on a Varian 400 MHz spectrometer. Chemical shifts were referenced to solvent resonances at δ_H 7.26 and δ_C 77.16 for $CDCl_3$, δ_H 5.32 and δ_C 53.84 for CD_2Cl_2, δ_H 2.05 and δ_C 29.84 for acetone-d_6.

^{31}P NMR chemical shifts were referenced against an external standard, 85% H_3PO_4 (aq), with a resonance at $\delta_P = 0.00$ ppm. Infrared spectra were recorded on samples as either KBr pellets or as acetone solutions with cells having KBr windows using a Nicolet Magna-IR 560 spectrometer. Melting point determinations were made on samples contained in glass capillaries using an Electrothermal 9100 apparatus and are uncorrected.

Ligand Syntheses.

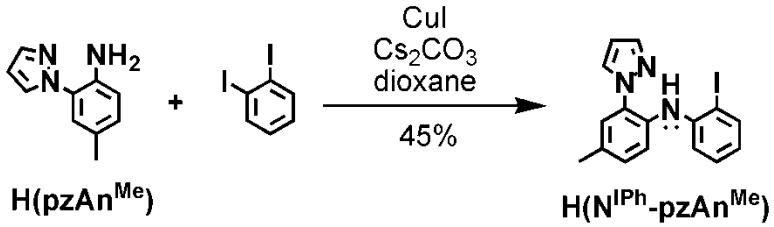

N-(2-iodophenyl)-4-methyl-2-(1H-pyrazol-1-yl)benzenamine, **H(N^{IPh}-pzAn^{Me})**. A Schlenk flask charged with 5.32 g (30.7 mmol) H(pzAn^{Me}), 11.14 g (33.8 mmol, 1.1 eq) 1,2-diiodobenzene, and 12.00 g (36.8 mmol, 1.2 eq) Cs_2CO_3 was deoxygenated by three evacuation and nitrogen back-fill cycles. Then, 30 mL of dry deoxygenated dioxane and 1.17 g (6.14 mmol, 20 mol %) CuI were added under nitrogen blanket. The reaction mixture was heated at reflux for 15 h under nitrogen. After cooling to room temperature, dioxane was removed by vacuum distillation. The solid product mixture was extracted with four 20 mL portions of Et_2O and then Et_2O was removed by vacuum distillation to afford a residue that was further purified by column chromatography on silica gel. After elution with 8:1 hexane: ethyl acetate ($R_f = 0.6$) and removal of solvents the desired product was obtained as a white solid. Yield: 5.230 g , 45 %. Mp: 218-221 ^oC. ^1H NMR ($CDCl_3$): δ_H 8.01 (s, 1 H), 7.79 (d, *J* = 2 Hz, 1 H), 7.75 (m, 2 H), 7.33 (d, *J* = 8 Hz, 1H),

7.19 (m, 1 H), 7.16 (m, 2 H), 7.09 (dd, *J* = 8.3, 1.6 Hz, 1 H), 6.59 (m, 1 H), 6.44 (t, J = 2.1 Hz, 1 H), 2.36 (s, 3 H) ppm. ^{13} C NMR ($CDCl_3$): δ_C 144.2, 140.9, 139.8, 133.8, 131.6, 130.4, 129.8, 128.84, 128.76, 125.1, 122.2, 120.2, 116.4, 106.8, 89.6, 20.8 ppm.

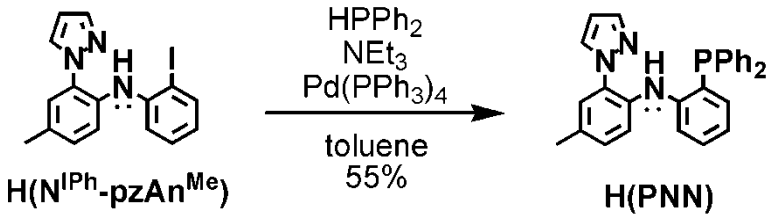

4-methyl-N-(2-(diphenylphosphino)phenyl)-2-(1H-pyrazol-1-yl)benzenamine, **H(PNN).** A Schlenk flask charged with 4.29 g (11.4 mmol) **H(N^{IPh}-pzAn^{Me})**, 1.75 mL (12.6 mmol, 1.1 eq) Et_3N, 2.00 mL (11.4 mmol) $HPPh_2$ and was deoxygenated by three evacuation and nitrogen back-fill cycles. Then, 40 mL dry, deoxygenated toluene and 0.067 g (0.058 mmol, 0.5 mol %) $Pd(PPh_3)_4$ were added, the mixture was purged with a nitrogen stream for 10 min, and the mixture was heated at reflux for 40 h under nitrogen. After cooling to room temperature, toluene was removed by vacuum distillation. The solid product mixture was extracted with three 25 mL portions dichloromethane. The combined organic fractions were washed with water then dried over $MgSO_4$, filtered, and volatiles were removed by vacuum distillation to afford an oily residue that was further purified by column chromatography on silica gel. After elution with 6:1 hexane: ethyl acetate (R_f = 0.6) and removal of solvents the desired product was obtained as a white solid. Yield: 3.56 g, 72 %. Mp: 141-143 ^oC. Anal. Calcd. (found) for $C_{28}H_{24}N_3P$: C, 77.27 (77.09), H, 5.56 (5.69), N, 9.66 (9.63). ^{1}H NMR (acetone-d_6): δ_H 8.55 (s, 1H), 7.97 (m, 1H), 7.39 (m, 6 H), 7.27 (m, 9 H), 7.04 (m, 1 H), 6.86 (m, 1 H), 6.77 (m, 1 H), 6.34 (m, 1 H), 2.30

(s, 3 H) ppm. ^{13}C NMR (acetone-d_6): δ_C 147.1 (d, J = 20.8 Hz), 147.0 (d, J = 20.7 Hz), 140.74, 140.73, 137.1 (d, J = 10.4 Hz), 135.4 (d, J = 1 Hz), 135.3 (d, J = 11 Hz), 134.8, 134.82, 134.7 (d, J = 20.0 Hz), 131.07, 131.05, 130.6, 130.3, 130.2, 129.8, 129.5 (d, J = 7.0 Hz), 129.0, 128.1 (d, J = 11.2 Hz), 128.0 (d, J = 11.3 Hz), 124.92, 124.91, 122.5 (d, J = 0.9 Hz), 119.8, 119.34 (d, J = 2.5 Hz), 119.28, 107.1, 20.5 ppm. ^{31}P NMR (acetone-d_6): δ_P -18.3 ppm. ^{1}H NMR (CD_2Cl_2): δ_H 8.04 (d, 1 H, J = 3.5 Hz, N-H), 7.67 (dd, 1 H, J = 2.5, 0.6 Hz), 7.40 – 7.25 (m, 11 H), 7.21 (m,3 H), 7.12 (d, 1 H, J = 2 Hz), 7.02 (m, 1 H), 6.84 (m, 1 H), 6.77 (m, 1 H), 6.28 (dd, 1 H, J = 2.5, 1.9 Hz), 2.31 (s, 3 H) ppm. ^{31}P NMR (CD_2Cl_2): δ_P -20.4 ppm.

Metal Complexes.

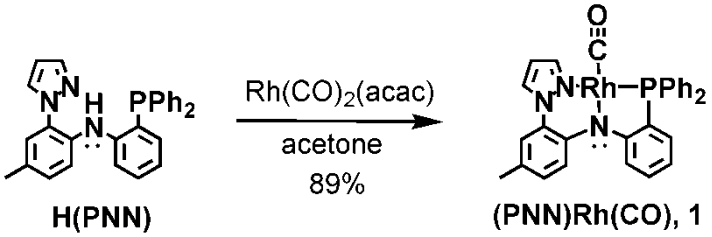

H(PNN) (PNN)Rh(CO), 1

(PNN)Rh(CO), **1**. A mixture of 1.04 g (2.41 mmol) H(PNN) and 0.621 g (2.41 mmol) $Rh(CO)_2(acac)$ in 20 mL acetone was heated at reflux for 15 minutes. After cooling to room temperature, volatiles were removed under vacuum to leave 1.21 g (89 %) of pure **1** as a yellow crystalline solid. Mp: 161-71 ^{o}C (dec.). Anal. Calcd. (found) for $C_{29}H_{23}N_3OPRh$: C, 61.82 (61.52), H, 4.12 (4.52), N, 7.46 (6.94). IR (ν_{CO}, cm^{-1}): 1957 (KBr pellet). 1961 (acetone). ^{1}H NMR (acetone-d_6): δ_H 8.45 (m, 1 H), 8.12 (d, *J* = 1.7 Hz, 1 H), 7.76 (m, 2 H), 7.69 (m, 2 H), 7.49 (m, 6 H), 7.37 (d, *J* = 8.4 Hz, 1 H), 7.14 (m, 4 H), 6.86 (dd, *J* = 8.4, 1.5 Hz, 1 H,), 6.76 (t, *J* = 2.1 Hz, 1 H), 6.61 (m, 1 H), 2.21 (s, 3 H) ppm. ^{13} C NMR (acetone-d_6): δ_C 193.2 (dd, J_{Rh-C} = 67.1, J_{P-C} =18.3 Hz, Rh-CO),

164.1 (dd, *J* = 26.1, 2.6 Hz), 146.3 (d, *J* = 1.4 Hz), 144.0, 135.4, 134.9, 134.5 (d, J = 1.8 Hz), 134.1, 134.0, 133.8, 133.6, 133.5, 132.5 (d, *J* = 1.3 Hz), 131.5 (d, *J* = 1.9 Hz), 131.2 (d, *J* = 1.8 Hz), 130.8, 130.4, 129.9, 129.6 (d, *J* = 10.4 Hz), 129.4 (d, *J* = 10.9 Hz), 127.8, 125.8, 124.7, 124.2, 120.3, 120.2, 118.8 (d, *J* = 7.3 Hz), 108.4, 20.3 ppm. ^{31}P NMR (acetone-d_6): δ_P 60.7 (d, *J* = 167 Hz) ppm.

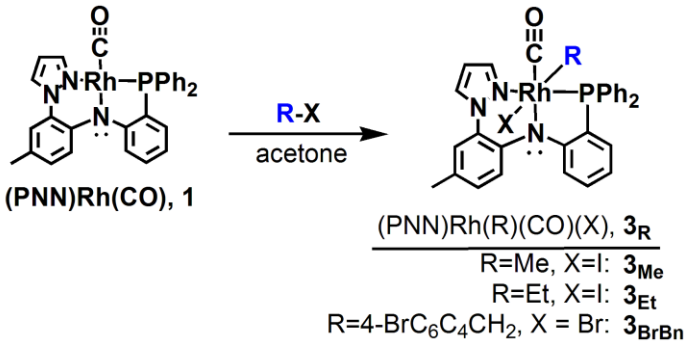

As indicated by Figure 7.8, the following two compounds (**3$_{Me}$** and **3$_{Et}$**) decompose by migratory insertion in solution to give the appropriate **5$_{Me}$** or **5$_{Et}$**. Thus, far, mixtures of **3** and **5** have proven to be inseparable by common methods. Although **3$_{Me}$** seems to be pure in solution from ^{1}H NMR spectroscopic experiments, it has not yet been isolated pure in the solid state. A mixture of 94% **3$_{Me}$** versus 6% **5$_{Me}$** (by NMR integration of a redissolved solid) represents the most enriched sample we have been able to obtain, vide infra. The subsequent transfer hydrogenation studies using "**3$_{Me}$**" were performed with this mixture. The **3$_{Me}$** or **3$_{Et}$** species can be identified spectroscopically, as indicated by the data below. Each **3$_{Me}$** or **3$_{Et}$** occurs as two isomers as outlined in Figure 7.4 and in the NMR discussion section 7.6

(PNN)Rh(Me)(CO)(I), **3$_{Me}$**. A 0.12 mL (0.187 mmol) aliquot of iodomethane was added by syringe to a solution of 0.105 g (0.187 mmol) **1** in 10 mL acetone. After the resultant

red solution had been stirred at room temperature for 10 min, acetone was removed by vacuum distillation. The residue was dried under vacuum to give 0.119 g (90% yield) of a red solid that is a mixture of **3_{Me}** (94% by NMR integration, two isomers) and **5_{Me}** (6%). The following spectroscopic data are only for **3_{Me}**. Data for **5_{Me}** are given after the synthetic scale preparation, described later. IR(ν_{CO}, cm^{-1}): 2046 (KBr pellet); 2052 (acetone). ^{1}H NMR (acetone-d_6): δ_H 8.52 (m, 0.3 H, pz), 8.50 (m, 0.7 H, pz), 8.42 (m, 1.3 H), 8.28 (m, 0.6 H), 8.01 (s, 0.6 H), 7.83 (m, 0.6 H), 7.71-7.65 (br m, 2.4 H), 7.62-7.56 (br m, 2.1 H), 7.51-7.46 (br m, 2.7 H), 7.44-7.31 (br m, 1.8 H), 7.28-7.14 (br m, 5.5 H), 6.96 (psd, J_{app} = 8.5 Hz, 0.7 H), 6.91 (psd, J_{app} = 8.5 Hz, 0.3 H), 6.79 (m, 1H, H_4pz), 6.74 (mt, J_{app} = 7.4 Hz, 0.3 H), 6.68 (mt, J_{app} = 7.4 Hz, 0.7 H), 2.25 (s, 0.9 H, $ArCH_3$), 2.24 (s, 2.1 H, $ArCH_3$), 1.05 (dd, J = 3.2, 2.9 Hz, 2.1 H), 0.36 (dd, J = 3.2, 2.9 Hz, 2.1 H) ppm, see Figure 7.4. ^{1}H NMR (CD_2Cl_2): δ_H 8.33 (m, J_{app} = 11.6, 8.0 Hz, 1H), 8.23 (s, 0.4 H), 8.15 (s, 0.6 H), 7.79 (m, J_{app} = 11.6, 8.5 Hz, 0.6 H), 7.71-7.51 (br m, 4.6 H), 7.30-7.14 (br m, 3.4 H), 7.09 (s, 0.4 H), 7.03 (s, 0.6 H), 6.97 (m, 1H), 6.72 (m, 1.4 H), 2.32 (s, 0.7 H, $ArCH_3$), 2.27 (s, 1.4 H, $ArCH_3$), 1.06 (s, 0.7 H), 0.37 (s, 1.4 H) ppm. ^{31}P NMR (CD_2Cl_2): δ_P 59.7 (d, J = 121.4 Hz, major isomer, 67%), 59.0 (d, J = 121.4 Hz, minor isomer, 33%).

Figure 7.4. Portions of the ^{1}H NMR spectrum of $\mathbf{3_{Me}}$ in acetone-d_6 showing two isomers. (*) demarcates a solvent impurity.

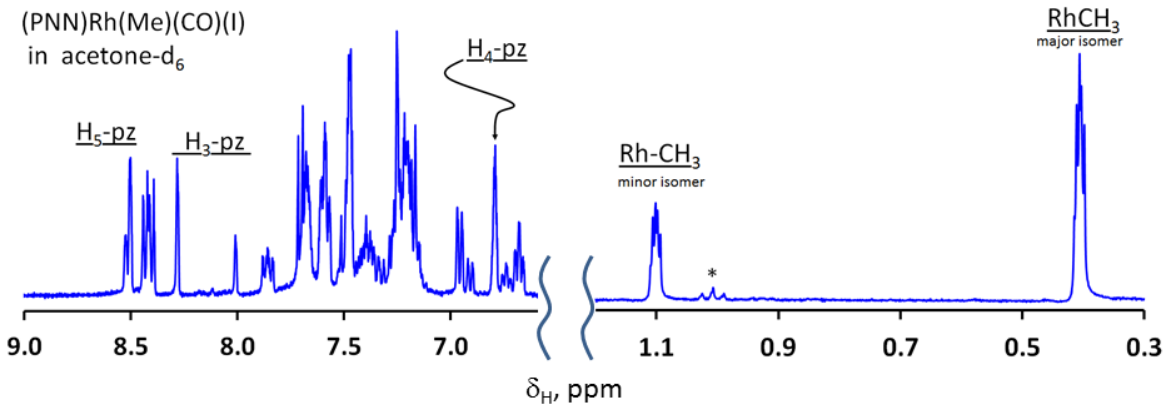

(PNN)Rh(Et)(CO)(I), $\mathbf{3_{Et}}$. This species is formed transiently during the reaction of **1** and EtI to give $\mathbf{5_{Et}}$, see Figure 7.8 (b) for example. The spectroscopic data reported here are deduced by examining data of the mixtures, subtracting signals known to be for **1** and $\mathbf{5_{Et}}$. Note that it was not possible to identify all resonances for hydrogens in the aromatic region owing to extensive overlap of multiplet resonances. IR(ν_{CO}, cm^{-1}): 2042 (KBr pellet); 2050 (acetone). ^{1}H NMR (acetone-d_6): δ_H 8.56 (s, 0.33H, pz), 8.54 (s, 0.67 H, pz), 8.41 (m, J_{app} = 11.9, 7.2 Hz, 0.66 H), 8.27 (s, 0.33 H), 7.87 (m, J_{app} = 11.5, 10.6 Hz, 0.67 H), 7.82-7.04 (br m), 7.00 (m, J_{app} = 8.8 Hz, 0.33 H), 6.79 (m, J_{app} = 2, 1 Hz, 0.33 H, pz), 6.77 (m, J_{app} = 2, 1 Hz, 0.67 H, pz), 2.37 (m, 0.33 H, $RhCH_2$), 2.27 (s, 2 H, tolyl-CH_3), 2.25 (s, 1 H, tolyl-CH_3), 2.06 (m, 0.67 H, $RhCH_2$), 1.47 (m, 0.66 H, $RhCH_2$), 1.41 (m, 0.67 H, $RhCH_2$), 0.41 (t, J = 7.4 Hz, 2 H, Et-CH_3), 0.36 (t, J = 7.4 Hz, 1 H, Et-CH_3). ^{31}P NMR (CD_2Cl_2): δ_P 59.6 (d, J = 127 Hz, major isomer, 67%), 57.1 (d, J = 127 Hz, minor isomer, 33%).

(PNN)Rh(BrBn)(CO)(Br), **3$_{BrBn}$**. A mixture of 0.0620 g (0.110 mmol) (PNN)Rh(CO) and 0.0275 g (0.110 mmol) 4-bromobenzylbromide in 15 mL acetone was maintained at room temperature for 2 days. During this time, bright red X-ray quality crystals of pure **3$_{BrBn}$** precipitated from the red solution. The red solution was concentrated under vacuum and washed with diethyl ether to give a red crystalline powder. Combined yield of crystals and powder: 0.0769 g (86 %). Mp: 191-193 ^{o}C. Anal. Calcd. (found) for $C_{36}H_{29}Br_2N_3OPRh$: C, 53.16 (53.15), H, 3.59 (3.51), N, 5.17 (5.06). IR (ν_{CO}, cm^{-1}): 2050 (KBr pellet); 2055 (acetone). ^{1}H NMR (CD_2Cl_2): δ_H 8.37 (m, 2 H), 8.10 (m, 1 H), 7.81 (m, 1 H), 7.62 (m, 1 H), 7.53 (m, 5 H), 7.35 (m, 3 H), 7.14 (m, 2 H), 7.06 (m, 2 H), 6.90 (d, *J* = 8.5 Hz, 2 H), 6.61 (m, 2 H), 6.13 (m, 2 H), 2.60 (m, 1 H), 2.34 (s, 3 H), 2.17 (m, 1 H) ppm. ^{31}P NMR (CD_2Cl_2): δ_P 55.8 (d, *J* = 124 Hz) ppm.

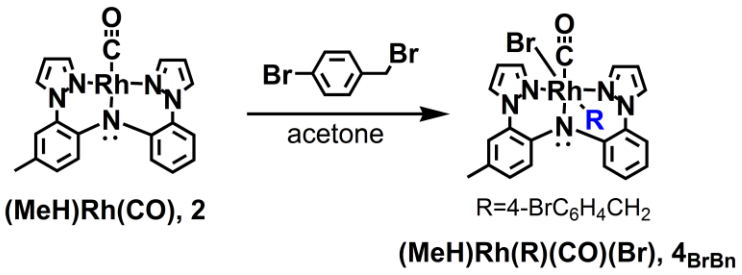

(MeH)Rh(BrBn)(CO)(Br), **4$_{BrBn}$**. A 0.0291 g (0.116 mmol) sample of 4-bromobenzylbromide was added as a solid to a solution of 0.0518 g (0.116 mmol) (MeH)Rh(CO) in 15 mL CH_2Cl_2. After the resulting bright red solution had been stirred at room temperature for 30 min, solvent was removed by vacuum distillation to give 0.119 g of a red-brown powder. As with other such complexes of the type (NNN)Rh(alkyl)(CO)(halide),[15] the sample is likely contaminated with poorly soluble red brown $[(MeH)Rh(Br)(\mu\text{-}Br)]_2$, as evident by a characteristic broadened baseline in the aromatic region of the ^{1}H NMR spectrum, see Fig 7.5. Also, microcrystalline red-brown

needles begin to deposit within minutes of re-dissolving the red-brown sample in CD_2Cl_2. The transfer hydrogenation experiments were run using the as-isolated red-brown powder. The spectroscopic data below are for the solid, the solid re-dissolved in CD_2Cl_2, or for a sample generated in-situ using acetone-d_6 as a solvent, as indicated. The spectroscopic data indicate that two isomers of $\mathbf{4_{BrBn}}$ coexist in a 5:4 ratio. These are most easily detected via the appearance of the two singlet resonances for the tolyl-CH_3 hydrogens and the two sets of second-order multiplet resonances for prochiral (diastereotopic) hydrogens of the Rh-CH_2Ar moiety. IR (ν_{CO}, cm^{-1}): 2062 (KBr pellet); 2069 (acetone). ^{1}H NMR (CD_2Cl_2): δ_H 8.21 (m, 4 H), 7.83 (s, 1 H, pz), 7.50 (d, J_{app} = 8.8 Hz, 1H), 7.46-7.40 (m, 4 H), 7.30 (m, 3 H), 7.27 (d, J_{app} = 1 Hz, 2 H, pz), 7.22 (d, J_{app} = 8.5 Hz, 1 H), 7.17 (d, J_{app} = 8.0 Hz, 2 H), 7.08 (m, 2 H), 7.04 (m, 2 H), 6.92, (m, 2 H), 6.83 (m, 2 H), 6.71-6.64 (br m, 8 H), 3.28 (m, 4 H), 2.36 (s, 3 H), 2.34 (s, 3 H) ppm. ^{1}H NMR (acetone-d_6): δ_H 8.61 (d, J_{app} = 2.8 Hz, 1 H, pz), 8.59 (dd, J_{app} = 4.3, 4.1 Hz, 1 H), 8.44 (dd, J_{app} = 8.5, 3 Hz, 1H), 7.92 (pst, J_{app} = 2.9 Hz, 1H), 7.83 (m, 0.44 H), 7.77 (d, J_{app} = 2Hz, 1 H), 7.70 (dd, J_{app} = 8, 1 Hz, 0.44 H), 7.56 (d, J_{app} = 1Hz, 0.55 H), 7.41 (m, 2H), 7.30 (m, 1.7 H), 7.15 (m, 1 H), 7.08 (d, J_{app} = 8.5 Hz, 0.55 H), 7.04-6.83 (br m, 4.6 H), 6.78 (m, 2 H), 6.76 (m, 1 H), 6.71 (m, 2 H), 6.67 (m, 0.7 H), 3.42 (m, 1H, RhCH_2), 3.16 (m, 1H, RhCH_2), 2.25 (s, 1.32 H, tolylCH_3), 2.24 (s, 1.66 H, tolylCH_3) ppm.

Figure 7.5. Portions of the ^{1}H NMR spectrum of impure $\mathbf{4_{BnBr}}$ in acetone-d_6 showing: *i*) characteristic broadening of aromatic region (pink shading) due to $[(MeH)Rh(Br)(\mu\text{-}Br)]_2$ dimer formation; *ii*) second-order resonances of diasterotopic hydrogens of $RhCH_2Ar$ moieties, and; *iii*) two tolyl-CH_3 resonances for different isomers.

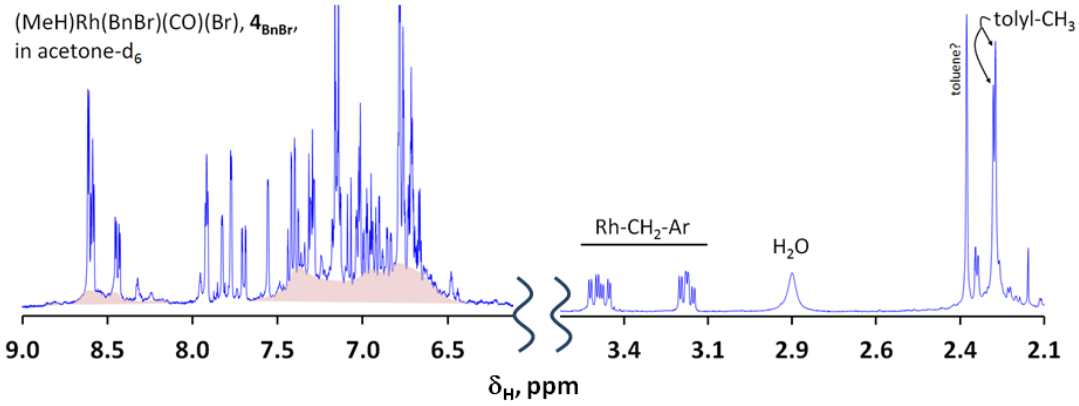

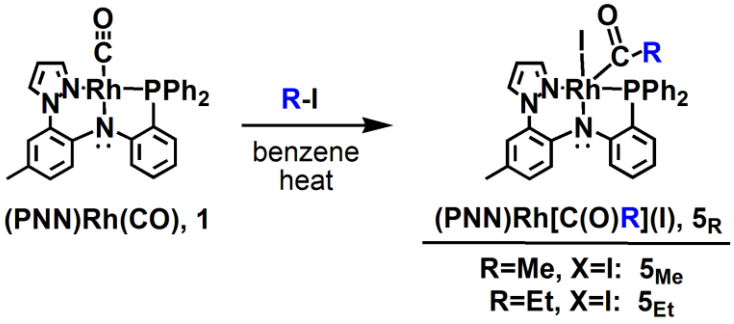

(PNN)Rh[C(O)Me](I), $\mathbf{5_{Me}}$. A mixture of 0.156 g (0.277 mmol) **1** and 0.17 mL (2.8 mmol, 10 eq) iodomethane in 15 mL benzene was heated at 70°C for 1 h. After cooling to room temperature, volatiles were removed by vacuum distillation. The resulting dark red powder was washed with two 5 mL portions Et_2O and was dried under vacuum to give 0.186 g (95 %) of pure $\mathbf{5_{Me}}$ as a red solid. Mp: 225-228 °C. Anal. Calcd. (found) for $C_{30}H_{26}IN_3OPRh$: C, 51.08 (51.31), H, 3.72 (3.79), N, 5.96 (5.88). IR(ν_{CO},

cm^{-1}): 1713 (KBr pellet); 1718 (CH_2Cl_2). ^1H NMR (acetone-d_6): δ_H 9.45 (d, *J* = 2.2 Hz, 1 H), 8.56 (dd, *J* = 7.8, 1.8 Hz, 1 H), 8.53 (dd, *J* = 7.8, 1.8 Hz, 1 H), 7.18 (d, 1 H, J = 8.6 Hz), 7.60 (dd, *J* = 8.5, 4.8 Hz, 1 H), 7.39 (m, 2 H), 7.26 (d, *J* = 2.5 Hz, 1 H), 7.24 – 7.10 (m, 4 H), 6.94 (m, 1 H), 6.82 (m, 3 H), 6.63 (dd, *J* = 8.5, 1.8 Hz, 1 H), 6.55 (m, 1 H), 6.44 (d, J = 1.7 Hz, 1 H), 6.01 (m, 1 H), 2.42 (s, 3 H), 1.96 (s, 3 H) ppm. ^{31}P NMR (acetone-d_6): δ_P 60.2 (d, J = 161.3 Hz) ppm. ^1H NMR ($CDCl_3$): δ_H 9.19 (d, *J* = 1.5 Hz,1 H), 8.19 (d, *J* = 1.5 Hz,1 H), 8.14 (m, J_{app} = 11.9, 7.9 Hz, 2 H), 7.53 (d, *J* = 7.8, 1.8 Hz, 1 H,), 7.53 (d, *J* = 8.6 Hz, 1 H), 7.49 (dd, J = 7.4, 1.7 Hz, 1 H), 7.43 (m, 2 H), 7.37 (m, J_{app} = 8.6, 4.9 Hz, 1 H), 7.34 – 7.10 (m, 9 H), 7.08 (m, 1 H), 6.97 (m, 1 H), 6.87 (dd, J = 8.4, 1.1 Hz, 1 H), 6.72-6.11 (m, 2 H), 2.25 (s, 3 H), 2.24 (s, 3 H) ppm. ^{13}C NMR ($CDCl_3$): δ_C 210.7 (dd, $J_{Rh\text{-}C}$ = 28.2, $J_{P\text{-}C}$ = 6.3 Hz, Rh-C(O)Me), 163.3 (d, *J* = 21.4 Hz), 147.5, 145.4, 136.6, 136.0, 135.0, 134.7 (d, *J* = 9.3 Hz), 133.2 (d, *J* = 10.8 Hz), 131.4, 130.9 (d, *J* = 2.7 Hz), 130.60, 130.58, 130.2, 130.1, 129.5, 129.2, 128.6, 128.5, 128.3 (d, *J* = 4.6 Hz), 128.2 (d, *J* = 4.9 Hz), 124.8, 122.7, 121.8, 121.6, 121.1, 119.4 (d, *J* = 7.3 Hz), 108.5, 39.2 (Rh-$COCH_3$), 20.7. ^{31}P NMR ($CDCl_3$): δ_P 60.8 (d, *J* = 160 Hz) ppm.

(PNN)Rh[C(O)Et](I), **5_{Et}**. A mixture of 0.097 g (0.17 mmol) **1** and 0.14 mL (1.7 mmol) iodoethane in 15 mL dichloromethane was heated at reflux for 7 hours and then at room temperature for an additional 15 h. Volatiles were removed by vacuum distillation. The resulting red powder was washed with two 5 mL portions Et_2O and then was dried under vacuum to give 0.075 g (61%) of pure **5_{Et}** as a red solid. Mp: 218-221 ^oC (dec). Anal. Calcd. (found) for $C_{31}H_{28}IN_3OPRh$: C, 51.76 (52.03), H, 3.92 (3.88), N, 5.47 (5.66). IR(ν_{CO}, cm^{-1}): 1703 (KBr pellet). 1707 (CH_2Cl_2). ^1H NMR (CD_2Cl_2): δ_H 9.16 (d, *J* = 2.1 Hz, 1 H), 8.28 (d, *J* = 2.5 Hz, 1 H), 8.15 (m, 2 H), 7.56 (m, 1 H), 7.49 (m, 3 H),

7.42 – 7.22 (m, 6 H), 7.15 (m, 2 H), 7.06 (d, *J* = 1.5 Hz, 1 H), 6.92 (dd, *J* = 8.7, 1.7 Hz, 1 H), 6.77 (m, 1 H), 6.72 (m, 1 H), 2.89 (m, 1 H), 2.74 (m, 1 H), 2.28 (s, 3 H), 0.27 (t, *J* = 7.3 Hz, 3 H) ppm. ^{13}C NMR (CD_2Cl_2): δ_C 215.7 (dd, $J_{Rh\text{-}C}$ = 30.4, $J_{P\text{-}C}$ = 6.1 Hz, Rh-C(O)Et), 163.4 (dd, *J* = 21, 2 Hz), 147.5, 145.8, 136.6, 136.1, 135.1, 134.8 (d, *J* = 9.5 Hz), 133.3 (d, *J* = 10.4 Hz), 131.50, 131.48, 131.0 (d, *J* = 2.9 Hz), 130.7 (m), 130.5, 130.2, 129.7, 129.5, 128.8, 128.7, 128.4 (d, J = 2 Hz), 128.3 (d, *J* = 3 Hz), 124.9, 122.8, 121.9, 121.7 (dd, *J* = 13.7, 1 Hz), 121.2, 119.4 (d, *J* = 7.4 Hz), 108.5, 77.5, 48.8, 20.8, 11.5. ^{31}P NMR ($CDCl_3$): δ_P 59.0 (d, *J* = 161 Hz) ppm.

7.5. Single crystal X-ray crystallography

X-ray intensity data from a colorless prism of **H(PNN)**, a brown plate of $\mathbf{3_{BrBn}}$·acetone, and a brown plate of $\mathbf{5_{Me}}$ were measured with an Oxford Diffraction Ltd. Supernova diffractometer equipped with a 135 mm Atlas CCD detector using Mo(Kα) radiation. Raw data frame integration and Lp corrections were performed with CrysAlis Pro (Oxford Diffraction, Ltd.).[17] Final unit cell parameters were determined by least-squares refinement of 31802, 15808, and 22417 reflections from the data sets of **H(PNN)**, $\mathbf{3_{BrBn}}$·acetone, and $\mathbf{5_{Me}}$, respectively, with $I > 2\sigma(I)$ for each. Analysis of the data showed negligible crystal decay during collection in each case. Direct methods structure solutions, difference Fourier calculations and full-matrix least-squares refinements against F^2 were performed with OLEX2.[18] Empirical absorption corrections were applied to the data of **H(PNN)** using spherical harmonics implemented in the SCALE3 ABSPACK multi-scan method.[19] Numerical absorption corrections based on gaussian integration over a multifaceted crystal model were applied to the data of the remaining complexes. All non-hydrogen atoms were refined with anisotropic displacement parameters. Hydrogen atoms were placed in geometrically idealized positions and included as riding atoms. The X-ray crystallographic parameters and further details of data collection and structure refinements are presented in Table 7.2.

Table 7.2. Crystallographic Data Collection and Structure Refinement for **H(PNN)**, **3$_{BrBn}$**·acetone, and **5$_{Me}$**.

Compound	**H(PNN)**	**3$_{BrBn}$**·acetone	**5$_{Me}$**
Formula	$C_{28}H_{24}N_3P$	$C_{39}H_{35}Br_2N_3O_2PRh$	$C_{30}H_{26}IN_3OPRh$
Formula weight	433.47	871.40	705.32
Crystal system	triclinic	triclinic	monoclinic
Space group	P -1	P -1	P 2_1/c
Temp. [K]	100.6	100.9	100.7
a [Å]	9.8762(3)	9.8237(3)	11.52569(17)
b [Å]	10.5856(3)	12.7478(4)	12.68988(18)
c [Å]	12.9701(4)	15.8893(4)	18.6791(3)
α[°]	72.002(3)	74.525(3)	90
β[°]	69.415(3)	73.605(3)	95.8469(13)
γ [°]	64.541(3)	70.710(3)	90
V [Å^3]	1125.96(6)	1768.33(10)	2717.79(7)
Z	2	2	4
D_{calcd}. [gcm^{-3}]	1.279	1.637	1.724
λ[Å] (Mo or Cu Kα)	0.71073	0.71073	0.71073
μ.[mm^{-1}]	0.143	2.827	1.852
Abs. Correction	multi-scan	numerical	numerical
F(000)	456	872	1392
2θ range [°]	6.74 to 58.92	6.82 to 59.22	6.74 to 59.14
Reflections collected	63636	39949	54004
Independent reflections	6000[R(int) = 0.0271]	9098[R(int) = 0.0354]	7161[R(int) = 0.0332]
T_min/max	0.85229/1.00000	0.592/0.876	0.711/0.936
Data/restraints/ parameters	6000/0/294	9098/6/455	7161/0/336
Goodness-of-fit on F^2	1.069	1.032	1.083
*R*1/*wR*2[*I*>2σ(*I*)][a]	0.0354/0.0866	0.0281/0.0608	0.0241/0.0503
*R*1/*wR*2 (all data)[a]	0.0391/0.0894	0.0365/0.0649	0.0330/0.0552
Largest diff. peak/hole / e Å^{-3}	0.405/-0.294	0.562/-0.562	1.237/-0.868

[a] $R = \Sigma||F_o|-||F_c||/\Sigma|F_o|$. [d] $wR = [\Sigma w(|F_o^2|-|F_c^2|)^2/\Sigma w|F_o^2|^2]^{1/2}$

Figure 7.6. Molecular Structure and atom labeling for **H(PNN)**.

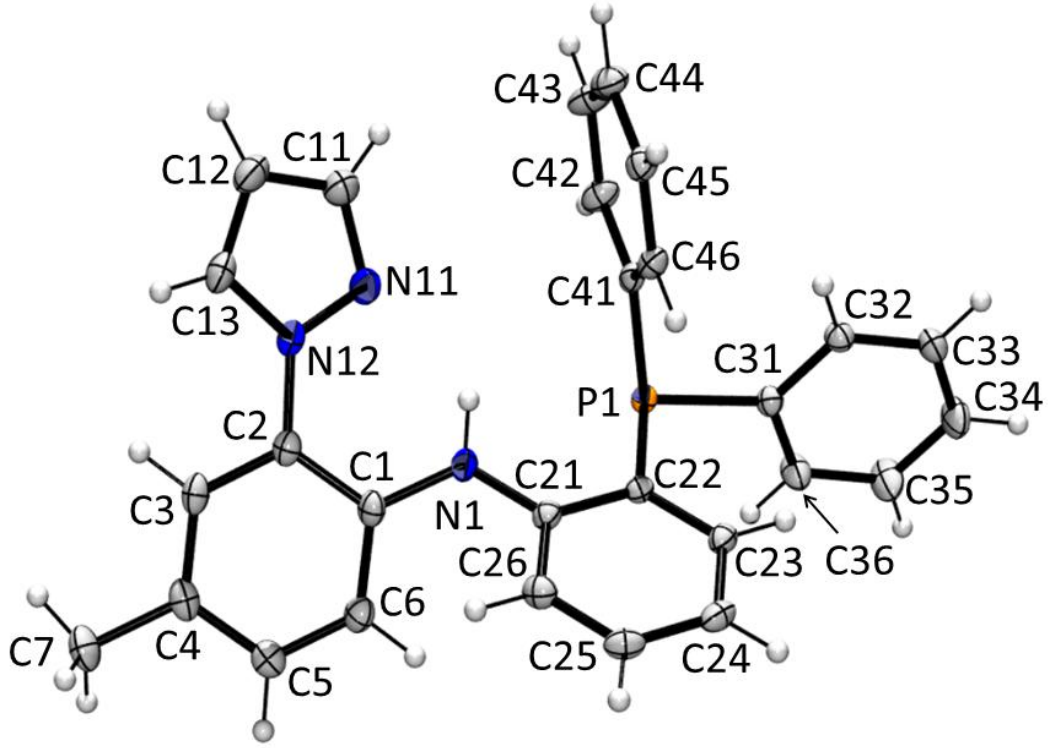

7.6. Discussion of NMR spectral data.

The multinuclear NMR spectra of analytically pure **3$_{Me}$** are complicated because of the co-existence of two isomers that can be differentiated by whether the iodide is located proximal to the pyrazolyltolyl or the arylphosphine arm, (see Figures 7.7 and 7.8.). A 7:3

Figure 7.7 Semi-empirical (PM3) energy-minimized structures of the two possible isomers of 3Me. The isomer on the right is lower energy than the other.

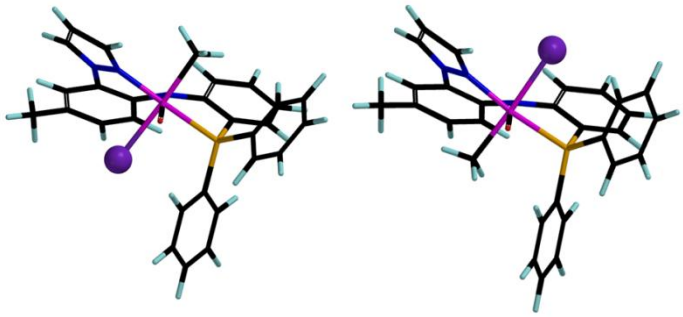

ratio of two isomers is found experimentally by relative integration of the two doublet resonances in the ^{31}P NMR spectrum of **3$_{Me}$** at δ_P 59.4 ppm (J_{Rh-P} = 121 Hz) (major) and δ_P 59.0 ppm (J_{Rh-P} = 121 Hz) (minor), as can be seen in Figure 7.8a (blue and yellow shaded resonances), for example. The similarity in chemical shifts and coupling constants for the two sets doublet resonances provides an indication that the two sets of signals are for comparable six-coordinate rhodium(III) species rather than for complexes with disparate metal coordination geometries or oxidation states. The same 7:3 ratio is found in the ^{1}H NMR spectrum by integration of the well-resolved resonances for the tolyl-CH_3 and Rh-CH_3 hydrogen nuclei. Semi-empirical equilibrium geometry calculations (or even simple molecular mechanics) indicate that the isomer with the iodide closer to the arylphosphine arm is lower energy than that with the iodide closer to

the pyrazolyltolyl arm (Figure 7.7). Similarly, a 5:2 ratio of two isomers of (PNN)Rh(Et)(CO)(I), $\mathbf{3_{Et}}$, is found from ^{1}H and ^{31}P NMR spectroscopic studies. On the other hand, only one isomer of (PNN)Rh($CH_2C_6H_4Br$)(CO)(Br), $\mathbf{3_{BrBn}}$, was found spectroscopically (presumably the same isomer as that found in the solid state structure) because of unfavorable steric interactions involving the bulky bromophenyl group and phenyl substituents of the diarylphosphine arm gives rise to a highly preferential conformation.

Figure 7.8.. ^{31}P NMR (acetone-d_6) spectra acquired after heating a mixture of **1** and (A) MeI in C_6H_6 (60^{o}C) or (B) EtI in acetone-d_6 (50^{o}C) for labeled time intervals. Key: Resonances for starting complex **1**, shaded violet, for isomers of (PNN)Rh(Me or Et)(CO)(I) shaded blue (major) and yellow (minor), and for complex 5_{Me} or 5_{Et}, shaded green.

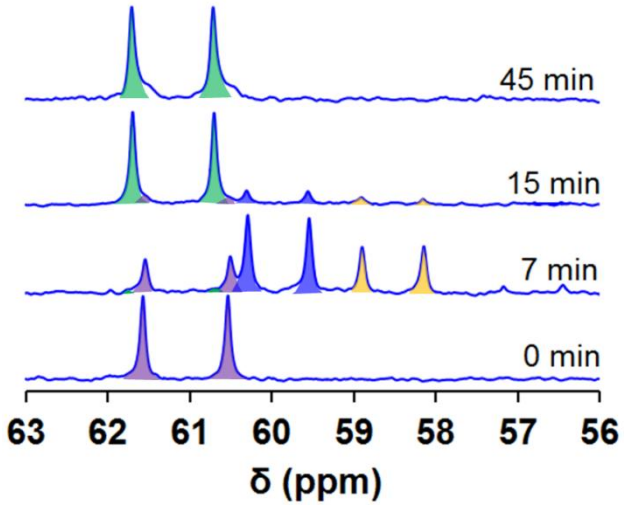

(A)

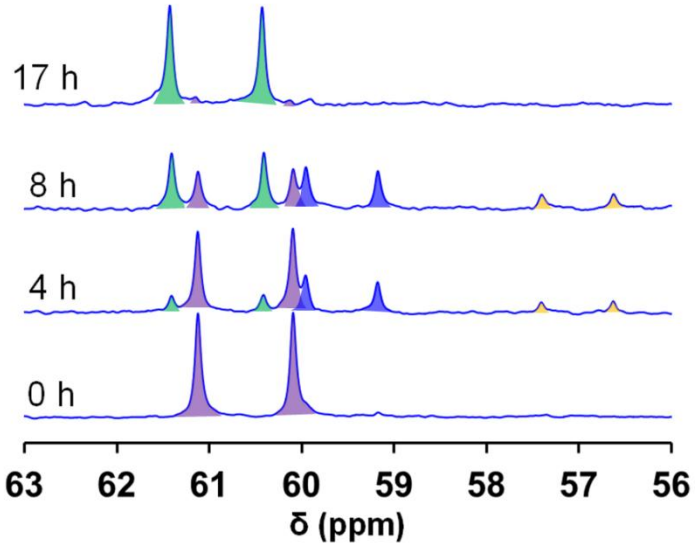

(B)

Transfer Hydrogenation (Kinetic Studies). **General Procedure.** The catalyst (5-8 mg, 0.5 mol %, 0.01 mmol), 0.0112 g KOH (0.2 mmol) and 10 mL *i*-PrOH were heated at reflux for 5 minutes and then 0.23 mL (2 mmol) acetophenone was added at once by syringe. The mixture was heated at reflux under N_2. At fixed times (2 h and 5h) two 0.3 mL aliquots (0.3 mL) were taken from the reaction mixture to verify that the ensuing work-up procedure did not affect the ratios of products observed by NMR. The work up was the same for each aliquot. Each was quenched with 2 mL hexane and filtered through a short pad of silica. The silica pad was washed with 25 mL Et_2O. The low boiling volatile components of the mixture (solvent) were removed by rotary evaporation (water aspirator) under low heat (water bath < 30^oC). It was found that heating above 30^oC under aspirator pressure led to widely-variable results as a result of preferential evaporation of acetophenone, perhaps being entrained in the Et_2O distillate. The residue was analyzed by ^1H NMR spectroscopy ($CDCl_3$) using the relative integration of resonances for methyl hydrogens of acetophenone at 2.61 ppm and the doublet resonance for methyl hydrogens of the reduced product, 1-phenylethanol, at 1.50 ppm (J = 6.5 Hz). By using the optimized work-up above, the difference in relative integrations between different aliquots of a given sample run was typically less than 1%. The data reported in Table 1 of the main text were from the average of three different experimental runs (two aliquots each, six total points).

BIBLIOGRAPHY

CHAPTER 1

1.) J. I. van der Vlugt and J. N. H. Reek, *Angew. Chem. Int. Ed*. **2009**, *48*, 2-17., Wanniarachchi, S.; Liddle, B. J.; Lindeman, S. V.; Gardinier, J. R. *Journal of Organometallic Chemistry*, **2011,** *696, 3623-3636*

2.) *The Chemistry of Pincer Compounds*. D. Morales-Morales and C. M. Jensen, Elsevier,Amsterdam, 2007; G. van Koten, and R. J. M. Klein Gebbink, *Dalton Trans*., **2011**, *40*, 8731- 8732.

(3). Gatard, S.; C-elenligil-C-etin, R.; Guo, C.; Foxman, B. M.; Ozerov,O. V. *J. Am. Chem.Soc*.**2006**, *128*, 2808

(4). Yoon, M.; Ryu, D.; Kim, J, Ahn, K. H. *Organometallics*, **2006**, *25*, 2409–2411

(5) Kozlov, L. A.; Aleksanyan, D. V.; Nelyubina, Y. V.; Lyssenko, K. A.; Petrovskii, P. V.; Vasil'ev, A. A.; Odinets, I. L.*Organometallics*, **2011**, *30*, 2920–2932. Lipke, M. C.; Woloszynek, R. A.; Ma, L.; Protasiewicz, J. D.; *Organometallics*, **2009**, *28*, 188–196

(6). Baumann, R.; Davis, W. M.; Schrock, R. R. *J. Am. Chem. Soc.* **1997,** *119*, 3830

(7). Daugulis, O.; Brookhart, M. *Organometallics*, **2004**, *23* 527–534

(8). Aydin, J.; Kumar, K. S.; Sayah, M. J.; Wallner, O. A.; Szabó, K. J. *J. Org. Chem.*, **2007**, *72*, 4689–4697

(9). Naota, T.; Takaya, H.; Murahashi, S.-I.*Chem. Rev.* **1998**, *98*, 2599

(10). Macgregor, S. A.;Roe, D. C.; Marshall, W. J.; Bloch, K. M.; Bakhmutov, V. I.; Grushin,V. V.*J.Am. Chem. Soc*. **2005**, *127*, 15304.Douglas, T. M.; Chaplin,A. B.; eller, A. S. Organometallics **2008**, *27*, 2918. Chen, S.; Li, Y.;Zhao, J.; Li, X. *Inorg. Chem*. **2009**, *48*, 1198

(11). Konrad, F.; Fillol, J. L.; Wadepohl, H.; Gade, L. H. *Inorg. Chem*. **2009**, *48*, 8523-8532

(12). Wucher, B.; Moser, M.; Schumacher, S. A.; Rominger, F.; Kunz, D. *Angew. Chem. Int. Ed*.**2009**, *48*, 4417 –4421

(13). Gladialia, S and Alberico, E. *Chem. Soc. Rev*., **2006**, *35*, 226–236
(14). Backvall, J. *Journal of Organometallic Chemistry*. **2002**, *652*, 105-111.

(15). Naota, T.; Takaya, H.; Murahashi, S.-I. *Chem. Rev.* **1998**, *98*, 2599.

(16). Dani, P.; Karlen, T.; Gossage, R. A.; Gladiali, S.; van Koten, G. *Angew. Chem., Int. Ed.* **2000**, *39*, 743.

(17). Zweifel, T.; Naubron, J. V.; Buttner, T.; Ott, T.; Grutzmacher, H.*Angew. Chem. Int. Ed*. **2008**, *47*, 3245-3249.

(18.). Baratta, W.; Chelucci, G.; Gladiali, S.; Siega, K.; Toniutti, M.; Zanette, M.; Zangrando, E.; Rigo, P. *Angew.Chem., Int. Ed.* **2005**, *44*, 6214.

(19). Recent Advances in Hydride ChemistryH. Jacobsen, H. Berke (Eds.: M. Peruzzini, R. Poli), Elsevier, Amsterdam, 2001, p. 89

(20). Lindner, R.; van den Bosch, B.; Lutz, M.; Reek, J. N. H.; van der Vlugt, J.I. *Organometallics*, **2011**, *30*, 459-510.

(21) .Braunstein, P.; Fryzuk, M.D.; Le Dall, M.; Naud, F.; Rettig, S. J.; Speiser, F. *Chem. Soc., Dalton Trans.*, **2000**, 1067; Dulebohn, J. I.; Haefner, S. C.; Berglund, K. A.; Dunbar, K. R. *Chem. Mater*. **1992**, *4*, 506.

(22). Grtzmacher, H.*Angew. Chem. Int. Ed*. **2008**, *47*, 1814 – 1818

(23). Frauhiger, B. E.; White, P. S.; Templeton, J. L.*Organometallics*, **2012,***31*, 25–237

(24). Ruddy, A. J.; Mitton, S. J.; McDonald, R.; Turculet, L.*Chem. Commun*.**2012**, *48*, 1159-1161

(25). Vuzman, D.; Poverenov, E.; Shimon, L. J. W.; Posner, Y. D.; Milstein, D.*Organometallics***2008,***27*, 2627-2634. |

(26). Lindner,R.; van den Bosch, B.; Lutz, L.; Reek, J. N. H.; van der Vlugt, J. I. *Organometallics* **2011,***30*, 499–510

(27). Cundari, T. R.; Klinckman, T. R.; Wolczanski, P. T. *J. Am. Chem.Soc.***2002**, *124*, 1481, and references cited therein

(28). a) Noyori, R.;Ohkuma, T.*Angew. Chem.***2001**, *113*, 40; *Angew.Chem. Int. Ed*. **2001**, *40*, 40; b) Noyori, R.; Yamakawa, M.; Hashiguchi, S. *J. Org. Chem.***2001,***66*, 7931., MuViz, K.*Angew. Chem.* **2005**, *117*, 6780*; Angew.Chem. Int. Ed*. **2005**, *44*, 6622

(29). Gunanathan, C.; Milstein, D.*ACCOUNTS OF CHEMICAL RESEARCH*.**2011**, *44*,

588-602. (b). Gunanathan, C.; Gnanaprakasam, B.; Iron, M. A.; Shimon, L. J. W.; Milstein, D. *J. Am. Chem.Soc*. **2010**, *132*, 14763–14765

(30). Kohl, S.W.; Weiner, L.; Schwartsburd, L.; Konstantinovski, L.; Shimon, L. J.W.; Ben-David,Y.; Iron, M. A.; Milstein, D. *Science*.**2009**, *324*, 74–77

(31). Zhao, J.; Goldman, A. S.; Hartwig, J. F. *Science*.**2005**, *307*, 1080

(32). (a) *Inorg. Chem.*, **2011**,*50 (forum articles).* (b) Braunstein, O.; Naud, F. *Angew.Chem. Int. Ed*. **2001**, *40*, 680-699.(c). Jadzewski, B. A. and Tolman, W. B. *Coord. Chem. Rev*., **2000**, *200-202*, 633 (d) van der Vlugt, J. I.; Reek, J. N. H. *Angew.Chem. Int. Ed*. **2009**, *48*, 2-17

(33). Jorgensen, C. K. *Coord.Chem.Rev.* **1966**, *1*, 164

(34). da Silva, R. S.; Gorelsky, S. I.; Dodsworth, E. S.; Tfouniand, E.; Lever, A. B. P. *J. Chem. Soc., Dalton Trans.*, **2000**, 4078.

(35). A. Juris, V. Balzani, F. Barigeletti, S. Campagna, P. Belser andA. vonZelewsky, *Coord. Chem. Rev.*, 1988, **84**, 85

(36). Pierpont, C. G. *Coord. Chem. Rev*., **2001**, *219-221*, 415-433.

(37). Lever, A. B. P. *Coord. Chem. Rev*., **2010**, *254*, 1397-1405.C. G. Pierpont and C. W. Lange, *Prog. Inorg. Chem.*, **1994**, *41*, 331;C. G. Pierpont, *Coord. Chem. Rev.*, **2001**, *216*, 99.

(38). Jung,O.S.; Jo,D. H.; Lee,Y.A.; Conklin,B. J.; Pierpont, C. G.*Inorg. Chem.*, **1997**, *36*, 19

(39). Stubbe, J. and Van der Donk, W. A. *Chem. Rev*., 1998, *98*, 705.

(40.). Kaim, W.; Dchwederski, B.*Coord. Chem. Rev*., **2010**, 254, 1580-1588

(41). Heyduk, A.F.; Zarkesh, R. A.; Nguyen, A. I. *Inorg. Chem.***2011**, *50*, 9849-9863

42.). de Bruin,B.; Bill, E.; Bothe, E.; Weyhermuller, T.; Weighardt, K. *Inorg. Chem.* **2000,** *39*, 2936-2947

(43). Dzik, W. I.; van derVlugt, J. I.; Reek, J. N. H.; de Bruin, B. *Angew. Chem. Int. Ed*. **2011**, *50*, 3356- 3358.

(44). Adhikari, D.; Mossin,S.; Basuli, F.; Huffman, J. C.; Szilagyi, K.; Meyer, K.; Mindiola, D. J. *J. Am. Chem.Soc.* **2008**, 130, 3676-3682

(45). Reger, D. L.; Gardinier, J. R.; Semeniuc, R. F.; Smith, M. D. , *J. Chem. Soc., Dalton Trans.*, **2003**, 1712-1718

CHAPTER 2

(1). (a) Oliveira,B. L.; Correia, G. D. J.; Raposhinho, P. D.; Santos, I.; Ferreira, A.; Cordeiro, C.; Freire, A. P.; *Dalton Trans*. **2009**, 152-162. (b) Maria, L.; Cunha, S.; Videira, M.; Gano, L.; Paulo, A.; Santos, I. C.; Santos, I. *Dalton Trans*. **2007**, 3010-3019. (c) Alberto, R.; *Top. Curr. Chem.* **2005**, *252*, 1-44. (d) Dilworth, J. R.; Parrott, S. *J. Chem. Soc. Rev.* **1998**, *27*, 43-55.

(2). Kirgan, R. A.; Sullivan, B. P.; Rillema, D. P. *Top. Curr. Chem*. **2007**, *281*, 45-100.

(3). (a) Walther, M. E.; Wenger, O. S. *Dalton Trans*. **2008,** 6311-6318. (b) Vlcek, A.; Busby,M. *Coord. Chem. Rev*. **2006**, *250*, 1755-1762.

(4). (a) Si, Z.; Li, J.; Li, B.; Zhao, F.; Liu, S.; Li, W. *Inorg. Chem*. **2007,** *46*, 6155-6163. (b) Lundin, N. J.; Blackman, A. G.; Gordon, K. C.; .Officer, D. L. *Angew. Chem., Int. Ed.* **2006,** *45*, 2582-2584.

(5). (a) Meyer, J. R. *Inorg. Chem*. **2005**, *44*, 6852-6864. (b) Kalyanasundaram, K.; Gratzel, M. *Coord. Chem. Rev*. **1998,** *177*, 347-414.

(6). Liddle, B. J.; Silva, R. M.; Morin, T. J.; Macedo, F. P.; Shukla, R.; Lindeman, S. V.; Gardinier, J. R. *J. Org. Chem*. **2007**, *72*, 5637-5646.

(7). Morin, T. J.; Lindeman, S. V.; Gardinier, J. R.; *Eur. J. Inorg. Chem*. **2009**, 104-110.

(8).Liddle, B. J.; Lindeman, S. V.; Reger, D. L.; Gardinier, J. R. *Inorg. Chem*. **2007**, *46*, 8484-8486.

(9). (a) Mukherjee, A.; Subramanyam, U.; Puranik, V. G.; Mohandas, T. P.; Sarkar, A. *Eur. J. Inorg. Chem*. **2005,** 1254-1263. (b) Piers, W. E.; Bourke, S. C.; Conroy, K. D..*Angew. Chem. Int. Ed*. **2005**, *44*, 5016-5036. (c) Saha, N.; Saha, A.; Chaudhuri, S Mak, T. C. W.; Banerjee, T.; Roychoudhury, P. *Polyhedron*. **1992**, *11*, 2341-2349.

(10). Drew, M.G. B.; Mukherjee, G. A.; De, S.; Nag, S.; Datta, D. *Inorg. Chim. Acta* **2007**, *360*, 3448-3451.

(11). Schmidt, S.P.; Trogler, W.C.; Basolo, F. *Inorg. Synth*. **1990**, *28*, 160-165.

(12). Noviandri, K.N. Brown, D.S. Fleming, P.T. Gulyas, P.A. Lay, A.F. Masters, L. Phillips, J. Phys. Chem**. 1999,** 6713-6722.

(13). SMART APEX2 Version 2.0-2 Bruker Analytical X-ray Systems, Inc., Madison, Wisconsin, USA, 2005.
(14). SAINT+ Version 7.23a and SADABS Version 2.05. Bruker Analytical X-ray Systems, Inc., Madison, Wisconsin, USA, 2005.

(15). Sheldrick, G. M. SHELXTL Version 6.1; Bruker Analytical X-ray Systems, Inc., Madison, Wisconsin, USA, 2000.

(16). (a) Cristau, H.-J.; Cellier, P.P; Spindler, J.F. Taillefer, M *Eur. J. Org. Chem.* **2004**, 695-709. (b) Taillefer, M.; Xia, N.; Ouali, A. *Angew. Chem. Int. Ed*. **2007**, *46*, 934-936. (c) Christau, H. J.; Cellier, P.P.; Spindler, J. F.; Taillefer, M. *Chem. Eur. J.* **2004,** *10*, 5607-5622. (d) See also, Lindley, J. M.; McRobbie, I. M.; Meth-Cohn, O.; Suschitzky, H. *J. Chem. Soc., Perkin Trans. 1* **1980,** 982-994.

(17). Antilla, J. C.; Baskin, J. M.; Barder, T. E.; Buchwald, S. L. *J. Org. Chem.* **2004,** *69*, 5578-5587.

(18). See *Journal of Organometallic Chemistry*, **2010**, *695, 53-61*.

(19). Antón, N.; Arroyo, M.; Gómez-Iglesias, P.; Miguel, D.; Villifañe, F. *J. Organomet. Chem.* **2008**, *693*, 3074-3080.

(20). Reger, D. L.; Gardinier, G. R.; Pellechia, P. J.; Smith, M. D.; Brown, K. J. *Inorg. Chem.* **2003**, *42*, 7635-7643,

(21). Liaw, W. F.; Hsieh, C. K.; Lin, G. Y.; Lee, G. H. *Inorg. Chem*. **2001**, *40*, 3468-3475.

(22). Hevia, E.;. Perez, J.; Riera, V.; Miguel, D. *Organometallics.* **2002,** *21*, 1966-1974.

(23). Fester, V. P.; Houghton, P. J.; Main, L.; Nicholson, B. K. *Polyhedron.* **2007**, *26*, 430-433.

(24). Silva, R. M.; Liddle, B. J.; Lindeman, S. V.; Smith, M. D.; Gardinier, J. R. *Inorg. Chem.* **2006**, *45*, 6794-6802.

(25). (a) Bullock, J. P.; Carter, E.; Johnson, R.; Kennedy, A. T.; Key, S. E.; Kraft, B. J.; Saxon, D.; Underwood, P. *Inorg. Chem*. **2008**, *47*, 7880-7887. (b) Seeber, R.; Mazzocchin, G. A.; Mazzi, U.; Roncari, E.; Refosco, F. *Trans. Met. Chem*. **1984**, *9*, 315-318. (c) Gubin, S.P.; Denisovich, L.I.; Zakurin, N.V.; Ginzburg, A.G.; *Izv. Akad. Nauk SSSR, Ser. Khim*. **1978**, *6*, 1322-1327. (d) Denisovich, L. I.; Zakurin, N. V.; Gubin, S.P.; Ginzburg, A. G. *J. Organomet. Chem*. **1975,** *101*, C43-C44.

(26). Fenske, R. F.; Lichtenberger, D. L. *J. Am. Chem. Soc*. **1976,** *98*, 50-63.

(27). Hall, M. B. *J. Am. Chem. Soc*. **1975**, *97*, 2057-2065.

(28). Roy, L . E.; Batista, E. R.; Hay, P. J. *Inorg. Chem*. **2008**, *47*, 9228-9237.

(29). The electrochemical behavior of aniline derivatives relies on the availability of the lone pair of electrons on the NH_2 moiety to be in conjugation with the aryl π-system rendering the aromatic molecule electron-rich. Upon binding to Lewis acids, the nitrogen becomes quartenary and its lone pair of electrons is less energetically accessible. As will be detailed elsewhere, the oxidation potentials of the protonated ligand $[H_2(pzAn^{Me})](BF_4)$ and even that of the cationic $[Me_2C(N,N\text{-}pzAnMe)](BF_4)$ (with an sp^2-hybridized amino nitrogen) occur above 2.3 V.

(30). Koopmans, T. *Physica 1*. **1933** 104-113.

(31). (a) Figgis, B. N.; Hitchman, M. A. *Ligand Field Theory and Its Applications*; Wiley-VCH: New York, **2002**. (b). Lever, A. B. P. *Inorganic Electronic Spectroscopy*; Elsevier: New York, **1968**.

(31). Machura, B.; Kruszynski, R.; Jaworska, M.; Lodowski, P.; Penczek, R.; Kusz, J. *Polyhedron.* **2008,** *27*, 1767-1778.

(32). Liddle, B. J.; Waniarachchi, S.; Lindeman, S. V.; Gardinier, J. R. *J. Organomet.. Chem.* **2010**, *695*, 53.

CHAPTER 3

(1). *Molecular Nanoelectronics*; Reed, M. A.; Lee, T., Eds.; American Scientific Publishers: Stevenson Ranch, CA, **2003**; *Molecular Switches*, B.L. Feringa, Ed.; Wiley-VCH: New York. **2001**.

(2). Balzani,V.; Credi, A.; Venturi, M. *Molecular Devices and Machines: Concepts and Perspectives for the Nanoworld, 2nd Ed.*; Wiley-VCH: Weinheim, **2008,** Ch 8 and 9.

(3). Olivier, C.; Kim, B.; Touchard, D.; Rigaut, S. *Organometallics*, **2008**, *27*, 509; Chae, D. H.; Berry, J. F.; Jung, S.; Cotton, F. A.; Murillo, C. A.;Yao, Z. *Nano Letters*. **2006,** *6*, 165; Yin, B.; Niemeyer, F.; Williams, J. A. G.; Jiang, J.; Boucekkine, A.; Toupet, L.; Le Bozec, H.; Guerchais, V. *Inorg. Chem.* **2006**. ***45***, 8584. Evangelio, E.; Ruiz-Molina, D. *Eur. J. Inorg. Chem.* **2005**, 2957;

(4). *The Chemistry of Pincer Compounds*, D. Morales-Morales and C.M. Jensen, Eds; Elsevier: New York, **2007**.

(5). For instance, Rajca, A.; Vale, M.; Rajca, S. *J. Am. Chem. Soc*., **2008,** *130*, 9099.

(6). Adhikari, D.; Mossin, S.; Basuli, F.; Huffman, J. C.; Szilagyi, R. K.; Mayer, K.; Mindiola, D. J. *J. Am. Chem. Soc.* **2008**, *130*, 3676; Harkins, S. B.; Peters, J. C. *Inorg. Chem.*, **2006**, *45*, 4316; Harkins, S. B.; Peters, J. C. *J. Am. Chem. Soc.* **2005**, *127*, 2030; Harkins, S. B.; Peters, J. C. *J. Am. Chem. Soc.* **2004**, *126*, 2885;.

(7). Radosevich, A. T.; Melnick, J. G.; Stoian, S. A.; Bacciu, D.; Chen, C. H.; Foxman, B. M.; Ozerov, O. V.; Nocera, D. G. *Inorg. Chem.*, **2009**, *48*, 9214.

(8). van der Vlugt, J. I.; Reek, J. N. H. *Angew. Chem. Int. Ed.* **2009**, *48*, 8832 and references.

(9). Schmidt, S. P.; Trogler, W. C.; Basolo, F. *Inorg. Synth.* **1990**, *28*, 160.

(10**).** Fan, L.; Foxman, B. M.; Ozerov, O.V. *Organometallics* **2004**, ***23***, 326.

(11). Noviandri, I.; Brown, K. N.; Fleming, D. S.; Gulyas, P. T.; Lay, P. A.; Masters, A. F.; Phillips, L. *J. Phys. Chem. B* **1999**, *103*, 6713.

(12). Rathore, R.; Burns, C. L.; Deselinescu, M. I.; Denmark, S. E.; Bui,T. *Org. Synth.* **2005**, *82*, 1.

(13). SMART APEX2 Version 2.0-2 Bruker Analytical X-ray Systems, Inc., Madison, Wisconsin, USA, **2005**.

(14). SAINT+ Version 7.23a and SADABS Version 2.05. TWINABS Bruker Analytical X-ray Systems, Inc., Madison, Wisconsin, USA, **2007.**

(15) Sheldrick, G. M. SHELXTL Version 6.1; Bruker Analytical X-ray Systems, Inc., Madison, Wisconsin, USA, **2000.**

(16). CCDC 759658, 759659, 759660, 759661, and 759662 contain the supplementary crystallographic data for **H(L)**, **1**, **2·PF$_6$**, **2·OTf**, and **3**. These data can be obtained free of charge from The Cambridge Crystallographic Data Centre via www.ccdc.cam.ac.uk/data_request/cif.

(17). Fan, L.; Foxman, B. M.; Ozerov, O. V. *Organometallics* **2004**, *23*, 326.

(18). Morin, T. J.; Lindeman, S. V.; Gardinier, *J. R. Eur. J. Inorg. Chem.* **2009**, *104*; Liddle, B. J.; Silva, R. M.; Morin, T. J.; Macedo, F. P.; Shukla, R.; Lindeman, S. V.; Gardinier, J. R. *J. Org. Chem.* **2007**, *72*, 5637 and references.

(19). The quasi-reversible nature of the wave (and scan rate dependence) is retained in other solvents (CH_3CN, THF) and is likely a result of slow structural reorganization on the time-scale of the cyclic voltammetry experiment.

(20). Compare also to: DeLearie, L. A.; Haltiwanger, R. C.; Pierpont, C. G. *Inorg. Chem.*, **1989,** *28*, 644.

(21). Chong, D.; Laws, D. R.; Nafady, A.; Costa P. J.; Rheingold, A. L.; Calhorda, M. J.; Geiger, W. E. *J. Am. Chem. Soc.* **2008**, *130*, 2692; Cotton, F. A.; Dunbar, K. R.; Falvello, L. R.; Walton, R.A. *Inorg. Chem.*, **1985**, *24*, 4180.

(22). (a) Liddle, B. J.; Waniarachchi, S.; Lindeman, S. V.; Gardinier, J. R. *J. Organomet.. Chem.* **2010**, *695*, 53. (b) Wei, L.; Babich, j.; Eckelman, W. C.; Zubieta, J. *Inorg. Chem.*, **2005**, *44*, 2198. (c) Machura, B.; Kruszynski, R.; Jaworska, M.; Lodowski, P.; Penczek, R.; Kusz, J. *Polyhedron* **2008**, *27*, 1767. (c) Silva, R. M.; Liddle, B. J.; Lindeman, S. V.; Smith, M. D.; Gardinier, J. R. *Inorg. Chem.* **2006**, *45*, 6794.

(23). SPARTAN, Wavefunction, Inc., Irvine, CA, **1997**.

(24). For instance see: (a) Ref S-9a. (b) Takatani, T.; Sears, J. S.; Sherill, D. C. *J. Phys. Chem. A* **2009**, ***113***, 9231. (c) Rayon, V. M.; Frenking, G. *Chem. Eur. J.* **2002**, *8*, 4693. (d) Szilagyi, R. K.; Frenking, G. *Organometallics* **1997, 16**, 4807.

(25). Becke, A. D. *J. Chem. Phys.* **1993,** *98*, 5648.

(26). Lee, C.; Yang, W.; Parr, R. G. *Phys. Rev. B* **1988**, ***37***, 785.

(27). (a) Hay, P. J.; Wadt, W. R. *J. Chem. Phys.* **1985,** *82*, 270. (b) Wadt, W. R.; Hay, P. J. *J. Chem. Phys.* **1985**, ***82***, 284.

CHAPTER 4

(1) Ozerov,O.V.; *The Chemistry of Pincer Compounds*, D. Morales-Morales and C.M. Jensen, Eds; Elsevier: New York, Chapter 13, 2007.

(2) Radosevich, A.T.; Melnick, J.G.; Stoian, S.A.; Bacciu, D.: Chen, C. H.; Foxman, B. M.; Ozerov, O.V.; Nocera, D.G. *Inorg. Chem.*, **2009**, *48*, 9214; van der Vlugt, J.I.; Reek, J. N. H. *Angew. Chem. Int. Ed.*, **2009**, *48*, 8832 and references; Nguyen, A. I.; Blackmore, K. J.; Carter, S. M.; Zarkesh, R. A.; Heyduk, A. F. *J. Am. Chem. Soc.* **2009**, *131*, 3307 and references; Adhikari, D,. Mossin, S.; Basuli, F.; Huffman, J. C.; Szilagyi, R. K.; Mayer, K and Mindiola, G. J. *J. Am. Chem. Soc.*, **2008**, ***130***, 3676; Harkins, S. B.; and Peters, J. C.; *Inorg. Chem.*, **2006**, ***45***, 4316; Harkins, S. B.; and. Peters, J. C. *J. Am. Chem. Soc.*, **2005**, *127*, 2030; Harkins, S. B.; and Peters, J. C. *J. Am. Chem. Soc.*, **2004**, *126*, 2885.

(3) Wanniarachchi; S.; Liddle; B. J.; Toussaint; J.; Lindeman; S. V.; Bennett; B.; Gardinier, J. R. *Dalton Trans.*, **2010**, *39*, 3167.

(4) Liddle, B. J.; Silva, R. M.; Morin, T. J.; Macedo, F. P.; Shukla, R.; Lindeman, S. V.; Gardinier, J. R. *J. Org. Chem.*, **2007**, *72*, 5637; Taillefer, M.; Xia, N.; Ouali, A.; *Angew. Chem. Int. Ed*., **2007**, *46*, 934 and references; Antilla, J. C.; Baskin, J. M.; Barder, T. E.; Buchwald, S. L.; *J. Org. Chem***., 2004**, *69*, 5578

(5) Fan, L.; Foxman, B. M.; Ozerov, O. V. *Organometallics* **2004**, *23*, 326.

(6) Trofimenko, S.; Calabrese, J. C.; Domaille, P. J.; Thompson, J. S. *Inorg. Chem.*, **1989**, *28*, 1091.

(7) Chadwick, K.; Davey, R. J.; Pritchard,R. G.; Hunter, C. A.; Musumeci, D. *Cryst. Growth. Des.* **2009**, *9*, 1990; Zanker, V.; Mantsch; H. H.; Erhardt, E. *Anales de Quimica*, **1968,** *64*, 659; Salimov, M. A.; Tatevskii,V. M.. *Dokl. Akad. Nauk. SSSR*, **1957**, *112*, 890.

(8) Sharma, R. C.; Parashar, R. K. *J. Inorg. Biochem.* **1987**, *29*, 225; Savitskii, A. V.; Kosareva, T. M.. *Dokl. Akad. Nauk, SSSR*, **1971**, *197*, 359; Decker, J. S.; Frye, H. *Z. Naturforsch. Teil B*, **1966**, *21*, 527..

(9) Liddle, B. J.; Wanniarachchi, S.; Lindeman, S. V.; Gardinier, J. R. *J. Organomet. Chem.*, **2010**, *1*, 695.

(10) Alves, S.; Paulo, A.; Correia, J. D. G.; Domingos, A.: Santos, I. *J. Chem. Soc., Dalton Trans.*, **2002**, *47*, 4714.

(11) Machura, B.; Kruszynski, R.; Jaworska, M.; Lodowski, P.; Penczek, R.: Kusz, J. *Polyhedron*, **2008**, 1767.

(12) Parker, A. J. *J. Chem. Soc.*, **1961**, 1328.

(13) The average Re-N bond distance of 2.223 Å in $\mathbf{4^{iPr}}$ is similar to 2.219 Å found in $\mathbf{2^{iPr}}$ where the Re-N_{Ar} bond (2.306 Å) is longer and the two Re-N_{pz} (2.177, 2.185 Å) are shorter for the former than in the latter. It is also noted that the amino nitrogen is more pyramidal for $\mathbf{4^{iPr}}$ than $\mathbf{2^{iPr}}$ as evident from the smaller sum of angles around nitrogen not involving the methyl (326^o versus 333^o) and larger perpendicular distance of nitrogen from the mean plane of rhenium and aryl carbon atoms to which nitrogen is bound (0.576 Å versus 0.519 Å). The small but increased ligand distortion in $\mathbf{4^{iPr}}$ versus $\mathbf{2^{iPr}}$ is also found from the tolyl-tolyl and average pz-tolyl dihedral angles (73^o versus 70^o and 40^o versus 37^o, respectively).

(14) Rathore, R.; Burns, C. L.; Deselinescu, M. I.; Denmark, S. R.; Bui, T. *Org. Synth.* **2005**, *82*, 1.

(15) The difference in EPR signal line shapes between ($\mathbf{3^{H+}}$) and ($\mathbf{3^{Me+}}$) or ($\mathbf{3^{iPr+}}$) can be attributed to a number of factors. First, the rhenium hyperfine coupling is smaller than the overall line width in the latter two cases causing alteration of the hyperfine pattern. The relative intensities of the four middle lines (line 4 > 3 > 5 > 2) in the latter two spectra may also arise due to genuine asymmetry of the complexes to give higher order effects. The possibility for multiple conformers (where each has a slightly different g-value) and any dynamic equilibria involving these species may also contribute. Incomplete motional averaging seems unlikley given the small size of the molecule.

(16)..Chong, D.; Laws, D. R.; Nafady, A.; Costa, P. J.; Rheingold, A. L.; Calhorda, M. J.; Geiger, W. E. *J. Am. Chem. Soc.* **2008**, *130*, 2692; Cotton, F. A.; Dunbar, K. R.; Falvello,L. R.; Walton, R. A. *Inorg. Chem.*, **1985**, *24*, 4180.

(17) Schmidt, S. P.; Trogler, W.C.; Basolo, F. *Inorg. Synth.*, **1990**, *28*, 160.

(18) Noviandri, I.; Brown, K. N.; Fleming, D. S.; Gulyas, P. T.; Lay, P. A.; Masters, A. F.; Phillips,L. *J. Phys. Chem. B* **1999**, *103*, 6713.

(19)..SMART APEX2 Version 2.0-2 Bruker Analytical X-ray Systems, Inc., Madison, Wisconsin, USA, **2005**.

(20)..SAINT+ Version 7.23a and SADABS Version 2.05. TWINABS Bruker Analytical X-ray Systems, Inc., Madison, Wisconsin, USA, 2**007**.

(21) Sheldrick, G. M. SHELXTL Version 6.1; Bruker Analytical X-ray Systems, Inc., Madison, Wisconsin, USA, 2000.

CHAPTER 5

(1) (a) A recent forum Issue on Redox Non-Innocent Ligands: *Inorg. Chem.* **2011**, *50*, 9737−9914. (b) Caulton, K. G. *Eur. J. Inorg. Chem.* **2012**, 435-443.

(2) Lyaskovskyy, V.; de Bruin, Bas *ACS Catalysis* **2012**, *2*, 270-279. (b) Lu, F.; Zarkesh, R. A.; Heyduk, A. F. *Eur. J. Inorg. Chem.* **2012**, *2012*, 467-470.

(3) (a) Nishimori, Y.; Kanaizuka, K.; Kurita, T.; Nagatsu, T.; Segawa, Y.; Toshimitsu, F.; Muratsugu, S.; Utsuno, M.; Kume, S.; Murata, M.; Nishihara, H. *Chem. Asian J.* **2009**, *4*, 1361-1367. (b) Olivier, C.; Kim, B.; Touchard, D.; Rigaut, S. *Organometallics* **200**8, *27*, 509-518. (c) Dong, T.- Y.; Lin, M.- C.; Chiang, M. Y.- N.; Wu, J-. Y. *Organometallics* **2004**, *23*, 3921-3930.

(4) By Kundu, N.; Maity, M.; Chatterjee, P. B.; Teat, S. J.; Endo, A.; Chaudhury, M. J. Am. Chem. Soc. 2011, 133, 20104-20107. Dei, A.; Sorace, L. *Appl. Magn. Reson.* **2010**, *38*, 139-153. Evangelio, E.; Ruiz-Molina, D. *C. R. Chim.* **2008**, *11*, 1137-1154. Sato, O.; Cui, A.; Matsuda, R.; Tao, J.; Hayami, S. *Acc. Chem. Res.* **2007**, *40*, 361-369.

(5) (a) Wanniarachchi, S.; Liddle, B. J.; Toussaint, J.; Lindeman, S. V.; Bennett, B.; Gardinier, J. R. *Dalton Trans.* **2011**, *40*, 8776-8787. (b) Wanniarachchi, S.; Liddle, B. J.; Toussaint, J.; Lindeman, S. V.; Bennett, B.; Gardinier J. R. *Dalton Trans.* **2010**, *39*, 3167 – 3169.

(6) Wanniarachchi, S.; Liddle, B. J.; Lindeman, S. V.; Gardinier J. R *J. Organomet. Chem.* **2011**, *696*, 3623-3636.

(7) (a) Bursten, B. E.; Green, M. R.; Katovic, V; Kirk, J. R.; Lightner Jr., D. *Inorg. Chem.* **1986**, *25*, 831-834. (b) Bursten, B. E. *J. Am. Chem. Soc.* **1982**, *104*, 1299-1304.

(8) Chatt, J.; Kan, C. T.; Leigh, G. J.; Pickett, C. J.; Stanley, D. R. *J. Chem. Soc., Dalton Trans.* **1980**, 2032-2038.

(9) Lever, A. B. P. *Inorg. Chem.* **1990**, *29*, 1271-1285.

(10) Pombiero, A. J. L. *Eur. J. Inorg. Chem.* **2007**, 1473-1482.

(11) (a) Makedonas, C; Mitsopoulou, C. A. *Eur. J. Inorg. Chem.* **2007**, 4176-4189. (b) Ahrland, S.; Chatt, J. *J. Chem. Soc.* **1957**, 1379-1386.

(12) SMART APEX2 Version 2.1-4, SAINT+ Version 7.23a and SADABS Version 2004/1. Bruker Analytical Xray Systems, Inc., Madison, Wisconsin, USA, 2005.

(13) CrysAlisPro, Agilent Technologies,Version 1.171.34.46 (release 25-11-2010 CrysAlis171 .NET), (compiled Nov 25 2010,17:55:46)

(14) G. M. Sheldrick, SHELXTL Version 6.12; Bruker Analytical X-ray Systems, Inc., Madison Wisconsin, USA, 2001.

(15) See section 5.7

(16) (a) Coe, B. J.; Fielden, J.; Foxon, S. P. Asselberghs, I.; Clays, K.; Brunschwig, B. S. *Inorg. Chem.* **2010**, *49*, 10718-10726. (b) Shepherd, R. E.; Proctor, A.; Henderson, W. W.; Myser, T. K. *Inorg. Chem.* **1987,** *26*, 2440-2444. (c) Lavallee, D. K.; Fleischer, E. B. *J. Am. Chem. Soc.* **1972**, *94*, 2583-2599. (d) Krishna, V. G.; Chowdhury, M. *J. Phys. Chem.* **1963**, *67*, 1067-1069.

(17) Patra, S. Chandra; B., Manas K.; Maity, A. N.; Ghosh, P. *Inorg. Chem.* **2011**, *50*, 1331-1338.

(18) Kasha, M.; Rawls, R. *Photochem. Photobiol.* **1968**, *7* (6), 561-569.

(19) Rathore, R.; Burns, C.L.; Deselinescu, M.I.; Denmark, S.E.; Bui, T. *Org. Synth.* **2005**, *82*, 1-9.

(20) (a) Ellison, I. J.; Gillard, R. D.; Moszner ,M.; Wilgocki, M.; Ziolkowski, J. J. *J. Chem. Soc., Dalton Trans.* **1994**, 2531-2538. (b) Buckley, A. N.; Busby, J. A.; Ellison, I. J.; Gillard, R. D. *Polyhedron*, **1993**, *12*, 247-253. (c) Ellison, I. J. and R. D. Gillard, *J. Chem. Soc., Chem. Commun.*, **1992**, 851.

(21) Reger, D. L.; Gardinier, J. R.; Elgin, J. D.; Smith, M. D.; Hatout, D.; Long, G. J.; Grandjean, F. *Inorg. Chem.* **2006**, *45*, 8862-8875.

(22) It was ultimately found that the best agreement between calculated and experimental $E_{1/2}$ values was obtained by including ligands with diverse E_L parameters (Cl, -0.24; py, +0.24; for PEt_3 a value of +0.3 rather than +0.34 worked best presumably due to either solvent effects, CH_2Cl_2 versus CH_3CN, or a metal dependence) at a slight expense of linear correlation: ignoring PEt_3 complexes in the basis set data would improve linearity in Figure 7a, but would be detrimental to final correlation between experiment and model predictions for non-basis ligand sets. For non-basis complexes, the E_L value for Me of +0.8 in (**L**)Rh(Me)(CO)(I) (E_L CO = +0.99, E_L(I) = -0.24), a value for PPh_3, E_L (PPh_3), of +0.34 for (L)Rh(PPh_3)(py)(Cl), and the tabulated value for pyrazine, E_L (pyz), of +0.33 worked best for predictions of $E_{1/2}$.

(23). (a) Gagné, R. R.; Koval, C. A., Lisensky, G. C. *Inorg. Chem.* **1980**, *19*, 2855-2857. (b) Noviandri, I.; Brown, K. N.; Fleming, D. S.; Gulyas, P. T.; Lay, P. A.; Masters, A. F.; Phillips, L. *J. Phys. Chem. B*, **1999**, *103*, 6713-6722. (c) Bond, A. M.; Oldham, K.B.; Snook, G. A. *Anal. Chem.* **2000**, *72*, 3492-3496. (d) Bao, D.;

Millare, B.; Xia, W.; Steyer, B. G.; Gerasimenko, A. A.; Ferreira, A.; Contreras, A.; Vullev, V. I. *J. Phys. Chem. A* **2009**, *113*, 1259-1267.

(24). Cotton, F. A.; Eglin, J. L.; Kang, S. –J. *J. Am. Chem. Soc.* **1992**, *114*, 4015-4016.

(25). (a) Coe, B. J.; Fielden, J.; Foxon, S. P. Asselberghs, I.; Clays, K.; Brunschwig, B. S. *Inorg. Chem.* **2010**, *49*, 10718-10726. (b) Shepherd, R. E.; Proctor, A.; Henderson, W. W.; Myser, T. K. *Inorg. Chem.* **1987,** *26*, 2440-2444. (c) Lavallee, D. K.; Fleischer, E. B. *J. Am. Chem. Soc.* **1972**, *94*, 2583-2599. (d) Krishna, V. G.; Chowdhury, M. *J. Phys. Chem.* **1963**, *67*, 1067-1069.

(26). (a) Long, G. J.; Grandjean, F.; Reger, D. L. Spin crossover in pyrazolylborate and pyrazolylmethane complexes. *Topics in Current Chemistry* (2004), 233(Spin Crossover in Transition Metal Compounds I), 91-122. (b) Graziani, O.; Hamon, P.; Thepot, J. -Y.; Toupet, L.; Szilagyi, P. A.; Molnar, G.; Bousseksou, A.; Tilset, M.; Hamon, J. -R. *Inorg. Chem.* **2006**, *45*, 5661-5674.

(27). (a) Ellison, I. J.; Gillard, R. D.; Moszner ,M.; Wilgocki, M.; Ziolkowski, J. J. *J. Chem. Soc., Dalton Trans.* **1994**, 2531-2538. (b) Buckley, A. N.; Busby, J. A.; Ellison, I. J.; Gillard, R. D. *Polyhedron*, **1993**, *12*, 247-253. (c) Ellison, I. J. and R. D. Gillard, *J. Chem. Soc., Chem. Commun.*, **1992**, 851.

CHAPTER 6

(1) Moulton, C. J.; Shaw, B. L.; *J. Chem. Soc., Dalton Trans*.**1976**, 1020-1024.

(2) *The Chemistry of Pincer Compounds*; D. Morales-Morales, C. Jensen, Eds.; Elsevier: Amsterdam, 2007.

(3) (a) G. van Koten, J. T. B. H. Jastrzebski, J. G. Noltes, A. L. Spek, J. C. Schoone J. Organomet. Chem 148 (1978) 233-245. (b) G. van Koten, K. Timmer, J. G. Noltes, A. L. Spek J. Chem. Soc., Chem. Commun. (1978) 250-252. (c) G. van Koten, Pure Appl. Chem. 61 (1989), 1681-1694.

(4) (a)van der Zeijden, A. A. H.; van Koten, G.; Luijk, R.; Vrieze, K.; Slob, C.; Krabbendam, H.; Spek, A. L.*Inorg. Chem.***1988**, 27, 1014-1019. (b) van der Zeijden, A. A. H.; van Koten, G.; Nordemann, R. A.; Kojić-Rodić, B.; Spek, A. L.*Organometallic*. **1988**, *7*, 1957-1966. (c) van der Zeijden, A. A. H.; van Koten, G.; Ernsting, J. M.; Elsevier, C. J.; Krijnen, B.; Stam, C. H. *J. Chem. Soc., Dalton Trans.***1989**, 317-324.

(5) (a)Albrecht, M.; Lindner, M. M..*Dalton Trans*.**2011**, 40. Advanced Article, DOI: 10.1039/c1dt10339c. (b)Choi, J.; MacArthur, A. H. R.; Brookhart, M.; Goldman, A. S..*Chem. Rev*.**2011**, *111*, 1761-1779. (c)Selander, N.; Szabó, K. J.*Chem. Rev*.**2011,***111*, 2048-2076.

(6) (a) Liang, L. C.; Lin, J. M.; Hung, C.H.*Organometallics.***2003**,*22*,3007-3009. (b) See also asymmetric derivatives: Lansing, Jr. R. B.: Goldberg, K. I.; Kemp, R. A. *Dalton Trans*. **2011**, *40*.Advanced Article, DOI 10.1039/c1dt10265f.

(7) (a) Surawatanawong, P.; Ozerov, O. V. *Organometallics***.2011**, *30*, 2972-2980. (b) Puri, M.; Gatard, S.; Smith, D. A.; Ozerov, O. V. *Organometallics***. 2011,***30* 2472-2485. (c) Gatard, S.; Chen, C. H.; Foxman, B. M.; Ozerov, O. V.*Organometallics*. **2008**, *27*, 6257-6267. (d) Gatard, S.; Guo, C.; Foxman, B. M.; Ozerov, O. V. *Organometallics*. **2007**, *26*, 6066-6075. (e) Gatard, S.; Çelenligil-Çetin, R.; Guo,C.; Foxman, B. M.; Ozerov, O. V. *J. Am. Chem. Soc***. 2006**, *128*, 2808-2809.

(8) Winter, A. M.; Eichele, K.; Mack, H. G.; Potuznik, S.; Mayer, H. A.;. Kaska, W. C.*J. Organomet. Chem*. **2003**, *682*, 149-154.

(9) Feller, M.; Iron, M. A.; Shimon, L. J. W.; Diskin-Posner, Y.;. Leitus, G.; Milstein, D.*J. Am. Chem. Soc*. **2008**, *130*,14374-14375.

(10) (a) Verat, A. Y.; Fan, H.; Pink, M.; Chen, Y. S.; Caulton, K. G.*Chem. Eur. J.***2008**, *14*, 7680-7686. (b) Verat, A. Y.; Pink, M.; Fan, H.; Tomaszewski, J.; Caulton, K. G.*Organometallics.***2008**, *27*, 166-168.

(11) (a) Xu, W. W.; Rosini, G. P.; Gupta, M.; Jensen, C. M.; Kaska, W. C.; Krogh-Jespersen, K.; Goldman, A. S. *Chem. Commun*. **1997**, 2273-2274. (b) Gupta, M.; Hagen, C.; Flesher, r. J.; Kaska, W. C.; Jensen, C. M..*Chem. Commun*.*1996* 2083-2084 and 2687.

(12) (a)Montag, M.; Efremenko, I.; Cohen, R.; Shimon, L. J. W.; Leitus, G.; Diskin-Y. Posner, Ben-David, Y.; Salem, H.; Martin, J. M. L.; Milstein, D.*Chem. Eur. J*. **2010**,*16*, 328 and references. (b) Frech, C. M.; Milstein, D. *J. Am. Chem. Soc*. **2006**, *128*,12434-12435.

(13) MacLean, D. F.; McDonald, R.; Ferguson, M. J.; Caddell, A. J.; Turculet, L.*Chem Commun*. **2008,** 5146-5148.

(14) Delferro, M.; Tegoni, M.; Verdolino, V.; Cauzzi, D.; Graiff, C.; Tiripicchio, A.*Organometallics***, 2009**, *28*, 2062-2071.

(15) Doux, M.; Ricard, L.; Le Foch, P.; Jean, Y.*Organometallics.* **2006**, *25*, 1101-1111.

(16) El-Zaria, M. E.; Arii, H.; Nakamura, H.*Inorg. Chem*. **2011**, *50*, 4149-4161.

(17) (a) Zweifel, T.; Naubron, J. V.; Grützmacher, H. *Angew. Chem. Int. Ed*. **2009,** *48***,** 559-563. (b) Büttner, T.; Geier, J.; Frison, G.; Harmer, J.; Calle, C.; Schweiger, A.; Schönberg, H.; Grützmacher, H. *Science*, **2005,** 307**,**235-238.

(18) (a) Wucher, B.; Moser, M.; Schumacher, S.A.; Rominger, F.; Kunz, D.;Angew. Chem. Int. Ed. **2009,** ***48,*** 4417-4421. (b) Moser,M.; Wucher, B.; Kunz, D.; Rominger, F.*Organometallics*.**2007,** *26***,** 1024-1030.

(19) Ligand**A**, Chart 1, n = 1: (a) Radi, S.; Tighadouini, S.; Toubi, Y.; Bacquet, M.; Hazard. Mater.**2011**, *185*, 494-503. (b)Yang, H.; Tang, Y.; Shang, C. F.; Han, X. L.;Zhang, Z. H.*Polyhedron***.2009**, *28*, 3491-3498. (c) Driessen, W. L.; Wiesmeijer, W. G. R.; Schipper-Zablotskaja, M.; De Graaff, R. A. G.; Reedijk, J. *Inorg.Chim.Acta*.**1989,***162*, 233-238. (d) Driessen, W. L.; De Graaff, R. A. G.; Ochocki, J.; Reedijk, J.*Inorg.Chim. Acta*.**1988**, *150*, 41-45.; Ligand **A**, Chart 1, n = 2: (e) Sorrell, T. N.; Malachowski, M. R.*Inorg. Chem*., **1983**, *21*, 1883-1887. (f) Alves, S.; Paulo, A.; Correia, J. D. G.; Domingos, A,; Santos, I.*J. Chem. Soc., Dalton Trans***., 2002**, 4714-4719. (g)Alves, S.; Paulo, A.; Correia, J. D. G.; Gano, L.; Smith,Hoffman, C. J.;Santos, I. C. J. *Bioconjugate Chem***. 2005,***16*, 438-449.

(20) Ligand **B**, Chart 1: (a) Dzik, W. I.; Arruga, L. F.; Siegler, M. A.; Spek, A. L.; Reek, J. N. H.; de Bruin, B.*Organometallics.* **2011**, *30*, 1902-1913. (b) Dzik, W.

I.; Creusen, C.; de Gelder, R.; Peters, T. P. J.; Smits, J. M. M.; de Bruin, B.*Organometallics*,**2010,***29*, 1629-1641. (c) Tejel, C.; del Río, M. P.; Ciriano, M. A.; Reijerse, E. J.; Hartl, F.; Záliŝ, S.; Hetterscheid, D. G. H.; Spithas, N. T. I.; de Bruin, B. *Chem. Eur. J*. **2009**, *15*, 11878-11889. (d) Tejel, C.; del Río, M. P.; Ciriano, M. A.; van den Bruele, F. J.; Hetterscheid, D. G. H.; Spithas, N. T. I.; de Bruin, B.*J. Am. Chem. Soc***. 2008**, *130*, 5844-5845. (e) Hetterscheid, D.; G.; H.; Klop, M.; Kicken, R. G. N. A. M.; Smits, J. M. M.; Reijerse, E. J.; de Bruin, B.*Chem. Eur. J*. **2007**, *13*, 3386-3405.

(21) Ligand **C**, Chart 1: Konrad, F.; Fillol, J. L.; Wadepohl, H.; Gade, H.*Inorg. Chem.* 2009, 48, 8523-8532.

(22) Ligand **D**, Chart 1: (a)Cryder, J. L.; Killgore, A, J.; Moore, C.; Golen, J. A .; Rheingold, A. L.; Daley, C. J. A..*Dalton Trans.***2010,***39*, 10671-10677. (b) Langlotz, B. K.; Wadepohl, H.; Gade, L. H.*Angew. Chem. Int. Ed*. 2008, 47, 4670-4674.

(23) Ligand **E**, Chart 1: (a) Inoue, M.; Nakada, M. *Heterocycles*.**2007**, *72*, 133-138. (b Inoue, M.; Nakada, M.*Angew. Chem. Int. Ed*. **2006**, *45*, 252-255.

(24) Ligand **F**, Chart 1: (a) Gaunt, J. A.; Gibson, V. C.; Haynes, A.; Spitzmesser, S. K.; White, A, J. P.; Williams, D. J. *Organometallics***. 2004**, *23*, 1015-1023. (b) For an alternative ligand preparation, see: Hollas, A. M.; Gu, W.; Bhuvanesh, N.; Ozerov, O. V. *Inorg. Chem*. **2011**, *50*, 3673-3679.

(25) Ligand **G**, Chart 1: Mudadu, M. S.; Singh, A. N.; Thummel, R. P.*J. Org. Chem.***2008**, *73*, 6513-6520.

(26) Ligand **H**, Chart 1: (a) Inagaki, T.; Ito, A.; Ito, J. I.; Nishiyama, H. *Angew. Chem. Int. Ed.*,**2010,***49*, 9384-9387. (b) Liu, H.; Du, D. M. *Eur. J. Org. Chem.* **2010**, 2121-2131.

(27) Ligand **I**, Chart 1: (a) Black, D. S. C.; Rothnie, N. E.*Tetrahedron Lett.***1978,** *31*2835-2838. (b) Black, D. S. C.; Rothnie, N. E. *Aust. J. Chem*. **1983**, *36*, 2395-2406. (c) Cameron, S. A.; Brooker, S.*Inorg. Chem*. **2011**, *50*, 3697-3699.

(28) Ligand **J**, Chart 1: (a) Ren, P.; Vechorkin, O.; Csok, Z.; Salihu, I.; Scopelliti, R.; Hu, X.. *Dalton Trans*.,**2011**, *40*, Advance Article, DOI: 10.1039/c1dt10195a. (b) Breitenfeld, J.; Vechorkin, O.; Corminboeuf, C.; Scopelliti, R.; Hu, X. *Organometallics*. **2010**, *29*, 3686-3689. (c)Csok, Z.; Vechorkin, O.; Harkins, S. B.; Scopelliti, R.; Hu, X.*J. Am. Chem. Soc.***2008**, *130*,8156-8157.

(29) Ligands **K** and **L**, Chart 1: (a) Peters, J. C.; Harkins, S. B.; Brown, S. D.; Day, M. W. *Inorg. Chem.***2001**, *40*, 5083-5091. (b) Betley, T. A.; Qian, B. A.; . Peters, J. C. *Inorg. Chem***. 2008**, *47*, 11570-11582.

(30) Other rhodium complexes of NNN-pincers: (a) Ho, J. H. H.; St Clair Black, D.; Messerle, B. A.; Clegg, J. K.; Turner, P.*Organometallics.* **2006**, *25*, 5800-5810. (b) Kooistra, M.; Hetterscheid, D. G. H.; Schwartz, E.; Knijnenburg, Q.; Budzelaar, P. H. M.; Gal, A. W.*Inorg. Chim.Acta.***2004**, *357*, 2945-2952.

(31) (a) Wanniarachchi, s.; Liddle, B. J.; Toussaint, J.; Lindeman, S. V.; Bennett, B.; Gardinier, J. R.*Dalton Trans*.2011, 40.Advanced Article, DOI:10.1039/C1DT10030K. (b) Wanniarachchi, S.; Liddle, B. J.; Toussaint, J.; Lindeman, S. V.; Bennett, B.; Gardinier, J. R.*Dalton Trans*.**2010**, *39*, 3167-3169.

(32) Montag, M.; Schwartsburd, L.; Cohen, R.; Leitus, G.; Ben-David, Y.; Martin, J. M. L.; Milstein, D.*Angew. Chem., Int. Ed.***2007**, *46*, 1901-1903.

(33) Hernandez-Gruel, M. A. F.; Pérez-Torrente, J. J.; Ciriano, M. A.; Oro, L. A.*Inorg. Synth*.**2004**, *34*, 128.

(34) (a) Liddle, B. J.; Silva, R. M.; Morin, T. J.; Macedo, F. P.; Shukla, R.; Lindeman, S. V.; Gardinier, J. R. *J. Org. Chem.* **2007**, *72*, 5637-5646. (b) Morin, T. J.; Lindeman, S. V.; Gardinier G. R. *Eur. J. Inorg. Chem.* **2009**, 104-110.

(35) SMART APEX2 Version 2.1-4, SAINT+ Version 7.23a and SADABS Version 2004/1. Bruker Analytical Xray Systems, Inc., Madison, Wisconsin, USA, 2005.

(36) CrysAlisPro, Agilent Technologies,Version 1.171.34.46 (release 25-11-2010 CrysAlis171 .NET), (compiled Nov 25 2010,17:55:46)

(37) G. M. Sheldrick, SHELXTL Version 6.12; Bruker Analytical X-ray Systems, Inc., Madison Wisconsin, USA, 2001.

(38) SCALE3 ABSPACK - *An Oxford Diffraction program* (1.0.4,gui:1.0.3) (C) 2005 Oxford Diffraction Ltd.

(39) (a) H.-J. Cristau, P.P. Cellier,; J.-F. Spindler, M. Taillefer, Eur. J. Org. Chem.(2004) 695-709. (b) M. Taillefer, N. Xia, A. Ouali, Angew. Chem. Int. Ed. 46 (2007) 934-936. (c) H.-J. Christau, P.P. Cellier, J.-F. Spindler, M. Taillefer, Chem. Eur. J. 10 (2004), 5607-5622. (d) See also, J.M. Lindley, I.M. McRobbie, O. Meth-Cohn, H. Suschitzky, J. Chem. Soc., Perkin Trans. 1 (1980) 982-994.(e) Antilla, J. C.; Baskin, J. M.; Barder, T. E.; Buchwald, S. L.. *J. Org. Chem.* **2004,** *69*, 5578-5587.

(40) (a) Liddle, B. J.; Silva, R. M.; Morin, T. J.; Macedo, F. P.; Shukla, R.; Lindeman, S. V.; Gardinier, J. R. *J. Org. Chem*. **2007**, *72*, 5637-5646. (b) Morin, T. J.; Lindeman, S. V.; Gardinier, J. R.. *Eur. J. Inorg. Chem*. **2009**, 104-110.

(41) Liddle, B. J.; .Gardinier, J. R. *J. Org. Chem*, **2007**, *72*, 9794-9797.

(42) Mathieu, R.; Esquius, G.; Lugan, N.; Pons, J.; Ros, J. *Eur. J. Inorg. Chem*. **2001** 2683-2688.

(43) Boixassa, A.; Pons, J.; Ros, J.; Mathieu, R.; Lugan, N. *J. Organomet. Chem*. **2003**, *682*, 233-239.

(44) García-Anton, J.; Mathieu, R.; Lugan, N.; Picart, J. P.; Ros, J. *J. Organomet. Chem.* **2004**, *689*, 1599-1602.

(45) Huang, J.; Haar, C. M.; Nolan, S. P.; Marshall, W. J.; Moloy, K. G. *J. Am. Chem. Soc.* **1998**, *120*, 7806-7815.

(46) Hansch, C.; Leo, A. *Substituent Constants for Correlation Analysis in Chemistry and Biology*, Wiley-Interscience: New York, 1979.

(47) Wilson, J. M.; Sunley, G. J.; Adams, H.; Haynes, A. *J. Organomet. Chem*. **2005**, *690*, 6089-6095.

(48) Rankin, J.; Benyei, A. C.; Poole, A. D.; Cole-Hamilton, D. J. *J. Chem. Soc., Dalton Trans.* **1999**, 3771-3782.

(49) Hart-Davis, A. J.; Graham, W. A. G. *Inorg. Chem*. **1970**, *9*, 2658-2663.

(50) (a) J.P. Collmann, L. S. Hegedus, J. R Norton, R. G. Finke *Principles and Applications of Organotransition Metal Chemisty*, 2nd Ed.; University Science Books: Mill Valley, CA, **1987**. (b) R. H. Crabtree, *The Organometallic Chemistry of the Transition Metals*, 5th Ed.; Wiley-Interscience: New York, 2009, Ch. 6 and 12. (c) P. W. N. M. van Leeuwen, *Homogeneous Catalysis: Understanding the Art*; Kluwer Academic Publishers: Dordrecht, 2004; Ch. 2 and 6. (d) J. Hartwig *Organotransition Metal Chemsitry: From Bonding to Catalysis*; University Science Books: Mill Valley, CA, 2010; Chapters 5-7.

(51) Ellis, P. R.; Pearson, J. M.; Haynes, A.; Adams, H.; Bailey, N. A.; Maitlis, P. M. *Organometallics.* **1994,** *13*, 3215-3226 and references.

(52) (a) Rubio, R. J.; Andavan, G. T. S.; Bauer, E. B.; Hollis, T. K.; Cho, J.; Than, F. S.; Donnadieu B., *J. Organomet. Chem*. **2005**, *690*, 5353-5364. (b) Haynes, A.; Maitlis, P. M.; Stanbridge, I. A.; Haak, S.; Pearson, J. M.; Adams, H.; Bailey, N. A. *Inorg. Chim. Acta*. **2004**, *357*, 3027-3037.

(53) Fustero, S.; Sánchez-Roselló, M.; Barrio, P.; Simón-Fuentes, A. *Chem. Rev*. **2011**, *111*, ASAP, dx.doi.org/10.1021/cr2000459.

CHAPTER 7

(1). For leading references, see: *The Chemistry of Pincer Compounds*, ed. D. Morales-Morales and C. M. Jensen, Elsevier, Amsterdam, 2007; G. van Koten, and R. J. M.. Klein Gebbink, *Dalton Trans.*, 2011, 40, 8731-8732 and ensuing articles.

(2). S. Wanniarachchi, B. J. Liddle, S. V. Lindeman, J. R. Gardinier, *J. Organomet. Chem.* 2011, 696, 3623-3636.

(3). C. J. Moulton, B. L. Shaw, *J. Chem. Soc., Dalton Trans.* 1976, 1020-1024.

(4). G. van Koten, J. T. B. H. Jastrzebski, J. G. Noltes, A. L. Spek, J. C. Schoone *J. Organomet. Chem.*, 1978, 148, 233-245; G. van Koten, K. Timmer, J. G. Noltes, A. L. Spek *J. Chem. Soc., Chem. Commun.* 1978 250-252; G. van Koten, *Pure Appl. Chem.*, 1989, 61, 1681-1694.

(5). B. J. Liddle, R. M. Silva, T. J. Morin, F. P. Macedo, R. Shukla; S. V. Lindeman, J. R. Gardinier *J.Org. Chem.* 2007, 72, 5637-5646.

(6). A. R. Katritzky, A. E. Abdel-Rahman; D. E. Leahy, O. A. Schwartz, *Tetrahedron* 1983, 39, 4133-4142.

(7). A. M. Winter, K. Eichele, H. -G. Mack, S. Potuznik, H. A. Mayer, W. C. Kaska, *J. Organomet. Chem.*, 2003, 682, 149-154.

(8). Y.-R. Luo, *Comprehensive Handbook of Chemical Bond Energies*, CRC Press, Boca Raton, FL, 2007.

(9). S. Wanniarachchi, B. J. Liddle, S. V. Lindeman, J. R. Gardinier, *Dalton Trans.* 2011, 40, 8776-8787.

(10). J. S. M. Samec, J. –E. Bäckvall, P. G. Andersson; Brandt, P. *Chem. Soc. Rev.* 2006, 35, 237-248.

(11)). For examples: Mao, D.C. Baker *Org. Lett.* 1999, *1*, 841-843; M. Albrecht; R. H. Crabtree; J. Mata, E. Peris, *Chem. Commun.* 2002, 32-33; L. Yang; A. Kruger; A. Neels; M. Albrecht, *Organometallics*, 2008, 27, 3161-3171; M. U. Raja, R. Ramesh, K. H. Ahn, *Tetrahedron Lett.* 2009, 50, 7014-7017; J. M. V. Jiménez, J. Fernández-Tornos, J. J. Pérez-Torrente, F. J. Modrego, S. Winterle, C. Chunchillos, F. J. Lahoz, L. A. Oro *Organometallics* 2011, 30, 5493-5508.

(12). T. Zweifel. D. Scheschkewitz, T. Ott, M. Vogt, H. Grützmacher, *Eur. J. Inorg. Chem.* 2009, 36, 5561-5576; T. Zweifel, J. –V. Naubron, T. Büttner, T. Ott, H, Grutzmacher, *Angew. Chem. Int. Ed.* 2008, 47, 3245-3249**.**

(13). D. R. Coulson *Inorg. Synth.* 1990, **28**, 107-109.

(14). M.A.F. Hernandez-Gruel, J.J. Pérez-Torrente, M.A. Ciriano, L.A. Oro, *Inorg. Synth.* 2004, **34**, 128.

(15). S. Wanniarachchi, B. J. Liddle, S. V. Lindeman, J. R. *J. Organomet. Chem.* 2011, **696**, 3623-3636.

(16). (a) B. J. Liddle, R. M. Silva, T. J. Morin, F. P. Macedo, R. Shukla, S. V. Lindeman, J. R. Gardinier, *J. Org. Chem.* 2007, **72**, 5637-5646. (b) T. J. Morin, S. V. Lindeman, J. R. Gardinier, *Eur. J. Inorg. Chem.* 2009, 104-110.

(17). CrysAlisPro, Agilent Technologies,Version 1.171.34.46 (release 25-11-2010 CrysAlis171 .NET), (compiled Nov 25 2010,17:55:46)

(18). O. V. Dolomanov, L. J. Bourhis, R. J. Gildea, J. A. K. Howard, H. Puschmann, OLEX2: A complete structure solution, refinement and analysis program. *J. Appl. Cryst.*, 2009, **42**, 339-341.

(19). SCALE3 ABSPACK - *An Oxford Diffraction program* (1.0.4,gui:1.0.3) (C) 2005 Oxford Diffraction Ltd.